DOCTOR OF PHILOSOPHY

Targeted Drug Delivery with Cyclodextrin-based Nanocarriers and Focused Ultrasound Triggering

Xu, Doudou

Award date:
2014

DOCTOR OF PHILOSOPHY

Targeted Drug Delivery with Cyclodextrin-based Nanocarriers and Focused Ultrasound Triggering

Doudou Xu

2014

University of Dundee

Targeted Drug Delivery with Cyclodextrin-based Nanocarriers and Focused Ultrasound Triggering

By

Doudou Xu

Thesis

Submitted to the University of Dundee for the degree of

Doctor of Philosophy (Ph.D.)

Institute for Medical Science and Technology,

Division of Imaging & Technology,

School of Medicine,

College of Medicine, Dentistry & Nursing

May 2014

This page was intentionally left blank

Table of Contents

ACKNOWLEDGMENTS

I would like to gratefully and sincerely thank my primary supervisor Prof. Andreas Melzer for his guidance, understanding, patience and constant support during my studies at Institute for Medical Science and Technology (IMSaT). His mentorship was paramount in providing a well-rounded experience consistent with my long-term career goals. For everything you've done for me, Prof. Andreas Melzer, I thank you.

I am deeply grateful to my second supervisor, Dr. Lijun Wang, for her direct experimental and writing skill guidance, and most importantly, her friendship during my whole studies and social life in IMSaT and Dundee. She has oriented and supported me with promptness and care, and has always been patient and encouraging in times of new ideas and difficulties; she has listened to my ideas and discussions frequently led to key insights.

Furthermore, I am very grateful to thank another supervisor of mine, Prof. Sandy Cochran, for his constant support and encouragement, especially during my thesis preparation. His precious suggestions and grateful patience endowed endless energy for me during the toughest writing up period. Without him, I could never trust myself to complete the final but the most important step of my PhD journey.

I would also like to acknowledge other wonderful people during my studies, without whom much of this could not have been achieved: Dr. Jallal Gnaim, Dr. Fabian Arditti, Dr. Eihab Kabha, Dr. Mariana Bobeica, Dr. Paul Prentice, Dr. Dun Liu, Miss Yue Min, Dr. Dana Gourevich, Dr. Bjoern Gerold and Dr. Ritu Malik, as well as all the support staff in IMSaT.

Finally, and most importantly, I would like to thank my dear husband Mr. Pengjue Fan. His sustained companionship, support, encouragement, patience and unwavering love were undeniably the bedrock for the past ten years of my life. His tolerance of my occasional bad moods is a testament in itself of his unyielding devotion and love. I also thank my parents and parents-in-law, for allowing me to be as ambitious as I wanted. It was under their watchful eyes that I gained so much drive and an ability to tackle challenges head on.

DECLARATION

I hereby declare that this thesis has been compiled by me, which it is a record of work completed by myself and that it has not previously been accepted by whole or part for a higher degree at this University or any other institution of learning.

Doudou Xu

Date: 29. May 2014

CERTIFICATE

This is to certify that Doudou Xu has done this research under my supervision and that she has fulfilled the conditions and requirements for of the University of Dundee, so that she is qualified to submit for the Degree of Doctor of Philosophy.

Prof. Andreas Melzer

Institute for Medical Science and Technology, School of Medicine

Date: 29. May 2014

List of Figures

List of Tables

List of Equations

List of Reactions

List of Symbols and Abbreviation

AuNPs	Gold NPs
AFM	Atomic force microscopy
AcN	Acetonitrile
ATCC	American Tissue Culture Collection
BCA	Bicinchoninic acid
BSA	Bovine serum albumin
CNTs	Carbon nanotubes
CTX	Chlorotoxin
CDs	Cyclodextrins
COSY	Correlation spectroscopy
C_2H_6CO	Acetone
$C_{61}H9_1NO_{41}$	mono-6’-deoxy-6-[3-(naphthalen-2-yl)-2-(amino)propionylamino]-γ-CD
CH_3OH	methanol
Cu	Copper
CM	Complete medium
C18	Octadecyl Carbon Chain Bonded Silica
CH_2C_{l2}	Dichloromethane
C	Cage
DOX	Doxorubicin
DMNPs	Drug-delivering magnetic nanoparticles
DMF	Dimethylformamide
DMSO	Dimethyl sulphoxide
DMAP	4,4-Dimethylaminopyridine
D_2O	Deuterated water
DMEM	Dulbecco’s modified Eagle’s medium
d	tumour’s horizontal/vertical diameter
EGFR	Epidermal growth factor receptor
ELP-DOX	Elastin-like polypeptide-DOX
ESI-MS	Electrospraying
EDC	1-Ethyl-3-(3-dimethylaminopropyl) carbodiimidehydrochloride
EMEM	Eagle's minimal essential medium
ECM	Extracellular matrix
EDTA	Ethylenediaminetetraacetic acid
FUS	Focused ultrasound
FBS	Fetal bovine serum
FR	Folate receptors
GC-MS	Gas chromatography-mass spectroscopy
H	Host compound
HPβCD	hydroxypropyl-β-cyclodextrin
HIFU	High intensity focused ultrasound

HPLC	High performance liquid chromatography
HPLC-MS	High performance liquid chromatography-mass spectroscopy
HOBt	1-Hydroxybenzotriazole
HCl	Hydrochloric acid
$_{dd}H_2O$	Distilled/deionized water
HCT116	Human colorectal carcinoma
HTA	Hydroxyterephthalic acid
HEPA	High-efficiency particulate absorption
IR	Infrared
IVC	Internally ventilated cages
I_0	Fluorescence intensity of DOX in the absence of carrier
I_x	Fluorescence intensity of DOX in the presence of carrier at concentration of x
I	Square number(s) of hemocytometer
IC_{50}	Inhibitory concentration
I	Acoustic intensity
K	Binding constant
KCl	Potassium chloride
KB	Human epidermal carcinoma
LTSLs	Low temperature-sensitive liposomes
MW	Molecular weight
MBs	Microbubbles
MR	Magnetic resonance
MRgFUS	Magnetic resonance guided focused ultrasound
MRI	Magnetic resonance imaging
MR-iLTST	MR imagable low temperature sensitive liposomes
MS	Mass spectroscopy
MP	Melting point
MEM	Minimum Essential Medium
MTT	Methylthiazoldiphenyltetrazolium
MTS	3-(4,5-dimethylthiazol-2-yl)-5-(3-carboxymethoxyphenyl)-2-(4-sulfophenyl)-2H-tetrazolium
MI	Mechanical index
NPs	Nanoparticles
NMR	Nuclear magnetic resonance
NOESY	Nuclear overhauser effect spectroscopy
NH_4OH	Ammonium hydroxide
NH_3	Ammonia
Na_2HPO_4	Dibasic sodium phosphate
$NaH_2PO_4{\cdot}H_2O$	Sodium phosphate monobasic
N	Total cell number/mL
n_i	Unit cell numbers in hemocytometer
NCI	National Cancer Institute
NM	No Mark

ODs	Outer diameters
OD	Absorbance values
PEG	poly(ethylene glycol)
PSA	prostate-specific antigen
polyHis	poly(L-histidine)
PLLA	poly(L-lactic acid)
P2O5	phosphorus pentoxide
Pen-Strep	penicillin and streptomycin
PMS	Phenazine methosulfate
PBS	Phosphate buffer solution
PTC	Positive Thermal Coefficient
PRF	Pulse repetition frequency
Pac	Acoustic power
P	Acoustic pressure
PNP	Peak negative pressure normalised to 1MPa
PTFE	Polytetrafluoroethylene
QDs	Quantum dots
QNM	Quantitative Nano Mechanics
RFA	Radiofrequency ablation
RPCC	Reversed-phase column chromatography
RPMI	Roswell Park Memorial Institute
RU	Resource unit
SWCNTs	Single-wall CNTs
SBEβCD	Sulfobutylether-β-CD
SDS	Sodium dodecyl sulfate
SPM	Scanning probe microscopy
SNR	Signal-to-Noise Ratio
SD	Standard deviation
S	Area of the acoustic beam
TDD	Targeted drug delivery
TLC	Thin layer chromatography
TMS$(CH_3)_4$Si	Tetramethylsilane
TFA	Trifluoroacetic Acid
TA	Terephthalic Acid
TPP	Techno Plastic Products
USCA	Ultrasound contrast agent
UV	Ultraviolet
UV-Vis	Ultraviolet-visible
UF	Uterine fibroid
UKCCCR	United Kingdom Coordinating Committee on Cancer Research
V	Tumour volume
WSTs	Water soluble tetrazolium salts
XTT	2,3-bis-(2-methoxy-4-nitro-5-sulfophenyl)-2H-tetrazolium-5-carboxanilide)

2D	Two-dimensional
Z	Acoustic impedance of the medium
P	Density of the medium
C	Speed of sound
Λ	Wavelength
$\delta(\Delta\nu)$	Chemical shift

Abstract

Background: The Nanoporation project set out to explore specific solutions to overcome the current challenges of targeted drug delivery (TDD) to tumours using magnetic resonance imaging guided focused ultrasound (MRgFUS) to cavitate microbubbles (MBs) for increasing cell permeability and to open 'drug nano-capsules' to release proven active anticancer drugs directly to the tumour site with reduction of systemic drug dosage needed for the desired therapeutic effect.

Objective: The work reported here aimed to develop novel nano-carriers for existing anticancer drugs, by establishment of human cancer cell models to evaluate the carriers' encapsulation efficiency *in vitro* and *in vivo*, by using animal models and a clinical MRgFUS system to investigate the carrier-drug vehicles' *in vivo* distribution and localised drug release / cellular drug uptake.

Methods: A novel γ-cyclodextrin (γ-CD) based carrier for encapsulation of doxorubicin (DOX) was synthesised and fully characterised. The encapsulation efficiency was assessed under various temperatures and pH levels by both chemical analysis and *in vitro* human cancer cell modeling with KB and HCT116 cells. A high-throughput *in vitro* FUS device was designed and applied, in combination with carrier-DOX inclusion. SonoVue® MBs was used to investigate TDD in cell monolayers. *Ex vivo* and *in vivo* trials were carried out with a clinically approved ExAblate MRgFUS system (InSightec, Israel) to establish a safe and efficient clinical TDD protocol on small rodents.

Results: The desired γ-CD based carrier greatly reduced DOX's toxicity and the carrier-DOX inclusion was highly stable under physiological temperature conditions as well as under a wide range of acidic conditions (pH 1.0 ~ 7.0); the encapsulated DOX is slowly released under hyperthermic conditions (up to 50 ℃). In the presence of MBs, application of FUS with low mechanical indexes, under which no thermal effect was observed, enhanced the drug uptake into tumour cells for both encapsulated and free DOX. Optimal setups of MR parameters and FUS parameters were identified *ex vivo*

and *in vivo*, allowing application of MRgFUS treatments to 4 live mice bearing tumours (human colorectal carcinoma, up to 1059.71 mm^3) under anaesthesia with full recovery.

Conclusions: The study demonstrated the possibility of translation of the constructed γ-CD derivative to potential clinical use as a delivery vehicle for DOX using combined thermal and mechanical release mechanisms by clinically applicable MRgFUS–triggered TDD with the potential for cancer therapy.

Chapter 1

Introduction

The main modalities of treatment for cancer patients are conventional surgery, chemotherapy and radiation therapy. Chemotherapy is particularly challenging primarily because of limited uptake of drugs by the tumour cells and the significant systemic toxicity. Better understanding of tumour biology in recent years and new targeted drug delivery (TDD) approaches that are being explored using different nanosystems, bioconjugates, administration routes and controlled delivery devices provide optimism in developing successful targeted and well controlled cancer therapy (Vasir and Labhasetwar 2005).

In spite of that, the current drug delivery systems exhibit many specific problems: 1) potencies and therapeutic effects of drugs are limited or otherwise reduced because of the partial degradation that occurs before drugs reach a desired target in the body; 2) time-release dependent drugs deliver treatment continuously once ingested, rather than providing relief of symptoms and protection from adverse events solely when necessary; and 3) *in vivo* circulation and distribution of drugs cannot be well monitored and controlled for their targeted delivery and release. Methods are not yet established to safely target drugs to specific areas of the body. Therefore, the purpose of reliable drug delivery systems is to deploy drugs intact to specifically targeted parts of the body through a medium that can control the therapy's administration by means of either a physiological or chemical trigger combined with a visualised monitoring tool (Vogelson 2001). To achieve this aim, nanotechnology (nanocarrier) and energy-mediated delivery with real-time visualisation based monitoring systems were proposed and developed to improve TDD by many researchers during the last decade.

1.1 Targeted Drug Delivery (TDD)

TDD is an intensive research area encompassing several engineering branches, physics, physical chemistry, and biology, combined with molecular pharmaceutics and etc. It essentially involves connecting a drug release site to a predetermined anatomical site with the objectives of high efficacy and safety via controlled drug release location, timing, dosage and transport (Kleinstreuer, Childress et al. 2013). The key requirements of an effective TDD system include retention, evasion, targeting and release. However, many obstacles exist to the purpose of strengthening the therapeutic index of a TDD system by selectively delivering it to target areas. Some of these concerns have been addressed by recent developments in areas such as liposomes, prodrugs, external targeting, controlled gene expression and antibodies (Mills and Needham 1999).

In the various TDD systems, the physico-biochemical properties of the drug carrier, the delivery device and optimisation of targeting methodology are the most critical factors for successful TDD (Kleinstreuer, Childress et al. 2013). To improve the efficiency of TDD, various targeting mechanisms have been proposed. The most widely used TDD strategies are **passive targeting** by accumulation of nanomedicines through the leaky vasculature of a tumour or enhancement of permeability and retention effects, and **active targeting** by attaching specific ligands on the surface of the carriers to increase affinity towards the site of interest (Torchilin 2000; Farokhzad and Langer 2009).

Besides, researchers have investigated a number of physical energy triggers to improve the efficiency of *in vivo* TDD, which are (Figure 1.1): ultrasound-mediated sonoporation, light intervention optoporation, electric field impelled electroporation, magnetic field forced magnetoporation, and temperature gradient triggered thermoporation, by using, for example, thermal effects or mechanical forces to enhance drug delivery within the targeted cells or tissues and to activate the drugs using a similar or a different external trigger (Lakshmanan, Gupta et al. 2013).

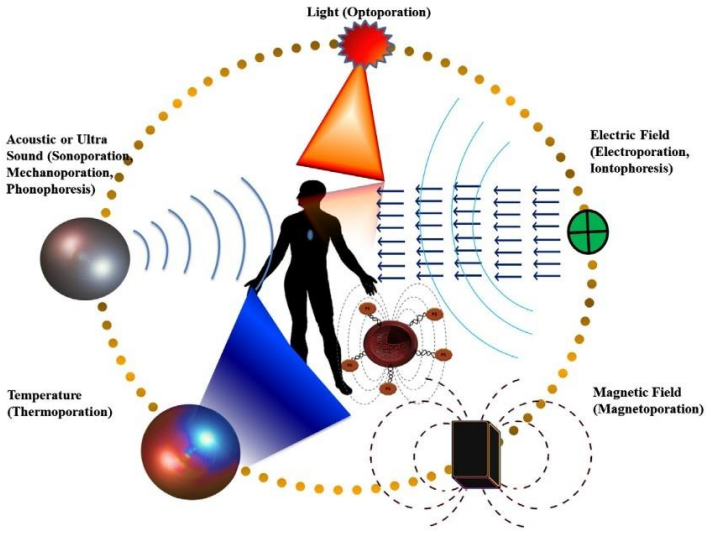

Figure 1.1 Different physical energy modalities used for drug delivery. Drug delivery enhancement through sonoporation, optoporation, electroporation, magnetoporation, and thermoporation are illustrated (Lakshmanan, Gupta et al. 2013).

1.2 Nanocarrier

A nanocarrier is a nanomaterial that is used to transport another substance, such as a chemotherapy agent. Widely used nanocarriers include micelles, polymers, dendrimers, carbon-based materials, liposomes and some other substances (Qian, Sun et al. 2012). Nanocarriers have the potential to improve the therapeutic effect of drugs that suffer from poor solubility and poor stability. This is done by improving their pharmacokinetics by tailoring the release rate (Blanco, Hsiao et al. 2011; Grazú, Moros et al. 2012; Venditto and Szoka Jr 2013), thereby reducing unwanted toxicity and changing the distribution of the drug in tissue. Sarker and Workman (Sarker and Workman 2007) stated that many existing cytotoxic agents discovered during the 1960s such as the platinates, camptothecins and adriamycins, which all suffer from poor solubility, poor pharmacokinetics, reduction of therapeutic efficacy and various harmful side effects, are currently being improved by researchers through the use of nanomedicine for anticancer treatments (Davis, Chen et al. 2008). Therefore, nanocarriers are increasingly being used to improve the solubility and pharmacokinetics of the drug and show promising reductions of adverse side effects (Blanco, Hsiao et al. 2011). Figure 1.2 shows advantages of nanocarriers.

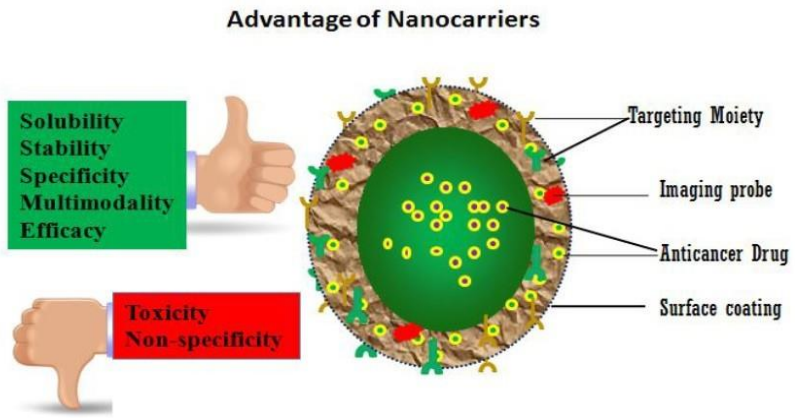

Figure 1.2 Advantages of nanocarriers for cancer nanomedicines (Mousa and Bharali 2011).

1.3 Motivation

- **TDD trigger: Why focused ultrasound (FUS) and magnetic resonance guided FUS (MRgFUS)?**

One of the recently developed physical TDD drivers is **focused ultrasound (FUS)** (Dromi, Frenkel et al. 2007; Ibsen, Benchimol et al. 2011) that allows the deposition of ultrasound bio-effects including heating, cavitation and radiation force in deep tissues in order to: 1) enhance the permeability of pathological cells; 2) localise drug release from nanocarriers; 3) increase extravasation of drugs from carriers; and 4) improve diffusivity of drugs (Husseini and Pitt 2008; Deckers and Moonen 2010). For example, certain tumour microenvironments are characterised by mild hyperthermia (1 – 2 ℃ above physiological temperature) (Vaupel, Kallinowski et al. 1989; Venditto and Szoka Jr 2013) where thermo-responsive drug-carrier nanosystems can be used. In addition, ultrasound contrast agent (USCA) microbubbles (MBs) are playing an important role in diagnosis of cancer. Nowadays, USCA can not only help to distinguish tissues and improve imaging, but can also induce local drug delivery by enhancing accumulation of drugs at a targeted tumour site and by increasing tumour vascular permeability because of cavitation and oscillatory effects such as microstreaming within the sonic field (Lin, Li et al. 2012).

Based on the treatment strategy of FUS, a new method developed very recently in

TDD is the combination of **magnetic resonance guidance with FUS** such that, by using MR imaging (MRI) as a tool, the safety profile of FUS-mediated targeted drug release and uptake (Dick and Gedroyc 2010) can be improved. Clinical MRgFUS systems have been developed by InSightec (work with GE MRI, Haifa, Israel) and Philips Healthcare (Amsterdam, The Netherlands). Specifically, many reports state that TDD applications to overcome the blood-brain barrier (BBB) can be applied safely, reliably and in a controlled manner on rhesus macaques by using an ExAblate MRgFUS system (from InSightec) (Vykhodtseva 2010; McDannold, Arvanitis et al. 2012; Burgess and Hynynen 2013; Jolesz and McDannold 2014). Additionally, Treat *et al.* (Treat, McDannold et al. 2012) have reported their *in vivo* work using MRgFUS for TDD with liposomal doxorubicin in which result in rats have shown that FUS can temporarily permeabilise the BBB but without causing evident tissue damage (Figure 1.3). This indicates that the approach may significantly increase the antineoplastic efficacy of the cytotoxic agent in the brain. Further authors have proposed that the therapeutic benefit of combined MRgFUS-enhanced chemotherapy, achieved with a single treatment, is an important step forward in the development of this technique for the improved treatment of patients with malignancies.

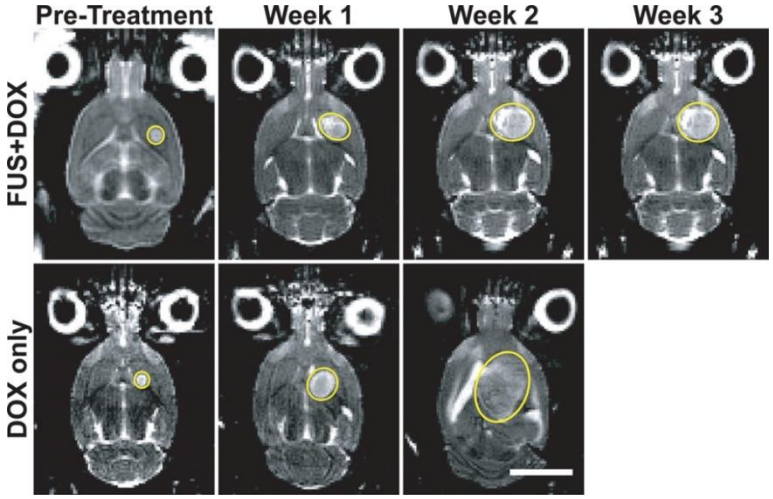

Figure 1.3 T2-weighted MR images of a rat brain with implanted 9 L gliosarcoma (outlined) before and 1, 2 and 3 weeks after treatment with focused ultrasound and liposomal doxorubicin (FUS+DOX; top row) and treatment with liposomal doxorubicin (DOX only; bottom row). While the tumour in the rat treated with DOX only continued to grow exponentially (R^2 = 0.999) even after treatment, tumour growth in the rat treated with FUS+DOX was visibly slowed in comparison (Treat, McDannold et al. 2012).

Additionally, researchers from Philips reported their advanced TDD study using drug release from temperature-sensitive liposomes (ThermoDox) mediated by Sonalleve MR-HIFU (high intensity focused ultrasound) in combination with gadolinium-based MRI contrast agent. They found the drug uptake in the targeted tumour was increased between 2 to 5-fold (http://www.newscenter.philips.com/main/research/news/backgrounders/2011/20110207-mr-hifu-backgrounder.wpd#.UxRsE4UyOSr). The same scientists also stated that the visualisation results by MR guidance may provide an indication if the treatment was effective and may be capable of identifying regions within a tumour that are poorly perfused with blood.

Therefore, MRgFUS system was selected as a TDD tool in this thesis as it has benefits of: 1) being completely non-invasive; 2) providing high-resolution tissue imaging guidance; and 3) providing real-time temperature mapping feedback of the treatment region.

- **Nanocarrier: Why cyclodextrin (CD) modification?**

In terms of drug carrier development, Venditto and Szoka Jr. (Venditto and Szoka Jr 2013) summarised the approved nanomedicines for cancer therapy, where the phases of invention, innovation and imitation were identified. As can be seen in Figure 1.4, monoclonal antibodies (Figure 1.4 C) and liposomes (Figure 1.4 B) have passed the invention and innovation phases and entered the imitation phase before 2000. However, polymer based nanomedicine (Figure 1.4 A), especially CD synthesis, began after 1980. To date, clinical trials are still in the innovation phase for all CD polymer modification and CD-based anticancer nanomedicine such as a remarkable nanoparticle assembly containing CD-based polymer and camptothecin (CRLX101), reported by Davis' team (Gaur, Chen et al. 2012).

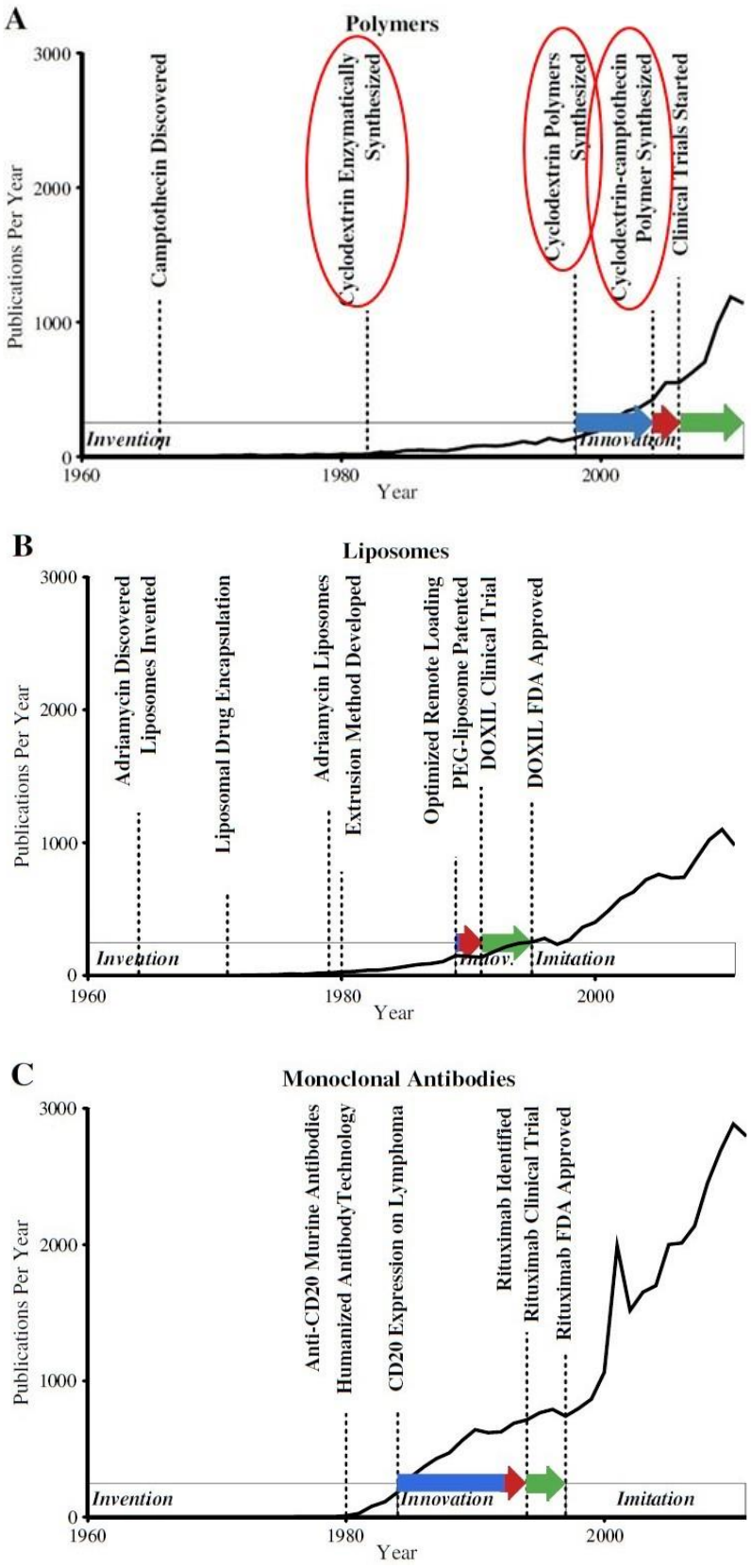

Figure 1.4 Invention, innovation and imitation timeline on the plot of publications per year with seminal publications highlighted. (A) Polymers; (B) Liposomes; (C) Monoclonal Antibodies (Venditto and Szoka Jr 2013).

For CDs, among the most common three native ones (α-, β- and γ-CD), α-CD and β-CD are known to be renally toxic and disruptive of biological membranes while γ-CD and some of its derivatives appear to be much safer (Stella and He 2008). Specifically, for the most frequently used cancer chemotherapeutic agent, doxorubicin (DOX), Anand *et al.* (Anand, Ottani et al. 2012) studied since the 90s the binding between DOX and unmodified natural CDs. Bekers and coworkers (Bekers, Beijnen et al. 1990; Bekers, Beijnen et al. 1991) as well as Dromi *et al.* (Dromi, Frenkel et al. 2007) experimentally demonstrated that DOX bonds significantly to γ-CD, whereas it possesses lower affinity to α-CD and β-CD.

To summarise, two factors: 1) the modification of natural CDs is regarded as novel and has unexplored potential; and 2) γ-CD appears to be less toxic and exhibits higher binding affinity towards the anticancer agent DOX; have served as the motivation for undertaking the rational design and chemical modification of γ-CD as the delivery nanocarrier for DOX reported in this thesis.

1.4 Structure of Thesis

This thesis reports:

1) The latest research progress in the field of nanocarriers in anticancer therapy and FUS-mediated TDD systems;

2) The design, synthesis and evaluation of a novel γ-CD based nanocarrier for encapsulation and delivery of DOX;

3) *In vitro* application of the carrier-drug inclusion by establishment of human cancer cell modelling through cytotoxicity assays and drug uptake investigations;

4) *In vitro* application of a unique high throughput FUS device (a ‘sonicator’) in combination with USCA – SonoVue® MBs to release the drug and/or increase cellular drug uptake;

5) *Ex vivo* and *in vivo* pre-clinical trials of TDD in nude mice with a clinical ExAblate MRgFUS system.

Chapters 1 & 2: Introduction & Literature review. This first chapter briefly

introduces the motivation of this work as well as the outline of this thesis. Chapter 2 overviews the literature in the field and summarises the latest advances in nanocarriers in anticancer therapy and prospective applications of FUS-mediated TDD systems.

Chapter 3: Development of a novel γ-cyclodextrin (γ-CD) based nanocarrier for doxorubicin (DOX). This chapter presents the detailed design, synthesis and evaluation of a novel γ-CD derivative: **mono-6'-deoxy-6-[3-(naphthalen-2-yl)-2-(amino)propionylamino]-γ-cyclodextrin** (**carrier 3b**) with a β-naphthyl alanine residue attached to the primary face of γ-CD. DOX encapsulation efficiency by **carrier 3b** was evaluated under various temperatures and pH levels and the potential of the **carrier 3b** conjugate as a thermo-sensitive carrier for DOX is discussed.

Chapter 4: *In vitro* study by human cancer cell modelling. This chapter provides information on *in vitro* experimental modelling undertaken on two human cancer cell lines: **KB** (human nasopharyngeal epidermal carcinoma) and **HCT116** (human colorectal carcinoma). It reports a series of cytotoxic and cellular drug uptake assays carried out to further validate the encapsulation capability of the **carrier 3b** for DOX under normal physiological conditions. Hyperthermia (up to 50 ℃) was employed to investigate the potential unloading factors of DOX from the **carrier 3b**. The biological observation of the encapsulation capacity of **carrier 3b** and the potential application of the vehicle in TDD are addressed.

Chapter 5: FUS mediated TDD: application of a unique *in vitro* sonicator device. A high-throughput *in vitro* sonicator device with FUS transducers was designed and implemented, in combination with USCA, in the form of SonoVue® MBs, to test cells' viability, drug release and cellular uptake of DOX from the drug-carrier inclusion. The results obtained by application of FUS in the absence and presence of MBs with low mechanical indexes, under which no thermal effects were observed, are discussed. Atomic force microscopy (AFM) is reported, to analyse membrane morphology of cancer cells upon exposure to FUS. A thermal camera and thermocouples were employed to monitor the temperature change during the application of FUS. This section of the study thus suggests that the constructed γ-CD

derivative may serve as a delivery vehicle of DOX with combined thermal and mechanical mechanism, e.g., clinically applicable FUS, -triggered TDD.

Chapter 6: *Ex vivo* and *in vivo* trials with a clinically approved MRgFUS system. This chapter describes *ex vivo* and *in vivo* pre-clinical trials (without injection of drug and carriers) which have been carried out with the clinically approved ExAblate MRgFUS system, in order to establish a safe and efficient clinical TDD protocol on small rodents with subcutaneous human cancer xenografts. The optimal MRI and FUS parameters, as well as the setup of *in vivo* trials, are introduced to explain the possibility of allowing application of MRgFUS treatments in live nude mice bearing subcutaneous tumours under anaesthesia with full recovery.

Chapter 7: Conclusions. The final chapter summarises achievements of the entire study, and further discusses and raises remaining problems, suggestions and possible solutions for future work.

1.5 Contributions to Knowledge

❖ A novel γ-CD based **carrier 3b** was successfully designed, synthesised and fully characterised for molecular encapsulation of the anticancer agent DOX. The evaluation by chemical analysis techniques, *in vitro* cytotoxic testing and cellular drug uptake investigation all showed that the **carrier 3b** had potent encapsulation ability for DOX.

❖ Application of a unique *in vitro* sonicator device as a FUS source to expose cancer cells cultivated in 96-well plate. The use of this standardised device and experimental method reduced instrument-related variability in reported results, reduced the time associated with the FUS exposure of a large number of wells of a 96 well-plate and thus increase the accuracy of exposure duration of cells to encapsulated and non-encapsulated drugs. Moreover, with this high throughput device, the established *in vitro* protocol provides an important platform for biologists to carry out FUS-induced TDD in cell culture.

❖ Successful evaluation and validation that the novel **carrier 3b** is thermally sensitive and stable under mechanical forces through bonding constant ($K_{binding}$)

investigation of the carrier-DOX inclusion by exposure to hyperthermia / FUS with no thermal effects.

❖ *Ex vivo* experiments offered a satisfactory simulation of *in vivo* studies, highlighting a series of questions and potential problems. A safe and efficient clinical TDD protocol was successfully established on small rodents. MRI and FUS parameters have been optimised. In addition, an optimal setup was identified that will allow the application of MRgFUS treatments to live mice with tumours under anaesthesia with full recovery.

❖ The first *in vivo* trial provided many insights into the application of MRgFUS for targeted drug release *in situ* in a small animal model. The presented experiment tested and confirmed the feasibility of the MRI and FUS sonication modes.

1.6 Publications

Journals

- **D. Xu**, L. Wang, D. Gourevich, E. Kabha, F. Arditti, M. Athamnab, S. Cochran, A. Melzer and J. Gnaim. **Synthesis and inclusion study of a novel γ-cyclodextrin derivative as a potential thermo-sensitive carrier for doxorubicin,** Chem Pharm Bull (Tokyo). 2014; 62(7):627-35.
- L. Wang, Y. Min, **D. Xu,** F. Yu, W. Zhou and A. Cuschieri. **Membrane lipid peroxidation by the peroxidase-like activity of magnetite nanoparticles,** Chem. Commun, online published on 30th July 2014, **DOI**: 10.1039/C4CC03082F.
- M. Bobeica, **D. Xu**, B. Gerold, R. Wang, R. Habeshaw, P. Prentice, S. Cochran, and A. Melzer. **An experimental method for standardised, high-throughput ultrasound-mediated targeted drug delivery *in-vitro,*** submitted to Ultrasonics.
- **D. Xu**, M. Bobeica, D. Liu, E. Kabha, L. Wang, S. Cochran, A. Melzer. **Ultrasound-mediated drug delivery of encapsulated doxorubicin into KB cells at low acoustic powers,** in preparation (intend to submit to Ultrasound in Medicine and Biology)

Proceedings

- **D. Xu**, L. Wang, E. Kabha, J. Ginam, and A. Melzer. **Synthesis and Evaluation of a γ-Cyclodextrin derivative for Doxorubicin Delivery**, European Summit on Clinical Nanomedicine (CLINAM 2013), Basel, Switzerland, 23rd-26th June, 2013, pp 229-230.
- Gourevich D, Gerold B, Arditti F, **Xu D**, Liu D, Volovick A, Wang L, Medan Y, Gnaim J, Prentice P, Cochran S, Melzer A. **Ultrasound activated nano-encapsulated targeted drug delivery and tumour cell poration**. (2012), Nano–Biotechnology for Biomedical and Diagnostic Research, in the "Advances in Experimental Medicine and Biology" (AEMB 733), pp.135-144. DOI 10.1007/978-94-007-2555-3_13, Springer Science+Business Media.
- F.D.Arditti, **D. Xu**, D. Liu, D. Gourevich, Y. Medan, J. Gnaim, S. Cochran, A. Meltzer. **Effect of Hyperthermia on the Cytotoxicity of Chemotherapeutic Drugs**, The Premier International and Multidisciplinary Meeting for Image-Guided Cancer Therapies, WCIO, 9-12 June, 2011, pp142-143
- Gerold B., Gourevich D., **Xu D**. , Arditti F., Prentice P.,Cochran S., Gnaim J., Yoav M., Wang L. and Melzer A. **Applicator for In vitro Ultrasound-activated Targeted Drug Delivery**,11th ISTU (The International Society for Therapeutic Ultrasound), New York City, 2011.
- Arditti. F, **Xu. D**, Liu. D, Gourevich. D, Medan. Y, Gnaim. J, Cochran. S, Melzer. **Encapsulation and controlled release of chemotherapeutic drugs by novel γ-cyclodextrin derived carriers**. Journal of Clinical Oncology, 2011 ASCO Annual Meeting Proceedings (Post-Meeting Edition). Vol 29, No 15_suppl (May 20 supplement), 2011: e13062.

Oral Presentations

- **Doudou Xu**. The 23rd International Conference of the Society for Medical Innovation and Technology (SMIT): **MRI guided focused ultrasound activated nano encapsulated targeted drug delivery**; Tel Aviv, Israel, 12-16 September, 2011.

❖ **Doudou Xu**, European Summit on Clinical Nanomedicine (CLINAM 2013): **MR-guided Focused Ultrasound Mediated Drug Delivery Trials in Moving Organs: a γ-cyclodextrin derivative for doxorubicin delivery**. Basel, Switzerland, 23-26 June, 2013.

Poster Presentations

❖ **D. Xu**, M. Bobeica, O. Volovyk, I. Karakitsios, L. Wang, E. Kabha, J. Gnaim and A. Melzer. MR-Guided Focused Ultrasound Mediated Doxorubicin Targeting Delivery by a Novel γ-Cyclodextrin Derivative. Focused Ultrasound Therapy – 2nd European Symposium. Rome, 10th-11th October, 2013.

❖ **D. Xu,** L. Wang, E.b Kabha, J. Ginam, and A. Melzer. Synthesis and Evaluation of a γ-Cyclodextrin derivative for Doxorubicin Delivery, European Summit on Clinical Nanomedicine (CLINAM 2013), Basel, Switzerland, 23rd-26th June, 2013.

❖ **D. Xu,** L. Wang, S. Cochran, M. Bobeica, P. Prentice, B. Gerold, D. Gourevich, J. Gnaim, F. D. Arditti, A. Volovick and A. Melzer. A novel sonicator for in vitro studies of focused ultrasound mediated release of nano-encapsulated drugs for MRgFUS pre-clinical research, The 9th International MRI Symposium, Boston, USA, September 22 - 23, 2012.

❖ D. Gourevich, O. Dogadkin, R. Malik, A. Volovick , B. Gerold, **D. Xu,** Y. Vachutinsky, F. D. Arditti, L. Wang, P. Prentice, Y. Medan, J. Gnaim, S. Cochran, A. Melzer. An in vitro study of increased drug uptake with MRI-guided focused ultrasound surgery, 28th ESMRMB (European Society for Magnetic Resonance in Medicine and Biology), Leipzig/DE, Germany, 6-8 October, 2011.

Awards

❖ **Doudou Xu**, "Technology Award" of the oral presentation: **MRI guided focused ultrasound activated nanoencapsulated targeted drug delivery,** for outstanding contribution during the 23rd International Conference of the Society for Medical Innovation and Technology (SMIT) in Tel Aviv, 12th-16th Sep, 2011

❖ **Doudou Xu**, Cell Culture Models for a Novel γ-cyclodextrin Drug Carrier for Doxorubicin in Focused Ultrasound targeted drug delivery, for **the best presentation prize** at the Symposium of School of Medicine, University of Dundee, 7th June, 2013

Chapter 2

Literature Review

2.1 Introduction

Cancer remains one of the leading causes of mortality worldwide, affecting over 10 million new patients every year (Jemal, Siegel et al. 2010). At present, cancer treatments include surgical resection, chemotherapy and radiation. However, although over 90 chemotherapeutic drugs have been approved for clinical use, their efficacy has been severely hindered by dose-restriction toxicity and patient morbidity (Blanco, Kessinger et al. 2009). Since two decades ago, nanoscale (10 – 200 nm) therapeutic systems have emerged as one of the most novel therapeutic modalities for cancer treatment (Duncan 2003; Ferrari 2005; Peer, Karp et al. 2007).

This chapter reviews the arsenal of nanosystems and molecules available in TDD systems for cancer therapy and emphasises the challenges for these nanosystems in the same applications. Cyclodextrin derivatives discussed particularly, as they are still regarded as novel excipients of unexplored potential (Brewster and Loftsson 2007). In addition, factors that may trigger release of anti-cancer agents from nano-vehicles, such as temperature, physiological pH environments and ultrasound, are introduced, focusing particularly on the MRgFUS mediated TDD that has been proposed as a powerful strategy. Finally, a summary discusses the contributions of the literature to the field of TDD in cancer therapy and the overall strengths and weaknesses of current progress as well as future research directions.

2.2 Nanosystems for TDD in Cancer Therapy: Potential and Challenges

Nanotechnology has the potential to revolutionise cancer diagnosis and treatment. Pioneers' contributions from protein engineering and materials science have given new hope to novel nano-scale targeting approaches that may bring benefits to cancer patients. To date, however, only a few clinically approved nanocarriers exist, incorporating anti-cancer molecules to selectively target and bind to cancer cells (Peer, Karp et al. 2007). These include organic nanocarriers such as liposomes, micelles, polymer-based carriers and dendrimers; inorganic particulates like metal (gold and iron oxide) particles; and carbon nanotubes (Figure 2.1). In comparison to conventional small molecule-based therapies, nanotherapeutic systems have many potential advantages for cancer therapy, including higher payload capacity, prolonged blood circulation times, reduced toxicity to healthy tissues and improved anti-tumour efficacy (Blanco, Kessinger et al. 2009).

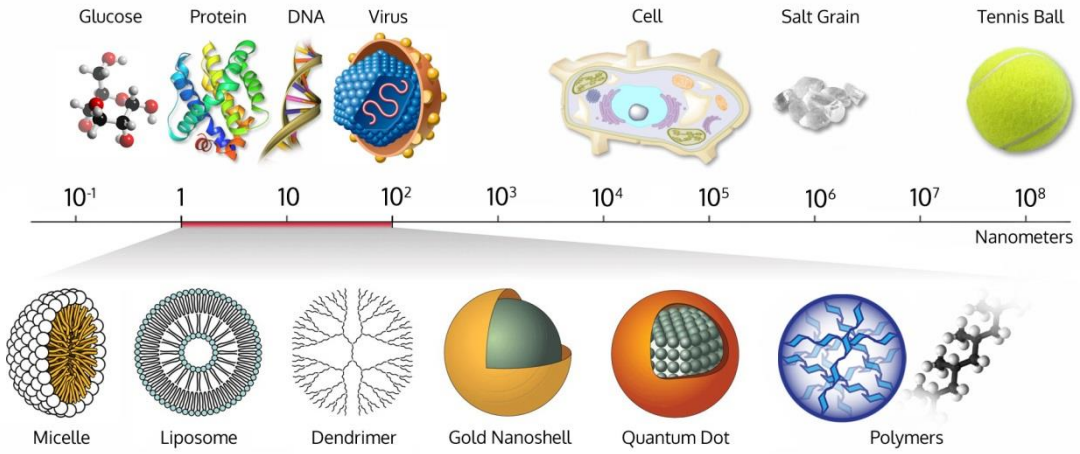

Figure 2.1 Different nanocarriers for cancer nanomedicines (From: http://wichlab.com/research/)

2.2.1 Organic Nanosystems for Cancer Treatment

Liposomes

Liposomes are one of the most attractive nanosystems. The interesting property is their natural ability to target cancer. Liposomes of certain sizes, typically less than

400 nm, can rapidly enter tumour sites from the blood, but are kept in the bloodstream by the endothelial wall in healthy tissue vasculature. Anti-cancer drugs such as doxorubicin (Doxil®, Ben Venue Laboratories, Bedford, Ohio, USA), camptothecin and daunorubicin (DaunoXome®, Nexstar Pharmaceuticals (Gilead Sciences), Foster City, California, USA) are currently being marketed in liposome delivery systems in cancer therapy.

Most of the medical applications of liposomes that have reached the preclinical stage are in cancer treatment (Gregoriadis and Wiley 1988; Gregoriadis 1995; Lasic and Papahadjopoulos 1998). Kobayashi *et al*. (Kobayashi, Tsukagoshi et al. 1975), and Mayhew *et al*. (Mayhew, Papahadjopoulos et al. 1976) first demonstrated *in vivo* application of a liposome-encapsulated anti-cancer agent, cytosine arabinoside, in animal models, showing that liposome-protected cytosine arabinoside prolonged the survival time of mice suffering from L1210 leukemia. Presant *et al*. (Presant, Proffitt et al. 1988) first revealed human solid tumours (Kaposi's sarcoma and malignant lymphoma) to be successfully imaged by accumulation of indium 111-labeled liposomes in regions of enhanced vascular permeability (Presant, Blayney et al. 1990). Gabizon *et al*. (Gabizon, Peretz et al. 1989) presented the first clinical trial, in which liposome-associated DOX improved the tolerance of liver cancer patients by reducing side-effects such as nausea and vomiting.

In contrast, Lasic (Lasic 1998) proposed that most early studies showed that liposome-entrapped drug molecules were only poorly bioavailable, which caused reduction of cytotoxicity but with a severe negative effect on efficacy. For instance, Lasic and Papahadjopoulos (Lasic and Papahadjopoulos 1998), Gabizon *et al.* (Gabizon, Chisin et al. 1991) and Barenholz *et al.* (Barenholz, Amselem et al. 1993) showed in several clinical studies that liposome-associated drugs were rapidly cleared by the reticuloendothelial system and had drug leakage during circulation. Therefore, the concept of ‘stealth liposomes’ was suggested to revive targeted liposomal drug delivery (Lasic 1998).

Stealth liposomes, also known as long-circulating liposomes, are stabilised by polymers such as polyethylene glycol (PEG) (Allen and Cullis 2013). Several studies

(Blume and Cevc 1990; Klibanov, Maruyama et al. 1990; Allen, Hansen et al. 1991; Maruyama, Yuda et al. 1991; Papahadjopoulos, Allen et al. 1991; Senior, Delgado et al. 1991) demonstrated that PEG-associated liposomes reduced the mononuclear phagocyte system (MPS) clearance. Senior *et al.* (Senior, Delgado et al. 1991) further reported that stealth liposomes have dose-independent pharmacokinetics. Following this, other studies demonstrated the therapeutic improvement of PEG-liposomes in animal models (Bakker-Woudenberg, Lokerse et al. 1992; Mayhew, Lasic et al. 1992; T.M. Allen 1992; Vaage, Mayhew et al. 1992; Woodle, Allen et al. 1992; Woodle, Storm et al. 1992). Gabizon *et al.*(Gabizon, Catane et al. 1994) first published the use of stealth liposomes in human studies, followed by a study by James *et al.* (James, Coker et al. 1994) that reported the first clinical trials of PEG-liposomes as DOX carriers (Doxil®) for Kaposi's sarcoma treatment in HIV patients.

In parallel, receptor-mediated endocytosis liposomes were demonstrated by Leserman *et al.* (Leserman, Weinstein et al. 1980), Straubinger *et al.* (Straubinger, Hong et al. 1983) and Leamon and Low (Leamon and Low 1991), and developed by Heath *et al.* (Heath, Fraley et al. 1980) and Martin *et al.* (Martin, Hubbell et al. 1981). Shortly after these publications, Heath *et al.* (Heath, Montgomery et al. 1983) showed that antibody-targeted liposomes improved selective cytotoxicity of liposomal anti-cancer drugs to cancer cells. However, Papahadjopoulos and Gabizon (Papahadjopoulos and Gabizon 1987) proved that antibody-targeted liposomes could not overcome rapid clearance by the mononuclear phagocyte system as well, which restricted their *in vivo* distribution. Therefore, more coupling techniques such as newer attachment of antibodies, their fragments and some other ligands to the terminus of PEG molecules were investigated to develop the stability of liposomes-drug system (Ahmad and Allen 1992; Blume, Cevc et al. 1993; Allen, Agrawal et al. 1994; Lee and Low 1994; Allen, Brandeis et al. 1995; Hansen, Kao et al. 1995; Maruyama, Takizawa et al. 1995; Suzuki, Watanabe et al. 1995). Ahmad *et al.* (Ahmad, Longenecker et al. 1993) introduced the improved *in vivo* survival of targeted-liposomes in a mice lung tumour model. Figure 2.2 further shows the evolution processes of liposomes.

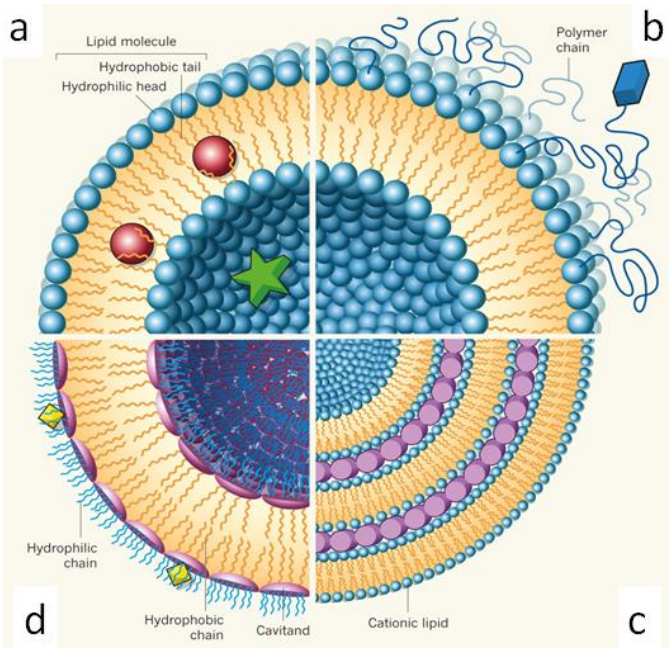

Figure 2.2 The evolution of liposomes: a) Simple liposomes are vesicles that have a shell consisting of a lipid bilayer; b) 'Stealth' liposomes developed for TDD applications, contain target specific biological targets (blue rectangle); c) Cationic liposome: DNA complexes have an onion-like structure, with DNA (purple rods) sandwiched between cationic membranes; d) Liposome bilayer are assembled from cavitands: vase-shaped molecules, with attached hydrophobic and hydrophilic chains which can trap angstrom-sized guest compounds (yellow diamonds)
(Safinya and Ewert 2012).

Overall, liposomes have been developed innovatively from the very simple bilayers through stealth targeted liposomes and cationic liposomes, to the very recent deep cavitand vesicles as drug carriers for anti-cancer agents (Figure 2.2). Notably, liposomes have many advantages because of their potency to encapsulate both hydrophobic and hydrophilic drugs to achieve reduction of unwanted cytotoxicity.

In contrast, techniques for developing targeted liposomes are tedious and difficult to control. Moreover, liposomes are often cleared out by blood circulation rapidly (Allen and Cullis 2013). As mentioned in Chapter 1, Venditto and Szoka Jr. (Venditto and Szoka Jr 2013) reported that liposome-mediated nanomedicine had entered an imitation stage and that many liposomal anti-cancer nanomedicines have obtained FDA approval since mid-1990s. However, from 2000 to 2012, only a couple of anti-cancer liposomal-medicines, Lipo-Dox (Allen and Cullis 2013) and Marqibo (Sarris,

Hagemeister et al. 2000; Rodriguez, Pytlik et al. 2009) have been approved by the FDA Conversely, many other liposomes-based anti-cancer medicines are in the clinical trial stage. Therefore, more efforts are needed in order to improve the 'targeting ligand' on the surface of liposomes to promote the clinical approval.

Micelles

Polymeric micelles are supramolecular (Figure 2.3), core-shell nanoparticles that offer considerable advantages for cancer diagnosis and therapy. They are relatively small (typically in the range of 10 – 100 nm), and have the capacity to solubilise hydrophobic drugs as well as imaging agents. In addition their improved pharmacokinetics provide a useful bioengineering platform for cancer applications (Blanco, Kessinger et al. 2009).

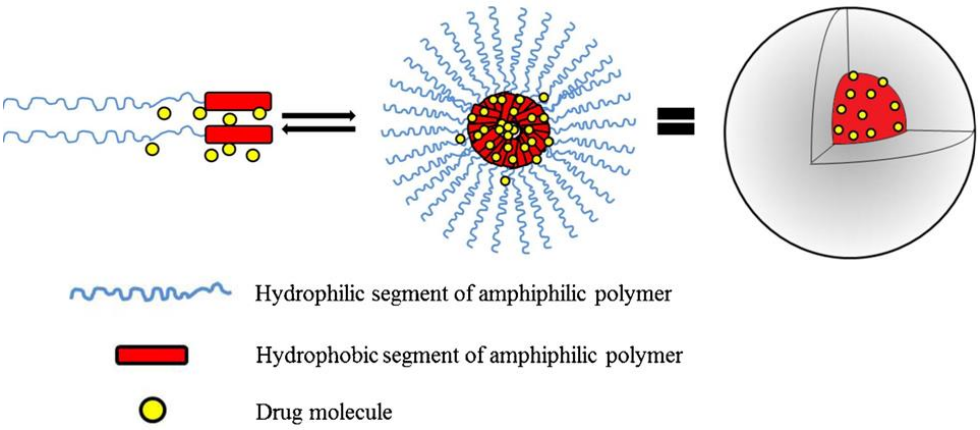

Figure 2.3 Schematic representation of supramolecular structure of polymeric micelles (Lu and Park 2013).

Ringsdorf *et al.* (Gros, Ringsdorf et al. 1981) reported the first use of micelles for cancer treatment in the early 1980s and they were first proposed by Bader *at al.* as drug carriers in 1984 (Bader, Ringsdorf et al. 1984). During the next three decades, micelle-mediated anti-cancer drug delivery developed rapidly. For example, Tokoama's group (Yokoyama, Inoue et al. 1987; Yokoyama, Inoue et al. 1989; Masayuki, Mizue et al. 1990) found DOX-conjugated PEG-*b*-poly (aspartate) copolymers spontaneously formed polymeric micelles in an aqueous environment. Yokoyama *et al.* (Yokoyama, Okano et al. 1991) and Kwon *et al.* (Kwon, Suwa et al. 1994; Yokoyama, Okano et al. 1999) then concluded that polymeric micelles significantly prolonged the blood

circulation time of associated anti-cancer agents. Shortly after, Kohori *et al.* (Kohori, Sakai et al. 1998) and Kim *et al.* (Kim, Kim et al. 2004) reported micelle-associated paclitaxel (Genexol-PM®) which has been approved for the treatment of breast, lung, and ovarian cancers in South Korea. At the same time, Matsumura *et al.* (Matsumura, Hamaguchi et al. 2004; Matsumura and Kataoka 2009) published micellar anti-cancer drug formulations that have entered different phases of clinical trials including NK911®, NK105® (Hamaguchi, Matsumura et al. 2005; Hamaguchi, Kato et al. 2007), and NC6004®. Furthermore, several biodegradable micellar anticancer drugs, NK012 (Hamaguchi, Doi et al. 2010), NC4016 (Gilchrist, Bunemann et al. 1999; Gong, Chen et al. 2012) and BIND-014 (Hrkach, Von Hoff et al. 2012) also have been approved in different phase clinical trials in Japan, USA and UK recently. Blanco *et al.* (Blanco, Kessinger et al. 2009) noted that polymeric micelles provided a unique and complementary nano-platform to the nanosystems including liposomes, polymer-drug conjugates and dendrimers in anti-tumour drug delivery applications.

Nevertheless, many challenges still exist, despite the fact that polymer micelles have shown many advantages in drug delivery applications, with an active field of research to address them,. Allen *et al.* (Allen, Maysinger et al. 1999) and Gaucher *et al.* (Gaucher, Dufresne et al. 2005) indicated that the small size of micelles restricts the amount of drug that can be loaded in the core. Higher drug loading requires increasing micelle size and aggregation. Thus, Kim *et al.* (Kim, Shin et al. 1998) suggested that drugs would be released faster from the micelles because of their small size and limited drug loading, causing to premature release before the micelle reaches its desired targeted site. Additionally, Jones and Leroux (Jones and Leroux 1999) have raised several questions regarding the long-term stability of polymer micelles. In response to these concerns, several groups such as Bontha and coworkers (Bontha, Kabanov et al. 2006) and Xu *et al.* (Xu, Tang et al. 2004) started examining core-cross linked micelles to improve micelle-drug stability *in vivo*. Finally, problems of anti-tumour efficacy of micelles in the clinical setting have been raised as well. To solve these issues, many researchers have explored new methods to ensure the accumulation of the micelles at the tumour site and release of their contents in a controlled, predetermined fashion

(Blanco, Kessinger et al. 2009).

Dendrimers

A dendrimer is tree-like polymer, generally described as a spherical body with a high degree of surface functionality and versatility (Holister, Vas et al. 2003). Two approaches have been developed to synthesise dendrimers. The first, called 'divergent synthesis' was reported by Vögtle's group (E.Buhleier 1978). Pioneers, including Denkewalter's team (Denkewalter, Kolc et al. 1981) from Allied Corporation, Tomalia and coworkers (James R. Dewald 1983; Tomalia, Baker et al. 1985) at The Dow Chemical Corporation and Newkome *et al.* (Newkome, Yao et al. 1985), described the first generation of dendrimers independently. Shortly after, Fréchet *et al.* (Hawker and Frechet 1990) introduced another new approach named 'convergent synthesis' of dendrimers.

The family of dendrimers has been greatly developed by the above two methods and especially in applications of drug delivery, gene delivery and chemotherapy. From 2000, Bosman *et al.* (Bosman, Janssen et al. 1999), Fréchet (Fréchet 2001), Donald (Donald 2005) reported over 100 compositionally different dendrimer families as well as over 1000 surface chemical modification methods (Nanjwade, Bechra et al. 2009).

Lee and coworkers (Lee, MacKay et al. 2005), Svenson and Tomalia (Svenson and Tomalia 2005) and Yang and Kao (Yang and Kao 2006) identified and reviewed the potency of dendrimers as nanocarriers, particularly in biological and pharmaceutical applications. Gillies and Frechet (Gillies and Frechet 2005), Khan *et al.* (Khan, Nigavekar et al. 2005), and Tomalia *et al.* (Tomalia, Reyna et al. 2007) raised the increasing significance of dendrimer-based nanosystems in oncological applications as dendrimers' unique properties are highly suitable for effective delivery of anti-cancer agents. In 2008, Wolinsky and Grinstaff (Wolinsky and Grinstaff 2008) described more dendrimer derivatives developed for greater specificity and functionality in pharmacokinetics and targeted delivery as the relationships between architecture, biocompatibility, retention and delivery of dendrimer families have become clearer. Wolinsky and Grinstaff further showed substantial progress in dendrimers applications for cancer diagnosis and treatment, including advances in the delivery of both

anti-neoplastic and contrast agents.

After dendrimers started to be used clinically, in the early 1990s, Wu *et al.* (Wu, Brechbiel et al. 1994) and Wiener *et al.* (Wiener, Brechbiel et al. 1994) introduced the application of dendrimers conjugates in MRI of tumours. Kukowska-Latallo *et al.* (Kukowska-Latallo, Candido et al. 2005) reported preliminary results showing that methotrexate-containing polyamidoamine (PAMAM) dendrimers significantly reduced subcutaneous tumours in mice. In the same year, Patri *et al.* (Patri, Kukowska-Latallo et al. 2005) and Choi *et al.* (Choi, Thomas et al. 2005) further reported PAMAM with methotrexate-containing / generation 5 (G5) that was covalently conjugated with folic acid specifically to target high folate receptor-expressing cancer cells after intracellular delivery of the drug through receptor-mediated endocyctosis. Independently, Quintana *et al.* (Quintana, Raczka et al. 2002) synthesised an ethylenediamine core PAMAM of G5 dendrimer which was covalently attached to folic acid, fluorescein, and methotrexate. Kasai *et al.* (Kasai, Nagasawa et al. 2002) and Shimamura *et al.* (Shimamura, Kasai et al. 2006) provided research data relating to novel arginine-rich dendrimers, TX-1943 (with 8 Arg residues) and TX-1944 (16 Arg residues), that can be used to suppress the growth and metastasis of solid tumours. To date, many researchers (Hu and Zhang 2012; Lim and Simanek 2012; Mattheolabakis, Rigas et al. 2012) reported frequent employment of DOX and paclitaxel that were covalently bonded to dendrimers in cancer treatment research.

Cheng *et al.* (Cheng, Wang et al. 2008) and Bawarski *et al.* (Bawarski, Chidlowsky et al. 2008) discussed the ideal size, tenability, and multifunctional capability that make dendrimers an excellent nanocarrier to enhance multiple drug interactions to deliver chemotherapeutic agents to specific tumour sites for tumour targeting and therapy. Those advances achieved in dendrimer-based delivery systems over the last two decades have led to development of large number of dendrimer technologies in oncology applications (Wolinsky and Grinstaff 2008). However, the continued research in the area of targeting to a specific cancer (Figure 2.4) still needs to be improved to increase specificity and efficacy towards the diagnoses and treatment of cancer in the clinic.

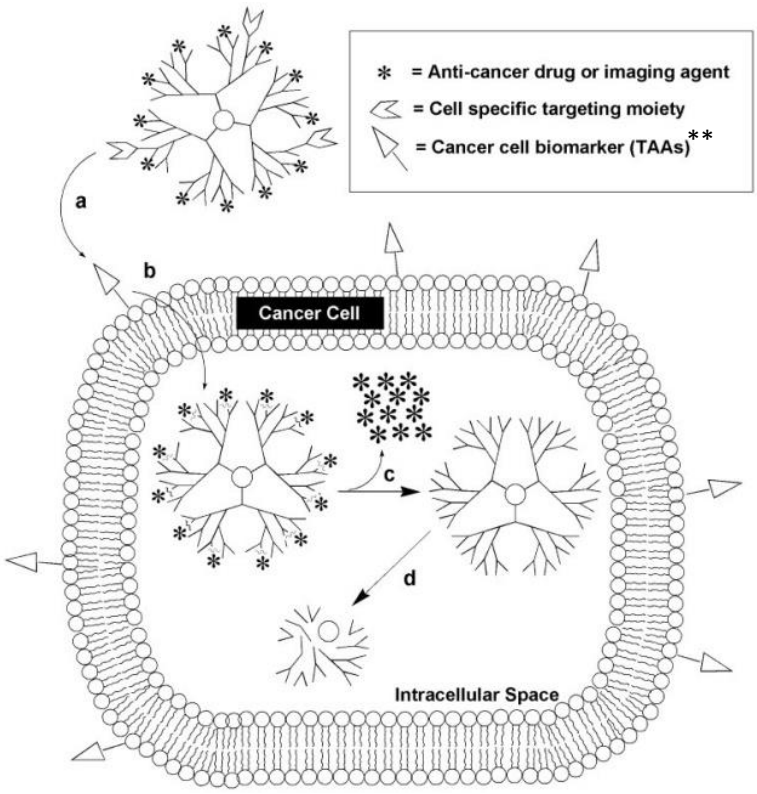

Figure 2.4 Dendrimer-based, cancer-targeted drug delivery. (a) Dendrimers with multiple surface functional groups can be directed to cancer cells by tumour-targeting entities. (b) The next step is intake into the cell, which occurs by membrane receptor-mediated endocytosis in the case of targeting group. (c) Once inside the cell, the drug generally must be released from the dendrimer. (d) Finally, the dendritic scaffold disintegrates.TAAs refers to tumor associated antigens (Sampathkumar and Yarema 2007).**

2.2.2 Inorganic Nanosystems

Inorganic nanosystems are attracting increasing attention in nanomedicine since many investigations on metal / metal oxide nanoparticles (NPs), quantum dots (QDs) and carbon nanotubes (CNTs) have shown that the biocompatibility of these nanosystems might be determined by functionalisation rather than by size, shape or the material, as summarised by Son *et al.* (Son, Bai et al. 2007). Specifically, Son *et al.* addressed the fact that inorganic nanosystems permit a wide range of functionality arising from their unique optical, electrical and physical properties, and that they might also provide novel solutions to overcome many physical barriers into the cell that restrict biomedical applications.

Metallic NPs

Metallic NPs are versatile agents with a variety of biomedical applications including: highly sensitive diagnostic assays (Baptista, Pereira et al. 2008; Selvan, Tan et al. 2009); radiotherapy enhancement (Hainfeld, Slatkin et al. 2004; Huang, Jain et al. 2007); and drug and gene delivery (Thomas and Klibanov 2003; Han, Ghosh et al. 2007). The nanostructured metal powders are typically reduced to the necessary particle size using metal salts or some type of corrosive alcohol. Metallic NPs include Au, Fe, Cu, Ag, Pt, Ru and Re etc. as well as their oxides, Al_2O_3, MgO, ZrO_2, CeO_2, TiO_2, ZnO, Fe_2O_3, SnO and so on. The most popular are gold NPs (AuNPs) and iron oxide NPs.

AuNPs, also known as colloidal gold, are nanosized Au particles in suspension. Specifically in cancer diagnosis and therapy, for example, El Sayed *et al.* (Huang, Jain et al. 2007) established that AuNPs assist cancer imaging through selectively transportation into the nuclei of cancer cells. Shortly after, Qian *et al.* (Qian, Peng et al. 2008) introduced the development of cancer targeted AuNPs as a probe for Raman scattering *in vivo* and suggested that the highly specific recognition and detection of human cancer cells and active targeting of epidermal growth factor receptor (EGFR)-positive tumour xenografts in animal models can be made using surface-enhanced Raman scattering. Moreover, as previous spherical AuNPs absorptions were not optimal for applications *in vivo*, the invention of rod-shaped AuNPs by Murphy's team (Busbee, Obare et al. 2003) circumvented the issue by tuning the absorption peak of the AuNP rods then making them selectively accumulate in tumours under laser light (IR region). Surrounding tissue is barely warmed as nanorods convert light into heat to kill the malignant cells. Several types of AuNPs were able to do this, up to 70 ℃ through near-IR light excitation or oscillating magnetic field stimulation, reported by Paciotti *et al.* (Paciotti, Myer et al. 2004), Visaria *et al.* (Visaria, Griffin et al. 2006) and Cheng *et al.* (Cheng, A et al. 2008), respectively.

Iron oxide NPs include three main oxides of Fe_2O_3, FeO and Fe_3O_4 that are reddish brown and usually magnetic. Their biomedical applications in cancer treatment include TDD, gene delivery and stem cell tracking due to their ultrafine size, magnetic properties and biocompatibility (Mody, Siwale et al. 2010). For example, Sun and coworkers (Sun, Veiseh et al. 2008) developed a chlorotoxin (CTX)-conjugated superparamagnetic iron

oxide nanoprobe coated with PEG, which permits detection of glioma tumours via the surface-bound targeting peptide. Johannsen *et al.* (Johannsen, Gneveckow et al. 2007) presented another Phase I clinical study in which magnetic iron oxide NPs locally killed prostate tumour cells. Furthermore, iron oxide coated with aminosilane (Nanotherm M01) has been in Phase II clinical trials in Germany for treatment of brain cancer and recurrent prostate cancer using hyperthermia as well as thermal ablation methods (Alexis, Pridgen et al. 2010). Further development and modification of iron oxide is possible in combination with dendrimers, polymer-based NPs and liposomes. However, the toxicity of these magnetic NPs to certain types of neuronal cells is still a matter of concern (Pisanic, Blackwell et al. 2007).

Quantum Dots (QDs)

QDs, nanoscale light-emitting particles, are emerging as a new class of fluorescent probe for *in vivo* biomolecular and cellular imaging (Gao, Yang et al. 2005). Major advances have been made in their use for highly sensitive cellular imaging applications because of the particular properties of narrow and size-tunable emissions with superior signal brightness and greater resistance to photobleaching. QDs can also be functionalised with targeting ligands such as antibodies (Howarth, Liu et al. 2008), peptides (Akerman, Chan et al. 2002), DNA (Farlow, Seo et al. 2013), and small molecules that simultaneously passivate the inorganic core and provide the particles with additional functionalities (Kim, Tonga et al. 2013). These properties make QDs versatile nanoscale bases for designing multifunctional NPs with both imaging and therapeutic functions (Smith, Duan et al. 2008).

Many attempts have been made to use QDs for tumour targeting under *in vivo* conditions. In the case of active targeting, QDs were functionalised with tumour-targeting molecules to selectively bind to cancer cells (Gao, Yang et al. 2005). While QDs involving passive targeting use the enhanced permeation and retention of tumour cells (Jain 1999; Jain 2001) for delivery, the first use of QD-peptide conjugates for targeting tumour vasculatures was reported by Akerman *et al*. (Akerman, Chan et al. 2002) in 2002, but unfortunately the QD probes were not detected in living animals. Shortly after, Gao *et al*. (Gao, Cui et al. 2004) demonstrate successful application of a new class of

multifunctional QD probes for simultaneous targeting and imaging of tumours in live animals.

The remaining issue of QDs is their cytotoxicity *in vivo*. For example, Derfus *et al.* (Derfus, Chan et al. 2004) reported that CdSe nanocrystals were highly toxic to cultured cells under UV illumination, as the QDs can be dissolved under the energy of UV irradiation which is close to the covalent chemical bond energy of CdSe nanocrystals. In contrast, Ballou *et al.* (Ballou, Lagerholm et al. 2004) found that QDs with a stable PEG coating showed no toxicity in mice. Finally, many other questions such as how to find the optical and electrical properties to explain QDs' energy states in theirs structures is an essential step (Mohammadi and Bahrami 2014) and must be carefully evaluated before QD applications in tumour or other diseases can be approved for human use.

Carbon Nanotubes (CNTs)

CNTs are the leading inorganic nanosystem for biomedical application. Kostarelos' group (Lacerda, Bianco et al. 2006; Kostarelos, Lacerda et al. 2007) discussed their toxicology and pharmacology properties extensively. As the electrical conductance of CNTs is sensitive and changes with their surface adsorption, CNTs have been proposed as a sensor element for detection of biological molecules such as cancer markers (Collins, Bradley et al. 2000; Kong, Franklin et al. 2000; Shim, Javey et al. 2001). Specifically, a bio-molecular detector based on single-wall CNTs (SWCNTs) has been reported as a highly specific electronic sensor to detect important bio-molecules in the human body (Chen, Bangsaruntip et al. 2003). In 2005, Li *et al.* (Li, Curreli et al. 2005) introduced another type of biosensor based on SWNTs which were integrated into a biosensor for the detection of prostate cancer and, in the same year, Li *et al.* (Li, Zhang et al. 2005) successfully detected prostate-specific antigen (PSA), an interesting target for both imaging and therapeutic intervention in prostate cancer (Schülke, Varlamova et al. 2003), using SWCNTs.

Although CNTs have attracted particular growing attention as new vectors for the delivery of therapeutic molecules because of their ease of translocation across cell membranes and the low toxicity demonstrated by many researchers (Bianco and Prato 2003; Pantarotto, Singh et al. 2004; Vardharajula, Ali et al. 2012), issues of ultimate

biocompatibility of CNTs have limited their widespread use in biomedical applications. For instance, SWCNTs' pulmonary toxicity was proved by Lam *et al.* (Lam, James et al. 2004) who showed, through animal models, that they are much more toxic than carbon black and can be more toxic than quartz.

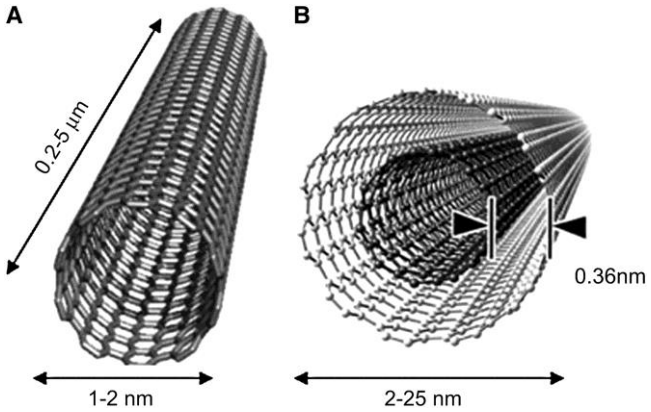

Figure 2.5 Conceptual diagram of (A) single-walled carbon nanotube (SWCNT) and (B) multi-walled carbon nanotube (MWCNT), showing typical dimensions of length, width, and separation distance between graphene layers in MWCNTs (Reilly 2007).

2.2.3 Summary

To sum up, non-specific accumulation into healthy tissues is always a concern for NP drug delivery systems. Typically, inorganic nanosystems such as metallic NPs use local sensitisation through light or temperature which may reduce overall toxicity but are expected to damage adjacent healthy tissues as well. In most applications, organic bio-nanosystems such as liposomes (Park 2002) and biodegradable polymers (El-Sayed, Hoffman et al. 2005) have played key roles in nanomedicine because they are considered to be safer in the human body. Inorganic nanosystems such as metals and metal oxide NPs as well as CNTs have been limited by safety issues and may not provide advantageous over organic nanosystems as they are not biodegradable, have low payloads, and have no controlled release properties (Alexis, Pridgen et al. 2010). On the other hand, Ferrari (Ferrari 2005) and Hillebrenner *et al.* (Hillebrenner, Buyukserin et al. 2006) have suggested that inorganic nanomaterials have fundamental advantages over bioorganic nanosystems such as liposomes, dendrimers, and biodegradable polymers in terms of size, shape control and surface functionalisation.

2.2.3 Cyclodextrin (CDs) Based Nanocarriers

Overview

CDs are natural, cyclic torus-shaped oligosaccharides mostly composed of 6, 7, or 8 D(+)-glucose units, named α-, β-, and γ-CD, respectively (Szejtli 1988; Allegre and Deratani 1994). CDs have a variety of applications in the pharmaceutical industry due to their complexation ability and other versatile characteristics (Arun, Ashok et al. 2008). One of the most noteworthy of these is the application of CDs as drug encapsulants in controlled release systems. As drug encapsulants, Uekama *et al.* (Uekama, Hirayama et al. 1998; Uekama 2004) noted that, because of the unique capability of forming inclusion complexes in the inner cavities and many other favourable physicochemical and biological properties, natural CDs and their derivatives have been applied in drug delivery systems to improve the solubility, stability, bioavailability, therapeutic index, efficacy, pharmacokinetics and biosafety of many hydrophobic drugs, with many concomitant pharmacological benefits such as reducing unwanted side effects.

The interior cavity of a CD molecule is considerably more lipophilic than the aqueous environment while its exterior surface is relatively hydrophilic. These properties account for its capability to act as a complexing agent to increase solubility of lipophilic drugs, to further assist in increasing their stability and bioavailability (Brewster and Loftsson 2007; Tafazzoli and Ghiasi 2009). Generally, CDs do not penetrate lipophilic membranes as they are large, with a number of hydrogen donors and acceptors (Arun, Ashok et al. 2008) and they normally carry and transport non-covalently bound drugs to the targeted cells (Yamanoi, Kobayashia et al. 2006). Figure 2.6 summarises the characteristics of natural CDs.

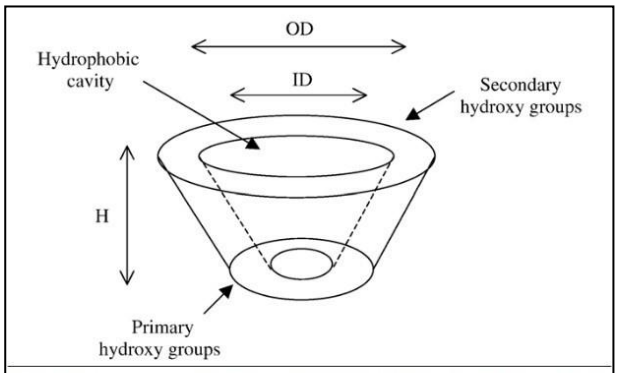

Cyclodextrin	Number of glucose units	Dimensions (nm)			$t_{1/2}$ of ring opening (h)	Mean $K_{1:1}$ [a] (M^{-1})
		H	OD	ID		
α-Cyclodextrin (αCD)	6	0.78	1.37	0.57	33	130±8
β-Cyclodextrin (βCD)	7	0.78	1.53	0.78	29	490±8
γ-Cyclodextrin (γCD)	8	0.78	1.69	0.95	15	350±9

Figure 2.6 Characteristics of natural CDs; *a*: Stability constants ($K_{1:1}$) of 1:1 guest/CD complexes in aqueous solutions at 25 ± 5 ℃ (Connors 1995; Brewster and Loftsson 2007).

Research studies in animals and humans have shown that CDs and their derivatives can be used to improve drug delivery for almost any type of drug formulation from anti-cancer drugs to anti-viral drugs (Tiwari, Tiwari et al. 2010). When some cancer drugs are combined with CDs, their bioavailability increases. It takes far less of a drug to produce cancer killing effects if its bioavailability can be controlled in the bloodstream and acceptable drug levels are reached more effectively and precisely. CDs can thus make cancer treatment far less debilitating for a patient undergoing chemotherapy: less of a toxic drug in a person's system may lead to fewer side effects.

History of CD development

CDs were first introduced in 1891 (Villiers 1891). Schardinger (Schardinger 1903; Schardinger 1911) then laid the foundation of CD chemistry and identified both α-and β-CD during the period 1903 – 11. In the 1930s, γ-CD was discovered by Freudenberg and Jacobi (Freudenberg and Jacobi 1935), and the hypothesis that larger CDs might exist was suggested in 1948 (Freudenberg and Cramer 1948). This hypothesis was later verified by French (French 1965) in 1965. Freudenberg *et al.* further demonstrated that CDs are cyclic oligosaccharides formed by glucose units, and shortly after, Cramer and coworkers described their ability to form inclusion complexes (Cramer 1954). By the early 1950s, the basic physicochemical characteristics of CDs had been discovered,

including their ability to solubilise and stabilise drugs. The first CD-based patent was issued in 1953 (Freudenberg 1953). However, pure CDs suitable for pharmaceutical applications did not become available until about two decades later, when the first CD-containing pharmaceutical product was marketed in Japan. CD-containing products appeared on the European market later and in 1997 also in the US. New CD-based technologies are constantly being developed and, thus, 100 years after their discovery, they are still regarded as novel excipients of unexplored potential (Brewster and Loftsson 2007).

Chemical and Biological Properties of CDs

CDs are relatively large, with molecular weight (MW) 1000 – 2000. They are chemically stable in aqueous alkaline solutions but are susceptible to hydrolytic cleavage under strong acidic conditions (Bender and Komiyama 1978; Hirayama, Yamamoto et al. 1992). CDs and their complexes will penetrate hydrophobic bio-membranes only with considerable difficulty under normal conditions.

Arima *et al.* (Arima, Adachi et al. 1990) and Uekama *et al.* (Uekama, Adachi et al. 1992) concluded stratum corneum was the main barrier to percutaneous absorption of CDs, and that penetration enhancers which decreased the barrier properties would enhance penetration of hydrophilic CDs into skin. For instance, Gerlóczy *et al.* (Gerlóczy, Antal et al. 1988) demonstrated that the absorption of heptakis(2,6-di-O-methyl)-β-CD (^{14}C-DIMEB/DMβCD) was negligible even it was assumed that the absorption might be greater into skin. Another study reported by Tanaka *et al.* (Tanaka, Iwata et al. 1995) in 1995 showed that only 0.02% of topically applied radio-labelled hydroxypropyl-β-cyclodextrin (HPβCD) was absorbed by intact skin of nude mice under occlusive conditions. However, within the same study, around 24% of HPβCD was absorbed into stripped skin. Some other bio-membranes were found to be slightly more permeable towards CDs, as summarised by Irie and Uekama (Irie and Uekama 1997) and Merkus *et al.* (Merkus, Verhoef et al. 1999). For example, Reeuwijk *et al.* (Reeuwijk, Irth et al. 1993) illustrated that 2.5 – 4% of nasally administered DMβCD was recovered in the urine in one clinical study. Another example addressed by Szatmári and Vargay (Szatmári and Vargay 1988) showed that

less than 10% of orally administered DMβCD was absorbed in rat trials.

In terms of CDs becoming drug carriers, Bergeron (Bergeron 1984) proposed that, in theory, water molecules entrapped in CD's interior cavity cannot satisfy their hydrogen-bonding potential and have higher enthalpy than bulk water molecules located in the aqueous environment. Therefore, in the aqueous environment, CDs can form inclusion complexes with many hydrophobic drugs through a process in which Loftsson and Masson (Loftsson and Masson 2001) suggested that water molecules located inside the central cavity are replaced by either the whole drug molecule, or more frequently, by some hydrophobic part of the drug. The driving force of complex formation was suggested by Loftsson and Brewster (Loftsson and Brewster 1996) to be enthalpy-rich water molecules releasing from CD's interior cavity and thus lowering the energy of the whole system. However, Loftsson and Brewster also proposed that other forces may also be involved in CD-drug inclusion complexes including *van der Waals* interactions, hydrogen bonding, hydrophobic interactions, release of structural strains and changes in surface tension. Figure 2.7 shows CD-based nanocarriers carrying anti-cancer drug to bio-systems.

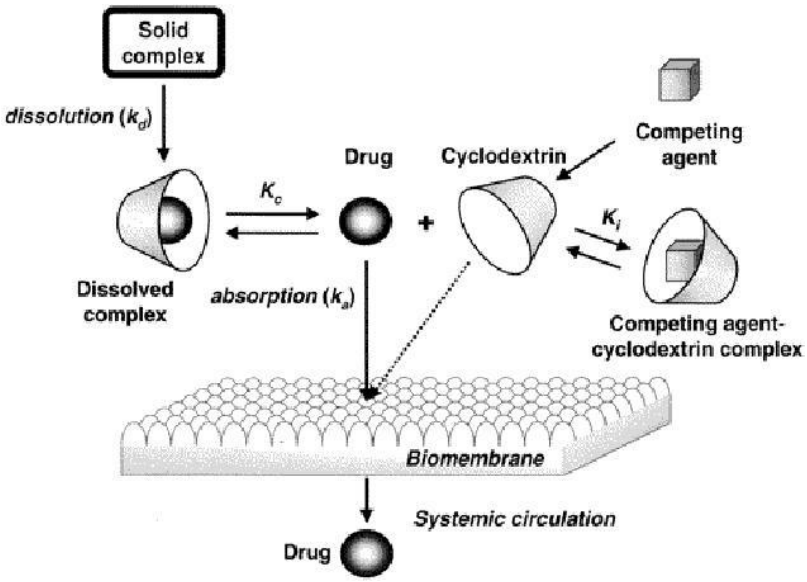

Figure 2.7 Schematic representation of the systemic absorption of drug from its CD complex through biological membranes (Uekama, Hirayama et al. 1998).

In summary, with regard to CDs' permeability, it is generally believed that drug uptake by tissues is not possible with CD-drug complexes or free CDs, as stated by

Loftsson and Bodor (Loftsson and Bodor 1995), Rajewski and Stella (Rajewski and Stella 1996), and Uekama *et al.* (Uekama, Hirayama et al. 1998), respectively. On the aspect of the form of CD-drug inclusions, Stella and Rajewski (Stella and Rajewski 1997) proposed that no covalent bonds were involved in CD-drug complex formation and drug molecules located within the interior cavity were in a very dynamic equilibrium with free drug molecules in the solution.

Modification of CDs as anticancer drug carriers

With the properties of drug-CD inclusion as a basis, from 2000, more and more modified CDs have been employed to improve the native CDs' efficacy in transportation of anticancer agents and reduction of unwanted side-effects in TDD system for cancer therapy.

Bhardwaj *et al.* (Bhardwaj, Dorr et al. 2000) reported the result of increased binding between the anticancer drug Mitomycin C and 2-hydroxypropyl-β-CD (2-HPβCD) and an attempt to reduce skin necrosis by employing the complex. Two years later, Xiang and Anderson (Xiang and Anderson 2002) found that the generation of supersaturated solutions of another anti-cancer agent, Silatecan, was possible by converting a precursor to the lactone at an appropriate pH in a sulfobutylether-β-CD (SBEβCD) solution. Shortly after, Sætern *et al.* (Sætern, Nguyen et al. 2004) proved that the solubility of Camptothecin had been increased by 30 to 50-fold by adding HPβCD-complexation. In parallel, Cheng *et al.* (Cheng, Khin et al. 2003) redesigned the linear β-CD polymer as a protection carrier for camptothecin on the basis of a linear CD copolymer patent obtained by Davis *et al.* (Davis, Gonzalez et al. 2004) in 2003. A year later, Cheng's team (Cheng, Khin et al. 2004) further reported optimised conditions for β-CD polymer-camptothecin conjugates including HGGG6, LGGG10, HG6 and HGGG10 in small animal studies.

In 2006, Phase I clinical trials with the CD-based polymer CRLX101 were first reported, then Davis (Davis 2009) took Insert Therapeutics-101 (IT-101, a CD polymer-camptothecin conjugate) into a Phase II trial in 2008 and was expected to complete the entire trial in 2013. At the same time, Yurkovetskiy and Fram (Yurkovetskiy and Fram 2009) also introduced another CRLX101-containing

camptothecin (XMT-1001) into a Phase II clinical study with Cerulean Pharma Inc. Since then, Davis *et al.* and their industrial partners have taken CD-based carrier transport anti-cancer agent/siRNA conjugates into clinical study (Venditto and Szoka Jr 2013).

As can be seen, β-CD is the most commonly applied medical research (Giordano, Novak et al. 2001; Loftsson and Masson 2001; Singh, Sharma et al. 2002; Loftsson and Duchene 2007) taking in 83.9% of all CD applications, while the application of γ-CD is only 6.5% (Kurkov and Loftsson 2012). However, as γ-CD is constituted by 8 glucopyranoside units, it has the largest toroid compared to α- and β-CD and has demonstrated the highest solubility, the lowest toxicity and better complexing ability (Giordano, Novak et al. 2001). Additionally, both α-CD and β-CD and a number of alkylated CDs are known to be renally toxic and disruptive of biological membranes. γ-CD and some of its derivatives appear to be much safer (Stella and He 2008). These are key issues in the present study and are the reasons why native γ-CD has been selected as the modification model for delivery of DOX.

Overall, CDs are potent nanocarriers to overcome some of the formulation and delivery limitations of highly hydrophobic drugs. However, just as with other nano-systems, they have both strengths and weaknesses. The major strengths of CDs are: 1) the specific form of the equilibrium interaction between CDs and drug molecules; and 2) their capability to deliver a number of intractable and cytotoxic drug molecules safely. However, this specific nature of their interaction is also a weakness, in that the inclusion complex of drug-CD is applicable only to those molecules with suitable size, geometry, and intrinsic solubility properties. This is also the reason that modifications are essential for improving CD's encapsulation ability towards different drug molecules.

Binding constant determination of CD-drug inclusion by fluorescence spectroscopy

CDs and their derivatives can behave as fluorophore quenchers for fluorescent drug molecules such as DOX, under the premise of the drugs being trapped by CDs dynamically. This property and the binding constant between CDs and different guest molecules were validated and calculated, respectively, by Yorozu *et al.* (Yorozu,

Hoshino et al. 1982; Yorozu, Hoshino et al. 1982).

As discussed in the above section, the complexation interaction between CDs and their guests is a dynamic process because no covalent bonds exist during the CD-guest complex formulation (Tafazzoli and Ghiasi 2009). Moreover, the rates of fluorophore entry into and exit from CD cavities are considered much slower than the rate of fluorescence decay of the fluorophore. For example, the fluorescence decay of free DOX in aqueous solution corresponds to a lifetime of 1.1 nsec, independent of its concentration (Dai, Yue et al. 2008). Thus, there is very little possibility for fluorophore guests to enter or exit CD cavities during the lifetime of their excited state. Therefore, fluorescence intensity change of CD-fluorophore inclusion is in the steady-state fluorescence of the fluorophore upon complexation with CDs.

The above interaction model makes it possible to analyse binding affinity of CD-fluorophore complexation by steady-state fluorescence theory (Park 2006) through modified Stern-Volmer correlation (Equation 2.1) (Lehrer 1971; Yorozu, Hoshino et al. 1982; Yorozu, Hoshino et al. 1982; Lee and Okura 1998; Lee, Shin et al. 2001; Lo, Chu et al. 2008; Sorokin, Fylymonova et al. 2012).

$$\frac{I_0}{I_0 - I_x} = \frac{1}{fK[H]_x} + \frac{1}{f}$$

Equation 2.1 Modified Stern-Volmer equation.

In Equation 2.1, I_o is the fluorescence intensity of fluorophores in the absence of CD carriers, I_x is the fluorescence intensity of fluorophores in the presence of different concentrations (x) of CDs, $[H]_x$ is the concentration of CD carriers as a host compound, and $1 / f$ should be one in the study if only one fluorescence quencher is employed (Lee and Okura 1998). In this thesis, only one fluorophore, DOX, was employed and the corresponding K binding was calculated by the relationship of the intercept / slope value which is equal to $(1 / f) / (1 / fK)$ and derived from the linear plot $y = ax + b$ generated from $I_0 / (I_0 - I_x)$ *vs.* $1 / [H]_x$. Hence, the binding constant K can be calculated by the following equation:

$$K = \frac{intercept}{slope} = \frac{b}{a}$$

Equation 2.2 Calculation of binding constant *K*.

To summarise, the fluorimetric properties of a fluorophore are affected by its encapsulation by CDs. Hence, the binding affinity between CDs and guest molecules with fluorimetric characteristics can be evaluated by measuring their fluorescence intensities. It should be noted that this method has to be applied at low concentrations of a fluorophore to afford information on the monomer complexation, since the dimer is known to be not emissive at all (Agrawal, Barthwal et al. 2009).

2.3 Triggers Involved in TDD for Cancer Therapy

2.3.1 Temperature

Topical temperature increases, also called hyperthermia, are a type of cancer treatment by exposure of body tissue to high temperatures, up to 45 ℃. However, hyperthermia treatment by itself is still under clinical trial and is not widely available (Wust, Hildebrandt et al. 2002). Instead, it is usually combined with other forms of cancer therapy as warmer temperatures can make the cells more likely to be affected by treatments such as chemotherapy and radiation therapy (van der Zee 2002; Wust, Hildebrandt et al. 2002). Hence, hyperthermia was also highlighted as a useful trigger tool in nanosystem-associated anti-cancer agents in chemotherapy / radiation therapy in order to: 1) enhance the effects of certain anticancer drugs; 2) enlarge the pore size of tumour microvessels (Lefor, Makohon et al. 1985) to increase tumour perfusion (Karino, Koga et al. 1988); and 3) control release of drugs from thermally-sensitive drug-protection carriers (Gaber, Wu et al. 1996; Kong, Braun et al. 2000; Kong, Braun et al. 2001) at targeted tumour sites.

Thermo-sensitive nanosystems in cancer TDD include thermo-sensitive liposomes (Drummond, Noble et al. 2008; Koning, Eggermont et al. 2010), thermo-responsive polymers (Schmaljohann 2006) and thermo-sensitive nanoparticles (Rahimi, Kilaru et al. 2008). For example, the development of thermo-responsive liposomes for cancer

therapy was first introduced in 1999 (Anyarambhatla and Needham 1999), when a novel method for preparing thermo-sensitive liposomes was described, which significantly enhanced the release of entrapped contents at mild hyperthermia temperatures, 39 – 40 ℃.

A year later, Needham and coworkers (Needham, Anyarambhatla et al. 2000) introduced a new lipid formulation of liposome-encapsulated DOX in combination with mild hyperthermia which appeared to be much more efficient than free DOX or other existing liposomes at reducing tumour growth in a human squamous cell carcinoma xenograft line. Then Celsion Corporation developed ThermoDox which can be triggered to release DOX by any heat-based treatment including radiofrequency ablation (RFA) and microwave hyperthermia as well as FUS. Apart from thermo-sensitive liposomes, Chilkoti *et al.* (Dreher, Raucher et al. 2003; Furgeson, Dreher et al. 2006) have designed a thermally responsive elastin-like polypeptide-DOX (ELP-DOX) conjugate for cancer therapy; Purushotham *et al.* (Purushotham, Chang et al. 2009) have presented a range of thermo-responsive polymer-coated magnetic NPs loaded with anti-cancer drugs and suggested they are of considerable interest for novel multi-modal cancer therapies.

2.3.2 pH

In most tumour tissues, the phenomenon of increased aerobic glycolysis (Gatenby and Gillies 2004) named the Warburg effect (Kim and Dang 2006), leads to lower extracellular pH (6.5 to 7.2) of cancer cells (Schmaljohann 2006; Alfarouk, Muddathir et al. 2011). The relative acidity of the extracellular / interstitial milieu of tumours compared to normal tissues provides a basis for the selective treatment of cancer (Gerweck and Seetharaman 1996). This has been actively exploited to develop drug carriers that can specifically respond to cancer cells with low pH values while staying inactive under normal physiological conditions (Gatenby, Gawlinski et al. 2006).

Many pH-triggered NP / nanocarrier-drug delivery systems have been developed during the last decade. Lim *et al.* (Lim, Huh et al. 2011) reported that pH-responsive drug-delivering magnetic nanoparticles (DMNPs) successfully released DOX under

acidic conditions within cancer cells. Schmaljohann (Schmaljohann 2006) introduced several types of thermo-responsive polymer-conjugated drugs such as pH-sensitive polymeric-micelles composed of poly(L-histidine) (polyHis)/PEG and poly(L-lactic acid) (PLLA)/PEG block copolymer associated-adriamycin (Lee, Na et al. 2003), with the drug released under acidic environment.

In summary, pH sensitive drug delivery system can effectively release drugs according to physiological pH levels in the local environment of diseases including tumours and are a promising TDD system in the future (Balamuralidhara, Pramodkumar et al. 2011).

2.3.3 Focused Ultrasound (FUS)

FUS allows the deposition of thermal and mechanical energies deep inside the human body non-invasively. One of the remarkable advantages of FUS is that it can be focused within pathological tissue in a region of about diameter 2 mm. Ultrasound-mediated techniques were proposed for TDD in the mid-1990s (Miller, Miller et al. 1996; Greenleaf, Bolander et al. 1998). The bio-effects of US can lead to local tissue heating, cavitation, and radiation force, which in TDD applications can be used to: 1) increase extravasation of drugs and / or carriers and enhance diffusivity of drugs; 2) increase the permeability of tumour cell membranes; and 3) control localised drug release from nanocarriers circulating in the blood stream.

When exposed through FUS to temperature / mechanical forces through oscillating ultrasound pressure waves, in sensitive nanocarrier-drug inclusion systems, entrapped drugs can be released locally. For example, thermo-sensitive liposomes have been suggested for targeted drug release in combination with local hyperthermia more than 25 years ago and MBs can be designed specifically to induce cavitation effects in order to cause sonoporation in pathological cell membranes. Moreover, real-time imaging methods, such as MRI, have led to insights and methods for ultrasound TDD. The following content discusses detailed thermal effects, cavitation and radiation force generated by FUS and MB-assisted TDD as well as therapeutic applications of

MRgFUS mediated TDD.

Heat

When US propagates through tissue, absorption of acoustic energy occurs and this energy normally will be converted into heat (Fry 1950). One widespread application of US heating is HIFU-induced solid tumour ablation. A HIFU pulse with several seconds duration generated by a high intensity ultrasound transducer is the basis of HIFU ablation. Because of the highly localised concentration of acoustic energy in the focused spot, the tissue in that small region is heated rapidly and a sharply-circumscribed lesion caused by thermal coagulation is induced. At the same time, tissue penetrated by unfocused ultrasound remains completely unaffected or shows negligible temperature rise. The temperature reached within the focal region during a single sonication should be between 60 to 95 ℃ to induce tissue lesions and necrosis.

To date, many clinical studies using HIFU ablation technique have been performed to treat solid tumours in different organs (Al-Bataineh, Jenne et al. 2012). HIFU therapy has been successfully employed in patients with prostate cancer (Lee, Hong et al. 2006; Ahmed, Zacharakis et al. 2009; El Fegoun, Barret et al. 2011), uterine fibroids (Fruehauf, Back et al. 2008; Okada, Morita et al. 2009; Zhang, Chen et al. 2010), breast cancer (Gianfelice, Khiat et al. 2003; Furusawa, Namba et al. 2007; Wu, Wang et al. 2007), liver (Li, Sha et al. 2007; Zhang, Zhu et al. 2009; Zhu, Zhou et al. 2009), kidney (Wu, Wang et al. 2003; Illing, Kennedy et al. 2005; Klingler, Susani et al. 2008) and pancreas tumours (Wu, Wang et al. 2005; Li, Sha et al. 2007; Xiong, Hwang et al. 2009).

Current methods of ablation can result in marginal recurrences of larger lesions and in difficulty treating tumours located near large blood vessels. The novel approach of applying FUS for the purpose of TDD to extend treatment out to the margins where temperatures do not provide complete treatment with ablation alone may be useful, by combining thermal ablation with drug-loaded thermo-sensitive nanocarriers (Dewhirst, Landon et al. 2013). Hence, the heat may cause the augmented inflow of drugs / drug-carriers and a significant enhancement of drug extravasation from the carriers. It is worth taking this into consideration for the potential application of low power of FUS in

TDD for cancer therapy. The approach is suitable for those thermal-responsive drug / drug-carriers combined with techniques such as chemotherapy and radiation therapy, as well as those patients with cancers that cannot be treated by thermal ablation.

To date, many heat-sensitive nanosystems for delivering anti-cancer agents in cancer therapy have been developed as discussed earlier in this chapter. Overall, the heating effect from US has been traditionally employed in physical therapy to warm up tissues (Draper, Castel et al. 1995), in TDD to melt drug-containing nanocarriers (Tacker and Anderson 1982) and in medical therapy to ablate pathological tissues (Huber, Jenne et al. 2001; Kennedy, Ter Haar et al. 2003; Madersbacher and Marberger 2003). Thus, US induced heating, especially mild hyperthermia in TDD, accomplishes the role of heating drugs / drug carriers and tissues to enhance drug efficient.

Cavitation

Acoustic cavitation is defined as the formation and / or activity of gas-filled bubbles in a medium exposed to US (Barnett, ter Haar et al. 1994). When the pressure wave passes through the medium, gas bubbles of any size will expand at low pressure and contract at high pressure. If the resulting oscillation within the bubbles is fairly stable and reversible, the cavitation is called stable or non-inertial cavitation (Leighton 1994). In contrast, if the amplitude of oscillation in the bubble increases with the sonic intensity up to a point that it cannot reverse the direction when the acoustic pressure reverses, the gas bubble will be continuously compressed to a very small volume until it collapses, creating extremely high pressures and temperatures (May, Allen et al. 2002). This type of cavitation is called transient or inertial cavitation (Leighton 1994).

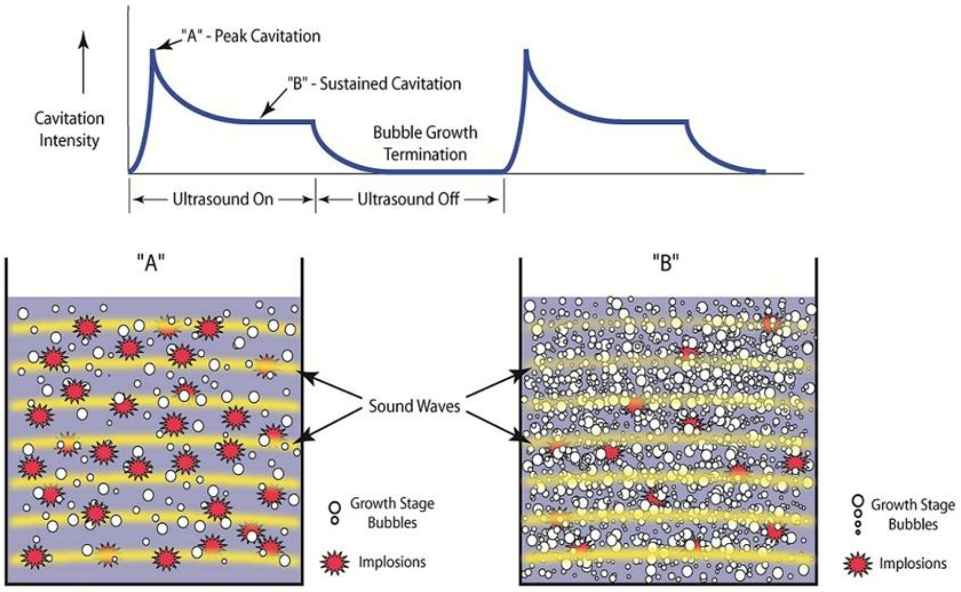

Figure 2.8 Cavitation bubbles are created when ultrasonic energy input is initiated. Bubbles require several cycles of sound waves to grow to a size which will result in an implosive collapse (A and B). The population of bubbles in the growth stage interferes with the transmission of sound waves thereby producing a diminished number of cavitation bubble implosions. (From http://www.ctgclean.com/tech-blog/2012/03/ultrasonics-pulse-more-about-pulsed-ultrasonics/, created by John Fuchs).

As US induced cavitation causes the permeability of cell membranes to increase the cellular drug uptake (Klibanov 2006; Deckers, Rome et al. 2008; Frenkel 2008), this property has led to US-mediated drug delivery as a novel strategy to assist non-permeable therapeutic agents to be internalised so as to enhance the cellular uptake of conventional drugs in cancer therapy (Deckers and Moonen 2010). US radiation is known to be the mechanism which induces cavitation (Larina, Evers et al. 2005) and *in vivo* application of US-mediated TDD is highly attractive as US radiation can be focused at almost any part of the body. Again, localised US induced cavitation may lead to highly selective and efficient drug delivery *in vivo*.

US-induced cavitation to deliver macromolecules *in vitro* has been considered by many research groups since the 1980s. In 1989, Kost *et al.* (Kost, Leong et al. 1989) first studied the effect of US on the degradation of polymers and the release rate of molecules incorporated within the polymers. The examination revealed 5-fold reversible

increases in degradation rate of polymers and 20-fold reversible increases in the release rate of incorporated molecules, with the authors observing that the release rate increased in proportion to the intensity of US and proposing that cavitation appeared to play a significant role. In 2003, Schaaf *et al.* (Schaaf, Langbein et al. 2003) reported that naked plasmid DNA can be easily and effectively delivered to malignant urothelial cancer cells *in vitro* upon exposure to acoustic shock-waves. Moreover, Guzman *et al*. (Guzman, Nguyen et al. 2002) measured the effects of cellular uptake of several different sizes of molecules including caicein (623 Da), bovine serum albumin (66 kDa) and two kinds of dextrans (42 Da and 464 kDa) by exposure of DU145 prostate cancer to 500 kHz US, with the results suggesting that the cellular uptake of all molecules were correlated with applied acoustic energy and thus providing a means to use US cavitation for laboratory and possibly clinical drug delivery applications.

As regards *in vivo* studies, Esenaliev *et al.* (Esenaliev, Larina et al. 2001) proposed an *in vivo* cavitation-induced drug delivery trial in nude mice bearing KM20 human colon tumours. They investigated the delivery of a macromolecular rhodamine-dextran and anti-cancer drug 5-FU under low cavitation US exposure in combination with radiation. The results showed significantly enhanced penetration of 5-FU in irradiated tumours and improvement of cancer therapy.

As US cavitation-enhanced drug delivery has a great potential for *in vivo* application in cancer chemotherapy and radiation therapy, optimisation of ultrasound-mediated cavitation in delivery of macromolecular drugs *in vitro* may provide a basic protocol that could routinely be employed in anti-cancer nanomedicine design and *in vivo* applications (Larina, Evers et al. 2005).

Microbubbles (MBs)

MBs are bubbles smaller than 1 mm in diameter but larger than 1 μm. They are used in medical diagnostics as USCA to assist imaging (Agrawal, Barthwal et al. 2009) because they oscillate and vibrate when applying an acoustic energy field. This behaviour helps to distinguish the MBs from surrounding tissues. MBs have gas cores and are usually entrapped by solid shells such as lipids, polymers or proteins (Bekers, Beijnen et al. 1991) as unshelled gas bubbles lack of stability in liquid environment.

With the exception of enhancement of molecular imaging through their use as functionalised contrast agents, MBs' utilisation as targeted delivery vehicles is one of the most popular research topics related to USCAs. As discussed above, cavitation generated by bubbles in an acoustic field can increase the permeability of endothelial vasculature, allowing small molecules to enter into tissues more easily from the blood stream; this technique is one form of sonoporation (Bekers, Beijnen et al. 1990). However, the exact mechanisms of induction of sonoporation are still unclear. It is generally believed that sonoporation is due to either direct penetration by inertial cavitation (Yorozu, Hoshino et al. 1982) or microstreaming around stable cavitation (Yorozu, Hoshino et al. 1982). Figure 2.9 shows the schematic sonoporation process for drug delivery.

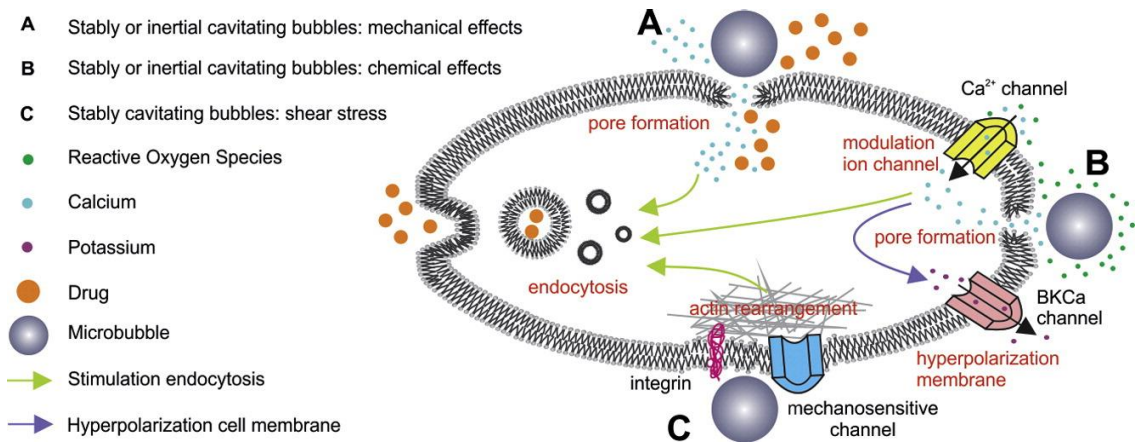

Figure 2.9 Sonoporation process on cell membrane for drug delivery (Lentacker, De Cock et al. 2013).

A range of *in vitro* exposures of US to prostate cancer cell suspensions in the presence of gradient concentrations of Optison MBs (see Table 2.1) were reported by Guzman *et al.* (Husain, Ndou et al. 1992). The results suggested extensive molecular uptake into cells at high viability occurs for low-energy US applied at a high cell-to-bubble ratio. Many studies have demonstrated that a combination of US sonication and MBs with chemotherapeutics may provide a promising way to treat animal tumours (Price, Chappell et al. 2006; Rapoport, Kennedy et al. 2009). For example, Anand *et al.* (Anand, Ottani et al. 2012) confirmed that MB-induced cellular

release of pre-loaded fluorescent dextrans evoked transient pore formation of primary endothelial cells after US exposure. Moreover, Lin and coworkers (Lin, Li et al. 2012) reported that US sonication with MBs significantly enhanced the accumulation of DOX in the sonicated tumour positions in animal models.

US-mediated drug delivery with MBs could also non-invasively enhance the transport of therapeutic agents to overcome the difficulties of drug delivery posed by vascular walls, which can provide a better transport for nanomedicines in tumour tissues and permit specific and effective cellular uptake to targeted tumours (Primeau, Rendon et al. 2005; Bohmer, Chlon et al. 2010; Lin, Huang et al. 2010).

Table 2.1 Commercially available ultrasound contrast agents (Frenkel, Etherington et al. 2006; Reilly 2007)

Contrast agent	Shell	Core (gas)	Market company	Registered region	Year of approval
Levovist	Phospholipids/ galactose	Air	Schering SA, Germany	Europe, China, Japan, Canada and USA	1995
Optison (Albunex)	Human albumin	Perfluoropropane	GE Healthcare	USA, Canada	1998
Definity (Luminity)	Phospholipids	Perfluoropropane	Bristol-Myers Squibb	USA, Canada, Europe	2001
SonoVue	Phospholipids	Sulfur hexafluoride	Bracco, Italy	Canada, Europe, China, India, Korea	2001
Imagent	Phospholipids	Perflexane	IMCOR	USA	2003

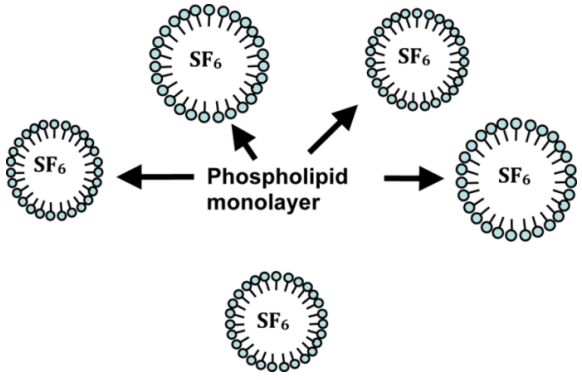

Figure 2.10 Schematic illustration of SonoVue MBs (Reilly 2007).

Table 2.1 lists commercially marketed MBs with their compositions and approved medical application year and regions. Figure 2.10 is the schematic picture of SonoVue® MBs, which was the type applied in this thesis. A detailed description of SonoVue® and its application is further introduced in Chapter 5.

FUS-mediated TDD and MRgFUS-TDD

FUS can be focused at defined locations in living tissues to generate thermal or mechanical effects as described in previous sections. During the last decade, a wide range of research has been conducted to demonstrate the concept of FUS-induced TDD *in vitro* and *in vivo*. In terms of FUS-mediated drug delivery, Frenkel *et al.* (Frenkel, Etherington et al. 2006) first applied pulsed HIFU, followed by tail vein injections of Doxil (liposomal DOX) in murine breast cancer tumours grown in the bilateral flanks of mice. However, the FUS exposure was not found to enhance the release of Doxil, nor did it allow for lower doses to obtain tumour regression. Nevertheless, this trial was the first to show that pulsed-HIFU exposure was safe *in vivo* and it also demonstrated that blood vessels treated with HIFU were dilated, as observed by using fluorescent dextran.

A year later, Dromi *et al.* (Dromi, Frenkel et al. 2007) reported both *in vitro* and *in vivo* studies using low temperature sensitive liposomes (LTSLs) in combination with pulsed HIFU at a thermal dose of 42 ℃ for 2 min, which resulted in 50% release of DOX from LTSLs and enhanced anti-tumour effects.

Therapeutic FUS induced thermal and mechanical effects have shown novel and potential trigger advantages for drug release at target tumour sites. Proper monitoring and guidance to control the acoustic treatment region is a useful adjunct to minimise unwanted damage to adjacent healthy structures (Thanou and Gedroyc 2013). Therefore, the combination of nanomedicines and non-invasive FUS triggering from outside the body together with techniques such as MR-guidance are providing novel approaches to achieve spatio-temporal control of drug delivery.

MRgFUS refers to FUS treatment within an MRI scanner. This setup allows tumour targeting and real-time treatment monitoring by MRI. In FUS-induced TDD, MRI guidance allows better control of the drug's bio-distribution, the pharmacokinetics and pharmacodynamics. Specifically, an MRgFUS system in the field of TDD can be used

for:

1) Real-time manipulation of drug guidance within the targeted area;

2) Spatio-temporal guidance of actions to control release or activate the drugs and / or permeabilise membranes;

3) Evaluation of a drug's bio-distribution, pharmacokinetics and pharmacodynamics;

4) Physiological readouts to evaluate therapeutic efficacy precisely (Thanou and Gedroyc 2013).

Kamaly *et al.* (Kamaly, Kalber et al. 2009) observed the effective accumulation of folate-targeted and fluorescent liposome delivery to solid tumours (IGROV-1 cells) induced in nude mice monitored by dynamic real-time MRI, providing MR-guided insight into the kinetics of nanoparticles targeted to solid tumours. Negussie and coworkers (Negussie, Yarmolenko et al. 2011) developed an MR imageable LTSL (MR-iLTSL) by co-loading liposome with the MRI contrast agent ProHance®Gd-HP-DO3A and DOX. MR-HIFU triggered experiments have been done both *in vitro* and *in vivo*, with the results showing that MR imaging had the greatest effect in the heated tumour region. A year later, Ranjan *et al.* (Ranjan, Jacobs et al. 2012) reported their MR-HIFU drug delivery trials in rabbits bearing tumours by injection of LTSL-based DOX. LTSL + MR-HIFU treatment suggested an improved distribution, with DOX found in both the tumour periphery and core.

The MRgFUS TDD technique is non-invasive, has excellent penetration depth with FUS and can be applied to different organs. It has real-time imaging as a guidance tool to provide accurate temperature mapping, high-resolution tissue imaging and precise targeting during FUS therapy. Therefore, the MRgFUS system may have an advantage over other methods for delivery of drugs to specific sites, especially for solid tumours. However, just as with sonoporation, the exact mechanism of FUS-mediated delivery is not completely understood. Multiple studies suggest that FUS and agents such as MBs facilitate the formation of transient pores in the plasma membrane via cavitation. These pores are known to spontaneously reseal within a short time (from seconds to minutes) (Schlicher, Radhakrishna et al. 2006; van Wamel, Kooiman et al. 2006; Kudo, Okada et

al. 2009). Moreover, MRI equipment is expensive; its use is labour-intensive and its spatial resolution is sometimes reduced (Thanou and Gedroyc 2013). Even allowing for these issues, the new field of MRgFUS triggered drug delivery opens up opportunities to expand applications for existing small drugs in cancer chemotherapy and radiation therapy.

2.4 Conclusions

To summarise, this chapter reviewed the literature which provided many contributions and insights into the invention of novel nanomedicines for TDD in cancer therapy, from design, synthesis, and evaluation *in vitro* and application *in vivo*, up to clinical trials. The improvement of nano-vehicles for carrying toxic and unstable anti-cancer drugs has never stopped; in contrast, their structures have been developed generation by generation as well as combinations of different nano-systems to improve their transportation abilities.

The combination of anti-cancer nanomedicines with traditional chemotherapy and radiation therapy, and with novel non-invasive thermal / ultrasound tumour ablation and drug delivery techniques has been successfully applied to many cancer patients. Numerous *in vivo* experiments and clinical trials have revealed valuable references for those new generations of researchers and clinicians.

Notwithstanding that many improvements and innovations have been achieved in TDD for cancer treatment, many problems remain, such as non-specific dosage, toxicity of nanocarriers themselves, fast clearance from the blood stream, low drug release rate and some unclear mechanism of trigger strategies. More efforts need to be made to overcome these weaknesses to promote more trustable and potent clinical cancer treatment protocols.

Chapter 3

Drug Carrier Development: Chemical Modification and Evaluation of a γ-cyclodextrin Derivative

3.1 Introduction

In aqueous solutions, CDs form inclusion complexes with anthracyclines (Grosse, Bressolle et al. 1999) which are potent antitumor antibiotics (Fujiwara, Hoshino et al. 1985). In present, cancer chemotherapeutic agent DOX, a DNA-intercalating antitumor agent, is the most frequently used member of the anthracycline group (Fernandez, derpoorten et al. 2001) in spite of being chemically unstable (Bekers, Beijnen et al. 1990) in aqueous media with major problems of acute and chronic toxicity (Muggia and Green 1991) and appearance of cellular multidrug-resistance. The best way to overcome serious side-effects associated with DOX administration is to limit the amount of DOX intake or alternatively, to encapsulate the drug in various drug-delivery systems. An ideal TDD vehicle should be able to solubilise, protect and transport the drug specifically to cancer cells and slowly release the drug molecules inside the cells to the site of their pharmacological activities. This can be achieved by attaching biological signals such as hormones, vitamins or antibodies (Willis and Forssen 1998), which can recognise cancer cells, to the surface of the vehicles (Low and Antony 2004; Lukyanov, Elbayoumi et al. 2004). Moreover, drug targeting can also be achieved by using drug vehicles sensitive to the surrounding enzymes, temperature or pH (Soppimath, Tan et al. 2005; Li, Zhang et al. 2006; Liu, Wiradharmaa et al. 2007)

Recently, several studies reported (Yamanoi, Yoshida et al. 2005; Hattori, Kenmoku et al. 2006; Yamanoi, Kobayashi et al. 2006; Oda, Kobayashi et al. 2008;

Oda, Yanagisawa et al. 2008; Oda, Miura et al. 2009; Kralova, Konak et al. 2010; Li, Zhao et al. 2012) that introduction of a suitable substituent (e.g., glucose, galactose, arbutin, hydroquinone α-glycoside, porphyrin or β-carboline) to the rim of α- and β-CDs, can enhance the binding affinity towards DOX through cooperative interactions between the CD's cavity and guest molecules. Although, α- and β-CD is the most exploited CDs, (Sorokin, Fylymonova et al. 2012) little has been published on γ-CD as targeted drug delivery system. Having 8 glucopyranoside units thus the largest cavity, the γ-CD possesses higher water solubility, better inclusion ability of large-size drugs, and orally and is parenterally administered non-toxic (Totterman, Schipper et al. 1997).

In the present study, a novel chemically modified γ-CD derivative, mono-6'-deoxy-6-[3-(naphthalen-2-yl)-2-(amino)propionylamino]-γ-cyclodextrin(**carrier 3b**), with a β-naphthyl alanine residue attached in the primary face of γ-CD, was rationally designed and synthesised. The DOX encapsulation efficiency by this carrier was evaluated under various temperatures and pH and the potential of the novel **carrier 3b** conjugate as a thermo-sensitive carrier for DOX was discussed.

3.2 Essential Chemical Synthesis and Analysis Techniques

3.2.1 Purification Techniques

3.2.1.1 Precipitation

Precipitation is a chemical reaction that uses a precipitant (precipitation agent) to extract desired substances or impurities, by decreasing their solubility to form a solid precipitate.

Precipitation is used in the applications such as making pigments, removing salts from water and in qualitative inorganic analysis, as well as to isolate some products during post-reactions. But ideally, the substance of the reaction is insoluble in the reaction solvent. Thus, when precipitate is formed, pure crystals is preferably formed (Adler, Longo et al. 1967). Precipitation may also occur when the environment is in

the presence of an anti-solvent (a solvent in which the substance is insoluble), which can drastically reduce the solubility of the desired substance. Therefore, the precipitate may easily be separated by filtration, decanting, or centrifugation (Adler, Longo et al. 1970). Precipitation is also useful in purifying products where it precipitates (Dupont, Consorti et al. 2003).

The precipitation method has been found to be very efficient in the isolation of CD based compounds from water, dimethylformamide (DMF) or dimethyl sulphoxide (DMSO) (Connors 1997). In particular, the reaction products in the synthesis within this thesis report were isolated by pouring the reaction mixture into acetone (Gorin, Riopelle et al. 1996).

3.2.1.2 Recrystallisation

Recrystallisation (Harwood 1989) is a procedure for purifying chemical compounds by dissolving both impurities and desired compound in an appropriate solvent. The most commonly used procedure for recrystallisation from a solution involves the following steps (Armarego and Chai 2003): 1) A near-saturated solution is obtained by dissolving the impure material in a suitable solvent, followed by shaking or vigorous stirring at or near its boiling point; 2) Insoluble particles are then removed by filtration of the above solution (a heated filter funnel can be used to prevent crystallisation during the filtration procedure, or the solution can be diluted with more solvent); 3) The solution is then allowed to cool slowly so that the dissolved substance can crystallise out; 4) The crystals are separated from the mother liquor, usually by filtering under vacuum suction through a sintered glass or a Büchner funnel; and 5) The pure crystals are finally washed by a little fresh cold solvent to remove traces of the mother liquor, and then dried.

3.2.1.3 Adsorption chromatography

Adsorption chromatography is based on the difference in the extent to which substances in solution are adsorbed onto a suitable surface. The main techniques in adsorption chromatography include thin layer chromatography (TLC), paper and

column chromatography (Armarego and Chai 2003). The chromatographic purification procedures employed in this thesis are TLC, reversed-phase column chromatography (RPCC) and high performance liquid chromatography (HPLC).

Thin layer chromatography (TLC)

TLC is a simple and inexpensive separation technique that can quickly reveal how many components are in a mixture. TLC is widely used to identifying a compound in a mixture by comparing R_f values (Figure 3.1) of a unknown compound to a known compound.

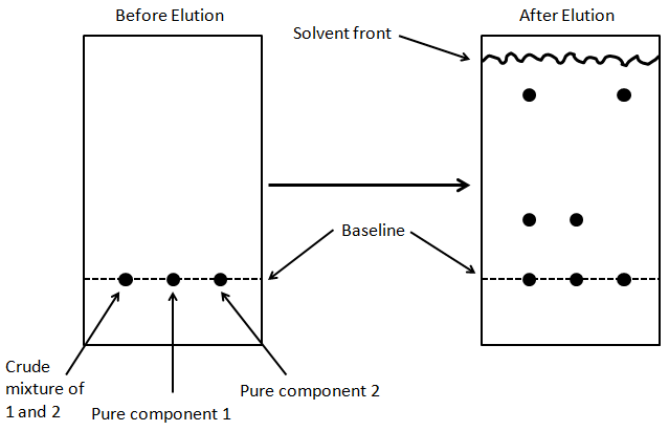

$$R_f = \frac{\text{Distance from baseline to spot}}{\text{Distance from baseline to solvent front}}$$

Figure 3.1 Schematic drawing of TLC experiment demonstration and R_f value calculation.

A TLC plate can be a sheet of glass, metal (aluminium foil), or plastic which is coated with a thin layer (0.2 – 2 mm) of a solid adsorbent (silica, alumina or cellulose) (Armarego and Chai 2003). A small amount of the mixture to be analysed is spotted near the bottom of the plate. The TLC plate is then placed in a shallow pool of a solvent in a developing chamber so that the bottom of the plate is in the liquid with the spotted mixture just above the solvent. This liquid, known as the eluent, or mobile phase and it slowly rises up the TLC plate by capillary action. At all times, the solid phase will adsorb a certain fraction of each component of the mixture and the remainder will be in the solution. Depending on different adsorption speed on TLC sheet, the components separation is achieved. The separated bands can be visualised conveniently by ultraviolet (UV) lamp if they are UV active or by treating the TLC

sheet with a suitable visualisation reagent such as iodine vapour (a good general reagent for hydrocarbon containing compounds) for few seconds or other more selective reagents.

Reversed-phase column chromatography (RPCC)

In RPCC, a non-polar or hydrophobic sorbent is usually filled in a vertical glass column as stationary phase (McNaught and Wilkinson 2012) leading to the separation of the sample components. The mobile phase is typically a mixture of water or aqueous buffers and organic solvents are used to elute analytic substrates. The substances to be purified are usually placed on the top of the column and the solvent runs down through the column by either gravity or external pressure such as vacuum suction. Fractions are collected and checked for compounds by using TLC (UV, heat, chemical spray and / or other means of visualisation) (Armarego and Chai 2003).

High performance liquid chromatography (HPLC)

HPLC is different to traditional liquid chromatography as its operational pressures are significantly higher between 50 to 350 bars, while ordinary liquid chromatography typically relies on the force of gravity to pass the mobile phase through the column.

HPLC utilises a liquid mobile phase to separate the components of a mixture. The stationary phase can be a liquid or a solid phase. Due to the small sample amount separated in analytical HPLC, typical column dimensions are 2.1 – 4.6 mm in diameter, and 30 – 250 mm in length. Also, HPLC columns are made with smaller sorbent particles size (2 – 50 μm) which gives HPLC superior resolving power when separating mixtures. Because of the improved efficiency of the columns, this technique has been referred to as high performance, high pressure, or high speed liquid chromatography and has found great importance in chemistry and biochemistry (Armarego and Chai 2003).

3.2.2 Characterisation and Analysis Techniques

3.2.2.1 Mass spectroscopy (MS)

MS is a powerful analytical technique that can be used to identify unknown compounds in a sample by comparison with a database of known compounds. It is particularly useful for identifying components of a mixture when combined with initial chromatographic separation: gas chromatography-MS (GC-MS) or HPLC-MS. The technique ionises the chemical compounds within a sample generating charged molecules (molecular ions) and/or molecule fragments and measures their mass-to-charge ratios (*m/z*) (Sparkman 2000). The distribution of masses (mass spectrum) is characteristic of a compound. Ions are generated by inducing either the loss or gain of a charge from a neutral species. The ions formed are electrostatically directed into a mass analyser where they are separated according to *m/z* and finally detected. The result of molecular ionisation, ion separation, and ion detection is a spectrum that can provide molecular mass and structural information (Wilson, Plumb et al. 2005; Djukovic, Nagana Gowda et al. 2013).

In the current study of the modification one hydroxyl proton on the primary rim of γ-CD, MS method is an essential tool applied to determine the final substituent, to prove the desired modification formula.

3.2.2.2 Nuclear magnetic resonance (NMR) methodology and spectroscopy

NMR is the phenomenon of nuclei absorbing and re-emitting electromagnetic radiation in a magnetic field (radiofrequency ν = 60 – 600 MHz). NMR spectroscopy is a powerful structural technique that provides information about changes in magnetic properties of certain NMR active atomic nuclei. ^{1}H and ^{13}C are the two most commonly studied nuclei, among others, for their different environment, and provide different signals for magnetically non-equivalent nuclei of the same atom present in the same molecule (Kumar 2006).

Chemical shift

Unlike infrared or ultraviolet-visible spectroscopy (section *3.2.2.3*), where absorption peaks are simply located at a frequency or a wavelength, however, in NMR spectroscopy, the location of different NMR signals is dependent upon both the external magnetic field strength and the reference frequency. The problem here is

resonance frequencies always vary as no two magnets have exactly the same field. Thus, it is necessary to find a method for characterising and specifying the location of NMR signals.

One suggestion to solve this problem is to report a reference signal from a standard compound, added to the investigated sample. Tetramethylsilane (TMS, $(CH_3)_4Si$), is a chemically inert compound and it can be easily removed from the tested sample (Balci 2005), has become the reference compound of choice for both proton and carbon NMR. The distance between the TMS signal and the sample signal is called the **chemical shift** ($\Delta\nu$) (Equation 3.1) of the corresponding proton/carbon.

$$\Delta\nu = \nu_{\text{sample}} - \nu_{\text{standard(TMS)}}$$

Equation 3.1 Signal distance of the reference signal and the sample signal.

In Equation 3.1, ν_{sample} is the resonance frequency of the sample, $\nu_{\text{standard(TMS)}}$ is the resonance frequency of the standard TMS, $\Delta\nu$ is the distance between the above two signals.

However, the chemical shift given in Hz will vary from on instrument to another as different NMR operating systems have different magnetic field strengths (1.4 – 21T), therefore, an additional step is needed to provide a uniform location unit which is independent of the strength of the external magnetic field. In order to correct these frequency differences, $\Delta\nu$ can be divided by the spectrometer frequency (dividing Hz by MHz). Since the chemical shifts area always very small number, the factor 10^6 is introduced to simplify the numerical values (Balci 2005), having units of parts-per-million (ppm) and designated by the symbol δ (Equation 3.2):

$$\delta = \frac{\Delta\nu}{\nu_{\text{spectrometer}}} \times 10^6$$

Equation 3.2 Chemical shift calculation.

Where, δ is the chemical shift, $\nu_{\text{spectrometer}}$ is the spectrometer frequency in Hz.

Two-dimensional (2D) NMR spectroscopy: correlation spectroscopy (COSY) and Nuclear Overhauser effect spectroscopy (NOESY)

Conventional (one-dimensional spectra) NMR, although potent to observe distinct peaks for the various functional groups of small chemical molecules, can be limited in use for more complex molecules having many overlapping resonances. The presence of overlapping peaks can make the interpretation of an NMR spectrum difficult. 2D NMR overcomes this problem by adding additional experimental variables and introducing a second dimension to the resulting spectrum, providing data that is easier to interpret and often more informative (Giraudeau, Guignard et al. 2007).

Specifically, one-dimensional NMR spectra are plots of intensity *vs*. frequency while in 2D spectroscopy intensity is plotted as a function of two frequencies. COSY and NOESY are two of the most common used 2D NMR methods. COSY is the most basic 2D NMR form among others; it is useful for determining the coupling between nuclei that are connected through one to three bond lengths. In 2D NOESY, the cross-peaks appear between protons that are within 6Å of each other, the closer in space the two protons are to each other, the more intense of the cross-peak. The NOESY experiment correlates all protons which are close enough. It also correlates protons which are distant in the amino acid sequence but close in space due to tertiary structure. Thus, 2D NOESY is the most important tool for the determination of protein structures.

NMR spectroscopy is not only a method for the determination of the structure of the molecule, but also a very functional spectroscopic method that explains the dynamic. Hence, NMR spectroscopy is widely utilised in CD complexation determination (Rekharsky and Inoue 1998; Schneider, Hacket et al. 1998). For example in the case of ^{1}H NMR, the observation of changes in the chemical shift of one or more protons on the guest, or those on the CD (host), particularly the hydroxyl protons can provide the geometrical information of CD-guest complex inclusion (Wagner 2006).

3.2.2.3 Ultraviolet-visible (UV-Vis) spectroscopy and fluorescence spectroscopy

UV-Vis spectroscopy (λ = 200 – 800 nm) studies the changes in electronic energy levels within the molecule arising due to transfer of electrons from π- or non-bonding orbitals (Kumar 2006). It is often called as electronic spectroscopy or reflectance spectroscopy in the ultraviolet-visible spectral region, where it uses light in the visible and adjacent (near-UV / near-infrared) ranges. UV-Vis spectroscopy has many applications especially in the quantitative determination of solutions of transition metal ions highly conjugated organic compounds and biological macromolecules. The information provided by UV-Vis spectroscopy when combined with the information obtained by NMR and infrared (IR) spectral data leads to valuable structural information (Kumar 2006). UV-Vis spectroscopy is a complementary technique to fluorescence spectroscopy, where, fluorescence deals with transitions from the excited state to the ground state, while absorption measures transitions from the ground state to the excited state (Skoog 2007).

CD / CD-inclusion complexes can be studied by a number of experimental techniques including UV-Vis spectroscopy (Busch, Swamidoss et al. 2003) and fluorescence spectroscopy (Li, Zhao et al. 2012). In the case of UV-Vis spectroscopy, a change in absorbance and/or absorption wavelength of the guest is observed; while in the case of fluorescence, a change in the emission intensity and/or emission wavelength maximum of the guest is observed (Wagner 2006).

Fluorescence is the most sensitive method for study of CD complexation and has many advantages in comparison to other methods, because: 1) it is high sensitivity and is applicable to complexation studies with large binding constant K values (the fluorescence method can be used to determine K values as high as 10^7 M^{-1}, whereas ^{1}H NMR measurement is used for $K < 10^4$ M^{-1} and UV-Vis spectroscopy is usually used for $10^2 < K < 10^4$ M^{-1}) (Wagner 2003); 2) upon complexation with a CD, the fluorescent properties usually change more sensitively than the other spectroscopic properties; and 3) it requires the lowest concentration of sample. Thus, fluorescence spectroscopy is an excellent technique for studying CD inclusion phenomena (Wagner 2006).

3.3 Materials and Methods

3.3.1 Materials

3.3.1.1 Reagents and solvents

Reagents/Solvents	Manufacturer and place of origin
γ-cyclodextrin	Mesochem Technology Co.,Ltd, Beijing, China
doxorubicin (DOX)	Mesochem Technology Co.,Ltd, Beijing, China
P_2O_5	Sigma Aldrich, Israel
4,4-Dimethylaminopyridine (DMAP)	Sigma Aldrich, USA
1-Hydroxybenzotriazole (HOBt)	Discovery fine chemicals, UK
N-Boc-3-(2-naphthyl)-D-alanine	Sigma Aldrich, Israel
1-Ethyl-3-(3-dimethylaminopropyl) carbodiimidehydrochloride (EDC)	Sigma Aldrich, Israel
Dimethylformamide (DMF)	Sigma Aldrich, Germany
Dimethyl sulphoxide (DMSO)	Sigma Aldrich, Israel
trifluoroacetic acid (TFA)	Sigma Aldrich, Israel
dichloromethane (CH_2Cl_2)	Sigma Aldrich, Israel
deuterated water (D_2O)	Sigma Aldrich, Israel
Acetonitrile (AcN)	Sigma Aldrich, Israel
acetone(C_2H_6CO)	YavinYedaa, Israel
1-butanol	Sigma Aldrich, Israel
sulfuric acid	Sigma Aldrich, Israel
Methanol	Sigma Aldrich, Israel
Ethanol	Sigma Aldrich, Israel
NH_3(aq)	Sigma Aldrich, Israel
PBS tablets	Oxoid, UK
dibasic sodium phosphate	Sigma Aldrich, UK
sodium phosphate monobasic	Sigma Aldrich, UK
citrate acid monohydrate	Sigma Aldrich, UK
potassium chloride	Sigma Aldrich, UK
hydrochloric acid	Sigma Aldrich, UK
Distilled/deionized water	Millipore, UK

3.3.1.2 Glassware, consumables and equipment

Glassware, consumables and equipment	Manufacturer and place of origin	Specification
TLC plates	Yavin-Yeda, Israel	Silica gel 60
PLC plates	Yavin-Yeda, Israel	Silica gel 60 F254
96-well plates	Greiner, Austria	Black Polystyrene without lid
UV Cuvettes	Yavin-Yeda, Israel	4mL volume clear
Reversed-phased column	Merck, Israel	LiChroprep RP-18, 40 – 63 μm
HPLC	Sedere, France	UV/Vis & ELSD (Sedex 75)
UV spectrophotometer	Thermo Electron Corporation Instrument, USA	Thermo Electron
Mass spectroscopy	Waters, USA	Micromass ZQ 2000
Melting Point Apparatus	Thermo Scientific, Israel	Electrothermal IA9100 Digital
Lyophilizer	Labconco, USA	Freezone 2.5 Plus
500 MHz NMR spectrometer	Bruker, USA	Advance III
400 MHz NMR spectrometer	Bruker, USA	Advance III
Fluorescence spectrophotometer	Agilent Technologies, USA	Varian Cary Eclipse
pH meter	Scientific Laboratory Supplies, UK	SevenEasy pH Mettler Toledo
Multi-mode plate reader	Tecan, Austria	Tecan infinite M200
Oven	Scientific Laboratory Supplies, UK	INV064
Vacuum oven	Swagelok, Israel	

3.3.2 Methods

3.3.2.1 Preparation of γ-CD derivative

a) General coupling reaction of pre-crude product: Mono-6'-deoxy-6-[3-(naphthalen-2-yl)-2-(tert-butyloxycarbonylamino)propionylamino]-γ-cyclodextrin (3a)

Native γ-CD was dried at 110 ℃/0.1 mmHg in the presence of P_2O_5 by vacuum oven for 24 hr. Dry γ-CD (12.97 g, 10 mmol), DMAP (1.22 g, 10 mmol), HOBt (1.35 g,

10 mmol), N-Boc-3-(2-naphthyl)-D-alanine (3.15 g, 10 mmol) and 1-Ethyl-3-(3-dimethylaminopropyl) carbodiimide hydrochloride (EDC) (4.12 g, 20 mmol), were dissolved in DMF (50 mL) and stirred at room temperature for 24 hr. The precipitate was removed by paper filtration and the filtrate solution was added drop wise with stirring to a hot acetone (500 mL, ~ 40 ℃). Then, TLC analysis was performed on silica gel plates to figure out the R_f value of **3a.** TLC eluent solution was prepared by mixing isobutanol: ethanol: $NH_4OH_{(aq)}$ at [4 : 5 : 6 (v / v / v)]. Then, spot detection was carried out by spraying with 5% (v / v) concentrated sulphuric acid in ethanol and heated up at 150 ℃ by means of hot plate for 5 min. After TLC analysis, the precipitate was filtered and dried under vacuum to obtain the pre-crude product of **3a:** mono-6'-deoxy-6-[3-(naphthalen-2-yl)-2-(tert-butyloxycarbonyl amino) propionylamino]- γ-cyclodextrin.

b) Purification of pre-crude product 3a by reversed-phase column chromatography

The pre-crude product **3a** was dissolved in 500 mL hot water (60 – 90 ℃) and the resulting solution was applied to a reversed-phased column (300 g of LiChroprep RP-18, 40 – 63 μm; 50 mm × 260 mm). The column was eluted with 100% $_{dd}H_2O$ (500 mL), methanol: water at 10 : 90 (1000 mL), 20 : 80 (1000 mL), 30 : 70 (1000 mL) and 100% methanol (500 mL), respectively. Collected column eluted samples 15 mL/tube, then, TLC analysis was performed to validate the R_f value of purified **3a**. (TLC eluent solution and performance were the same as described in section *3.2.2.1a*). After TLC analysis, fractions of 80 mL volume were collected. The solvent was removed by evaporation under reduced pressure affording white crystalline material (yield 50%) to obtain crude product of **3a**.

c) Removal of the tert-butoxycarbonyl protecting group from pre-crude product 3a to obtain final product of mono-6'-deoxy-6-[3-(naphthalen-2-yl)-2-(amino) propionylamino]-γ-cyclodextrin (carrier 3b)

Compound (**3a**, 5 g) from the above procedure was dissolved in TFA (20 mL) and CH_2Cl_2 (20 mL), and the mixture was stirred at room temperature for 3 hr. Then, the

solvent was removed by evaporation under reduced pressure (< 25 ℃). The residue was dissolved in water (5 mL) and poured in methanol (200 mL). The white precipitate was filtered and dried under vacuum (yield 84%). TLC was carried out (the method is the same as described in section *3.2.2.1a*) and showed one major spot which is the final residue of **carrier 3b**. The pure **carrier 3b** product was dissolved in $_{dd}H_2O$ (10 mL/g). The solution was filtered and freeze dried by Lyophilizer for 2 days.

d) Further purification of carrier 3b by TLC and HPLC

TLC analysis was conducted the same as mentioned described in section *3.2.2.1a*. HPLC analysis was performed on a Thermo Electron instrument equipped with UV/Vis & ELSD (Sedex 75) detectors. The column was by means of a Gemini 5 μm octadecyl carbon chain bonded silica (C18) (110 Å, 250 – 4.6 mm) mobile phase: H_2O / Acetonitrile (AcN), with a gradient ratios: 98% / 2%, 50% / 50%, 10% / 90%, 98% / 2% and 98% / 2% at 0 min, 10 min, 15 min, 20 min and 30 min respectively, under a constant flow rate of 1.2 mL/min.

3.3.2.2 Characterisation of carrier 3b

a) General characterisation

The UV spectroscopy signal of **carrier 3b** was measured at λ = 254 nm. UV analysis was performed on a UV spectrophotometer. MS was performed using Micromass ZQ 2000 detector, nitrogen flow 500 L/hr, nitrogen cone flow 70 L/hr, source temperature 110 ℃, desolvation temperature 350 ℃, and cone voltage 30 V. Melting point (MP) was performed by using Electrothermal IA9100 Digital Melting Point Apparatus. ^{1}H-NMR, ^{13}C-NMR, COSY and NOESY spectra were recorded on Bruker 400 MHz Advance III spectrometer with D_2O as a solvent. All the chemical shifts are expressed as δ units (ppm).

b) Fluorescence spectrometry analysis

<u>Inclusion association analysis of carrier 3b with DOX</u>

The inclusion association of **carrier 3b** with DOX was quantitatively evaluated by titration method by measuring the fluorescence intensity of DOX at constant concentration (5 μM) in the presence of different concentrations (0.67 to 5000 μM) of **carrier 3b**. The **carrier 3b** : DOX molar ratios, in the tested solutions, varied from 0.13 : 1 to 1000 : 1. Fluorescence spectra were measured by fluorescence spectrophotometer. Experiments were performed in 0.1 M PBS buffer solutions (pH = 7.4) at 37 ℃. A DOX stock solution (100 mM) was made by dissolving 58 mg DOX powder (purity ≥ 98%) by 1 mL DMSO and kept frozen. A solution of 5 μM DOX was prepared by dilution of 100 mM DOX stock solution (in DMSO) into PBS. The final concentration of DMSO in the diluted solution is 0.005%. To 10 mL of the final 5 μM DOX solution, 7.47 mg/mL of **carrier 3b** was added to obtain a carrier concentration of 5000 μM (1000 : 1 molar ratio of **carrier 3b** : DOX). Double dilutions from 1000 : 1 of **carrier 3b** : DOX solution by using 5 μM DOX solution was performed to obtain the various ratios of **carrier 3b** : DOX in the final solutions. Each solution was transferred into a 4 mL cuvette (Figure 3.2) and the fluorescence intensity was measured at $\lambda_{excitation}$ = 480 nm, $\lambda_{emission}$ = 500 − 800 nm (λ_{max} = 592 nm) (Kerry K. Karukstis and Rosenfeld 1998; Dai, Yue et al. 2008), with excitation and emission slits of 10 nm.

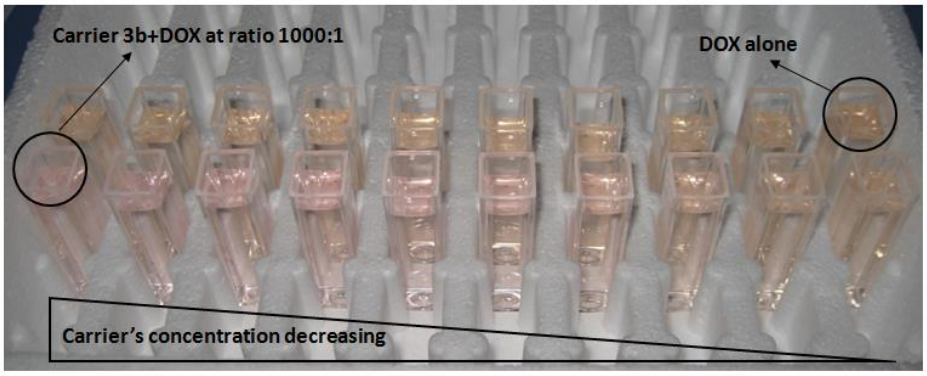

Figure 3.2 DOX at constant concentration of 5 μM in the presence of different concentrations (0.67 to 5000 μM) of carrier 3b in cuvette before measuring fluorescence intensity.

Thermal-responsivity of the inclusion complex of carrier 3b : DOX

In thermal-responsivity investigations, DOX concentrations were employed constant at 2, 5 and 12.5 μM, respectively. The ratio between **carrier 3b** and DOX was

from 0.13 : 1 to 1000 : 1 (20 gradients). Tested solutions were prepared the same as described above (the section right above) but were transferred 200 µL/well to a black 96-well plate (Figure 3.3 A) and test solutions arrangement can be seen from Figure 3.3 B.

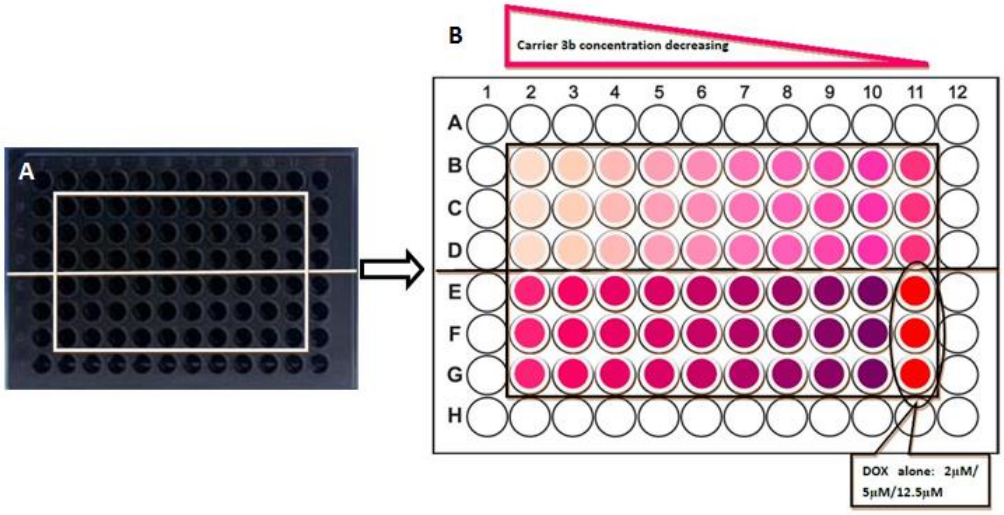

Figure 3.3 Black 96-well plate for fluorescence intensity investigation (A); Schematic drawing of test solutions arrangement in 96-well plate (B).

The first fluorescence intensity at room temperature (~ 25 ℃) was measured by multi-mode plate reader under fluorescence optimal gain mode. Then INV064 oven (–10 ℃ to 50 ℃) was used for achieving the higher desired temperatures (37 ℃, 42 ℃ and 50 ℃) by placing the same plate with the same test solutions 40 min with plate cover, fluorescence intensity at each temperature was recorded at the same setting of multi-mode plate reader. Then, the same plate was cooled down to room temperature again and the final set of fluorescence intensity was recorded.

pH-responsivity of the inclusion complex of carrier 3b : DOX

pH dependence of **carrier 3b** : DOX was assessed by dissolving the complex in different buffer solutions. The buffer solutions were prepared by using 0.2 M/0.1 M dibasic sodium phosphate (Na_2HPO_4), 0.1 M sodium phosphate monobasic ($NaH_2PO_4 \cdot H_2O$), 0.1 M citrate acid monohydrate, 0.1 M Potassium chloride (KCl) and 0.1 M hydrochloric acid (HCl) (Mohan 2003). Table 3.1 shows pH buffers ingredients in details and final pH values measured by pH meter at 25 ℃ and 37 ℃, respectively.

Table 3.1 pH buffers preparation and their final pH values at 25 ℃ and 37 ℃

	Ingredients (mL)								Final pH	
Aimed pH value	PBS	0.1 M Citric Acid	0.1 M Na_2HPO_4	0.2 M Na_2HPO_4	0.1 M $NaH_2PO_4 \cdot H_2O$	0.1 M KCl	0.1 M HCl	$_{dd}H_2O$	25 ℃	37 ℃
8.0			10		125			70	8.004	7.970
7.4	100								7.317	7.214
7.0		15		45				40	7.047	6.912
6.5		18.6		36.4				50	6.484	6.407
5.5		24.2		27.8				50	5.503	5.429
5.0		25		25				50	5.054	4.974
4.5		29		23				50	4.532	4.507
4.0		35		19				50	3.998	3.810
3.0		48		10				50	3.057	2.980
2.0						50	12	50	2.051	2.012
1.0						50	90	90	1.095	1.024

Tested solutions were prepared the same as the above section in a 96 well-plate with DOX concentration constant at 5 μM but by using different pH buffers instead of PBS. Fluorescence intensities of test solutions at room temperature (~ 25 ℃) and heated to 37 ℃ were measured by multi-mode plate reader under fluorescence optimal gain mode.

3.3.3 Calculations of encapsulation efficiency and binding constant

3.3.3.1 Calculation of encapsulation efficiency of carrier 3b to DOX

The encapsulation efficiency of **carrier 3b** to DOX was calculated by Equation 3.3:

$$Encapsulation\% = \frac{I_o - I_x}{I_o} \times 100\%$$

Equation 3.3 Encapsulation percentage of DOX by carrier 3b through fluorescence intensity measurement.

Where, I_0 is the fluorescence intensity of DOX in the absence of carrier and I_x is the fluorescence intensity of DOX in the presence of different concentrations (x) of **carrier 3b**.

3.3.3.2 Calculation of binding constant *K* of carrier 3b to DOX

It has been well reported that in the literature (Emara S 2000), addition of native γ-CD added to DOX at a ratio of up to 5000 : 1 can significantly stabilise DOX in aqueous solution via complex formation. Some other literatures (Swiech, Mieczkowska et al. 2012), where it has been shown that DOX encapsulation within CDs can significantly lower the fluorescence and absorbance signals of the guest molecule which means CDs can be considered as a fluorophore quencher for DOX molecular. Therefore, the binding constant can be calculated according to modified Stern-Volmer Equation 3.4 (Sorokin, Fylymonova et al. 2012) (which has been introduced in section *2.2.3* in Chapter 2):

$$\frac{I_o}{I_o - I_x} = \frac{1}{fK[H]_x} + \frac{1}{f}$$

Equation 3.4 Modified Stern-Volmer equation.

Where, $[H]_x$ is the concentration of the host compound **carrier 3b** and 1 / f is equal to 1 since only one fluorescence quencher was employed in the present study (Lee 1998). The corresponding K binding, was calculated by the relationship of the intercept/slope value which is equal to (1 / f) / (1 / fK) and derived from the linear plot of $I_0 / (I_0 - I_x)$ *vs.* 1 / $[H]_x$.

3.4 Results and Discussion

3.4.1 Characterisation of Carrier 3b

Mono-6'-deoxy-6-[3-(naphthalen-2-yl)-2-(tert-butyloxycarbo nylamino)propionylamino]-γ-cyclodextrin (**3a**) was prepared by direct coupling of dry γ-CD (**1**) with 2-((tert-butoxy carbonyl)amino)-3-(naphthalen-2-yl)propanoic acid (**2**)

using HOBt, DMAP and EDC in DMF at 25 ℃ for 24 hr as shown in Figure 3.4 (step 1). Precipitation of the crude product from hot acetone, vacuum filtration of the white solid, careful purification by RP-18 column chromatography (H_2O / CH_3OH), recrystallisation from hot water and drying, afforded colourless crystals of pure **3a** in 50% yield. **3a** was converted to mono-6'-deoxy-6-[3-(naphthalen-2-yl)-2-(amino) propionylamino]-γ-cyclodextrin (**carrier 3b**) by removal of the *tert*-butoxycarbonyl protecting group using TFA in CH_2Cl_2 (1 : 1) at 25 ℃ (Figure 3.4, step 2). Concentration of the solvents under reduced pressure (< 25 ℃), precipitation from hot acetone, vacuum filtration and freeze drying, afforded colourless crystals of pure **carrier 3b** in 84% yield (overall yield 42%). Compound **carrier 3b** was then fully characterised. Figure 3.5 shows γ-CD before and after modification.

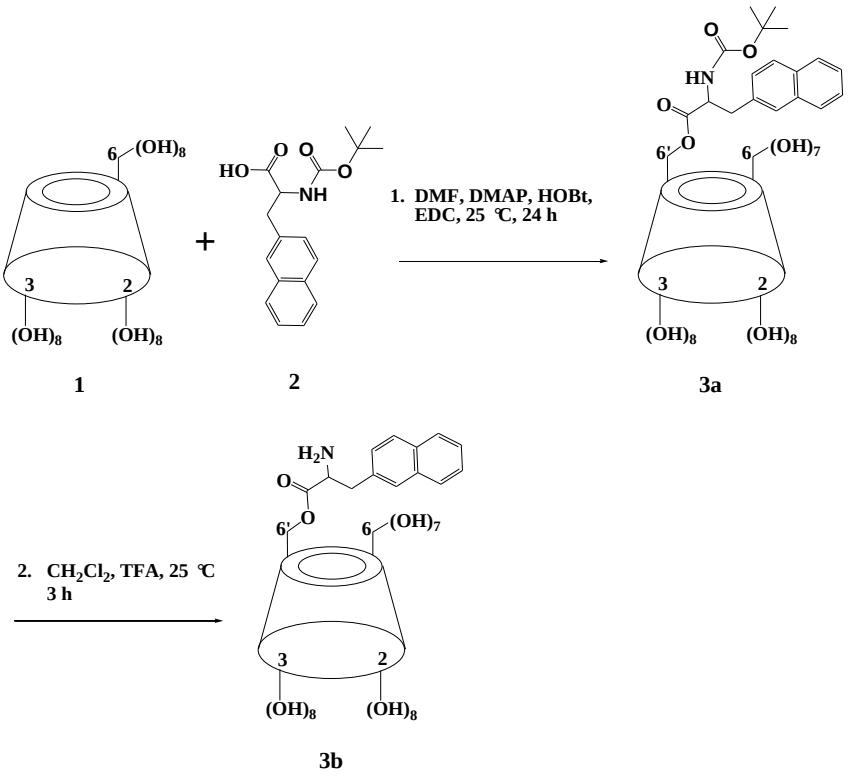

Figure 3.4 Synthetic approaches to 3a and carrier 3b.

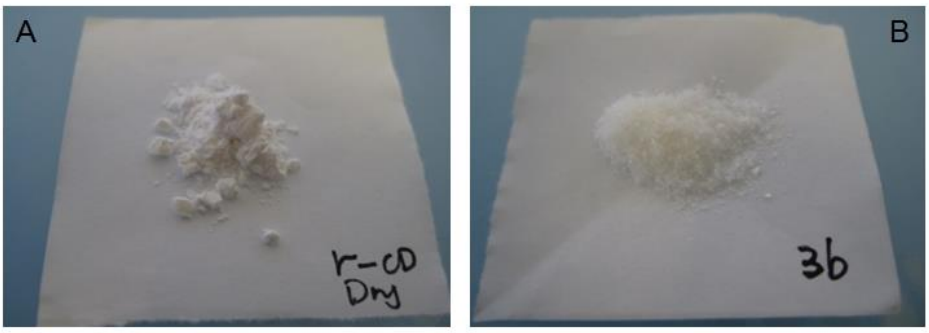

Figure 3.5 Dry γ-CD before modification (A); and modified γ-CD derivative carrier 3b after purification and freeze-dry (B).

3.4.1.1 TLC, HPLC, UV, MS and MP characterisation

To analyse the conjugated product of the carrier synthesis, TLC and HPLC were conducted. TLC analysis showed R_f (γ-CD) = 0.18, R_f (**3a**) = 0.48 and R_f (**carrier 3b**) = 0.25, respectively. The chromatogram obtained by HPLC (Figure 3.6) of crude **carrier 3b** contains the following peaks: 12.06 min (**carrier 3b**), 12.9, 13.5, 14.1 min (unknown impurities), 17.1, 17.8, 18.8 min (di-substituted γ-CD), 36.6, 37.5, 46.8 min (unknown impurities). Where, retention time of the monosubstituted carrier (83% of the product) was 12.06 min. The unwanted di-substituted and tri-substituted (14.1% in total) retention times were manily three parts happened from 12.9 min to 14.1 min, 17.1 min to 18.8 min and 36.6 min to 46.8 min, respectively, which depending on the relative position of the substituents to each other. As this is a non-specific reaction, it was stopped on purpose after 50% of the reagents had reacted and carefully purified. This action was done to avoid the creation of unwanted di- and tri-substitution on the rim of γ-CD.

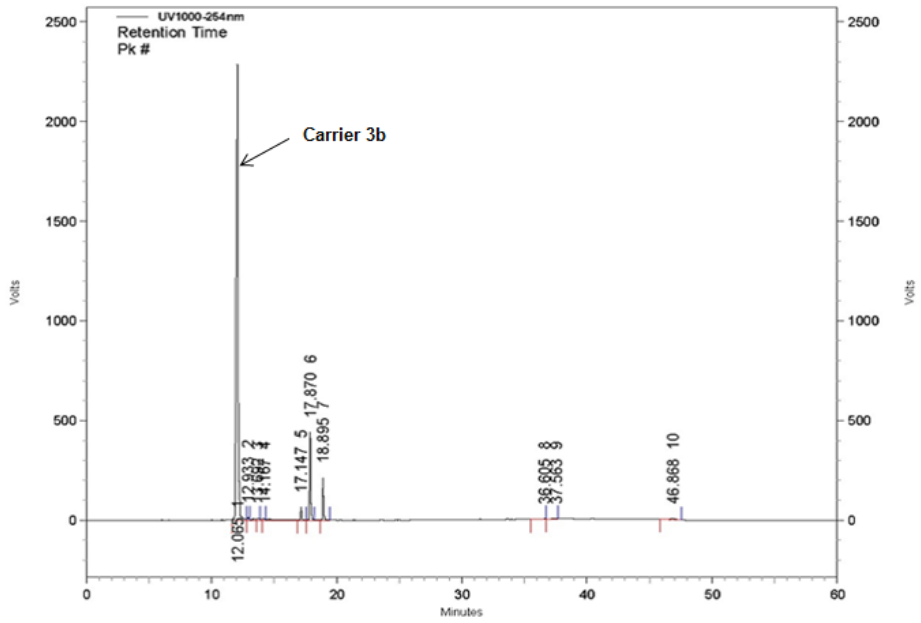

Figure 3.6 HPLC Chromatogram of crude carrier 3b. It contains the following peaks: 12.06 min (carrier 3b), 12.9, 13.5, 14.1 min (unknown impurities), 17.1, 17.8, 18.8 min (di-substituted γ-CD), 36.6, 37.5, 46.8 min (unknown impurities).

UV spectra found 8 peaks above -3.00 A between started wavelength at 190 nm and stop wavelength at 1100 nm which gave a highest peak at absorbance 0.895 of 278 nm (Figure 3.7). MS result of ESI-MS *m/z* calculated for $C_{61}H_{91}NO_{41}$ (**carrier 3b**) as 1494.51, measured as 1494.77 (Figure 3.8). MP (**carrier 3b**, H_2O) = 220 – 222 ℃.

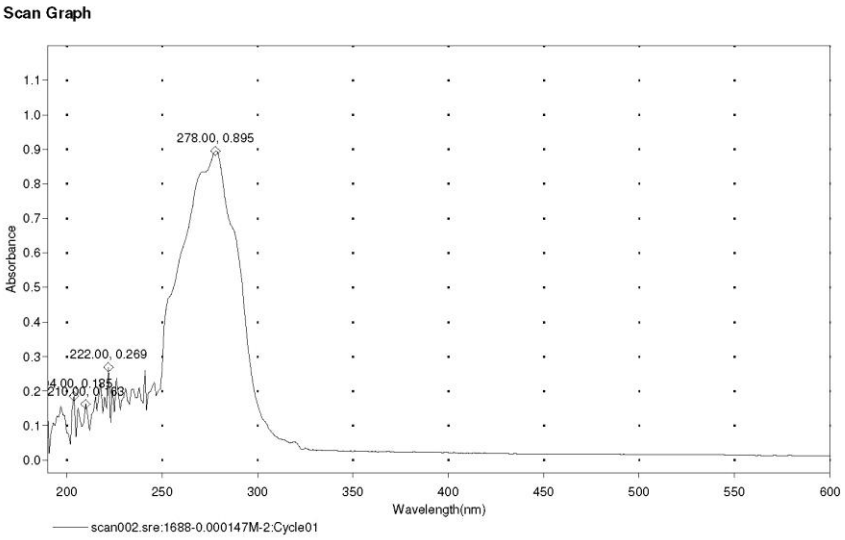

Results Table - scan002.sre,1688-0.000147M-2,Cycle01

nm	A	**Peak Pick Method**
204.00	0.185	Find 8 Peaks Above -3.0000 A
210.00	0.163	Start Wavelength 190.00 nm
222.00	0.269	Stop Wavelength 1100.00 nm
278.00	0.895	Sort By Wavelength

Figure 3.7 UV spectrum of carrier 3b.

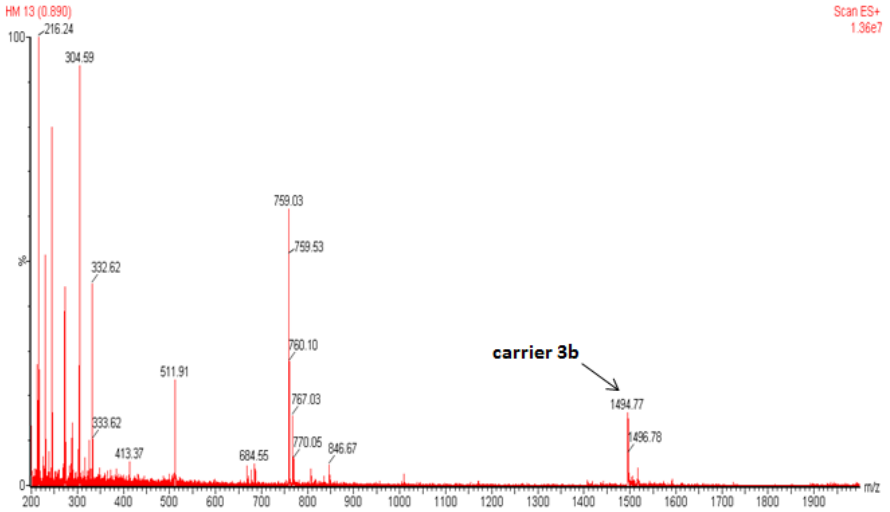

Figure 3.8 Electrospraying Ionisation Mass Spectroscopy (ESI-MS) (1.36×10^7) of carrier 3b.

3.4.1.2 NMR characterisation

^{1}H-NMR and ^{13}C-NMR mesurements were performed to validate the structure of desired **carrier 3b** (Gourevich, Dogadkin et al. 2013). The ^{1}H-NMR spectra (Figure 3.9 A) and especially ^{13}C-NMR spectra (Figure 3.9 B) suggested that the chemical structure of the carrier is consistent with the desired yield being the monosubstituted γ-CD with a β-naphthyl alanine residue on one of the hydroxyl groups on the primary face.

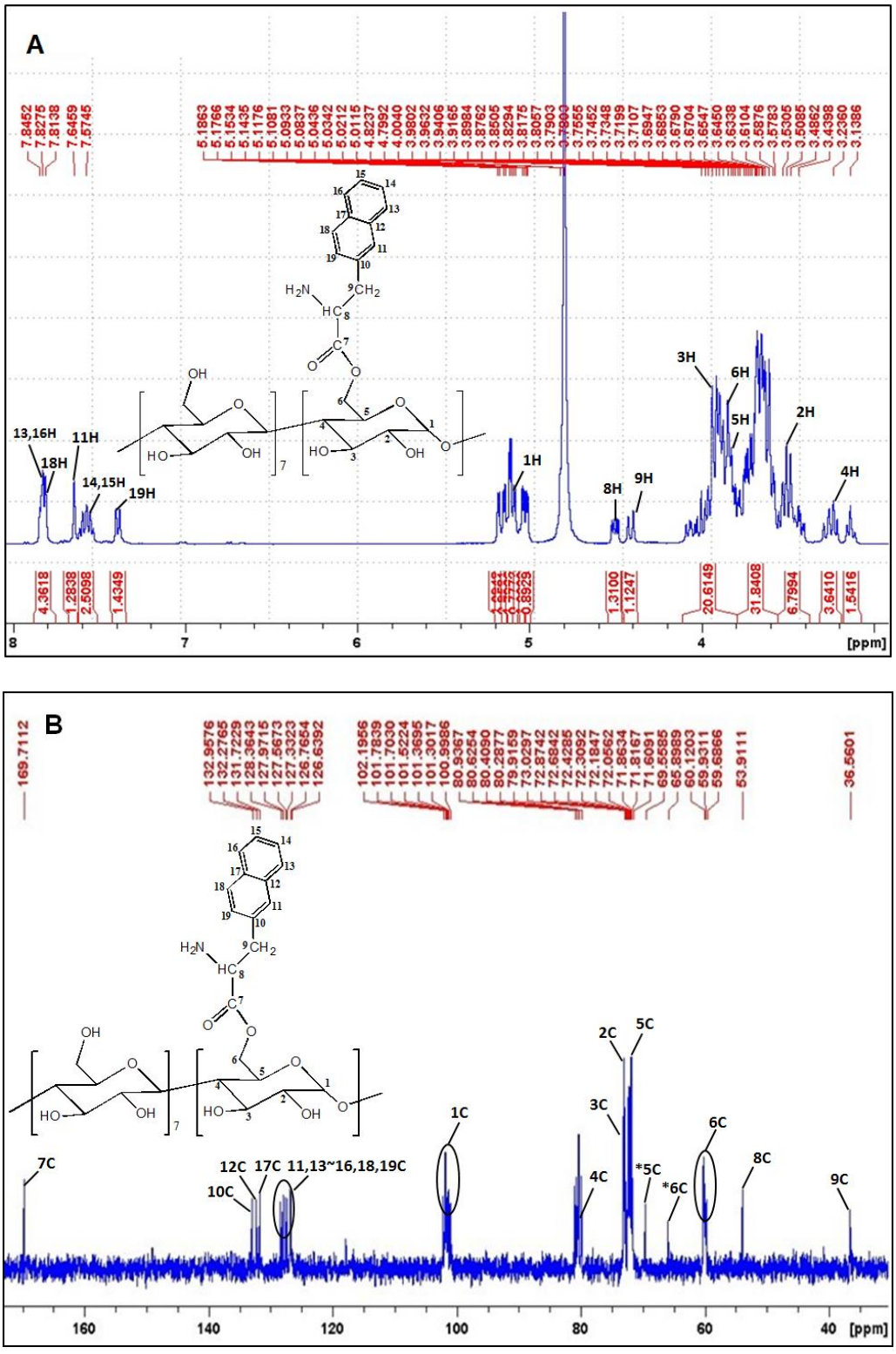

Figure 3.9 NMR spectra of carrier 3b (20 mM) in D_2O. ^{1}H-NMR spectrum (A); ^{13}C-NMR spectrum (B).

^{1}H-NMR (400 MHz, D_2O) of **carrier 3b**: 3.20 (d, 4H), 3.52 (d, 2H), 3.86 (s, 6H-6), 3.79 (t, 5H), 3.97 (d, 3H), 4.41 (d, 9H), 4.50 (s, 8H), 5.10 (d, 1H), 7.39 (s, 19H), 7.57 (m, 15H), 7.57 (m, 14H), 7.65 (m, 11H), 7.81 (m, 18H), 7.83 (m, 16H), 7.85 (m, 13H).

^{13}C-NMR (400 MHz, D_2O) of **carrier 3b**: 36.53 (9C), 53.87 (8C), 59.63-60.15 (6C), 65.84 (*6C), 69.52 (*5C), 71.56-71.82 (5C), 72.01-72.38 (2C), 72.64-73.06 (3C), 79.83-80.90 (4C), 100.97-102.17 (1C), 126.59 (15C), 126.73 (14C), 126.81 (18C-18), 127.31 (13C), 127.53 (16C), 127.94 (19C), 128.35 (11C), 131.69 (17C), 132.23 (12C), 132.92 (10C), 169.68 (7C). (*Carbon of the substituted ring)

It is well documented in the literature (Schneider, Hacket et al. 1998) that H-1, H-2, H-4 and H-6 protons in γ-CD are located on the exterior surface of the molecule and exposed to bulk environments, while H-3 (δ = 3.95 ppm) and H-5 (δ = 3.88 ppm) protons are located in the interior cavity of γ-CD. ^{1}H-NMR analysis of **carrier 3b** (Figure 3.9 A), shows that H-3 (δ = 3.97 ppm) and H-5 (δ = 3.79 ppm) protons experience magnetic perturbation and have a downfield shift of 0.02 ppm and an upfeild shift of 0.09 ppm, respectively. These observations suggest the existence of certain cooperative hydrophobic interactions between the CD's interior cavity and the β-naphthalene moeity. Such interaction could be achieved only by partial or fully self-assembly inclusion of the β-naphthalene subsituent within the hydrophobic cavity of **carrier 3b,** as suggested by 3D interaction modelling in work reported previously (Gourevich, Dogadkin et al. 2013).

3.4.2 Inclusion Association of Carrier 3b to DOX

3.4.2.1 NMR analysis of carrier 3b to DOX complexation

In order to investigate the inclusion behavior of DOX molecule as a guest to the host molecule of **carrier 3b**, further NMR measurements were performed in an aqueous solution D_2O. The NMR results showed significant changes (black circles positions in Figure 3.10) in the majority of the protons from both **carrier 3b** and DOX molecular.

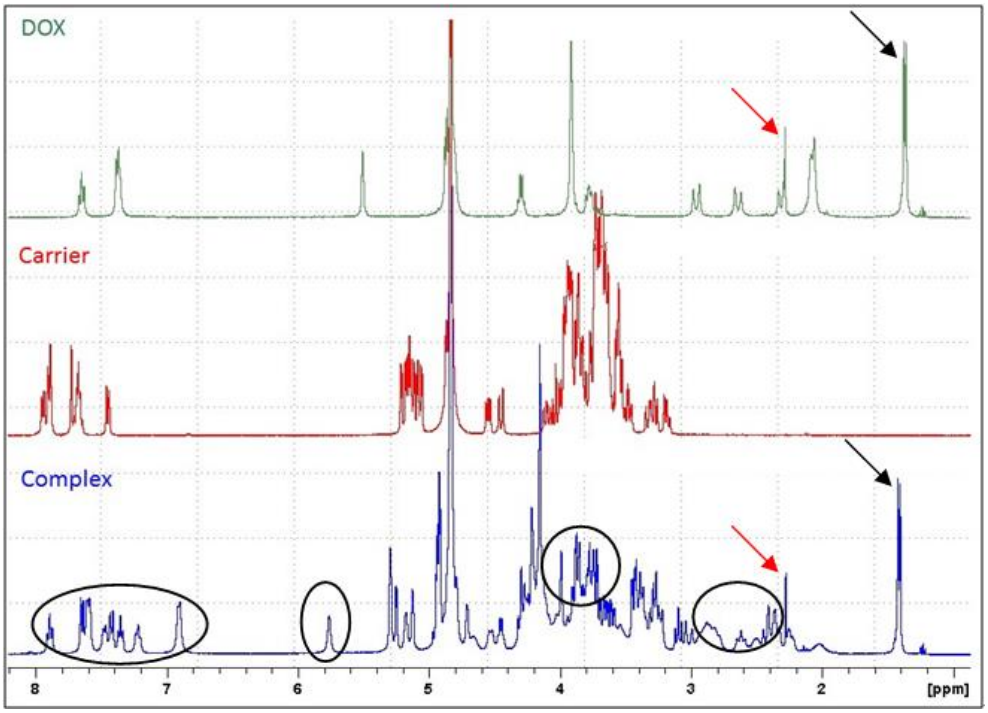

Figure 3.10 ^{1}H-NMR spectra of 10 mM DOX (top), 10 mM carrier 3b (middle), 1:1 of carrier 3b : DOX (10 mM each) complex (bottom) in D_2O with significant chemical shifts (black circle areas). 5'-CH_3(black arrow) δ = 1.33 ppm and 8-H_2 (red arrow) δ = 2.30 ppm are as indicated. Black circles indicate interations of (from left to right): 3H of DOX with protons on β-naphthalene; 1'H of DOX with 1H of CD's ring; 3H and 5H interior protons of CD's ring with 4-OCH_3 of DOX and protons on β-naphthalene; 10H_2 of DOX with protons on CD's ring.

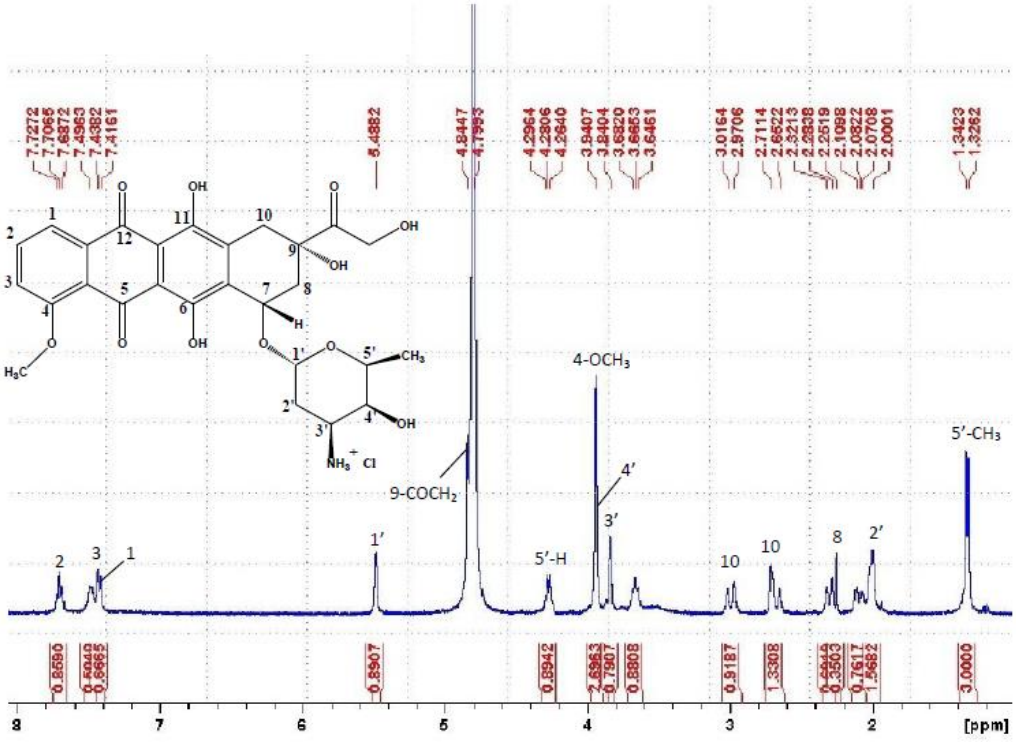

Figure 3.11 ^{1}H-NMR spectra of DOX (2 mM) in D_2O.

Where, the complex spectrum of **carrier 3b** and DOX mixture in D_2O is not a simple superposition of the carrier and DOX spectra (Figure 3.11) (Wang, Wang et al. 2010), which illustrating that there is indeed an interaction between these two molecules. Closer evaluation of the significant amount and manner of DOX and **carrier 3b**'s chemical shifts in aqueous solution suggested the encapsulation of DOX happens within **carrier 3b**'s cavity (Swiech, Mieczkowska et al. 2012).

As mentioned above in section *3.4.1.2*, H-3 and H-5 of **carrier 3b** are both facing the inner space of the cone and are affected by the removal of D_2O and DOX entrance (Singh 2010). Thus, explanations for the encapsulation might be found from the upfeild chemical shifts of the protons in the 3^{rd} and 5^{th} positions in the γ-CD ring. Additional information obtained from the ^{1}H-NMR spectrum of the complex can indicate the orientation of the DOX within the carrier. Again, as can be seen from Figure 3.10, the methyl moiety on the 5^{th} position of the amino sugar ring with the peak position of δ = 1.33 ppm (5'-CH_3, black arrow in Figure 3.10) and the proton on the 8^{th} position of the aromatic ring with peak position of δ = 2.30 ppm (8-H_2, red arrow in Figure 3.10) of the DOX molecule are not influenced by adding the **carrier 3b**, which suggested that moiety of DOX is located outside the γ-CD cavity.

Additional information on the 3D structure of the complex was achieved by NOESY and COSY measurements. Subtraction of the COSY and NOESY full spectrums (Figure 3.12, 3.13 and 3.14) provided the information on the non-covalently bonded protons present in proximity to each other in the 3D structure of the molecule. In the measurement of the ^{1}H-NOESY spectra of the **carrier 3b** and DOX (Agrawal, Barthwal et al. 2009) (1 : 1) complex in D_2O, the NOE interactions between the proton H-3 of DOX (6.9 ppm), which is located on the first phenyl ring next to the methyl group, and the β-naphthalene protons (7.6 ppm) of **carrier 3b** were observed (black arrow in Figure 3.13 C). This observation indicated that these protons were located close to each other and there was a strong probability of the formation of π-π stacking complex between the naphthyl group of **carrier 3b** and the included DOX (Figure 3.15).

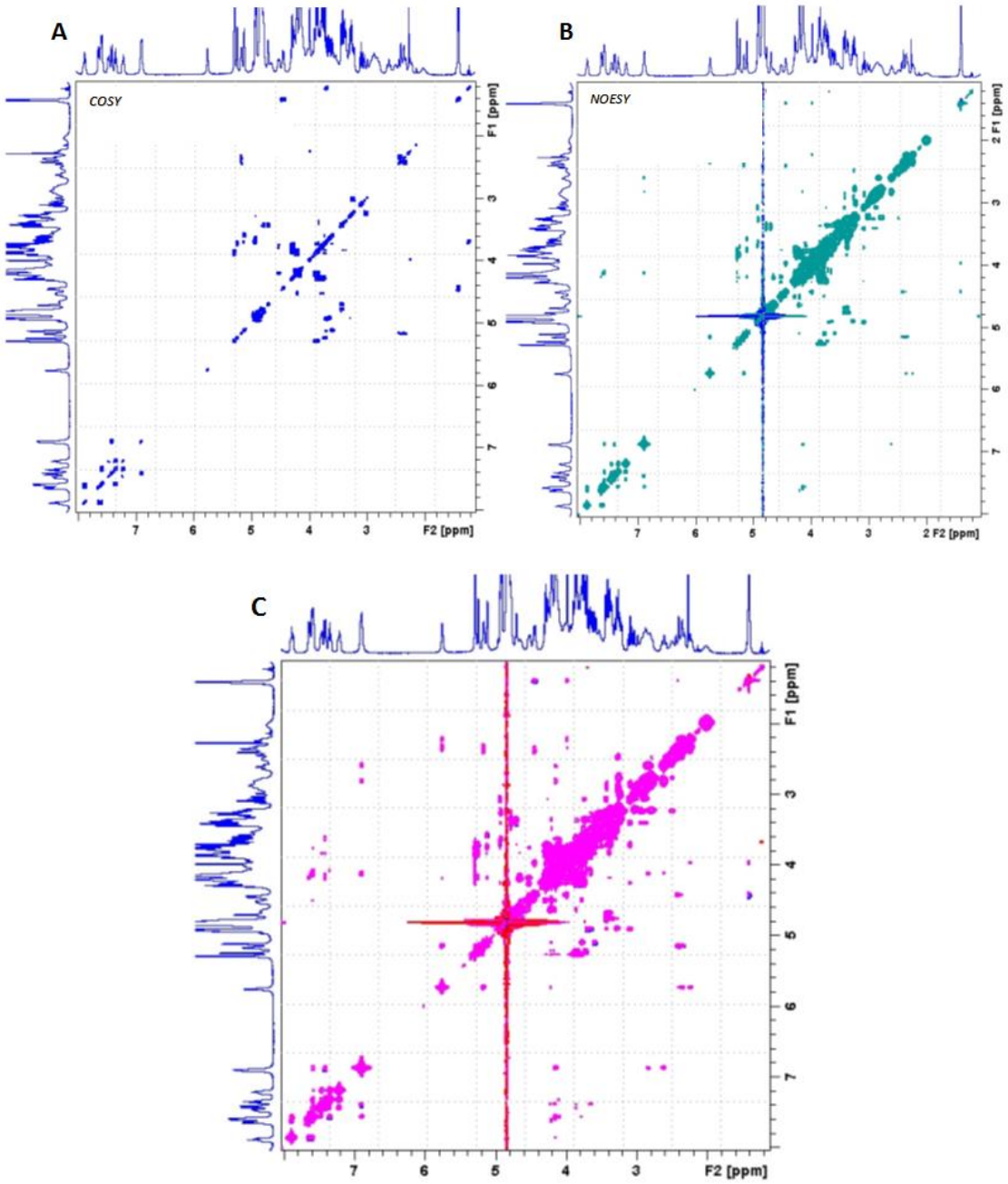

Figure 3.12 ^{1}H–NMR (A) COSY and (B) NOESY full spectra and (C) their subtraction of carrier 3b : DOX (1 : 1) complex in D_2O.

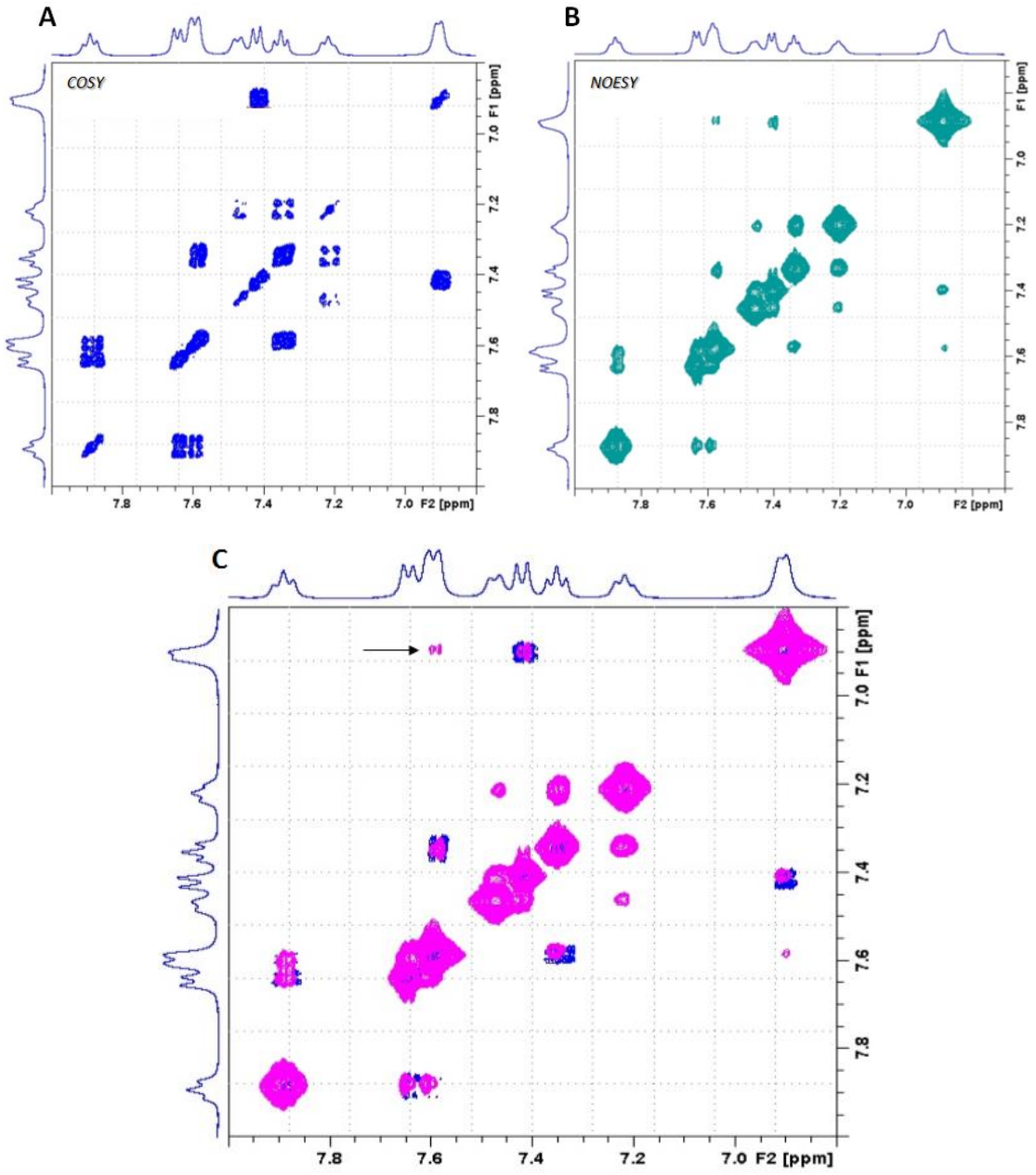

Figure 3.13 6 – 8ppm ^{1}H–NMR (A) COSY and (B) NOESY spectra and (C) their substraction of carrier 3b : DOX (1 : 1) complex in D_2O.

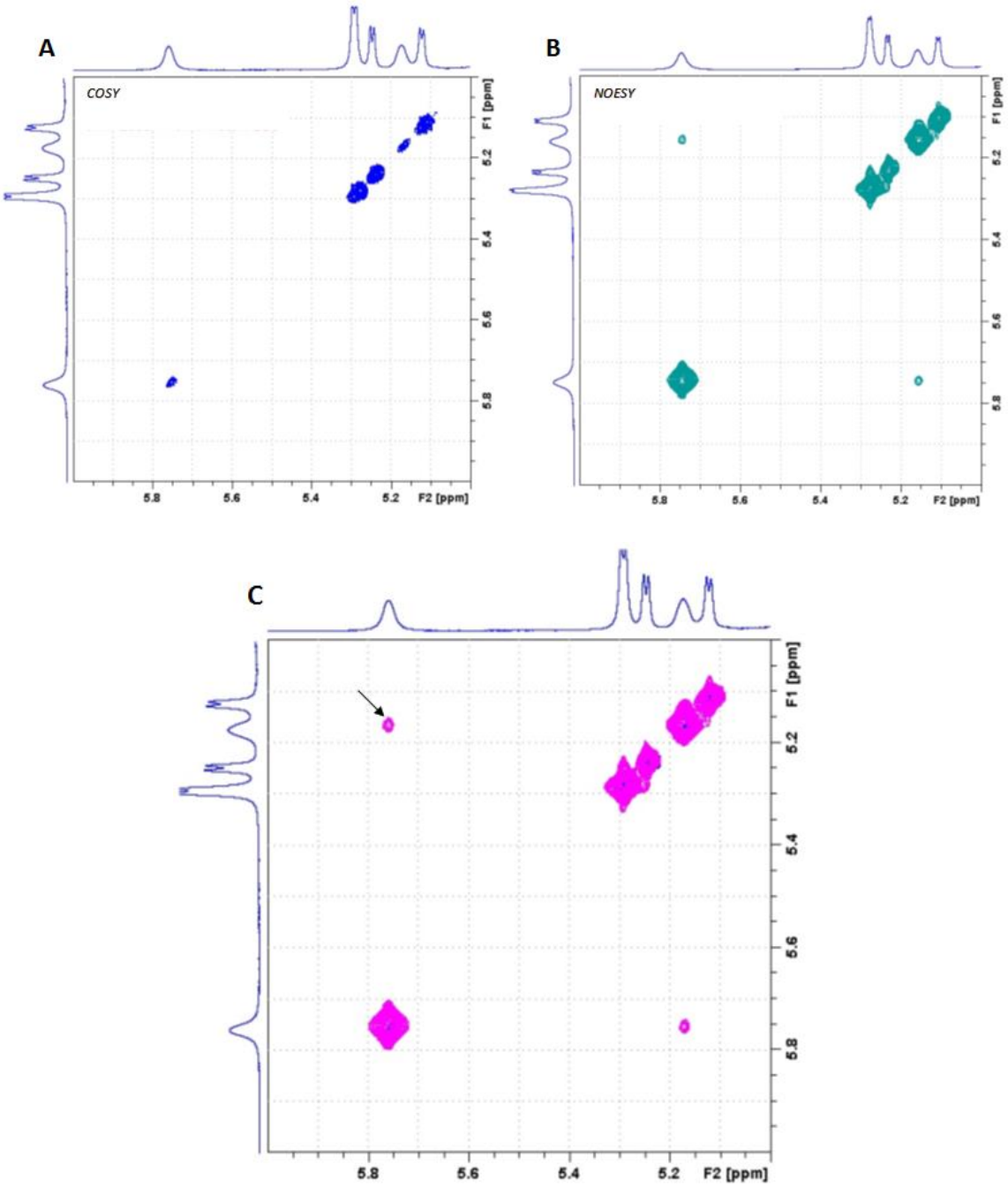

Figure 3.14 5 – 6ppm ^{1}H–NMR (A) COSY and (B) NOESY spectra and (C) their subtraction of carrier 3b : DOX (1 : 1) complex in D_2O.

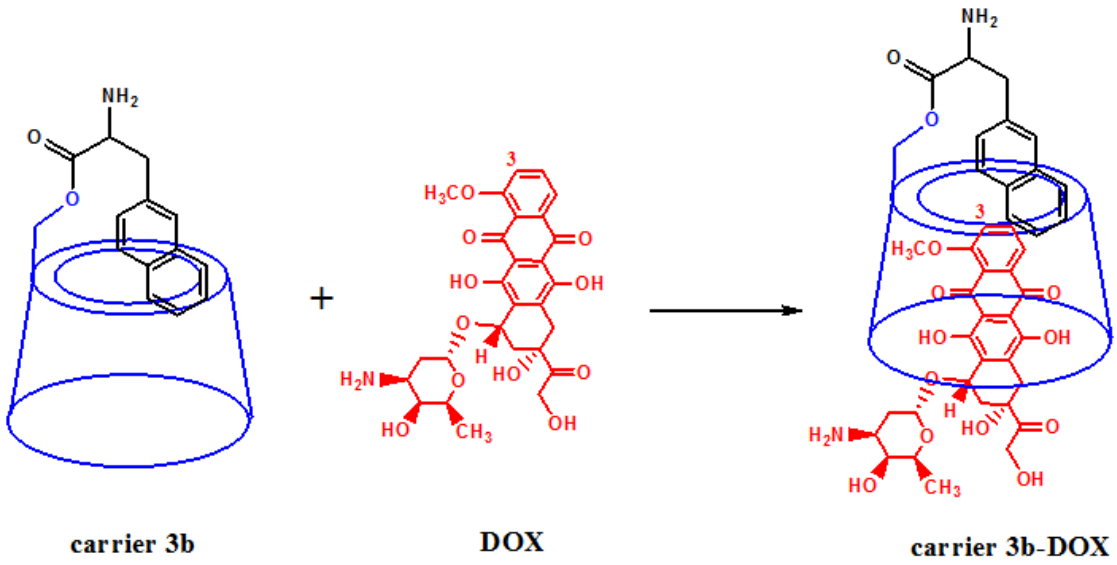

Figure 3.15 Interaction model of carrier 3b-DOX inclusion complex

3.4.2.2 Carrier 3b to DOX complexation analysed by fluorescence spectroscopy

The inclusion complex created between **carrier 3b** and DOX in the present study was detected through fluorescence measurements based on the DOX fluorescence signal at 592 nm. According to the fluorescence studies, the fluorescence intensity of DOX was gradually decreased with increasing **carrier 3b**'s concentrations (Figure 3.16). This signal decays in the presence of **carrier 3b**, suggesting that good coupling between the DOX and **carrier 3b** is formed due to encapsulation, which is allowing energy transfer between the guest and host molecule. Therefore, the DOX excited state decays non-radioactively leading to lower fluorescence signals. The experimental results also validated that **carrier 3b** is a fluorophore quencher for DOX, because the fluorescence intensities of the **carrier 3b** : DOX samples were constantly lower than those of the free DOX. The observed decrease in the fluorescence intensity of DOX is in a good correspondence with literatures (Wagner, Fitzpatrick et al. 2003; Park 2006).

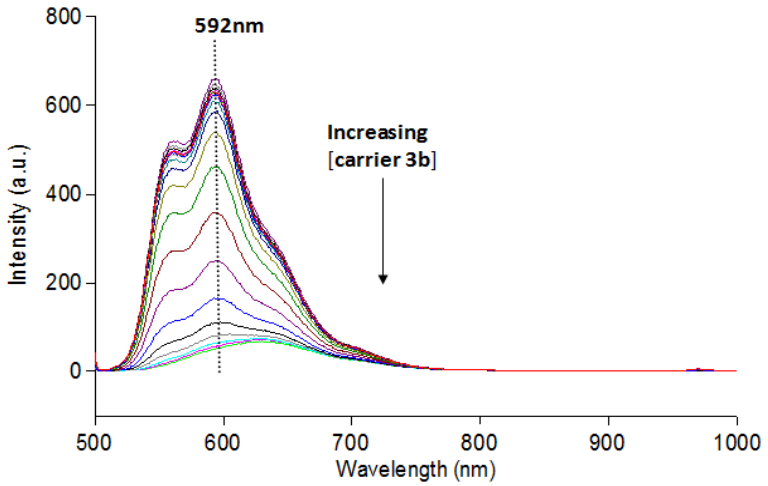

Figure 3.16 Fluorescence spectrum of DOX in the prescence of carrier 3b. 5 µM DOX with increasing concentrations (0.67 to 5000 µM) of carrier 3b in PBS was tested at $\lambda_{excitation}$ = 480 nm, $\lambda_{emission}$ = 500 – 800 nm (λ_{max} = 592 nm) with slits 10 nm

According to the calculation of encapsulation efficiency (Equation 3.3) between **carrier 3b** and DOX (Figure 3.17), DOX encapsulation efficiency was gradually enhanced with increasing concentration of **carrier 3b**, while no inclusion evidence was observed using the non-modified γ-CD with DOX, under similar conditions. Significant encapsulation of DOX within **carrier 3b** was observed at ratios as low as 1 : 1. Satisfying encapsulation was obtained of **carrier 3b** : DOX at the ratio of 10 : 1 which will be further discussed in section *3.4.4*.

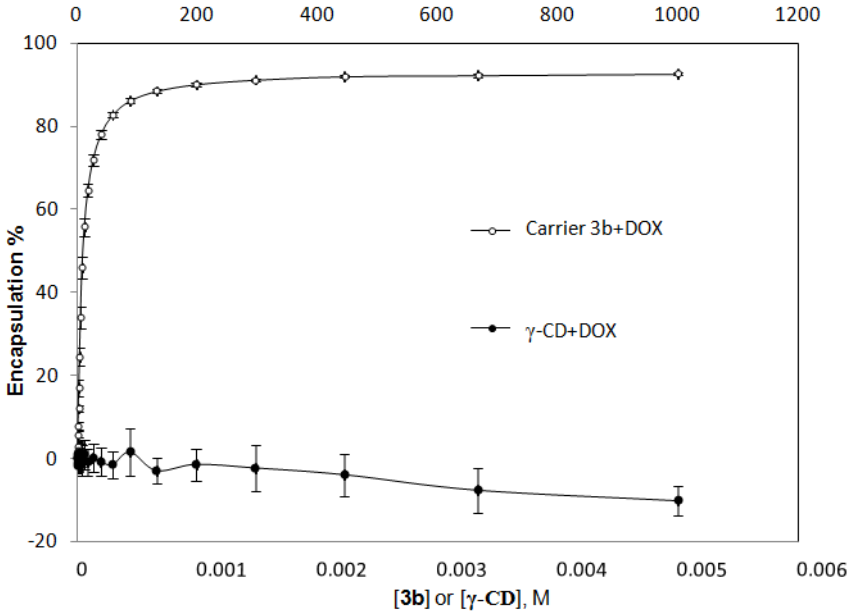

Figure 3.17 Encapsulation of DOX (5 µM) by carrier 3b (0.67 to 5000 µM) and γ-CD (0.67 to 5000 µM) analysed by fluorescence spectroscopy.

3.4.2.3 Binding constant calculation of carrier 3b to DOX by modified Stern-Volmer equation

Since a good correspondence function between 1 / ([**carrier 3b**], M^{-1}) and fluorescence intensity of DOX in the presence of *x* M **carrier 3b** was obtained above (Figure 3.17), the corresponding *K* binding value, was calculated by the obtained liner plot of $y = 5\times10^5 x+1.0263$ derived from the correspondence of $I_0 / (I_0-I_x)$ *vs.* $1 / [H]_x$ (*y* and *x* axis in Figure 3.18, respectively) at $R^2 = 0.9936$ through the intercept (1.0263) / slope (5×10^5) value which finally equal to 20,526 M^{-1} at physiological temperature. This value is a factor of 102 higher than the fluorescence established $K_{binding}$ reported by Anand *et al*. recently (Anand, Ottani et al. 2012) for the native γ-CD with DOX in 1 : 1 complex formation. The higher value of $K_{binding}$ of the modified **carrier 3b** can be attributed to the modification by the naphthalene group, which potentially exhibits π-π interactions between the aromatic rings of **carrier 3b** and DOX molecule. The analysis is consistent with the previous **carrier 3b** to DOX inclusion's NMR structure investigation.

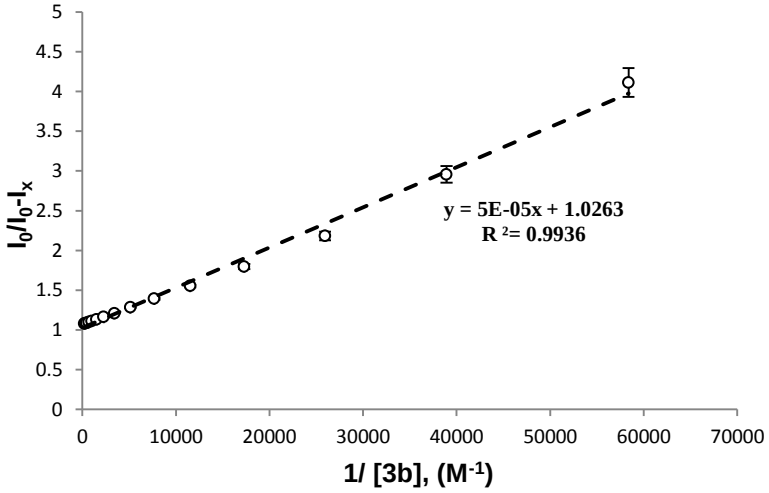

Figure 3.18 Binding constant K of carrier 3b with DOX. Fluorescence intensity of DOX (5 µM) mixed with carrier 3b (0.67 to 5000 µM) was measured and K binding was calculted as described in the Materials and Methods (K = 20526 M^{-1}).

3.4.2.4 Drug Loading efficiency of the carrier

An additional important factor in the complex formation is the concentrations of the reagents and their molar ratio in solution. As can be seen in the ^{1}H-NMR spectra of

carrier 3b : DOX at ratio 1 : 1 and 10 : 1 (Figure 3.19), the top spectrum has broader, which has more widely distributed peaks. This variation between the spectra suggests that, in the 1 : 1 solution, the created complexation has a more rigid structure than with excess of the **carrier 3b**. In the former case (10 : 1), several **carrier 3b** molecules can encapsulate a certain DOX encouraging it to exhibit a faster dynamic equilibrium between the free and encapsulated forms. Additionally, the comparison of the two spectra can aid in the attribution of the peaks to the appropriate molecules. The appearance of a certain peak (black circle in Figure 3.19) only in the 1 : 1 complex spectrum provides a strong indication that the peak belongs to DOX rather than the **carrier 3b**. A good example is the peak at 6.9 ppm which appears only in the 1 : 1 spectrum and corresponds to DOX H-3.

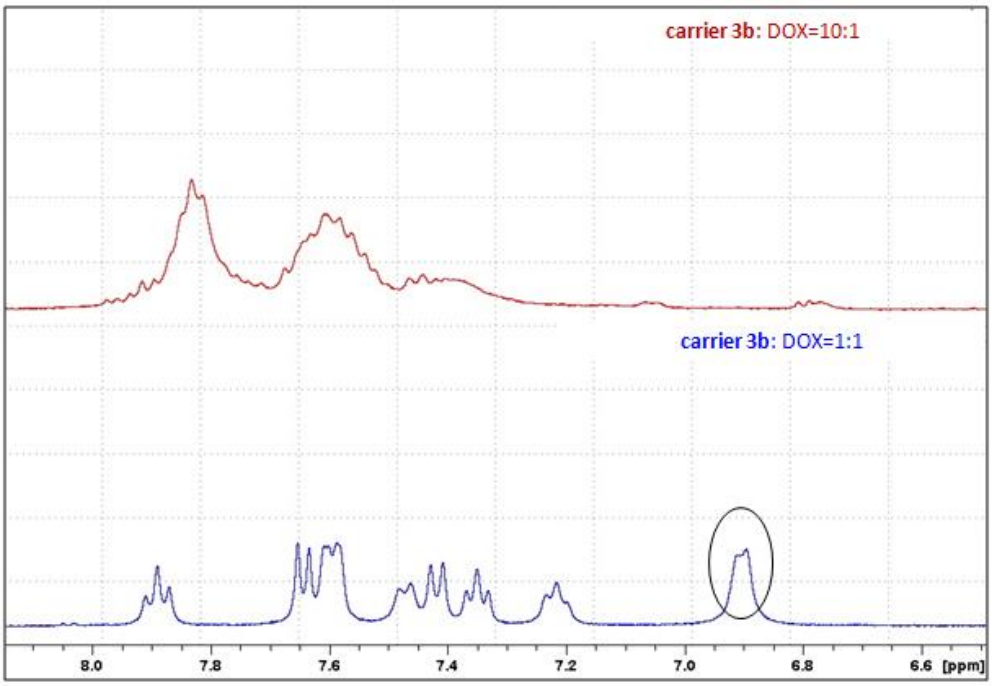

Figure 3.19 ^{1}H–NMR spectra of carrier 3b : DOX complexes at ratios 10 : 1 (top) and 1 : 1 (bottom) in D_2O, respectively. 20 mM carrier 3b and 2 mM DOX were applied for the 10 : 1 complex; and 10 mM carrier 3b and 10 mM DOX were applied for the 1 : 1 complex.

The drug loading efficiency was also validated by fluorescence spectroscopy in which increasing concentrations of DOX were used while **carrier 3b** : DOX was kept at the same ratio. The results suggested that increasing the concentration of DOX (2, 5 or 12.5 μM) led to increased drug loading (Figure 3.20), which further confirmed that

increasing either the concentration of the carrier or DOX will lead the equilibrium of the two molecules to the direction of forming more encapsulation. These results demonstrate the potential of this carrier in reducing the dose of DOX in chemotherapy.

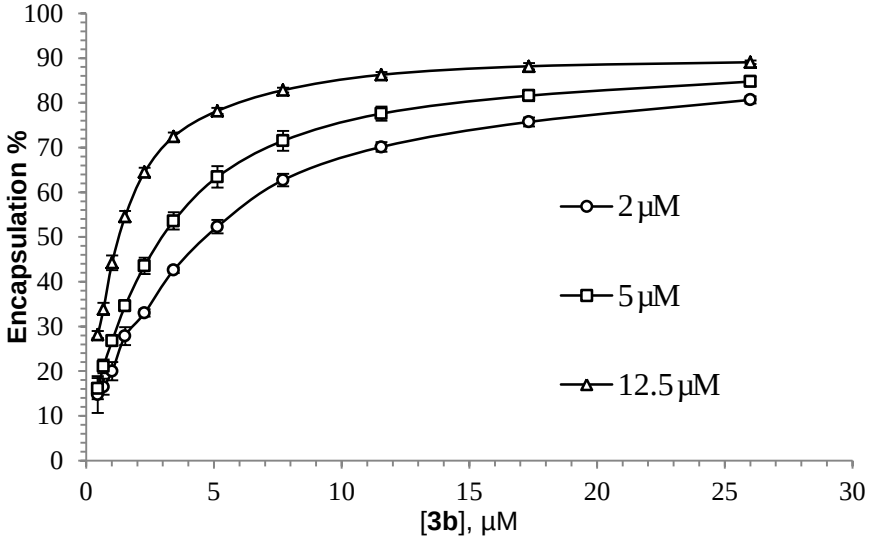

Figure 3.20 Loading efficiency of DOX by carrier 3b. The DOX concentrations were as indicated (2 μM, 5 μM and 12.5 μM) and carrier 3b was applied at the ratios to each concentration of DOX from 26 : 1 down to 0.5 : 1.

3.4.3 pH Stability of Carrier 3b : DOX Complex

The pH responsivity of **carrier 3b** for the inclusion of DOX was investigated by fluorescence spectroscopy. The fluorescence emission values of free DOX were found to be unaffected in different pH media (Figure 3.21). Therefore, any change in the fluorescence intensity of DOX will be a result of the encapsulation. The encapsulation efficiency of **carrier 3b** to the drug was estimated under a wide range of pH values (1.0 – 7.4) at 37 ℃ (Figure 3.22).

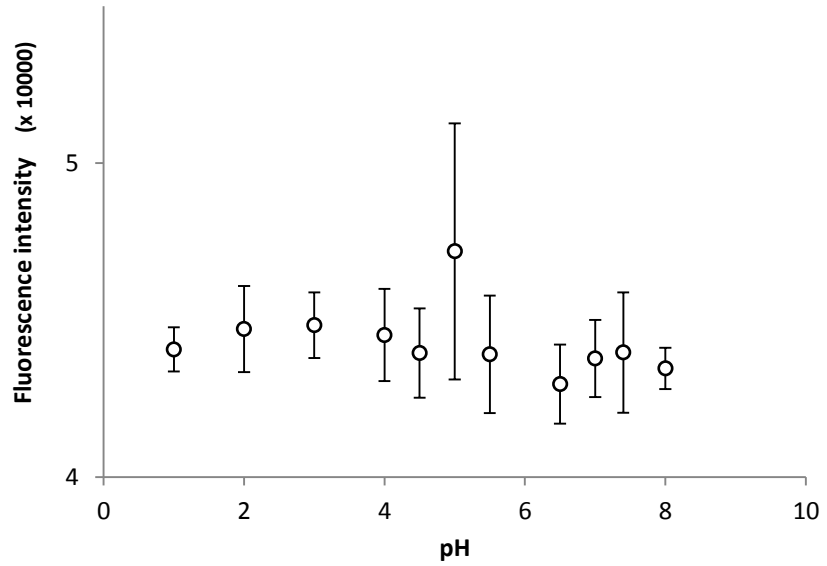

Figure 3.21 Fluorescence intensity of DOX in solutions of various pH values.

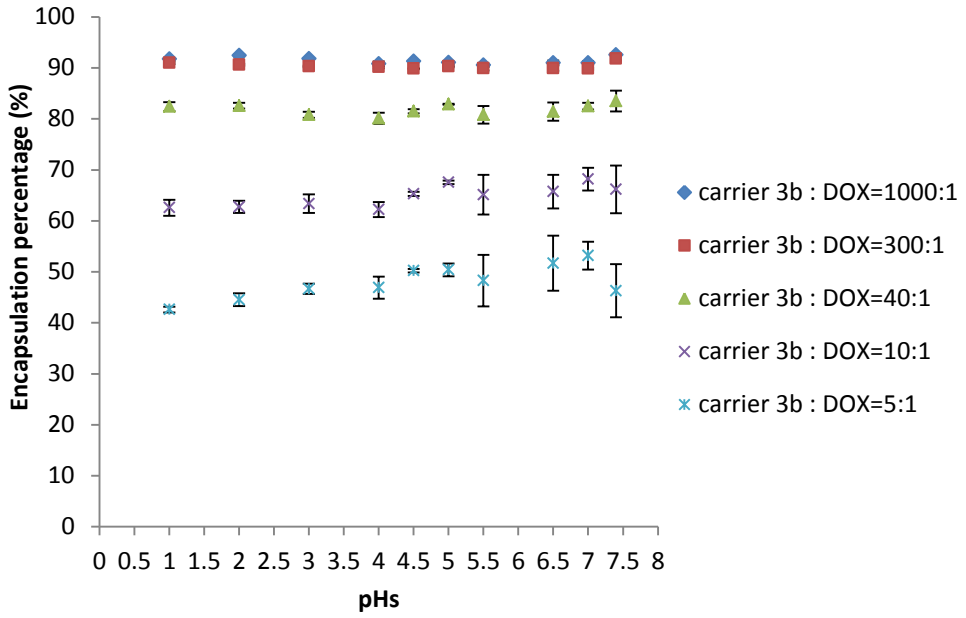

Figure 3.22 Encapsulation percentage (%) of DOX by carrier 3b in solutions of various pH values and at different carrier 3b : DOX ratios at 37 ℃

Since the encapsulation efficiencies are all in the same order of magnitude, the results indicate a similar chemical stability of the complex (Bekers, Beijnen et al. 1990; Emara S 2000) and comparable encapsulation mode in a wide range of acidic environments and at a wide range of **carrier 3b** : DOX ratios.

3.4.4 Thermal Responsivity of Carrier 3b : DOX Complex

The same method was utilised to evaluate the thermal responsivity (Schmaljohann 2006) of the inclusion complex **carrier 3b** : DOX. Testing temperatures were 25, 37, 42, 50 ℃ and then cool down at 25 ℃ (Figure 3.23). The modified Stern-Volmer plot shows a clear correlation between the encapsulation efficiency of **carrier 3b** with DOX and the temperature of the surrounding environment (Figure 3.24).

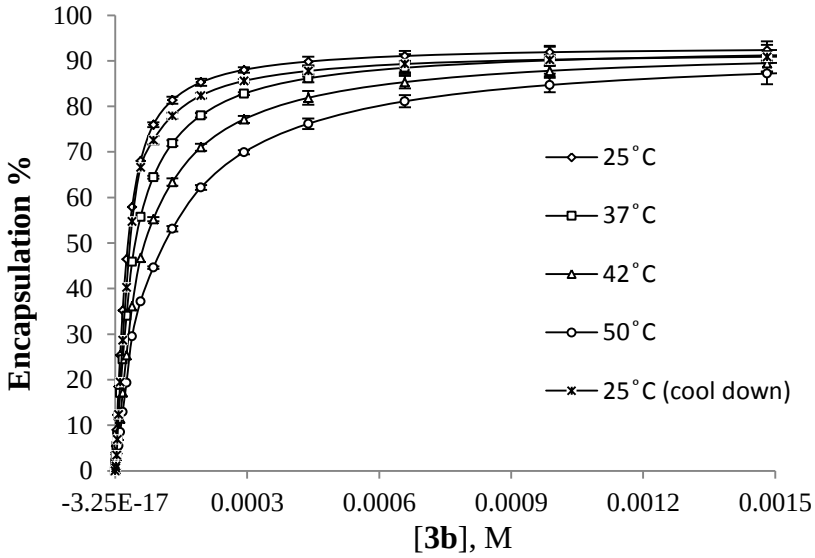

Figure 3.23 Thermal responsivity of carrier 3b : DOX inclusion complex at pH7.4.

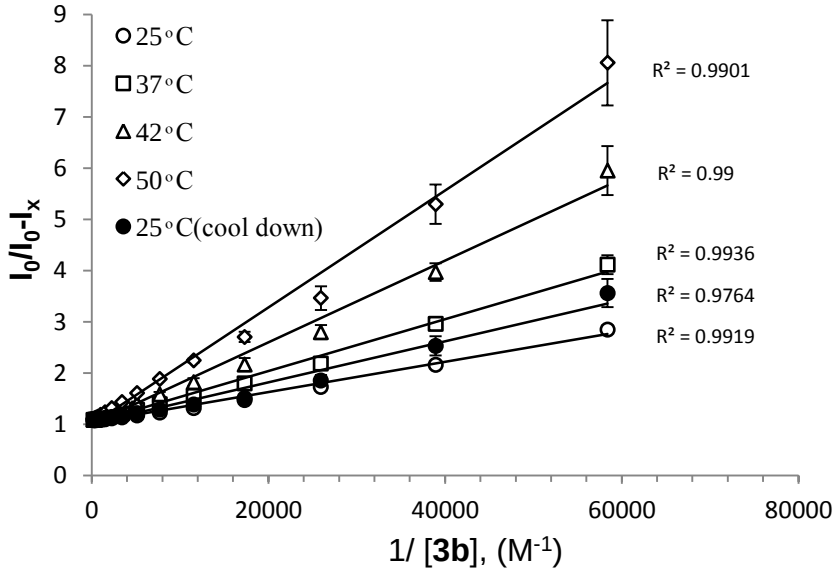

Figure 3.24 Modified Stern-Volmer plot showing binding affinities of carrier 3b (0.67 to 5000 μM) to DOX (5 μM) at varying temperatures. $K_{25\ ℃}$ = 34433, $K_{37\ ℃}$ = 20526, $K_{42\ ℃}$ = 12475, $K_{50\ ℃}$ = 9960, $K_{25\ ℃}$ (cool down) = 25377 M^{-1}.

Increasing the temperature from 25 to 50 ℃ led to a decrease of the $K_{binding}$ by ~ 3.5-fold and release of the DOX from the inclusion complex. In addition, after cooling down the testing solutions to 25 ℃, a re-encapsulation process of DOX by **carrier 3b** was observed. This phenomenon demonstrated the reversible equilibrium process of DOX + **carrier 3b** ⇆ **carrier 3b**-DOX and further confirmed the dynamic complexation interaction between DOX and **carrier 3b**. It is well known in the literature (Tabushi, Kiyosuke et al. 1978) that the complexation process of CDs is driven by enthalpy and entropy, typically exhibiting large negative enthalpy changes as well as small negative entropy changes. The negative enthalpy changes results from *van der Waals* interaction and hydrogen bonding between guests and the cavities of CDs, while the negative entropic change is due to the steric barrier caused by the molecule's geometrical shape and the limit of CD cavity to the freedom of shift and rotation of guest molecules (Chen, Xu et al. 2005).

Optimal (highest) DOX release from the inclusion by temperature changes occurred when the **carrier 3b** : DOX ratio was around 10 : 1 as indicated by the release rate (Table 3.2) calculated according to data obtained in Figure 3.23. This ratio formation was applied thereafter in *in vitro* cell culture studies in Chapter 4 and 5.

Table 3.2 DOX (5 μM) release from encapsulation by temperature changes

	Ratio of **carrier 3b** to DOX						
	39	26	17	**11**	8	5	3
Temperature	*Release rate (%)						
25 ℃ to 37 ℃	7.3	9.5	11.5	**12.3**	12.0	12.5	10.8
37 ℃ to 42 ℃	7.0	8.5	9.0	**9.8**	9.2	8.6	7.3
42 ℃ to 50 ℃	8.8	10.3	9.6	**10.6**	6.6	6.1	4.3

*Release rates were calculated by deducting the encapsulation efficiency (%) at lower temperature from that of at higher temperature.

3.5 Conclusions

In conclusion, a novel γ-CD derivative **carrier 3b** has been successfully designed and constructed which showed significantly improved encapsulation ability for DOX. The carrier possesses thermo-sensitivity and high pH stability. The delivery system was

designed to be used in combination with heat treatments, such as RFA, microwave hyperthermia and HIFU (May and Li 2013). However, whether this carrier would be efficient in encapsulation of DOX in *in vitro* and *in vivo* stages, and how the specific transportation and distribution of **carrier 3b**-DOX inclusion would be, are need to be further validated. The further investigation and application of this delivery system, *in vitro* and *in vivo,* are further introduced and discussed in Chapter 4, 5 and 6.

Chapter 4

Establishment of *in vitro* Evaluation of Doxorubicin Encapsulation by γ-cyclodextrin Derivative

4.1 Introduction

On the basis of chemical analysis for the encapsulation affinity between the novel modified γ-CD carrier and DOX discussed in last chapter, it is essential to establish proper human cancer cell models to verify the encapsulation ability of the carrier to DOX for potential pre-clinical studies in the future.

Cell culture plays an important role in the development and evaluation of novel anticancer drugs *in vitro* through carrying out experiments such as cellular drug uptake, drug efflux, cellular metabolism and cell proliferation assays. The development of methods for culturing human cancer cells *in vitro* has raised the question of whether it might be possible to use cell culture methods to model all of the features important for clinical anti-tumour activities. Such approaches might also lead to the development of novel nanocarriers for transportation of existing anticancer drugs that are selective for human tumour targets (Baguley, Hicks et al. 2002).

Cell cultures are often used to: 1) screen compounds for carcinogenicity or mutagenicity; 2) analyse of the cells themselves; 3) examine cell to cell communication; 4) assess cell's response to chemical compounds; and 5) produce cellular-derived protein products (Varga 2011).

The main theme of this chapter is the investigation of encapsulation capacity of the novel modified γ-CD carrier to DOX by cytotoxic and cellular drug uptake assays. Cytotoxic assays are particularly useful in evaluation of cell survival following exposure to novel compounds designed for anti-cancer treatments, while cellular drug

uptake evaluation is an efficient tool to investigate the encapsulation affinity of designed nanocarriers towards existing cytotoxic anti-cancer agents *in vitro*.

4.2 Human Cancer Cell Culture and Selection of Methodology

4.2.1 Selection of Suitable Human Cancer Cell Lines: KB and HCT116 (Langdon 2003)

KB, human nasopharyngeal epidermoid carcinoma, is a HeLa (cervical carcinoma) contaminant cell line according to American Tissue Culture Collection (ATCC, CCL-17). KB cell line is widely used as it contains the highest expression required in many studies (Antony, Kane et al. 1989; Elwood 1989; Saikawa, Knight et al. 1993; Lee and Low 1994). It is also relatively sensitive to doxorubicin (Shen, Lu et al. 1991; Kamimura, Furukawa et al. 2013).

HCT116 (ATCC, CCL-247) is a human colorectal carcinoma that has wild type p53. It carries a RAS mutation in codon 13 and is tumourigenic in nude mice. Cell lines from human colorectal cancers are useful tools in the study of cell biology and in the development and testing of new therapeutic modalities. In general, colorectal cancer cell lines are relatively easy to establish and grow (Langdon 2003).

4.2.2 Selection of Methodology: Anti-proliferative (Growth Inhibition) Assays

Anti-proliferative assays include cell cytotoxic assays and cellular drug uptake assays, which discuss the measurement of growth inhibition rather than cell killing (Baguley, Hicks et al. 2002). Cell cytotoxic assays such as the evaluation of the half maximal inhibitory concentration (IC_{50}) (Belotti 1996) of a certain drug to different cell lines, is a particularly important strategy for DNA-damaging drugs such as DOX which was employed in the thesis reported here. DNA damage generally arrests cells in G2

phase (Furnari, Rhind et al. 1997) especially when p53 function is present (Abedin and King 2010). IC_{50} determination is the most direct method of measuring cytotoxic activity of a drug by *in vitro*, which may provide useful pharmacokinetic information for *in vivo* application (Fridborg, Nygren et al. 1995).

Another commonly used anti-proliferative assay is cellular drug uptake. It provides a promising evaluation approach for drugs / nanomedicines such as those designed for selective activation by specific enzymes in tumour cells; those transportable by targeting ligands; and those released by physical or chemical triggers. In the above cases, useful activity depends not only on the ability of the drug to act as a substrate for the enzyme system but also on its ability to enter the tumour cells. This cell-based method is particularly suitable for detecting potential components such as cell targets that are difficult to represent in isolated biochemical systems.

Cytotoxicity investigation by MTT assay

Mitochondrial reduction of the dye methylthiazoldiphenyltetrazolium (MTT), has been first developed and reported as a rapid and quantitative assay for cell survival and proliferation investigation by Mosmann (Mosmann 1983).

In MTT assay, cells should be in their exponential phase of growth and are exposed to cytotoxic chemicals. The exposure duration of MTT assay is usually determined by the time required for maximal damage to occur but is also depends on the stability of the tested drugs. After removal of testing compounds, the cells are usually post-cultured to proliferate for two to three doubling times to distinguish between cells that remain viable and are capable of proliferation and those that remain viable but cannot proliferate (Langdon 2003). Surviving cell numbers are then determined indirectly by MTT dye reduction.

MTT reagent is a yellow water-soluble tetrazolium dye which is reduced by mitochondria of live cells (Liu, Peterson et al. 1997) by forming a blue formazan product that is insoluble in aqueous solutions (Figure 4.1 A). The amount of produced formazan can be determined spectrophotometrically once solubilised in a suitable solvent such as DMSO. The advantages of MTT assay are 1) it is a quick and easy screening procedure; 2) it allows a large number of assays to be carried out in one batch;

3) The results can be read on a multi-well scanning spectrophotometer and show a high degree of precision; and 4) No washing steps are used in the assay and lack of any radioisotope. But a drawback of the assay is that it cannot distinguish between a cytotoxic (cell kill) and a cytostatic (reduced growth rate) effect (Langdon 2003).

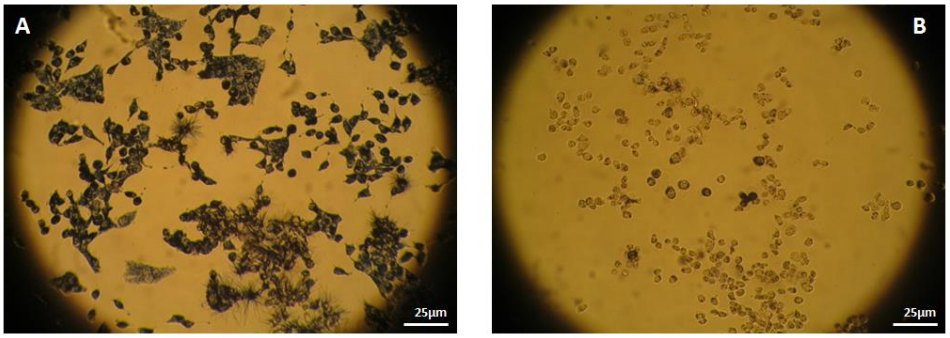

Figure 4.1 MTT assay formazan formed by live cells (A) and dead cells (B).

In terms of MTT application, the assay has been adapted successfully to measure growth and drug sensitivity of a variety of tumour cell lines by Finlay *et al.* (Finlay, Wilson et al. 1986) and Scudiero *et al.* (Scudiero, Shoemaker et al. 1988) in the 1980s. Moreover, the American National Cancer Institute (NCI) reported MTT dye reduction evaluation as a possible endpoint in a rapid screening assay (Alley, Scudiero et al. 1988). Shortly after, Berridge and Rao (Berridge and Rao 1993) further investigated the cellular reduction including sub-cellular localisation, substrate dependence, and involvement of mitochondrial electron transport in MTT reduction.

Many other tetrazolium salts such as XTT (2, 3-bis-(2-methoxy-4-nitro-5-sulfophenyl)-2H-tetrazolium-5-carboxanilide), MTS (3-(4,5-dimethylthiazol-2-yl)-5-(3-carboxymethoxyphenyl)-2-(4-sulfophenyl)-2H-tetrazolium) in the presence of phenazine methosulfate (PMS) (Cory, Owen et al. 1991) and water soluble tetrazolium salts (WSTs) have been developed as water soluble tetrazolium salts to alternatively replace MTT assay. However, no single cytotoxicity assay is ideal and it is always advisable to support results with those obtained from alternative assays where possible and applicable. In the thesis reported here, MTT assay was adopted to investigate cell viabilities.

Cellular drug uptake and cell total protein measurement by the bicinchoninic acid (BCA) assay

Cellular DOX uptake can be observed first of all by fluorescence microscopy. When DOX has been up-taken by cells, its fluorescence signal is visible under fluorescence microscopy by using a black glass fluorescence filter. The quantitation of DOX cellular uptake can be further determined by breaking down cells by lysis buffer and measuring cell lysate's fluorescence intensity. The obtained fluorescence intensities of cell lysates need to be normalised further by the total cellular protein using bicinchoninic acid (BCA) assay.

Tuszynski and Murphy (Tuszynski and Murphy 1990) reported BCA assay is a rapid and convenient method for the determination of the actual and relative cell numbers in tissue culture by using bicinchoninic acid to measure the total cellular protein of cultured cells.

In BCA assay, cells usually are treated by cell lysis buffer to ensure cell protein release. By adding BCA reagent to cell lysate, Cu^{2+} firstly oxidises the protein and is converted to Cu^{1+}, followed by bicinchoninic acid which complexes with the formed Cu^{1+} to form a purple colour. The oxidation reaction can be performed at room temperature for 2 hr, or at 37 ℃ for 30 min. The colour generated at the end of the incubation period is fairly stable. This assay is rapid and simple to perform. The data generated are also very reproducible and the assay is ideal for screening a large number of samples.

As Tuszynski and Murphy finally pointed that the cell-derived absorbance reading as determined by BCA protein assay was proportional to the number of cells, in this thesis, BCA assay has been adopted for the indication of total cell numbers for normalising the fluorescence intensity by DOX in cellular drug uptake assay.

4.3 Materials and Methods

4.3.1 Materials

4.3.1.1 In vitro cell culture, medium, supplementation and other reagents

Medium, supplementation and reagents	Manufacturer and place of origin	Specification
KB cell line	American Tissue Culture Collection, USA	CCL-17
HCT116 cell line	American Tissue Culture Collection, USA	CCL-247
Roswell Park Memorial Institute (RPMI)1640	Gibco® Invitrogen, UK	[+] L-Glutamine
Dulbecco's Modified Eagle's Medium (DMEM)	Gibco® Invitrogen, UK	[+] 4.5g/L D-Glucose [+] L-Glutamine [+] Pyruvate
Phenol Red Free Dulbecco's Modified Eagle's Medium (DMEM)	Gibco® Invitrogen, UK	[+] 4.5g/L D-Glucose [+] L-Glutamine [+] 25Mm HEPES [−] Sodium Pyruvate
Fetal Bovine Serum (FBS)	Gibco Invitrogen, UK	Origin: South America
Trypsin-Ethylenediaminetetraacetic acid (EDTA)	Gibco Invitrogen, UK	0.05%
Penicillin Streptomycin (Pen-Strep)	Sigma-Aldrich, UK	10,000 units penicillin and 10 mg streptomysin/mL
L-Glutamine	Sigma-Aldrich, UK	200 mM
Sodium Pyruvate	Gibco® Invitrogen, UK	100 mM
Non-Essential Amino Acids	Gibco® Invitrogen, UK	
HEPES buffer solution	Gibco® Invitrogen, UK	1 M
MycoAlert PLUS Mycoplasma Detection Kit	Lonza, USA	10 test kit
Dimethyl Sulphoxide (DMSO)	Sigma-Aldrich, UK	Biotechnology use, sterile filtered, endotoxin tested, hybridoma tested
Sodium Dodecyl Sulfate (SDS)	Sigma-Aldrich, UK	0.05% (w/v) in $_{dd}H_2O$
3-(4,5-Dimethylthiazol-2-yl)-2,5	Sigma-Aldrich, UK	5 mg/mL in PBS

- diphenyltetrazolium bromide (MTT)		
Bicinchoninic Acid (BCA) Protein Assay Kit	Sigma-Aldrich, UK	Solution A: bicinchoninic acid, sodium carbonate, sodium tartrate, sodium bicarbonate in 0.1 M NaOH (final pH 11.25). Solution B: 4% (w/v) copper(II) sulfate pentahydrate
Protein Standard (Bovine Serum Albumin-BSA)	Sigma-Aldrich, UK	1.0 mg/mL bovine serum albumin in 0.15 M NaCl with 0.05% sodium azide
doxorubicin (DOX)	Mesochem Technology Co.,Ltd, Beijing, China	Purity ≥ 98%
PBS tablets	Oxoid, UK	Typical Formual (g/L): Sodium chloride 8.0; Potassium chloride 0.2; Di-sodium hydrogen phosphate 1.15; Potassium dihydrogen phosphate 0.2. 1tablet/100mL, pH 7.3±0.2 at 25℃

4.3.1.2 Complete RPMI1640 and DMEM medium formulation

Complete RPMI1640	
Supplementation	**Supplementation**
Fetal bovine serum (FBS)	Fetal bovine serum (FBS)
L-Glutamine	L-Glutamine
Penicillin and Streptomycin (Pen-Strep)	Penicillin and Streptomycin (Pen-Strep)
Sodium Pyruvate	Sodium Pyruvate
Non-essential Amino Acids	Non-essential Amino Acids
HEPES buffer	HEPES buffer
Complete DMEM	
Supplementation	**Supplementation**
Fetal bovine serum (FBS)	Fetal bovine serum (FBS)
L-Glutamine	L-Glutamine
Penicillin and Streptomycin (Pen-Strep)	Penicillin and Streptomycin (Pen-Strep)

4.3.1.3 Cell culture consumables and equipment

Consumables and equipment	Manufacturer and place of origin	Specification
Cell culture flasks	Techno Plastic Products (TPP), Switzerland	75 cm^2
6-well, 12-well, 24-well and 96-well plate	Techno Plastic Products (TPP), Switzerland	transparent
Black 96-well plate	Greiner, Austria	Non cell culture treated black base microplates
Haemacytometer	Marienfeld, Germany	Depth: 0.1 mm Area: 0.0025 mm^2
Sterile Syringe filters	Fisher Scientific, UK	0.45 μm cellulose acetate membrane
Serological pipettes	Techno Plastic Products (TPP), Switzerland	5 mL, 10 mL and 25 mL
Multi-mode plate reader	Tecan, Austria	Tecan infinite M200
Oven	Scientific Laboratory Supplies, UK	INV064
Multi-channel pipettes	Eppendorf, UK	8-channel/12-channel
Distilled/deionized water	Millipore, UK	

4.3.2 Methods

4.3.2.1 IC_{50} evaluation of DOX for KB and HCT116 cell lines

Cultured KB / HCT116 cells were harvested and seeded at the density of 4000 per single well in a 96-well micro-plate 1 day prior to the assay. Cells were not plated in columns 1 and 12, rows A and H, but filled with complete medium (CM) because these are used as blank controls for the absorbance of the residual medium and MTT in the wells.

DOX stock solution was prepared by dissolving 58 mg DOX powder in 1 mL DMSO to obtain the stock DOX concentration at 100 mM and kept the solution frozen. A solution of 100 μM DOX was prepared by dilution of the DOX stock solution by CM. The final concentration of DMSO in the diluted solution was 0.1%. This solution was then filtered by 0.45 μm filter and was diluted by 3/4 dilution method by CM to obtain

DOX concentrations from 100 μM to 2.4 μM for KB cell line (14 DOX concentration gradients, Figure 4.2 A) experiments, and to obtain DOX concentrations from 100 μM to 0.56 μM for HCT116 cell line (19 DOX concentration gradients, Figure 4.2 B) experiments, respectively.

Cells were then exposed to the pre-heated (20 min at 37 ℃ water bath) test solutions by incubation with 100 μL of each solution/well for 30 min in triplicates. Experimental arrangement is presented as in Figure 4.2. At the end of incubation, test solutions and CM in control wells were removed and cells were washed by pre-heated CM twice and replaced with 100 μL/well fresh CM. Cells were then observed under the microscope to assess cell loss. Cell in the plate with refilled 100 μL/well fresh CM were further incubated for 48 hr.

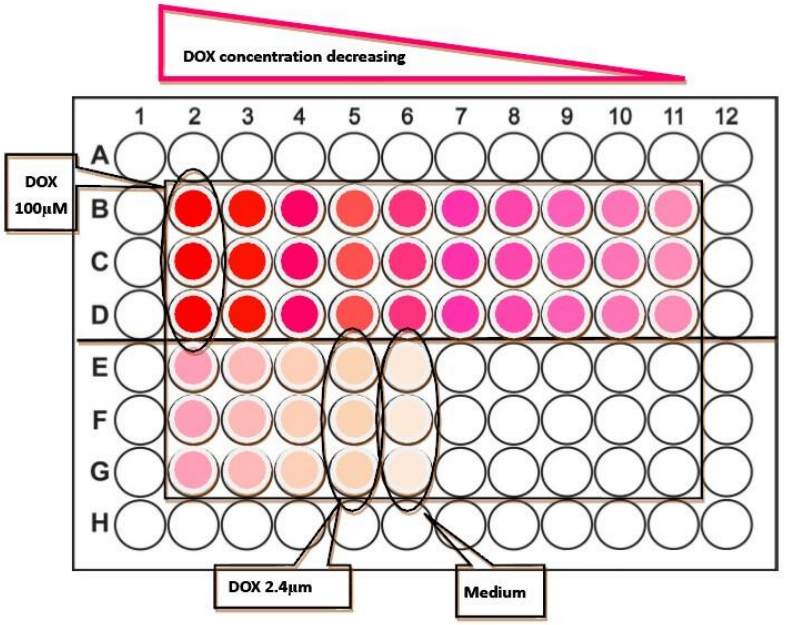

A: KB cells

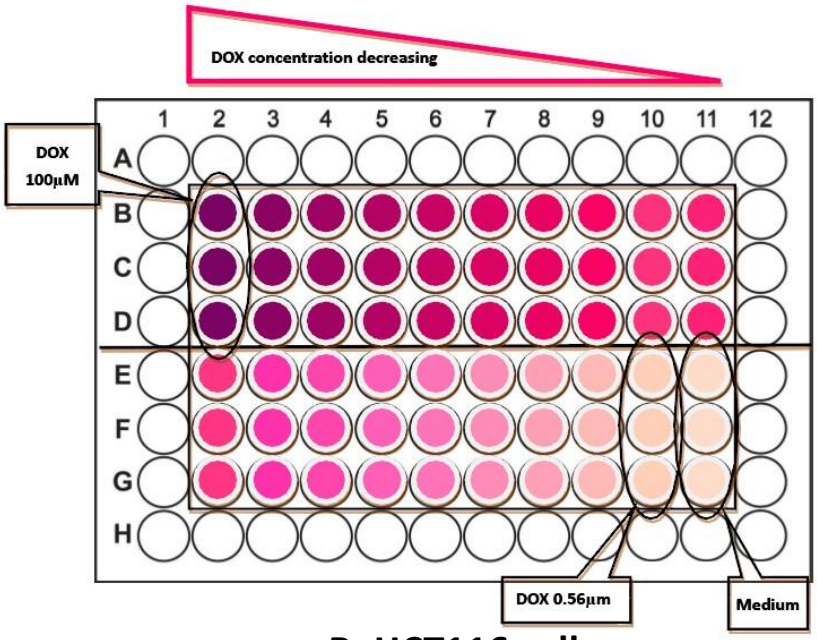

B: HCT116 cells

Figure 4.2 Experimental design for IC_{50} determination of DOX to KB cell line (A) and HCT116 cell line (B) in 96-well plates.

Cell viability was then evaluated by MTT colorimetric assay that uses the enzymatic activities of cells as a measure for their viability 48 hr post DOX exposure. For the MTT assay, 5 mg/mL MTT powder was dissolved in PBS and 20 µL of the prepared reagent was added directly into each well of cultured cells (100 µL CM) and

incubated for 3 hr in a standard incubator. After incubation, the liquid was gently aspirated from the wells with a multi-channel pipette without touching the bottom of wells. Then, 100 µL/well of DMSO was added to dissolve the formazan, an artificial chromogenic product created by the reduction of the tetrazolium salt in metabolically active cells. The absorbance for each well, which is proportional to the number of viable cells, was read using the multi-mode Infinite M200 plate reader at a wavelength of 550 nm with 2 min pre-shaking (this step helps to dissolve formed formazan thoroughly).

Cell inhibition percentages (Inhibition %) by DOX can be calculated based on the absorbance values (OD) at 550 nm obtained from MTT assay by Equation 4.1:

$$Inhibition\% = \left(1 - \frac{OD_{cell+DOX} - OD_{blank}}{OD_{cell\ control} - OD_{blank}}\right) \times 100\%$$

Equation 4. 1 Cell inhibition percentage upon exposure to DOX solutions.

Where, $OD_{cell+DOX}$ is the absorbance of cells exposed to gradient concentration of DOX solutions, $OD_{cell\ control}$ is the absorbance of cells with no DOX exposure and OD_{blank} is CM without cells. Then, a correlation between Inhibition% and common logarithm of DOX concentrations (Log_{10} [DOX, M]) (Stewart and Watson 1983; Martone, Zhou et al. 2009; Chavez-Gutierrez, Bammens et al. 2012) can be obtained as typically showed by Figure 4.3.

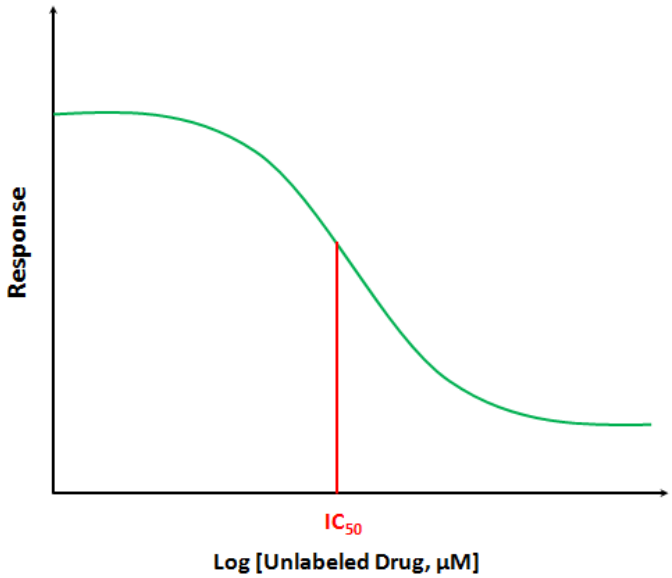

Figure 4.3 Determination of IC_{50} of unlabeled drug

As IC_{50} is the concentration at which the curve passes through the 50% inhibition, the inhibition at IC_{50} concentration ($Inhibition_{IC_{50}}\%$) can be then calculated according to Equation 4.2:

$$Inhibition_{IC_{50}}\% = [Inhibition_{max} - 50\% \times (Inhibition_{max} - Inhibition_{min})] \times \%$$

Equation 4.2 Inhibition at IC_{50} concentration

Where, $Inhibition_{max}$ is the maximum inhibition rate of DOX to this cell line, while $Inhibition_{min}$ is the minimum inhibition rate. Thus, the IC_{50} can be determined as the DOX concentration at which inhibition equals to $Inhibition_{IC_{50}}$ value.

4.3.2.2 Calibration curve of DOX

Two sets of calibration curves for DOX fluorescence intensity *vs.* DOX concentration were determined by preparation of two sets of gradient concentrations (2 µM to 0.034 µM and 1 µM to 0.017 µM) of DOX in 0.5% SDS cell lysis buffer. Then DOX solutions were transferred to a black plate 200 µL/well in triplicate per sample, and fluorescence intensities were obtained by infinite M200 multi-mode plate reader at $\lambda_{excitation}$ = 485 nm, $\lambda_{emission}$ = 500 – 800 nm and the fluorescence intensity at 592 nm (λ_{max}) was adopted for the calibration curves.

4.3.2.3 Cytotoxicity evaluation assays

Cultured KB / HCT116 cells were harvested and seeded at the density of 4000 per single well in a 96-well micro-plate 1 day prior to the assay. Cells were not plated in columns 1 and 12, rows A and H, but filled with CM as these are used as blank controls for the absorbance of the residual medium and MTT in the wells.

To test the modified carrier's cytotoxicity, a solution of 1250 / 2500 µM carrier was prepared by dissolving 1.875 / 3.75 mg/mL carrier in CM and filtered by 0.45 µm filter for KB and HCT116 cells respectively. For the mixture of carrier and DOX cytotoxic assays, a solution of 12.5 / 25 µM DOX (corresponding to the test for KB / HCT116 cell

lines, respectively) was prepared by dilution of the DOX stock solution (100 mM) in DMSO by CM. The final concentration of DMSO in the diluted solution is 0.0125 / 0.025%, respectively. To the final 12.5 / 25 μM DOX solution, 0.1875 / 0.375 mg/mL of carrier was added to obtain a concentration of 125 / 250μM (10 : 1 of carrier : DOX molar ratio). This solution was then filtered by 0.45 μm filter and was diluted by 12.5 / 25 μM DOX solution to obtain carrier : DOX molar ratio at 100 : 1, 50 : 1, 25 : 1, 10 : 1, 5 : 1 and 2.5 : 1, to keep the concentration of DOX constant at 12.5 / 25 μM. DOX solution of 12.5 / 25 μM with native γ-CD (100 : 1 of γ-CD : DOX molar ratio) was also experimented to compare the encapsulation affinity of γ-CD to DOX with the modified γ-CD.

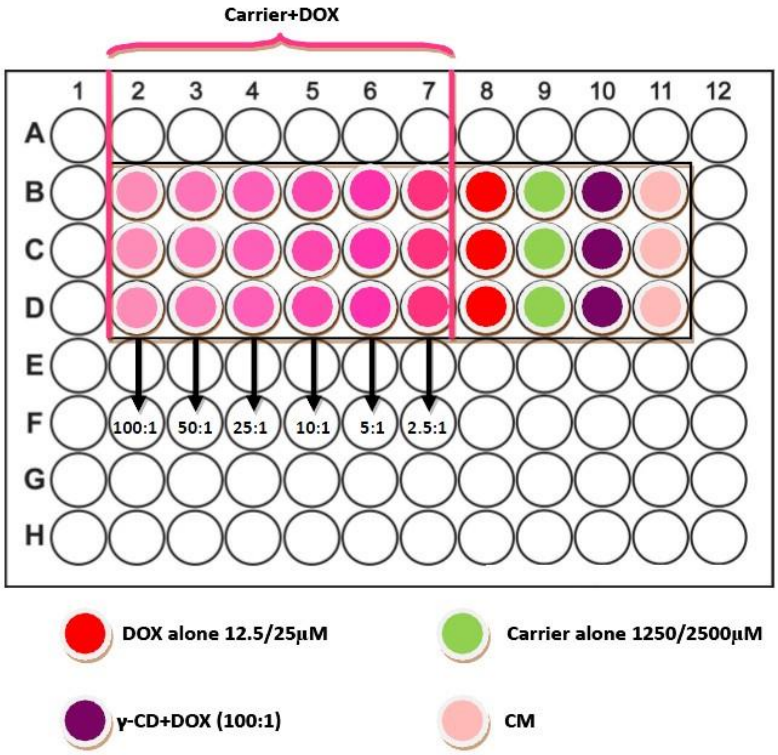

Figure 4.4 Cytotoxicity test by exposure KB / HCT116 cells to gradient concentrations of carrier in the presence of constant concentration of DOX (12.5 / 25 μM, respectively).

Cells were then exposed to the pre-heated (20 min at 37 ℃ water bath) test solutions by incubation with 100 μL of each solution/well for 30 min in triplicates according to Figure 4.4. At the end of incubation, test solutions and CM in control wells were removed and cells were washed by pre-heated CM twice and replaced with 100

μL/well fresh CM. Cells were then observed under the microscope to assess cell loss. Cells in the plate with refilled 100 μL/well fresh CM were further incubated for 48 hr.

Cell viability was evaluated with MTT colorimetric assay 48 hr post exposure, as described in section *4.3.2.1*.

4.3.2.4 Cellular drug uptake evaluation assays

KB / HCT116 cells were harvested and seeded at the density of 1.3×10^5 per well in a 24-well plate and allowed to grow over 3 days prior to the assay. A solution of 12.5 / 25 μM DOX (corresponding to the test for KB / HCT116 cells, respectively) was prepared by dilution of the DOX stock solution (100 mM) in DMSO by CM. The final concentration of DMSO in the diluted solution is 0.0125 / 0.025%, respectively. To the final 12.5 / 25 μM DOX solution, 0.1875 / 0.375 mg/mL of carrier was added to obtain a concentration of 125 / 250 μM (10 : 1 of carrier : DOX molar ratio). This solution was then filtered by 0.45 μm filter and was diluted by means of 12.5 / 25 μM DOX solution to obtain carrier : DOX molar ratio at 100 : 1, 50 : 1, 25 : 1, 10 : 1, 5 : 1 and 2.5 : 1, to keep the concentration of DOX is constant at 12.5 / 25 μM. Cells were exposed to DOX solution of 12.5 / 25 μM with native γ-CD (100 : 1 of γ-CD : DOX molar ratio) to compare the encapsulation affinity of unmodified γ-CD's to DOX with that of modified γ-CD to DOX.

For physiological temperature test, cells were exposed to the pre-heated (20 min at 37 ℃ water bath) test solutions by incubation with 300 μL/well of each solution for 30 min in triplicates / duplicates (see Figure 4.5). For thermal-responsivity test, cells were exposed to preheated (30 min at 42 ℃ and 50 ℃ oven) test solutions by incubation with 300 μL/well of each solution in triplicates / duplicates (Figure 4.5).

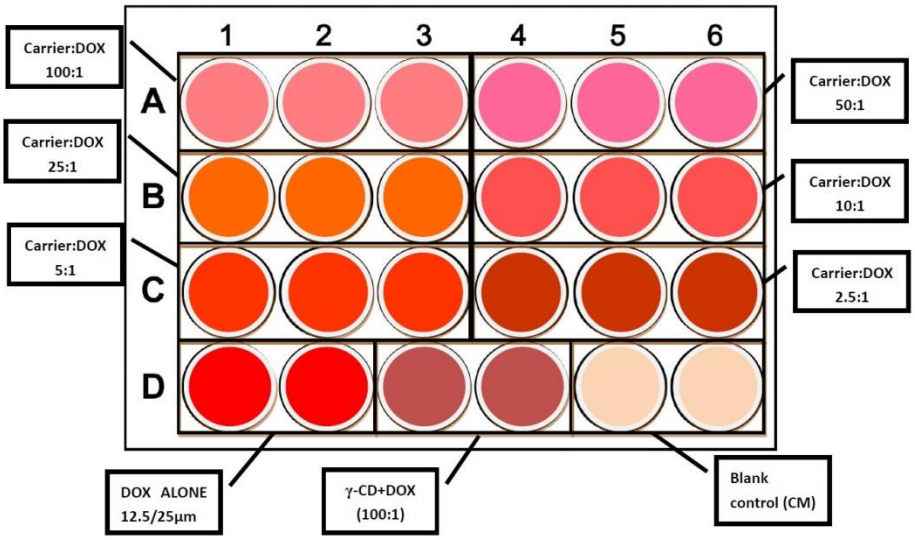

Figure 4.5 Cellular DOX uptake by exposure KB / HCT116 cells to carrier-protected DOX (12.5 / 25 μM). The arrangement was the same for all experimental conditions: physiological (37 ℃) and hyper-thermal temperatures (42 ℃ and 50 ℃).

At the end of the incubation time, test solutions were removed and the wells were washed twice with preheated (at 37 ℃ water bath) PBS. PBS was removed and 250 μL 0.5% SDS were added to each well. Following observation under the microscope to ensure complete cell disruption by SDS, 200 μL total cell lysates from each well were transferred into wells of a black 96-well plate with μ-clear bottom for the measurement of the fluorescence intensity of intracellular DOX. Meanwhile, 25 μL of cell lysates from the same samples were transferred to wells of a normal transparent 96-well cell culture plate for protein determination by the BCA assay.

BCA reagent was prepared by mixing 50 parts of bicinchoninic acid (reagent A) and 1 part of 4% (w / v) copper sulphate solution (reagent B). Standard bovine serum albumin (BSA) solutions from 25 μg/mL to 500 μg/mL were prepared by diluting the standard BSA solution (1000 μg/mL) in the BCA kit by using the same cell lysis buffer (0.5% SDS). BCA assay was then carried out by adding 200 μL BCA reagent into 25 μL of cell lysates samples or BSA standard solutions to obtain the ratio of reagent and protein sample at 8：1. The plate was shaken for 30 sec and incubated for 30 min at 37

℃. After incubation, the plate was cooled down to room temperature and the absorbance was recorded.

Both fluorescence intensity and absorbance were read by Infinite M200 multi-mode plate reader. Fluorescence intensity was measured at excitation and emission wavelengths at 485 nm and 592 nm, respectively. Absorbance of BCA assay was measured at a wavelength at 562 nm.

The cellular uptake of DOX (% of free DOX) can be calculated according to Equation 4.3:

$$Uptake\% = \frac{I_x/OD_x}{I_{DOX}/OD_{DOX}} \times 100$$

Equation 4.3 Cellular uptake of DOX (% of DOX alone).

Where, I_x (I_{DOX}) is the fluorescence intensity of cells exposed to DOX in the presence (or absence) of *x* concentration of carrier while OD_x (OD_{DOX}) is the absorbance of BCA test for corresponding samples. DOX calibration curve can be adopted further to calculate the amount of cellular DOX uptake in the unit of **μmol/μg total protein**.

4.4 Results and Discussion

4.4.1 Cytotoxicity Test

4.4.1.1 IC_{50} determination of DOX for KB and HCT116 cell lines

KB and HCT116 cells were exposed to gradient concentrations of DOX to determine the IC_{50} for both cell lines. IC_{50} is an important criterion for choosing proper DOX concentration for further cell culture studies presented later in this chapter and Chapter 5.

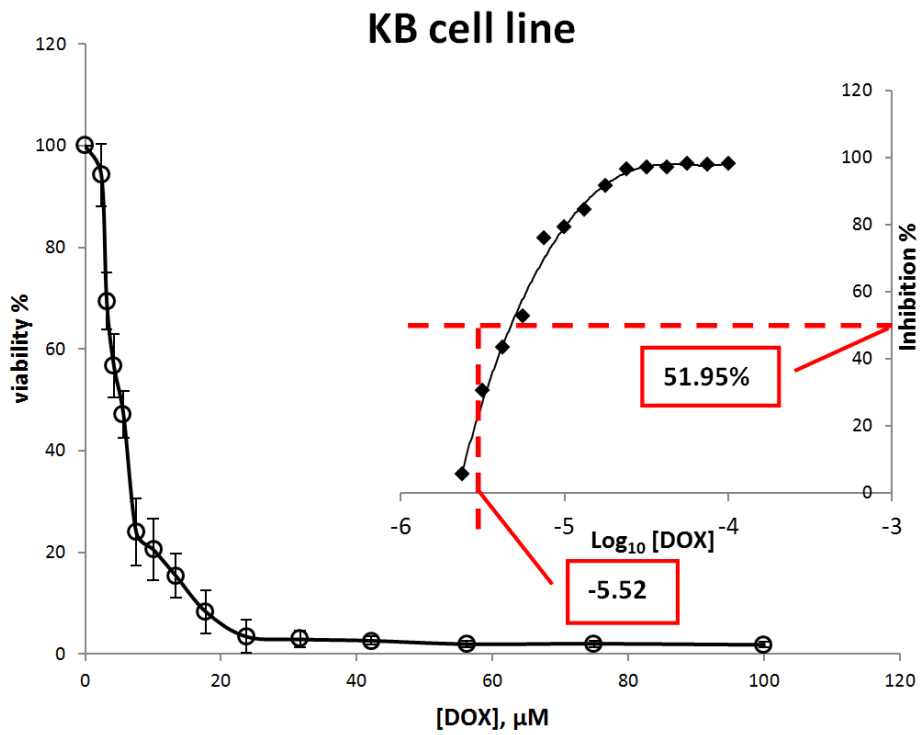

Figure 4.6 IC_{50} determination for DOX to KB cells expressed by the cell viability curve and the correlation between Inhibition% and Log_{10} [DOX, M] (Inset).

Figure 4.6 demonstrates the viability of KB cells against gradient concentrations of DOX (30 min exposure at 37 ℃), and the correlation curve and equation obtained by DOX inhibition rate for KB cells *vs.* the value of Log_{10} [DOX, M]. The viability of KB cells sharply decreased with increasing concentrations of DOX. When DOX concentrations went up to around 23.73 μM and higher, the viability of KB cells reached to a plateau where cell viable rate was only 2%, which gave the maximum inhibition rate at 98% ($Inhibition_{max}$). Accordingly, the maximum KB cell viability in the presence of DOX was 94.24%, thus, the minimum cell inhibition rate was 5.76% ($Inhibition_{min}$). Therefore, $Inhibition_{IC_{50}}$% was obtained as 51.95% according to Equation 4.2. Together with the correlation equation generated between inhibition rates and Log_{10} [DOX, M], the value of Log_{10} [DOX, M] is equal to −5.52 at $Inhibition_{IC50}$%, hence, DOX IC_{50} to KB human epidermal carcinoma cells was finally determined by Log_{10} [DOX, M] = −5.52 as **$IC_{50\ (DOX\ to\ KB)}$ = 5.01 μM.**

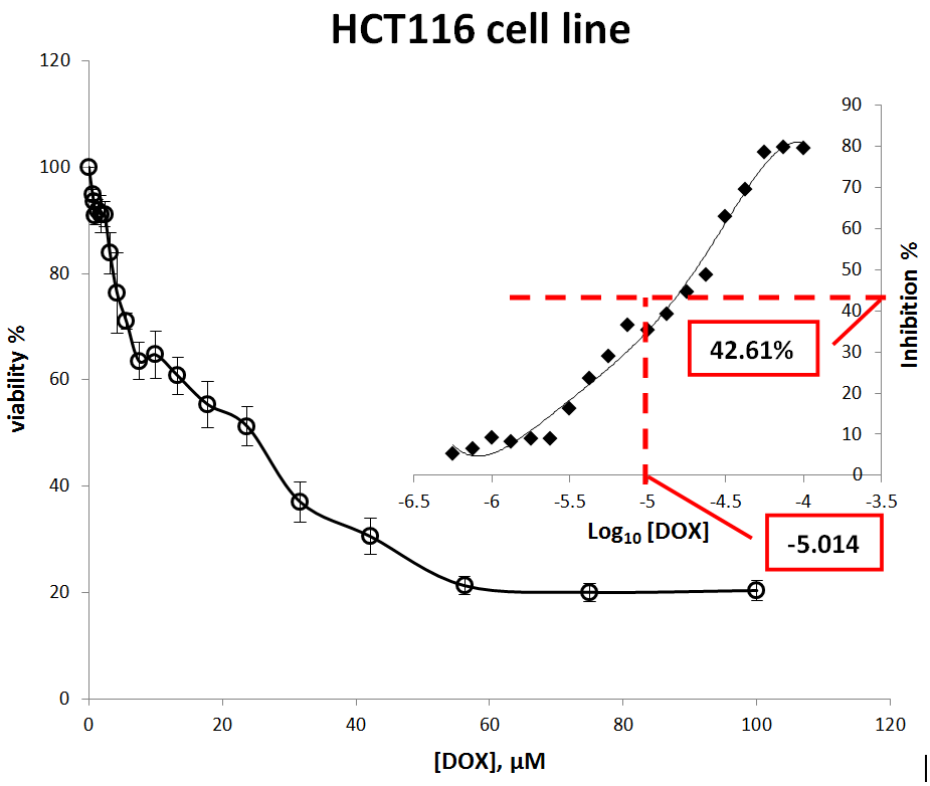

Figure 4.7 IC_{50} determination for DOX to HCT116 cells expressed by the cell viability curve and the correlation between Inhibition% and Log_{10} [DOX, M] (Inset).

Similar to KB cell line, Figure 4.7 depicts the viability of HCT116 cells exposed to DOX solutions (30 min exposure at 37 ℃) and the relationship between DOX inhibition rates to HCT116 cells and Log_{10} [DOX, M]. In comparison to KB cells, HCT116 human colorectal cell line showed more resistance to DOX, as the minimum cell viability of HCT116 to DOX was at 20% whereas KB cells showed only 2%. The maximum viability of HCT116 to DOX was similar to KB cells, which was at 94.80%. Hence, the maximum inhibition rate of DOX to HCT116 cells was 80% while the minimum inhibition rate was 5.2%. According to Equation 4.2 again, $Inhibition_{IC_{50}}\%$ was calculated as 42.6%, and Log_{10} [DOX, M] = −5.014 was obtained. Finally, IC_{50} of DOX to HCT116 human colorectal carcinoma cells was determined as **$IC_{50\ (DOX\ to\ HCT116)}$ = 9.68 µM.**

For easy calculation in future experiments, IC_{50} = 5 µM for KB cell line and IC_{50} = 10 µM for HCT116 cell line were adopted, respectively. Consequently, concentrations of 2.5 × IC_{50} (O'Neill, Ormerod et al. 1996; Keenan, Liang et al. 2004; Vandyke, White

et al. 2007) of DOX for the treatment of KB and HCT116, 12.5 μM and 25 μM respectively, were employed for the viability and drug uptake assays by exposure KB and HCT116 cells to DOX in the presence of carriers.

4.4.1.2 Cytotoxicity of encapsulated DOX by unmodified γ-CD and modified γ-CD carrier

To validate the encapsulation capability of the carrier, *in vitro* cytotoxicity experiments were performed at 37 ℃ for 30 min. Both KB and HCT116 cells were exposed to gradient ratios (100 : 1, 50 : 1, 25 : 1, 10 : 1, 5 : 1 and 2.5 : 1) of carrier-DOX complex and were compared with DOX alone and γ-CD associated DOX, while keeping constant concentration of DOX.

Table 4.1 Effect of carrier encapsulation on the viability of KB and HCT116 cells by DOX

		KB cells (Viability % of control)	HCT116 cells (Viability % of control)
Ratio of Carrier : DOX	100:1	95.5±3.4	92.7±3.4
	50:1	84.6±3.9	91.8±3.3
	25:1	84.1±6.8	78.7±2.0
	10:1	85.4±4.5	65.9±4.1
	5:1	66.5±2.4	59.2±4.8
	2.5:1	39.4±2.9	54.2±1.7
DOX alone	12.5 / 25 μM (KB / HCT116)	12.9±1.2	37.2±1.5
Carrier alone	1250 / 2500 μM (KB / HCT116)	100.7±2.6	97.8±2.0
γ-CD+DOX (100:1)	(125+12.5 μM)/(250+25 μM) (KB / HCT116)	24.7±3.5	37.9±0.8

*The data were compiled from five separate experiments performed in triplicates and were expressed as means±SD.

The MTT results (Table 4.1) show that this modified γ-CD derivative itself has no obvious cytotoxic effect on cancer cells, in which, 100.7 ± 2.6% viable KB cells and 97.8 ± 2.0% viable HCT116 cells were observed after exposure to 1250 μM and 2500 μM carrier, respectively. For both KB and HCT116 cell line, cell viability increased by increasing the concentration of carriers. Specifically, KB cells showed 85.4 ± 4.5%

viability when the ratio between carrier and DOX was 10 : 1, when the carrier to DOX ratio was increased to 25 : 1 and 50 : 1, The rates of viable KB cells (84.1 ± 6.8% and 84.6 ± 3.9%) were similar to that at 10 : 1, and at highest ratio of 100 : 1 of carrier to DOX, viability of KB cells increased to 95.5 ± 3.4%. In comparison to KB cells, HCT116 cells exhibited relatively lower cell viability when the same ratio of carrier and DOX was employed, 65.9 ± 4.1% at 10 : 1, 78.7 ± 2.0% at 25 : 1, and 92.7 ± 3.4% at 100 : 1.

In comparison to the exposure of DOX alone and DOX in the presence of unmodified γ-CD, inclusion of DOX by the modified carrier significantly reduced the toxicity of DOX in both KB and HCT116 cells: 12.9 ± 1.2 / 37.2 ± 1.5% of the cells were viable at the dose of 12.5 / 25 μM of DOX alone for KB / HCT116 cells; 24.7 ± 3.4 / 37.9 ± 0.8% of the KB/HCT116 cells were viable when exposed to DOX in the presence of unmodified γ-CD. In addition, 39.4 ± 2.9% of KB cells and 54.2 ± 1.7% of HCT116 cells were found viable in the presence of lowest concentration of modified γ-CD derivative when exposed to DOX, all higher than that of cells exposed to DOX alone or DOX associated by native γ-CD.

The above results indicate that the inclusion of DOX by the modified γ-CD derivative prevented DOX from eliciting cytotoxic effect on cultured human cancer cells. These results also validate that the encapsulation mechanism of CDs to drug molecules is in equilibrium: CDs+DOX⇆CDs-DOX; when the concentration of CDs is increasing, the equilibrium moves to the right side to form more CDs-DOX complex inclusion which causes higher encapsulation efficiency. Moreover, HCT116 cells showed again higher resistance (higher cell viability) to DOX than KB cells, which is consistent with the IC_{50} evaluation of DOX in both cell lines in section *4.4.1.1*. These results suggest that the optimal application ratio between the carrier and DOX is 10 : 1 especially for KB cell line, which further supported this conclusion obtained in section *3.4.4* in Chapter 3. Thus, ratio of 10 : 1 of carrier: DOX was adopted for a range of cellular drug uptake assays conducted in Chapter 5.

4.4.2 Cellular Drug Uptake

4.4.2.1 Cellular drug uptake under physiological conditions

Cellular DOX uptake investigation was performed to further confirm the encapsulation capability of the carrier. Similar to the above cytotoxicity assays, KB and HCT116 cells were exposure to gradient ratios (100 : 1, 50 : 1, 25 : 1, 10 : 1, 5 : 1 and 2.5 : 1) of carrier-DOX complex and were compared with DOX alone and γ-CD associated DOX, while keeping DOX's concentration constant. Drug exposure condition was 30 min at 37 ℃.

Table 4.2 Effect of carrier encapsulation on the uptake of DOX by KB cells and HCT116 cells

		KB cells (Uptake % of DOX alone)	HCT116 cells (Uptake % of DOX alone)
Ratio of Carrier : DOX	100:1	2.4±1.1	2.1±0.5
	50:1	4.6±0.6	3.6±0.2
	25:1	8.0±0.3	5.9±0.4
	10:1	13.3±2.4	11.5±0.5
	5:1	34.2±3.7	19.9±1.2
	2.5:1	53.1±4.5	35.7±2.9
γ-CD+DOX (100:1)	(125+12.5μM)/(250+25μM) (KB/HCT116)	61.7±5.3	58.9±3.6

*The results were compiled from five separate experiments performed in triplicates and were expressed as means±SD.

Table 4.2 presents the prevention effect of carrier on DOX from being up-taken by both KB and HCT116 cells. Cellular DOX uptake percentage gradually increased along with decreasing concentrations of carrier. In the presence of the carrier, DOX cellular uptake had minimum 46.9 ± 4.5% reduction to KB cells and 64.3 ± 2.9% reduction to HCT116 cells at carrier-DOX ratio of 2.5 : 1. In consistence with above DOX IC_{50} and cytotoxicity results, HCT116 cells behaved more resistant to DOX exposure as their DOX uptake was lower than those by KB cells in both absence and presence of carriers. Unmodified γ-CD demonstrated some encapsulation capacity towards DOX as cellular DOX uptake by KB and HCT116 cells was 61.7 ± 5.3% and

58.9 ± 3.6%, much lower than DOX alone exposure.

Overall, the cellular DOX uptake results confirmed the encapsulation capability of the carrier to DOX as well as validated that at carrier-DOX ratio of 10 : 1, the reduction of DOX uptake was as potent as 86.7 ± 2.4% and 88.5 ± 0.5% for KB and HCT116 cells. These results further suggested that the ratio of carrier and DOX at 10 : 1 may be suitable for future cell culture studies and *in vivo* trials.

To further quantify DOX uptake by cells in the unit of **μmol/μg total protein,** DOX calibration curves and BSA standard curve were obtained in each cellular uptake experiment. Figure 4.8 is an example of a DOX calibration curve up to DOX concentration of 1 μM (A), and a BSA standard curve (B).

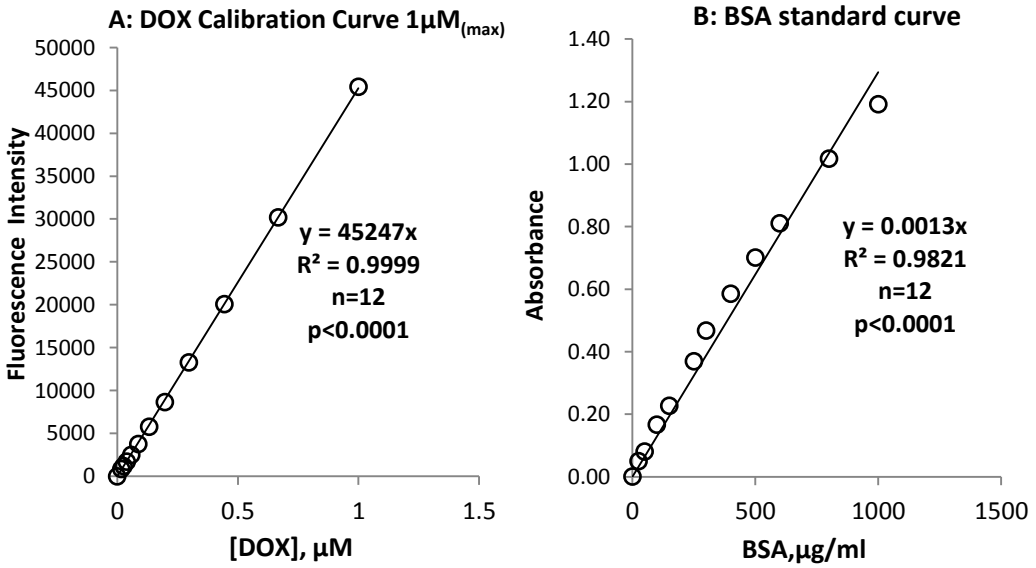

Figure 4.8 DOX calibration curve up to 1 μM at $\lambda_{excitation}$ = 485 nm, $\lambda_{emission}$ = 592 nm and optimal gain at 127 (A); BSA standard protein curve (B).

Taking the above Figure 4.8 as an example, if fluorescence intensity of tested sample is 30000, by substituting it into equation 30000 = 45247x_1, then x_1 = 30000 / 45247 = 0.66 (μM of DOX). If the same sample's BCA absorbance is 0.75, then 0.75 = 0.0013x_2, in which x_2 is equal to 0.75 / 0.0013 which is 576.92 (μg/mL). DOX cellular uptake per unit of total protein is then calculated as x_1 / x_2 = 0.66 / 576.92 = 1.14×10^{-6} μM/μg protein. This method will be applied in experiments wherever discussion of absolute amount of drug uptake is necessary.

4.4.2.2 Cellular drug uptake under hyperthermia

As described in Chapter 3, the modified γ-CD derivative was found to be thermo-sensitive. More cellular DOX uptake assays were performed by exposure of cancer cells to carrier-DOX under hyperthermia conditions (42 ℃ and 50 ℃) to validate carrier's thermo-responsivity in cell culture application. KB and HCT116 cells were exposed to various ratios (100 : 1, 50 : 1, 25 : 1, 10 : 1, 5 : 1 and 2.5 : 1) of carrier-DOX complex and the drug uptake was compared with DOX in the absence of carrier at 37 ℃, 42 ℃ and 50 ℃ for 5 min, respectively.

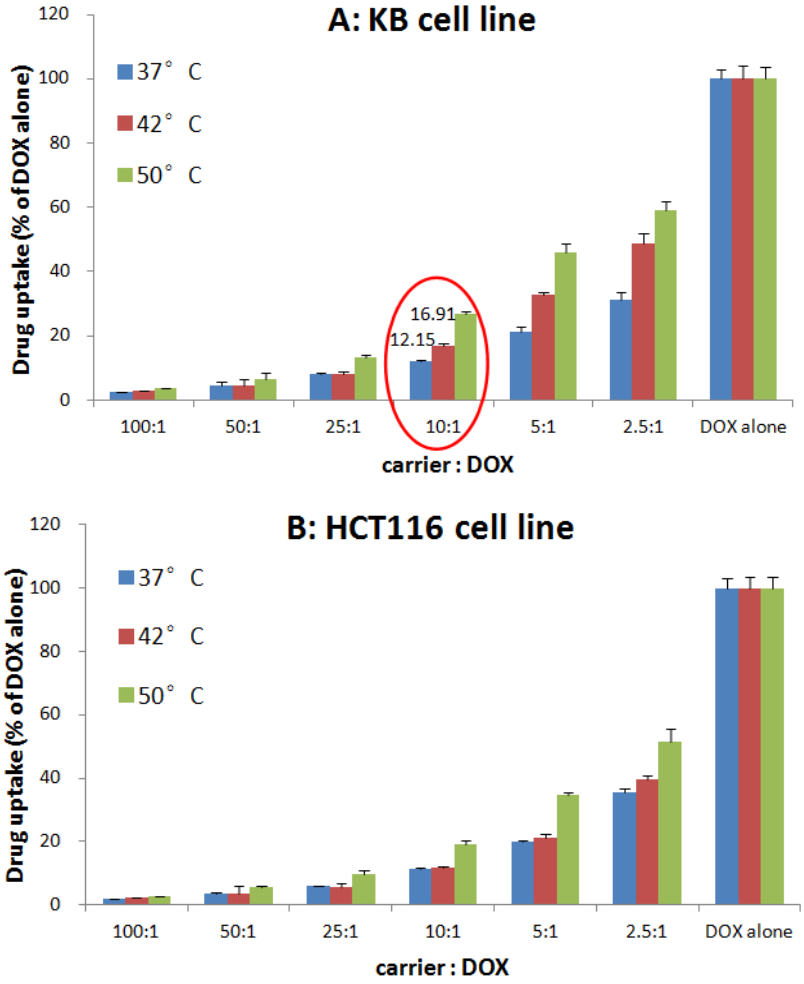

Figure 4.9 Effect of carrier encapsulation on the uptake of DOX by KB cells (A) and HCT116 cells (B) under hyperthermia conditions.

Figure 4.9 depicts DOX cellular uptake by exposure of human cancer cells to carrier-DOX complex under hyperthermia conditions, 42 ℃ and 50 ℃ in comparison to physiological temperature (37 ℃). DOX uptake by KB cells exhibited clear trend

that the uptake was increased by increasing exposure temperatures. For HCT116 cells, there was a slight increase of uptake when temperature was risen from 37 ℃ to 42 ℃. At higher temperatures (50 ℃) DOX cellular uptake was significantly increased compared to lower temperatures exposure.

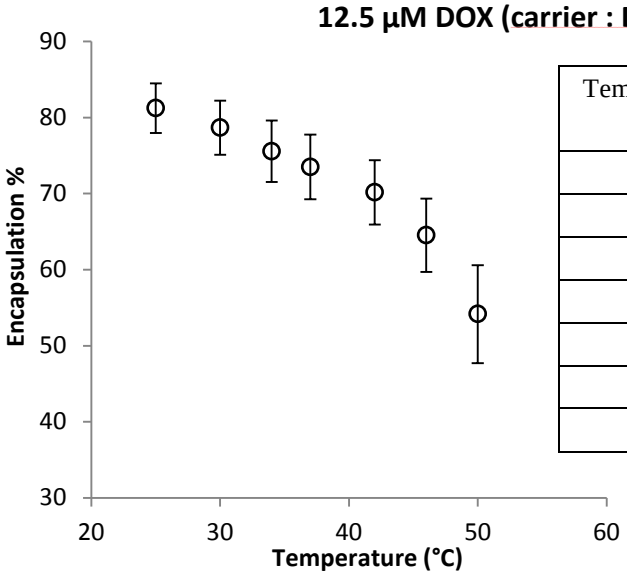

Temperature (℃)	Encapsulation (%)
25	81.23±3.25
30	78.66±3.56
34	75.55±4.03
37	73.50±4.25
42	70.16±4.23
46	64.53±4.82
50	54.17±6.44

Figure 4.10 DOX release correlation with temperature changes.

Figure 4.10 shows the correlation between temperature rise and DOX release rate from the carrier through carrier-DOX binding investigation. The drug release was 3.34% when temperature increased from 37 ℃ (73.50 ± 4.25% encapsulation) to 42 ℃ (70.16 ± 4.23% encapsulation) (see the table within Figure 4.10). And the increase of DOX cellular uptake in KB cells was 4.76% according to Figure 4.9 A (red circled), higher than DOX release rate of 3.34%. It should be noticed that the binding test between carrier and DOX conducted in Chapter 3 went through 30 min hyperthermia incubation without cells; while in the hyperthermia uptake assay reported here, cells were only treated by 5 min 'heat shock' and nonetheless showed higher uptake rate.

Therefore, these results suggest that hyperthermia may have two effects on cellular drug uptake. The first effect is hyperthermia triggered DOX release from the encapsulated carrier-DOX inclusion which has been confirmed in Chapter 3 by the observation that binding affinity between carrier and DOX decreased when

temperatures increased; the second effect is that hyperthermia may enable the enlargement of pore size of cell membranes to allow more DOX enter the tumour cells, as thermal treatment has been shown to enhance permeability of cells (Ponce, Vujaskovic et al. 2006; Cabuy 2011).

4.4.3 Statistical Analysis

All cytotoxicity and drug uptake data were expressed as mean ± SD (standard deviations). *P* values for expressing differences between DOX alone / carrier+DOX treated samples and controls were calculated by unpaired two-tailed equal variance Student's t-test. Statistical significance was set at $p < 0.05$.

4.5 Conclusions

To summarise, the encapsulation potency of modified γ-CD derivative for DOX has been validated and confirmed by a range of cytotoxicity and cellular drug uptake evaluations in comparison to the exposure of drug alone and drug plus unmodified γ-CD. The encapsulation efficiency was potent enough at 10 part of carrier with 1 part of DOX; the ratio of 10 : 1 was further employed in sonoporation experiments in Chapter 5. The cell culture studies further confirmed the thermo-sensitive property of the novel modified γ-CD carrier, suggesting that this delivery system may have the potential to be used in chemotherapy in combination with heat treatments, such as RFA, microwave hyperthermia and HIFU.

Chapter 5

In vitro FUS Sonication Investigation by A Standardised High Throughput Ultrasound Device

5.1 Introduction

As discussed in Chapter 2, US may play an increasing role in medical applications because of its thermal and mechanical effects on tissue, cells and bio-molecules, expanding its traditional applications from imaging and diagnostics to therapeutics. While hyperthermia and ablation with HIFU (ter Haar 2001) are better established therapeutic methods, there is very significant research interest in ultrasound-mediated delivery of therapeutic agents to cells and solid tumours (Lavon and Kost 2004; ter Haar 2007; Deckers and Moonen 2010) including chemotherapeutics, genetic material (Hernot and Klibanov 2008), proteins and small molecules (Pitt, Husseini et al. 2004).

US in focused form is thus expected to play an important role in future medical technologies (Jolesz and McDannold 2008) with potential major benefits including significantly reduced side effects via efficacious and targeted delivery of drugs. To translate the benefits of FUS into drug delivery for medical therapies, there is a need for an increase in experiments *in vitro* to form the basis of preclinical and *in vivo* studies.

Referring to the experimental methodology reported in pioneers' work on cell sonoporation, several common features of setups are:

1) Most of the *in vitro* ultrasound exposure was conducted for cell suspensions (Ashush, Rozenszajn et al. 2000; Sundaram, Mellein et al. 2003; Karshafian, Bevan et al. 2009);

2) Sonications were performed in dedicated chambers (Guzman, Nguyen et al. 2001; Feril, Kondo et al. 2002; Deng, Sieling et al. 2004), in Opti-cell environments

(Eisenbrey, Huang et al. 2009; Feril, Tachibana et al. 2010) or in wide petri-dishes (Hundt, Steinbach et al. 2009; Conti, Grimaldi et al. 2010);

3) Most of the acoustic sources were bespoke transducers (Wang, Xu et al. 2010; Yudina, Lepetit-Coiffe et al. 2011).

However, *in vitro* studies concerning the action of FUS by using piezoceramic bowl transducers with cells cultured in monolayers in a 96-well plate presently lack a standardised way to deliver the FUS and the comparative evaluation is difficult.

In this chapter, a new high-throughput *in vitro* sonicator device is described, which was designed in the Nanoporation project based on the results obtained by Gerold *et al.*(Gerold, Gourevich et al. 2012). Sonoporation procedures in combination with USCA SonoVue® MBs were applied to monolayers of human cancer cells cultured in 96-well plates and, through testing of cells' viability, the drug release and cellular uptake of DOX from the modified γ-CD carrier-DOX inclusion discussed in the previous two chapters was determined.

This chapter puts forward results obtained by application of FUS in the absence / presence of MBs with low mechanical indexes, under which negligible thermal effects were observed. AFM was employed for preliminary analysis of membrane morphology of cancer cells upon exposure to FUS. A thermal camera and thermocouples were employed to monitor temperature changes during the application of FUS.

5.2 In vitro Micro-scale Sonicator

5.2.1 FUS: Principles and FUS Device for TDD

Similar, in principle, to using magnifying glass to focus multiple beams of light to a single point, ultrasound can be focused: 1) geometrically via a lens such as a polystyrene lens or a spherically curved transducer; 2) electronically via a phased array (the relative phases of electrical signals to an array of elements that comprise a transducer); and 3) effectively by resonant electrical excitation of thin plates of a suitable piezoceramic, in the required frequency region (Hill and ter Haar 1995).

In general, the interaction between FUS waves and biological tissue can be divided into thermal and non-thermal (mechanical) effects (Jenne, Preusser et al. 2012), have been discussed in Chapter 2. However, thermal and mechanical effects of FUS propagation through tissue or cells can be described, and thus controlled, through a number of parameters that depend on the source characteristics and medium properties.

When ultrasound travels through a medium, the intensity decreases as the energy of the wave is absorbed by the medium and as a result, local heating can occur. The intensity (I, W/m^2) of a FUS beam (Hoskins, Martin et al. 2010) produced by a FUS source (transducer) is defined as the acoustic power (P_{ac}, W), or the rate at which the energy of the FUS is produced by the source, flowing through the cross sectional area of the beam (S, m^2), shown in Equation 5.1:

$$I = \frac{P_{ac}}{S}$$

Equation 5.1 Calculation of FUS beam intensity according to acoustic power.

The intensity is also proportional to the acoustic pressure, P (MPa), as shown by the following Equation 5.2 (Husseini and Pitt 2008):

$$I = \frac{P^2}{Z}$$

Equation 5.2 Calculation of FUS beam intensity according to acoustic pressure.

Where, Z (Pa · s/m or N · s/m^3) $= \rho \times c$, is the acoustic impedance of the medium, ρ (kg/m^3) is the density of the medium and c (m/s) is the speed of sound in that medium. Mechanical effects of ultrasound propagating through a medium can be estimated from P, which is a function of the acoustic power, calculated using both Equations 5.1 and 5.2 to obtain Equation 5.3:

$$P = \sqrt{\frac{P_{ac} \times \rho \times c}{S}}$$

Equation 5.3 Correlation between acoustic power and pressure.

If the medium contains gas MBs (ultrasound contrast agent), the FUS pressure waves can induce oscillations (volume changes) in the MBs at lower values, and generate violent collapse (inertial cavitation) at higher pressures. A useful parameter which can give a qualitative indication of the likelihood of cavitation is the mechanical index (MI) (Duck, Baker et al. 1998) expressed in Equation 5.4:

$$MI = \frac{PNP}{\sqrt{f}}$$

Equation 5.4 Calculation of mechanical index (MI).

Where, *PNP* is the peak negative pressure normalised to 1 MPa and *f* (MHz) is the centre frequency of the FUS field normalised to 1 MHz. As MI gives an estimation of the risk of the non-thermal effects including cavitation and streaming, thus, MI is most applicable with the use of ultrasound contrast agents. It is well documented that when MI < 0.3, it is preserving the contrast agents; while MI > 0.7 means cavitation risk is existing (De Jong 2002).

A large number of experimental and acoustic parameters are used in the relevant literature including frequency of acoustic field, intensity, power, pressure, mechanical index, exposure duration, total energy delivered and others, in relation to FUS field interacting with the biological material or gas MBs. When the large volume of studies in TDD is taken into account, this makes determining the optimum drug delivery system for a specific type of cancer virtually impossible. Moreover, the issue of repeatability in FUS-mediated TDD *in vitro* experiments has been highlighted in recent reports (Hensel, Mienkina et al. 2011; Leskinen and Hynynen 2012), which specifically note that the methods of FUS exposure and the experimental conditions vary greatly between investigators, making it difficult to compare results. It has also been highlighted that there is an increased need for standardisation of experimental conditions and the reporting of FUS exposure levels (ter Haar, Shaw et al. 2011).

5.2.2 Standardisation of *in vitro* FUS Device for TDD

It is common in FUS-mediated TDD experiments, to use a simple setup containing a transducer as an ultrasound source and a chamber containing a cell suspension as the target. However, a standard 96-well plate is best accommodated by most biological sample characterisation equipment. Transfer of biological samples for characterisation, after FUS exposure, from a suspension chamber to a 96-well plate, is likely to generate less accurate results. Therefore it was decided to carry out the experiments directly in the 96-well plates.

To address this fundamental issue, a high-throughput sonication device was designed (section 1 in Appendices) to be small, robust and portable, and capable of generating customised and highly reproducible FUS conditions for a wide range of experiments *in vitro*, allowing sonication of the contents in selected wells or sequences of wells within standard 96-well cell culture plates (or other plates) in a short period of time. The rationale behind using the 96-well cell culture plate is to allow a large number of repetitions and also accurate and identical sonication of various sample groups on the same plate, including control groups used as references for drug uptake, sonoporation or MBs effects, creating a *lab-on-a-bioplate* approach. One of the advantages of this device is that it allows a large number of experiments under similar US exposures, as well as significant flexibility in experiment design on the same 96-well plate and is, uniquely, reported in sufficient detail here for the work to be reproduced fully and accurately.

The high-throughput experiments were initially approached through a clinical MRgFUS system, ExAblate 2000/2100 for *in vitro* TDD experiments (Gourevich, Dogadkin et al. 2013). Although this approach could be useful for translation of *in vitro* results to *in vivo* experiments, due to limitations such as the multifocal sonication (16 foci) on the clinical multi-element transducer (ExAblate 2100 Conformal Bone System) only 16 wells per plate could be used. Moreover, a rapid sequence of sonications on the clinical machine is difficult to obtain since this would require the repetition of treatment planning procedures, which are time consuming. The very high costs associated with

such a clinical FUS device in combination with a bulky MR system, also render the approach impractical for *in vitro* testing in a laboratory.

5.3 Materials and Methods

5.3.1 Materials

5.3.1.1 *In vitro* cell culture, medium and supplementation

Medium, supplementation and reagents	Manufacturer and place of origin	Specification
KB cell line	American Tissue Culture Collection, USA	CCL-17
HCT116 cell line	American Tissue Culture Collection, USA	CCL-247
Fetal Bovine Serum (FBS)	Gibco Invitrogen, UK	Origin: South America
Roswell Park Memorial Institute (RPMI)1640 complete medium	Gibco® Invitrogen, UK	[+] 10% Fetal bovine serum (FBS) [+] 1% L-Glutamine [+] 1% Penicillin and Streptomycin (Pen-Strep) [+] 1% Sodium Pyruvate [+] 1% Non-essential Amino Acids [+] 0.5% HEPES buffer
Dulbecco's Modified Eagle's Medium (DMEM) complete medium	Gibco® Invitrogen, UK	[+] 10% Fetal bovine serum (FBS) [+] 4.5g/L D-Glucose [+] 1% L-Glutamine [+] Pyruvate [+] Penicillin and Streptomycin (Pen-Strep)
Phenol Red Free Dulbecco's Modified Eagle's Medium (DMEM)	Gibco® Invitrogen, UK	[+] 4.5g/L D-Glucose [+] L-Glutamine [+] 25Mm HEPES [−] Sodium Pyruvate

5.3.1.2 Other reagents

Medium, supplementation and reagents	Manufacturer and place of origin	Specification
Trypsin-Ethylenediaminetetraacetic acid (EDTA)	Gibco® Invitrogen, UK	0.05%
Dimethyl Sulphoxide (DMSO)	Sigma-Aldrich, UK	Biotechnology use, sterile filtered, endotoxin tested, hybridoma tested
Sodium Dodecyl Sulfate (SDS)	Sigma-Aldrich, UK	0.05% (w/v) in $_{dd}H_2O$
3-(4,5-Dimethylthiazol-2-yl)-2,5-diphenyltetrazolium bromide (MTT)	Sigma-Aldrich, UK	5 mg/mL in PBS
Bicinchoninic Acid (BCA) Protein Assay Kit	Sigma-Aldrich, UK	Solution A: bicinchoninic acid, sodium carbonate, sodium tartrate, sodium bicarbonate in 0.1 N NaOH (final pH 11.25). Solution B: 4% (w/v) copper(II) sulfate pentahydrate
Protein Standard (Bovine Serum Albumin –BSA)	Sigma-Aldrich, UK	1.0 mg/mL bovine serum albumin in 0.15 M NaCl with 0.05% sodium azide
Doxorubicin (DOX)	Mesochem Technology Co.,Ltd, Beijing, China	Purity ≥ 98%
Sonovue®	Bracco, Italy	
Terephthalic Acid (TA)	Sigma-Aldrich, UK	
Hydroxyterephthalic Acid (HTA)	Sigma-Aldrich, UK	
PBS tablets	Oxoid, UK	Typical Formual (g/L): Sodium chloride (8.0); Potassium chloride (0.2); Di-sodium hydrogen phosphate (1.15); Potassium dihydrogen phosphate (0.2). 1tablet/100mL, pH 7.3±0.2 at 25℃

5.3.1.3 Other consumables

Other consumables	Manufacturer and place of origin	Specification
Distilled/deionised water	Millipore, UK	
Cell culture flasks	Techno Plastic Products (TPP), Switzerland	75 cm^2
96-well plates	Greiner, Austria	Polystyrene cell culture black microplates with µClear® bottom
Titer Tops™ sealing film	ESM, USA	
Multi-mode plate reader	Tecan, Austria	Tecan infinite M200
Atomic Force Microscopy (AFM)	Bruker AXS, Cambridge, UK	BioScope Catalyst
Thermocouples	Omega, UK	Type T, PTFE-insulated Cu-Constantan, 0.076 mm wire diameters
Thermocouple data logger	Omega, UK	TC-08
Infrared (IR) thermo camera	FLIR, UK	JADE
RF power amplifier	Electronics and Innovation, Rochester, NY, USA	A075
LabVIEW	National Instruments, UK	

5.3.2 Methods

5.3.2.1 KB cell line viability screening

To demonstrate accuracy and repeatability combined with high-throughput, that all facilitate a standardised experimental system (sonicator, section 1 in Appendices) for TDD *in vitro*, a wide range of cell viability tests were performed under various sonication sequences with different set of FUS parameters (frequencies, MI, power, duration, mode: continuous or pulsed) for human nasopharyngeal epidermal carcinoma KB cell line.

In KB cells viability screening assays, FUS was applied at available frequencies: f = 0.4868, 1.142, 1.467 and 2.022 MHz, in continuous / pulsed FUS exposures with various acoustic intensities and sonication durations. Plate arrangement for sonications can be seen from Figure 5.1.

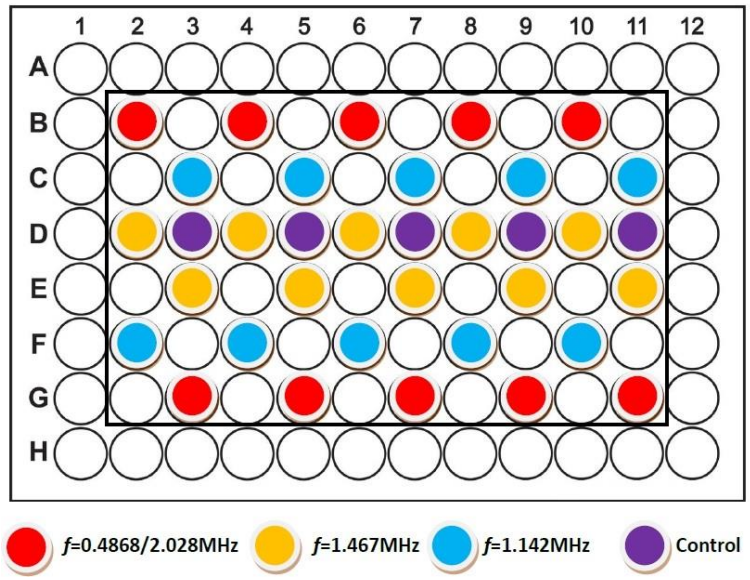

Figure 5.1 Protocols of KB cells viability screening by each transducer in a 96-well plate. Colour filled wells were treated by various sets of FUS parameters and selected control wells (purple) without FUS treatment.

KB cell viabilities were screened by sonications within the parameter range shows in Table 5.1 by four transducers.

Table 5.1 Sonication parameters range for KB cell viability screening

	Continuous Wave		Pulsed Wave		
Transducer frequency (MHz)	**Intensity (W/cm^2)**	**Duration (sec)**	**Intensity (W/cm^2)**	**Duration (sec)**	**Duty Cycle (%)**
0.4868	14.04 – 61.7	60 – 300	14.04 – 61.7	180 – 300	20
1.142	17.72 – 277.87	40 – 600	116.25 – 195.65	60 – 180	10, 15, 20
1.467	63.36 – 1339.51	40 – 300	575.12 – 1011.33	60 – 180	10, 15, 20
2.022	58.08 – 1665.94	40 – 300	623.3 – 1127.73	60 – 300	10, 15, 20

KB cell viability was calculated according to Equation 5.5:

$$Viability\% = \frac{OD_{cell+FUS} - OD_{blank}}{OD_{control} - OD_{blank}} \times 100\%$$

Equation 5.5 Cell viability calculation after sonication treatment.

Where, $OD_{cell+FUS}$ is the absorbance of cells sonicated by FUS, $OD_{control}$ is the absorbance of control cells without FUS treatment, OD_{blank} is the MTT reading of

CM without cultured cells.

5.3.2.2 Temperature evaluation in the 96 wells by thermal camera and thermo-couples

The thermal effect generated by the sonicator transducer at f = 0.4868 MHz was evaluated by FLIR thermal camera and Omega type T, PTFE-insulated Copper-Constantan thermocouples respectively to investigate temperature rising within selected sonication parameters in the absence / presence of SonoVue® MBs.

Thermal camera

Infrared (IR) camera is a device that forms an image by using IR radiation rather than visible light used by normal camera. Instead of the 450 – 750 nm range of the visible light camera, IR cameras operate in wavelengths as long as 14 μm. These IR rays were mainly devoted to thermal measurement (Herschel 1800; Corsi 2014).

Thermal camera was employed to monitor temperature changes of medium filled in wells of 96-well plate during sonication treatment. By using the IR thermal camera (Figure 5.2 A), which was placed above a partially submerged 96-well plate placed inverted inside the sonicator, focusing vertically against the transducer which is underneath of the focused single well of a 96-well plate (Figure 5.2 A). Temperatures within captured region can be selected and analysed according to points of interest, such as marked positions 4 (the well is being sonicated), 5 (the well will be sonicated next) and 6 (the well has just been sonicated) in Figure 5.2 B.

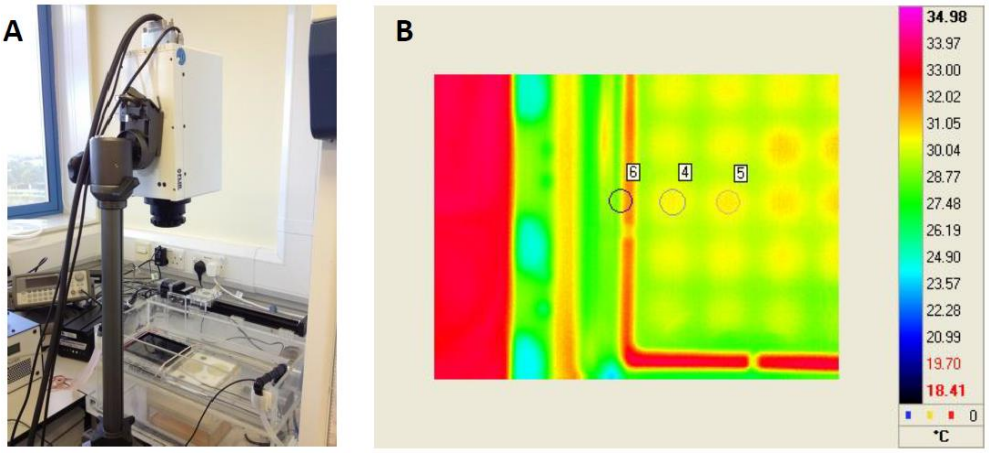

Figure 5.2 IR thermal camera vertically setting up on top of the plate placed inside the sonicator (A); Thermal camera imaging region of a 96-well plate, where, the transducer is focused at marked position 4 underneath the plate (B).

Thermocouples

Type T PTFE-insulated Copper-Constantan precision fine wire thermocouples (diameter 0.07 mm) were used to do the same temperature evaluation, aimed to confirm the results obtained from IR thermal camera experiments. Type T thermocouples were selected due to their wide range of temperature measurement (from –200 ℃ to 350 ℃) and relatively low error (1 ℃ or 0.75% above 0 ℃ and 1 ℃ or 1.5% below 0 ℃) (Omega-Thermocouple Reference Tables Type T).

In the current study, Type T thermocouples were placed inside of each well by drilling a small hole in the center of each well from the bottom of plate, and thermocouples were fixed and sealed by clear glue (Figure 5.3).

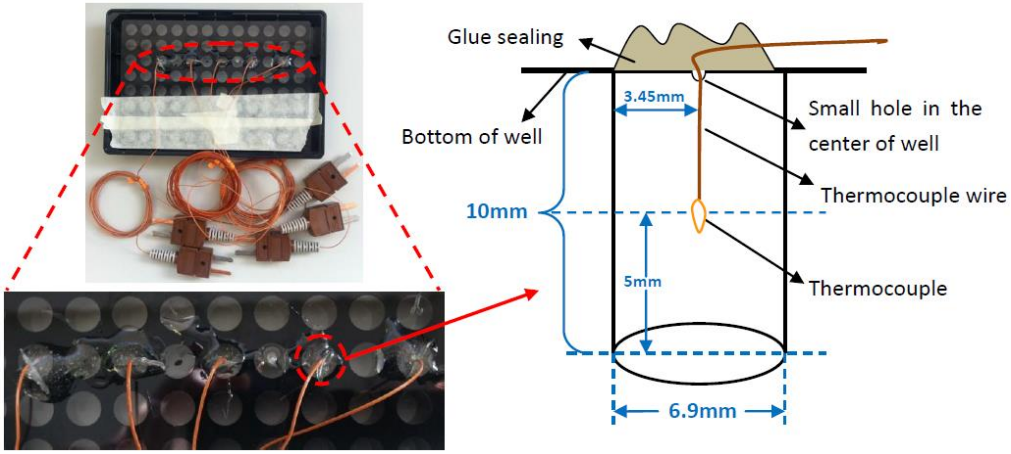

Figure 5.3 Thermocouples fixed inside wells from bottom of the μclear 96-well plate and sealed by glue.

Thermocouples were then connected to a Pico TC-08 thermocouple data logger (Figure 5.4) and real-time temperatures in wells were recorded by data acquisition software (Picolog).

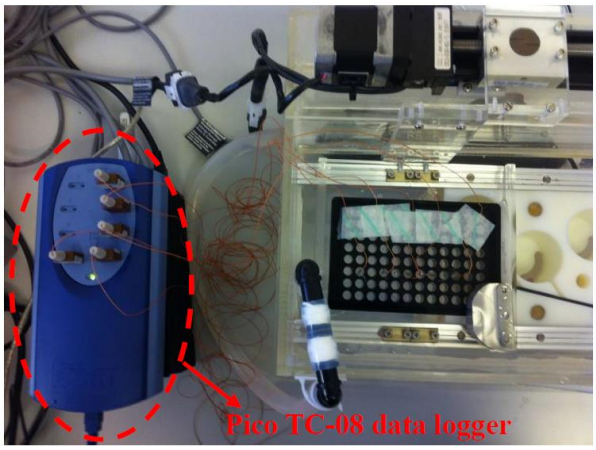

Figure 5.4 Thermocouples connected to a Pico TC-08 thermocouple data logger.

For both thermal camera and thermocouples temperature evaluations, test solution was prepared by using serum free PRMI1640 / DMEM medium in the absence / presence (0.1%, 1%, 2.5% and 5%) of SonoVue® MBs. Sonication parameters were applied at: MI = 0.24, 0.31 and 0.53; sonication duration = 10 sec at continuous FUS wave.

5.3.2.3 Stable / inertial cavitation detection

Although the mechanism of US-mediated TDD has not been fully understood (Pitt, Husseini et al. 2004; Myhr and Moan 2006), its function is normally divided into thermal effects and non-thermal effects (Afadzi, Davies Cde et al. 2012). Among all the non-thermal effects, as introduced in section *2.3.3* in Chapter 2, FUS induced acoustic cavitation is the most important non-thermal mechanism and it has been shown to play a critical role in a wide range of novel therapeutic ultrasound applications during last two decades (Coussios, Farny et al. 2007).

Cavitation can be classified into two types: stable cavitation and inertial cavitation (Naji Meidani and Hasan 2004). Stable cavitation generally refers to lower intensity insonations, whereby bubbles undergo stable, low amplitude oscillations. In contrast, inertial cavitation is associated with high intensity insonation, with bubbles undergoing significant volume fluctuations, and strong, violent collapses (Leighton 1994; Young 1999; Leighton, Cox et al. 2000). Such bubble collapses can produce intense local (core) heating (5000 K) and high pressure (~ 1000 atmospheres) (Leighton, Cox et al.

2000).

Inertial cavitation can also generate free radicals from the breakdown of water and other molecules to form radical-containing chemical species (McLean and Mortimer 1988; Mason, Lorimer et al. 1994; Fang, Mark et al. 1996). The specific mechanism is the acoustic energy level achieved which can lead to the homolytic cleavage of covalent bonds between the oxygen and hydrogen atoms comprising water molecules. Water sonolysis then leads to the formation of reactive oxygen species such as hydroxyl radicals (OH·) and hydrogen peroxide (H_2O_2) according to the following chemical reactions (Villeneuve, Alberti et al. 2009):

$H_2O \rightarrow H\cdot + OH\cdot$

$H\cdot + O_2 \rightarrow HO_2\cdot$

$HO_2\cdot + HO_2\cdot \rightarrow H_2O_2 + O_2$

$OH\cdot + OH\cdot \rightarrow H_2O_2$

$H + H_2O \rightarrow H_2OH\cdot$

In order to investigate whether inertial cavitation induced by FUS, the measurement of the OH radicals dissolved in sonication treated liquid was conducted by using chemical dosimetry method based on terephthalic acid (TA). TA is a well-known OH scavenger which has no chemical reactions with other radicals such as HO_2 and H_2O_2 (Kanazawa, Furuki et al.), TA is also a non-fluorescent compound. When inertial cavitation happens, the generated OH radical can convert TA to a fluorescent compound 2-hydroxyterephthalic acid (HTA) according to Reaction 1:

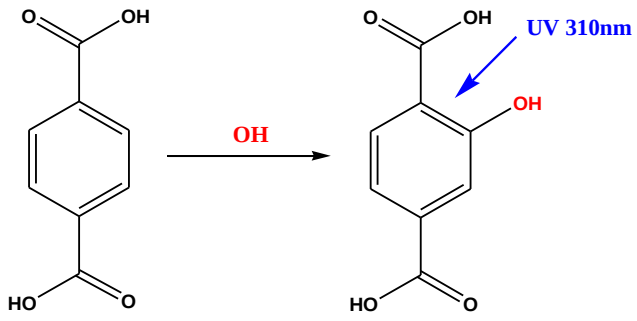

TA (Non-fluorescent) **HTA (Fluorescent 425nm)**

$C_6H_4(COOH)_2 + OH \rightarrow C_6H_4(COOH)_2OH$

Reaction 1 Terephthalic acid (TA) is converted by free OH radical to 2-hydroxyterephthalic acid (HTA).

Where, the fluorescence intensity of HTA can be detected by fluorescence spectroscopy with excitation and emission wavelengths at 310 nm and 425 nm respectively.

Initial TA solution was prepared by dissolving 16 mg TA powder by 0.5 ml NaOH (5 mM), as TA cannot be dissolved in acidic or neutral solutions (Mason, Lorimer et al. 1994). The solution of dissolved TA in NaOH was then diluted to 50 mL by $_{dd}H_2O$ to achieve the concentration of TA at 2 mM. Sonications were then performed by using transducer f = 0.4868 MHz, with $0.24 \leq$ MI ≤ 0.91 and sonication duration of 10 sec in the absence / presence of 2.5 / 5% SonoVue® MBs according to protocols in Figure 5.5. Fluorescence intensities of sonicated TA were recorded at $\lambda_{excitation}$ = 310 nm and $\lambda_{emission}$ = 425 nm before and after sonication.

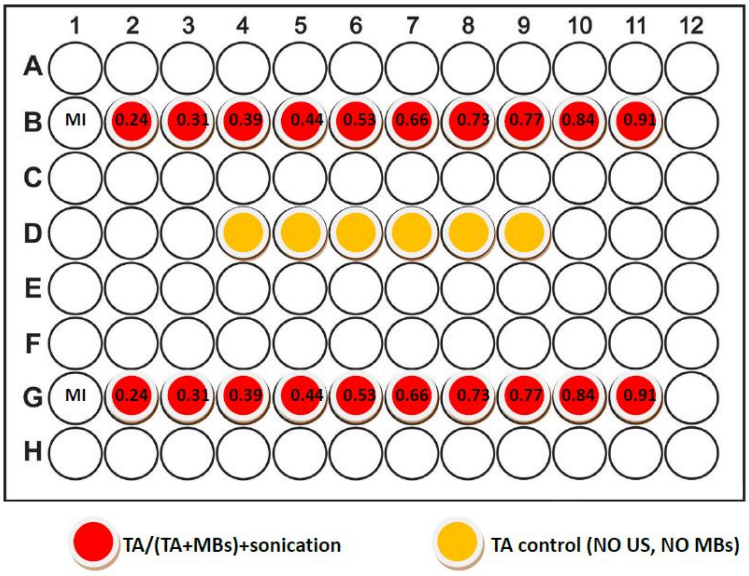

Figure 5.5 Protocols of TA solution sonication.

5.3.2.4 Carrier-DOX binding investigation by exposure to FUS

Certain groups of FUS parameters were employed to the carrier-DOX inclusion complex introduced in Chapter 3 by the *in vitro* sonicator, to investigate the responsivity of the carrier-drug system to FUS mechanical effects. Serum free RPMI1640 / DMEM medium was prepared as test solution in the absence / presence (0.1%, 1%, 2.5% and 5%) of SonoVue® MBs. Sonication parameters were: MI = 0.24, 0.31 and 0.53; sonication duration = 10 sec at continuous FUS wave.

Similar as the $K_{binding}$ investigation performed in section *3.3.2.2b* in Chapter 3, test

solutions' fluorescence intensities were recorded before and after FUS treatment, and the drug release rate after sonication was calculated according to Equation 5.6:

$$Encapsulation\% = \frac{I_{(carrier+DOX)}}{I_{DOX}} \times 100\% \quad (1)$$

$$Release_{DOX}\% = Encapsulation\%_{before\ US} - Encapsulation\%_{after\ US} \quad (2)$$

Equation 5.6 Encapsulation and release rate of DOX after FUS sonication treatment in the absence/presence of MBs.

In Equation 5.6 (1), $I_{(carrier+DOX)}$ is the fluorescence intensity of encapsulated DOX with / without FUS sonication treatment in the absence / presence of MBs, while I_{DOX} is fluorescence intensity of DOX alone solutions with / without FUS sonication treatment in the absence / presence of MBs. In Equation 5.6 (2), $Encapsulation\%_{before\ US}$ and $Encapsulation\%_{after\ US}$ were both obtained from Equation 5.6 (1) for each test samples before and after FUS treatment.

5.3.2.5 Cell viability test

After KB cells viability screening assays, more cell viability tests were focused on the application of f = 0.4868 MHz transducer in the presence (0.1%, 1%, 2.5% and 5%) of SonoVue® MBs. Two human cancer cell lines KB and HCT116 were selected. Various solutions were added to each well according to the defined protocols in 5 replicates (Figure 5.6). Sonication parameters were: MI = 0.24, 0.31 and 0.53; sonication duration = 10 sec at continuous wave.

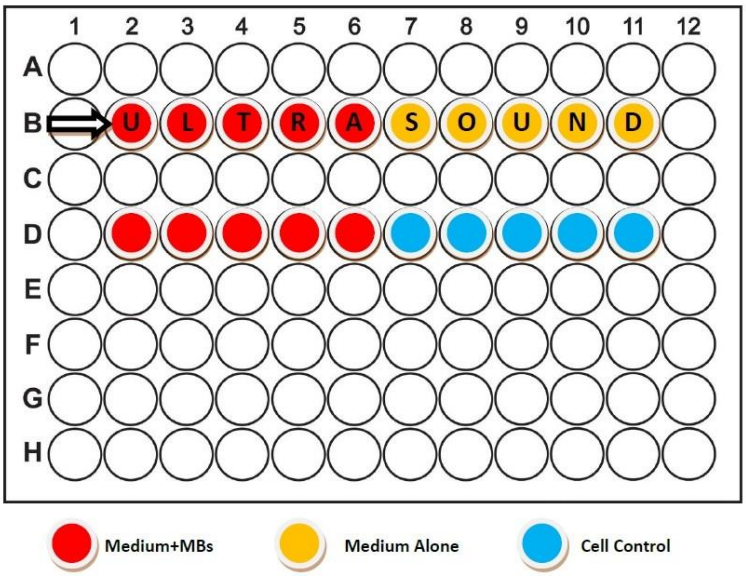

Figure 5.6 Protocols of cell viability sonication.

Cell viability in this section was calculated by Equation 5.7:

$$Viability\% = \frac{OD_{US/(US+MBs)} - OD_{blank}}{OD_{cell\ control} - OD_{blank}} \times 100\%$$

Equation 5.7 Cell viability calculation after FUS sonication treatment.

Where, $OD_{US/(US+MBs)}$ is the MTT absorbance of cells treated by FUS in the absence / presence of MBs, $OD_{cell\ control}$ is the MTT absorbance of cells without any treatment and OD_{blank} is the MTT absorbance of medium without cultured cells.

5.3.2.6 Cellular drug uptake test

Cellular drug uptake assay was performed to further investigate carrier-DOX inclusion's responsivity to FUS sonication, as well as the response of human cancer cells to FUS treatment. Sonication experiments were focused on the application of f = 0.4868 MHz transducer at FUS parameters without thermal effects but in the presence (0.1%, 1%, 2.5% and 5%) of SonoVue® MBs. DOX concentration was applied at 12.5 μM for KB cell line and at 25 μM for HCT116 cell line, the ratio of carrier-DOX was 10 : 1. Various solutions were added to each well according to the defined treatment groups in 5 replicates (Figure 5.7). Sonication parameters were: MI = 0.24, 0.31 and 0.53; sonication duration 10 sec at continuous wave.

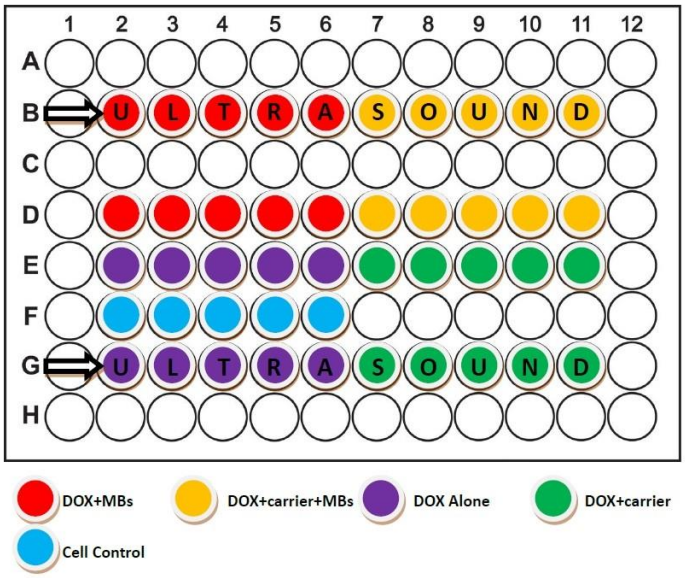

Figure 5.7 Protocols of cellular drug uptake sonication assays.

DOX cellular uptake calculation is according to Equation 5.8:

$$Uptake\% = \frac{I_{(US\pm MBs)_{DOX/(carrier+DOX)}} / OD_{(US\pm MBs)_{DOX/(carrier+DOX)}}}{I_{DOX\ NO\ US} / OD_{DOX\ NO\ US}} \times 100\%$$

Equation 5.8 Cellular drug uptake calculation after FUS sonication treatment.

Where, $I_{(US\pm MBs)_{DOX/(DOX+carrier)}}$ is the fluorescence intensity of the cell sample exposure to DOX alone / carrier+DOX with FUS treatment in the absence / presence of MBs, $OD_{(US\pm MBs)_{DOX/(carrier+DOX)}}$ is the BCA absorbance reading of those samples correspondingly. $I_{D□X\ NO\ US}$ is the fluorescence intensity of the cell sample exposed to DOX alone solution without FUS treatment, $OD_{DOX\ NO\ US}$ is the BCA absorbance of this cell sample.

5.3.2.7 Atomic Force Microscopy (AFM) cell membrane topography measurement

AFM is a high-resolution type of scanning probe microscopy (SPM). It utilises a fine tip to measure surface morphology and properties through an interaction between the tip and sample surface. In an AFM, a constant force is maintained between the probe and sample while the probe is raster scanned (parallel lines) across the surface.

By monitoring the motion of the probe as it is scanned across the surface, a three dimensional image of the surface is constructed (Quate and Gerber 1986). AFM thus becomes one of the foremost tools for imaging, measuring, and manipulating matter at the nanoscale.

In terms of biological applications, AFM is a well-established technique used to both image the topography of rigid / fixed samples (Langer and Koitschev 2002) and measure the mechanical properties of living material such as tissue and cells (Radmacher 1997). In this thesis report, Peak Force Quantitative Nano Mechanics (QNM), an extension of Peak Force Tapping mode in AFM was employed to investigate human cancer cell morphological and physico-mechanical behaviour changes in response to exposure to FUS.

AFM was employed to measure the short time membrane morphology changes of KB cells, which were exposed to different frequencies transducers for various sonication durations (sec), in the absence / presence of SonoVue® MBs. KB cells were seeded at a density of 8000 cells/well on sterilised glass cover slips (6 mm in diameter) placed in 96-well plates and incubated for 24 hr before FUS exposure. To be noticed that the glass cover slip did not influence the cells during sonication, as the cell culture plate was placed inverted and the monolayer of cells were facing to the transducer directly. Immediately after each FUS treatment, the medium was removed and cells were exposed directly to 200 μL/well of 2.5% (v/v) Glutaraldehyde fixed solution (freshly prepared on the day of the experiment), plates were placed in 4 ℃ fridge for 1 hr. After fixation, fixed solution was aspirated carefully; cells were then washed by PBS three times to remove residual fixed solution, and washed by distilled water for five times. After all washing procedure, the glass cover slips with fixed cells were taken out carefully from 96-well plates and fixed on the surface of glass slides, cells were allowed to dry at room temperature for another 2 hr.

Fixed and dried samples were then scanned in air at room temperature by BioScope Catalyst AFM in ScanAsyst imaging mode, using ScanAsyst in Air probe (tip radius: 2 nm), at scan frequency of 0.25 Hz with 384 scan lines per image.

5.3.2.8 General methods of cell seeding and solution preparation

Cell handling

KB and HCT116 were selected for FUS sonication experiments based on fundamental *in vitro* cell culture studies performed in Chapter 4. KB and HCT116 cells were cultured in complete RPMI1640 medium (section *4.3.1.2*, Chapter 4) and complete DMEM medium (section *4.3.1.2*, Chapter 4), respectively.

For cell viability investigations, KB / HCT116 cells were harvested from the flask and seeded in 96-well plates with μclear base at cell density 4000 cells/well in 100 μL complete medium (CM) 1 day prior to sonication. Cells were not plated in columns 1 and 12, rows A and H, but filled with CM as these are used as a blank for the plate reader to allow for the absorbance of the residual medium and MTT in the wells. Before sonication, up to 420 μL/well of CM was added in each well and the plate was sealed with Titer-Tops® (plate-sized US-transparent films, Figure 5.8 A), carefully avoiding air-bubble formation. After sealing, the plate was inverted and placed in the sonicator using the plate holder located above the FUS sources (Figure 5.8 B), so that the cells adherents to the μclear base were uppermost.

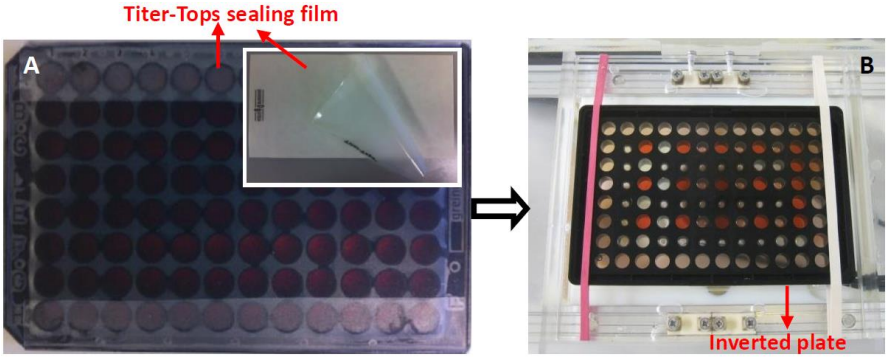

Figure 5.8 96-well plate fully filled with medium and sealed with Titer-Tops® sealing without air-bubble formation (A); Inverted plate with μclear bottom fixed in sonicator by plate holder and further fixed by rubber bands in both sides (B).

After sonication treatment, the wells were emptied of their entire volume of CM carefully and refilled with 100 μL/well fresh CM, cells were observed by microscope for cells detach inspection. Cells were then followed by incubation for a further 48 hr. Cell viability was evaluated by MTT colorimetric assay (section *4.3.2.1*, Chapter 4).

For cellular drug uptake investigations, KB / HCT116 cells were harvested from

flask and seeded in 96-well plate with μclear base at cell density 12000 cells/well in 100 μL CM and allowed to expand over 2 days prior to sonication. Before exposure to FUS, 420 μL of various solutions were added to each well according to the defined treatment groups in 5 replicates. After adding solutions, the plates were sealed with Titer-Tops® sealing film to maintain cell culture sterility. After sealing, the plate was inverted, so that the cells adherent to the μclear base were uppermost, and placed in the sonicator using the plate holder located above the FUS transducer sources and fixed.

At the end of FUS treatments, test solutions and CM in control wells were removed and the wells were washed by preheated PBS twice. Cells were observed under the microscope for cells lost inspection. PBS was then removed and 200 μL 0.5% SDS in $_{dd}H_2O$ were added to each well. Following observation under the microscope to ensure total cell disruption by SDS, quantification of the fluorescence intensity of intracellular DOX was recorded. The fluorescence readings were normalised by total protein amount by transferring 25 μL of cell lysates from the same samples to wells of a normal transparent 96-well cell culture plate for protein determination by using the BCA method (section *4.3.2.4*, Chapter 4).

5.3.2.9 Test solutions preparation

Solutions with SonoVue®

SonoVue® MBs stock solution (100%) were prepared according to its manufacture protocol (Figure 5.9) and kept in ice box after preparation.

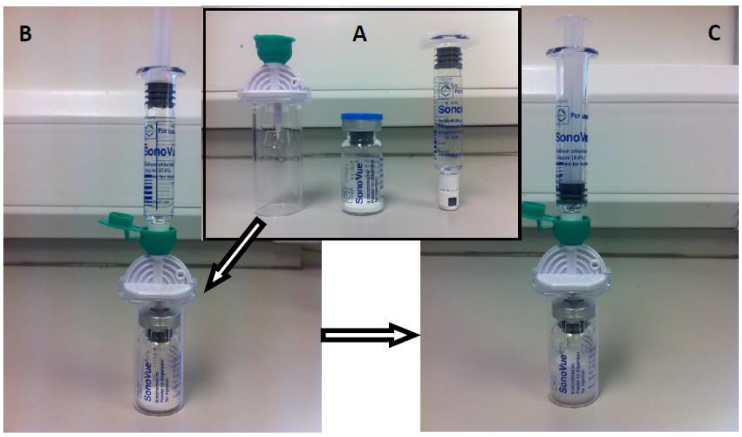

Figure 5.9 Preparation of SonoVue® stock solution.

In cell viability / AFM inspection assays, 1 μL/mL, 10 μL/mL, 25 μL/mL and 50 μL/mL MBs stock solution were added into CM to obtain SonoVue® MBs concentration at 0.1%, 1%, 2.5% and 5%, respectively. Similarly, in carrier-DOX binding investigation or cellular drug uptake assays, 1 μL/mL, 10 μL/mL, 25 μL/mL and 50 μL/mL MBs stock solution were added into DOX alone / carrier+DOX solutions to obtain SonoVue® MBs concentration at 0.1%, 1%, 2.5% and 5%, respectively.

DOX and carrier+DOX solutions

A solution of 100 mM DOX stock was prepared by dissolving 58 mg DOX powder in 1 mL DMSO and kept frozen. A solution of 12.5 / 25 μM DOX was prepared by dilution of the DOX stock solution (100 mM) by CM for KB and HCT116 cells accordingly. The final concentration of DMSO in the diluted solution is 0.0125 / 0.025%. To 50 mL of the final 12.5 / 25 μM DOX solution, 0.1875 / 0.375 mg/ml of carrier was added to obtain a concentration of 125 / 250 μM (10 : 1 carrier : DOX molar ratio). Preheated (20 min at 37 ℃) test solutions before exposure to cells. SonoVue® MBs stock solution (100%) were prepared according to its manufacture protocol and placed in ice box. 1 μL/mL, 10 μL/mL, 25 μL/mL and 50 μL/mL MBs stock solution were added into DOX / carrier+DOX and to obtain SonoVue® MBs concentration at 0.1%, 1%, 2.5% and 5% prior to sonication respectively.

SDS reagent

0.5% (w/v) SDS was prepared by dissolving 0.5 g SDS powder in 100 mL $_{dd}H_2O$, the solution was then stirred by magnetic plate stirrer until SDS salt dissolved completely.

MTT reagent

5 mg/ml MTT reagent was prepared by dissolving 250 mg of the MTT salt by 50 ml PBS. The solution was stirred by magnetic plate stirrer until all solid was dissolved. The solution was filtered using a 0.45 μm filter, then aliquoted 10 ml/tube and kept frozen (–20 ℃) until use.

BCA reagent

BCA reagent was freshly prepared on the day of the experiment, by mixing 50

parts of Bicinchoninic acid (reagent A) and 1 part of 4% (w/v) Copper sulphate solution (reagent B). Standard bovine serum albumin (BSA) solutions from 25 µg/mL to 500 µg/mL were prepared by diluting the standard BSA solution (1000 µg/mL) in the BCA kit by using the same cell lysis buffer (0.5% SDS).

5.4 Results and Discussion

5.4.1 Cell Viability Screening Results

An initial cell culture application by all frequencies (2.022, 1.467, 1.142 and 0.4868 MHz) of transducers has been employed through cell viability investigation by exposure KB cells to FUS source. Various combinations of US parameters (frequency, power, duration and US mode (continuous / pulsed), Table 5.1) have been applied in order to identify the optimal set of parameters in terms of safe mechanical response of equipment especially the power amplifier, FUS focused beam diameters, beam length (according to Table A.1 in Appendices) and temperature rising at different levels.

Transducer *f* = 2.022 MHz

For the transducer frequency of 2.022 MHz, KB cells were exposed to continuous FUS wave at power from 0.6 W to 17 W, and sonication duration from 40 sec to 300 sec; while in pulsed FUS wave mode, FUS power was applied from 6.5 W up to 12 W, sonication duration was from 60 sec to 300 sec, selected duty cycles were 10%, 15% and 20%.

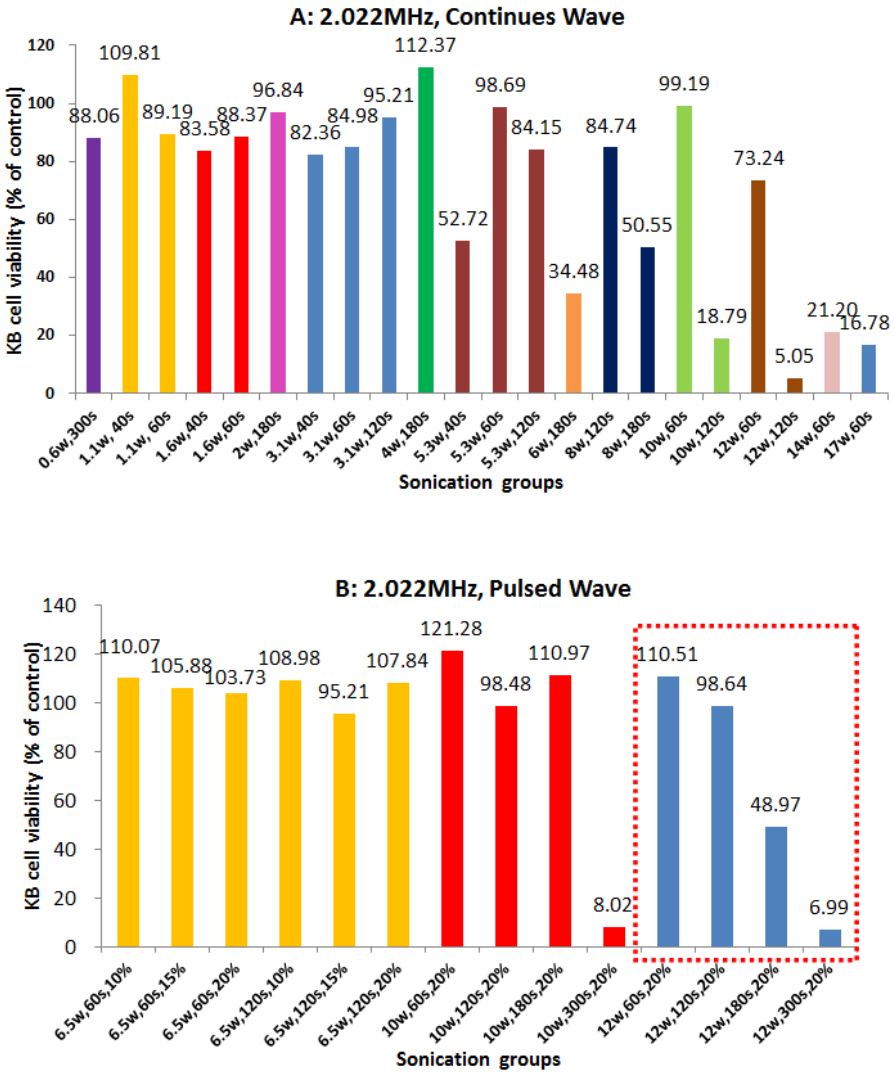

Figure 5.10 KB cells viability (% of control) 48 hr post transducer *f* = 2.022 MHz sonications. Continuous FUS wave mode (A); Pulsed FUS wave mode (B).

As can be seen from Figure 5.10 A, KB cell viabilities were all over 82.36% when continuous FUS was applied under or equal to 5.3 W (at sonication duration of 40 sec, viable KB cells of 52.72% was obtained; it is suggested that this is an error in comparison to other higher / longer treatments). When $6W \leq P_{ac} \leq 12$ W and sonication duration was under 120 sec, cell viabilities showed higher than 73.24%; while, within this power range but when longer durations (120 sec and over) were applied, cell viability had sharp decreases (all under 50.55%). Moreover, higher power of 14 W and 17 W induced lower cell viabilities when sonication duration was 60 sec.

In pulsed FUS sonications (Figure 5.10 B) mode, three FUS powers of 6.5 W, 10

W and 12 W were applied respectively, where, viable cells were over 95.21% when the power was lower than 10 W and sonication time was fewer than 180 sec. At FUS power of 12 W, cell viabilities decreased upon increased sonication durations at duty cycle of 20% (bars within the red square in Figure 5.10 B).

Transducer *f* = 1.467 MHz

In frequency of 1.467 MHz transducer's sonication, results obtained by employing continuous FUS wave (Figure 5.11 A) were similar in comparison to frequency of 2.022 MHz transducer. FUS power was applied from 0.78 W up to 17 W, sonication duration was from 40 sec to 300 sec. When FUS power was lower than 5.5 W, all treatment groups of cells responsed with high cell viabilities (over 74.39%); when FUS power was applied over 6 W (bars within the red square), KB cell death rate increased upon ever-increased both FUS power and sonication duration.

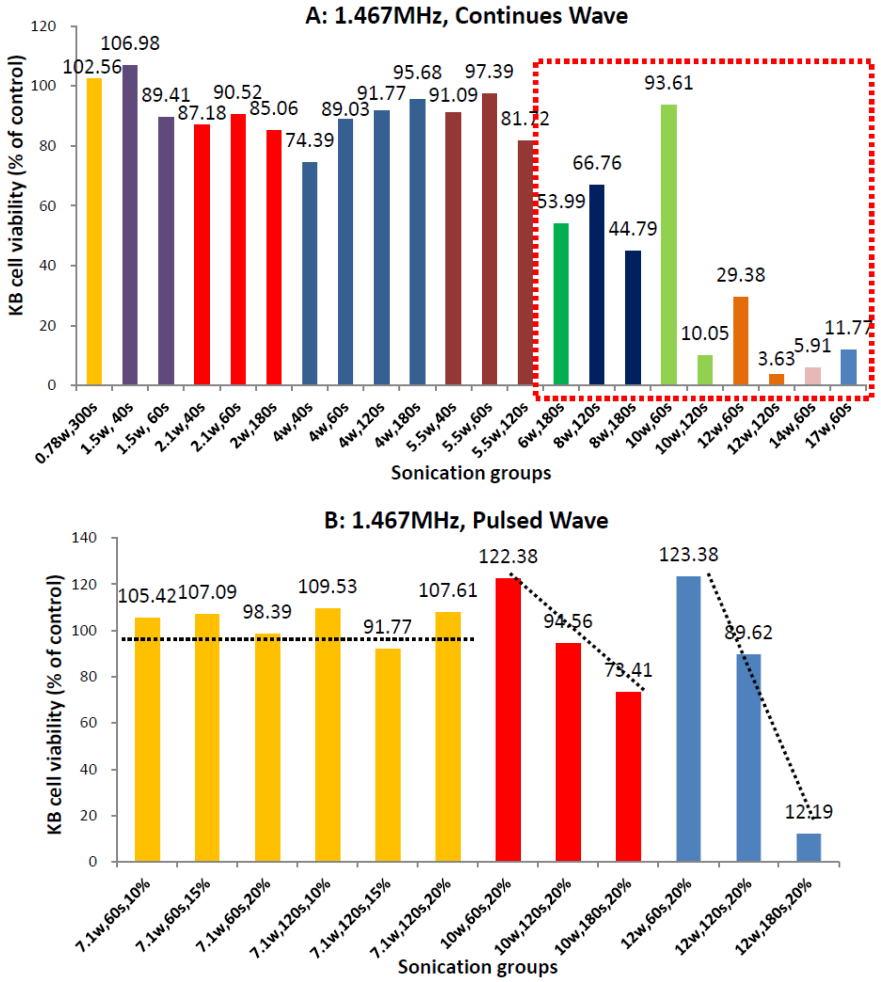

Figure 5.11 KB cells viability (% of control) 48 hr post transducer *f* = 1.467 MHz sonications. Continuous FUS wave mode (A); Pulsed FUS wave mode (B).

In 1.467 MHz pulsed FUS wave sonications, three powers of 7.1 W, 10 W and 12 W were employed. It is easy to conclude from Figure 5.11 B that at lowest power of 7.1 W, cell viabilities were not affected much by all sonication treatments as the lowest cell viable rate was 91.77%. At higher power of 10 W and 12 W applications, cell viabilities again decreased by increased sonication duration when keeping the duty cycle constantly at 20%.

Transducer *f* = 1.142 MHz

In the third transducer at frequency of 1.142 MHz sonication treatments, KB cell viabilities (Figure 5.12 A and B) exhibited not much affected by all sonication parameters combinations in both continuous and pulsed wave mode. Where, two extreme low cell viability values (red circled bars) obtained under continuous wave mode at 0.8 W for 300 sec duration (34.64%) and under pulsed wave mode at 3 W for 60 sec, 20% duty cycle induced viable cells were only 5.35% which was suggested to be error by comparing to those data obtained by higher FUS parameters.

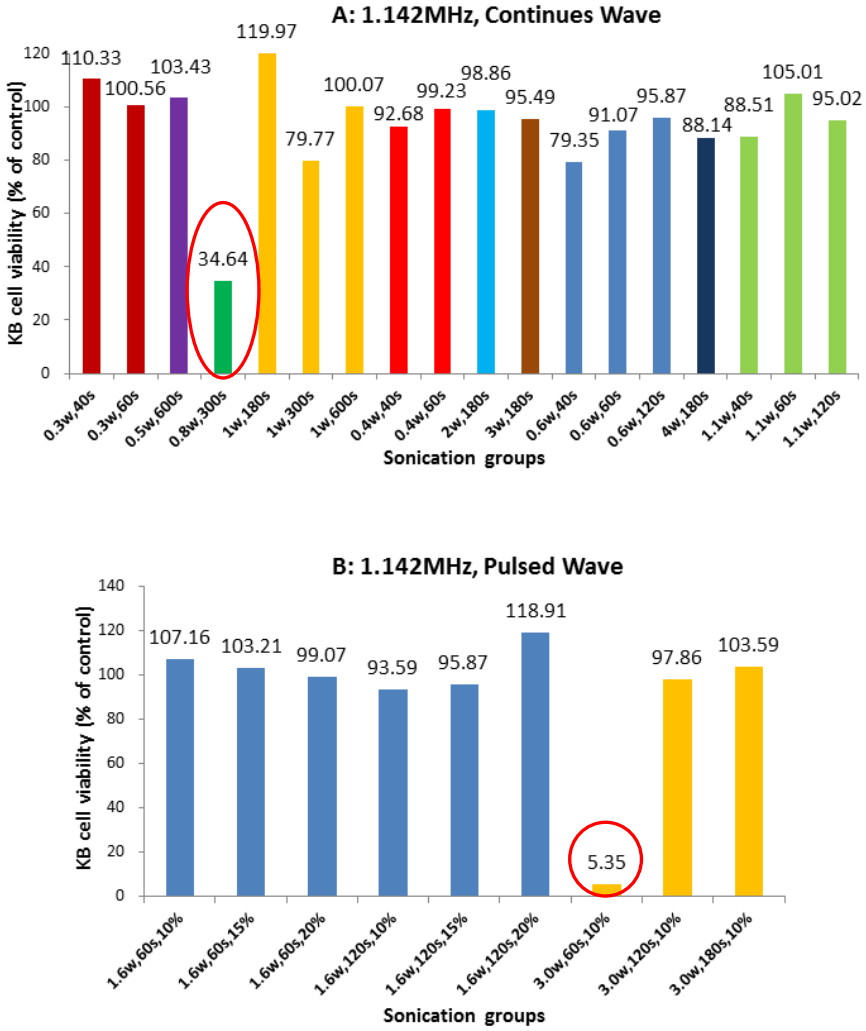

Figure 5.12 KB cells viability (% of control) 48 hr post transducer *f* = 1.142 MHz sonications continuous FUS wave mode (A); Pulsed FUS wave mode (B).

Transducer *f* = 0.4868 MHz

The lowest frequency (0.4868 MHz) of transducer, again, did not severely affect KB cell monolayer post sonications, except after longest duration of 300 sec with highest continuous power of 4.8 W applied, cell viable rate expressed at only 3.19%. For all the other parameters applied, cell viable rate were all over 81.22% (Figure 5.13 A and B).

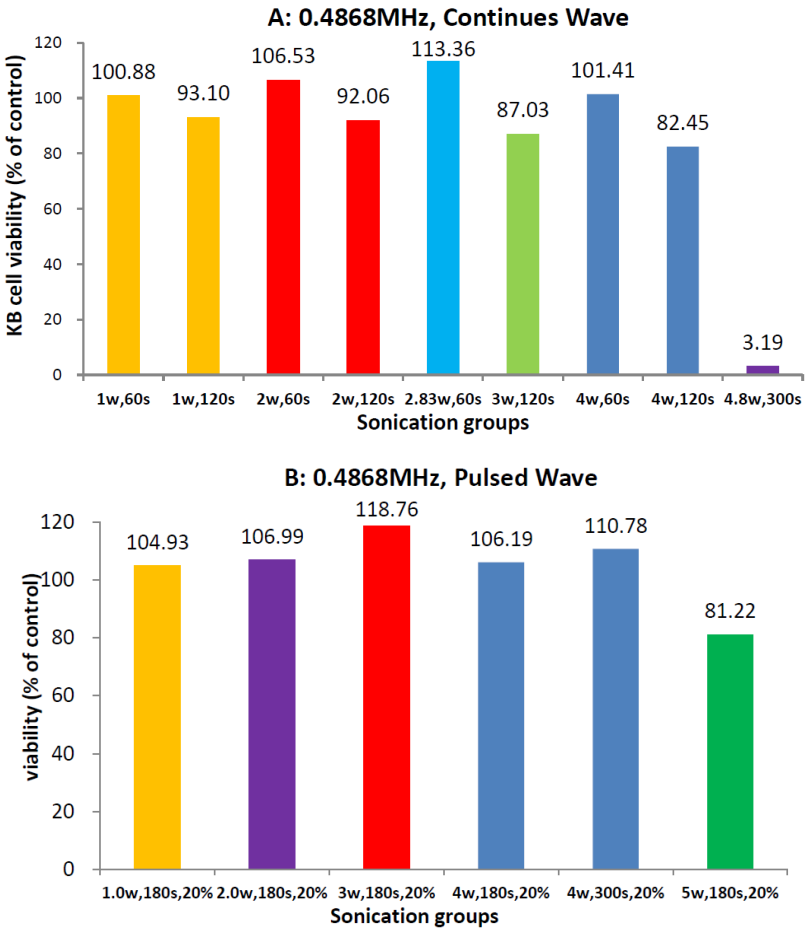

Figure 5.13 KB cells viability (% of control) 48 hr post transducer *f* = 0.4868 MHz sonications. Continuous FUS wave mode (A); Pulsed FUS wave mode (B).

Summary

To summarise, cell viability values were high (over 80%), for FUS exposures at *f* = 1.142 and 0.4868 MHz and power in the range of 0.3 – 5 W. This suggests that cell viability and proliferation is not much affected, as expected, or sometimes even enhanced / triggered by FUS at low acoustic intensity (Pitt and Ross 2003; Yu, Wang et al. 2004). Cell viabilities after 48 hr incubation post sonication at *f* = 2.022 and 1.467 MHz with continuous power under 6 W were still over 80%; with pulsed power under 10 W and duration under 180 sec were over 73%. Cell viabilities also observed drop dramatically below 50% for various combinations of higher acoustic intensity, frequency and exposure time. However it is desirable for TDD experiments to maintain high cell viability values (over 80%) for accurate control and repeatability.

Cell viable rate upon sonication is a crucial aspect in the following *in vitro* cellular

drug uptake assay and *in vivo* MRgFUS application to animals. As targeted drug release is an active process, and the energetic cavitational phenomena discussed in this chapter that may be detrimental to tissues are requisite in promoting the physical or chemical release of drugs from the nanocarriers, or the transport of drugs into cells. However, low acoustic intensity may not be adequate to effectively active TDD. Thus a proper level of cavitational activity must be compensated to achieve the medicinal purpose of FUS-mediated TDD. Somewhere between these harsh and mild extremes lies the desired realm of ultrasonic TDD – a cavitational level that produces cavitation activity sufficient to sonoporate cell membranes temporary without killing the cells, an energy level that creates a sufficient number of micro-jets to allow extravasation from capillary walls without killing the endothelial cells or causing thrombosis, or a level that generates sufficient microstreaming to break open desired γ-CD based nanocarriers or other vesicles without lysing red cells or other host cells (Pitt, Husseini et al. 2004).

5.4.2 Evaluation of MBs Related Temperature Effects

If the thermal effects of US are exploited, then a small focal zone, diameter 1 – 3 mm, and increased US durations may provide the energy necessary for the desired effects through heat transfer. However, the size of the focal zone is highly relevant for US-mediated TDD experiments, if carrier-drug insensitive to temperature or sensitive to mechanical effects are used, then those mechanical effects of FUS in conjunction with gas MBs as possible “tools” to open the carriers and release the drug in the vicinity of the cell membrane will benefit from a wider focal zone, and the coverage of US-exposed cell layers will improve.

According to mechanical characterisations of acoustic field and focused zone (section 2 in Appendices), efficiency (section 3 in Appendices) and temperature rising with various combinations of US parameters for each transducer (section 4 in Appendices), combined with the target carrier-drug system were found to be thermo-sensitive (Chapter 3 and Chapter 4), it is necessary to have rational

experiments design to figure out responsivity of the carrier-drug system under US mechanical effects only, in which, thermal effects need to be avoid.

Therefore, transducer f = 0.4868 MHz was selected for the following experiments, as 1) it shows lowest energy efficiency to delivery as low acoustic power as desired; 2) it has lowest temperature rising; and 3) its focused zone is the largest of 5.3 mm (obtained from experimental scan) to cover the most cells monolayer on a 6.9 mm well, among others. Together with SonoVue® MBs half-life time is 41.05 ± 1.83 sec when exposure to 1 MHz transducer at intensity of 4 W/cm^2 (Tinkov, Bekeredjian et al. 2009), desired plate sonication arrangement and total drug exposure time in drug cellular uptake investigation, sonication duration for the following experiments was determined for 10 sec per single well constantly. To assess the impact of FUS application on cells in the presence of MBs, selected MI between 0.2 to 0.6 was applied, as stable cavitation happen with MBs when 0.1 < MI < 0.6 (Hernot and Klibanov 2008) and MBs destruction (oblique implosion) reported to occur when MI is over 0.7 (Lindner 2002).

Moreover, it is well known that bubble collapsing is a microscopic implosion that generates high local turbulence and the release of heat energy. The consequence is a significant increase of temperature and pressure (Leong, Ashokkumar et al. 2011). Furthermore, it is reported that at 20 kHz ultrasound frequency, the bubbles generated in the acoustic field are relatively large and their collapse results in strong shockwaves (Leong, Wooster et al. 2009). However, acoustic frequency between 100 to 1000 kHz, their collapse induces a higher increase in temperature (Suslick and Crum 1998). Thus, the aim of experiments in this section is to evaluate whether MBs' concentration would affect temperature changes upon sonication. IR thermal camera and thermocouples have been adopted to investigate thermal effect within selected US parameters in the presence of different concentrations of MBs.

5.4.2.1 Temperature measurement by thermal camera

MI = 0.24

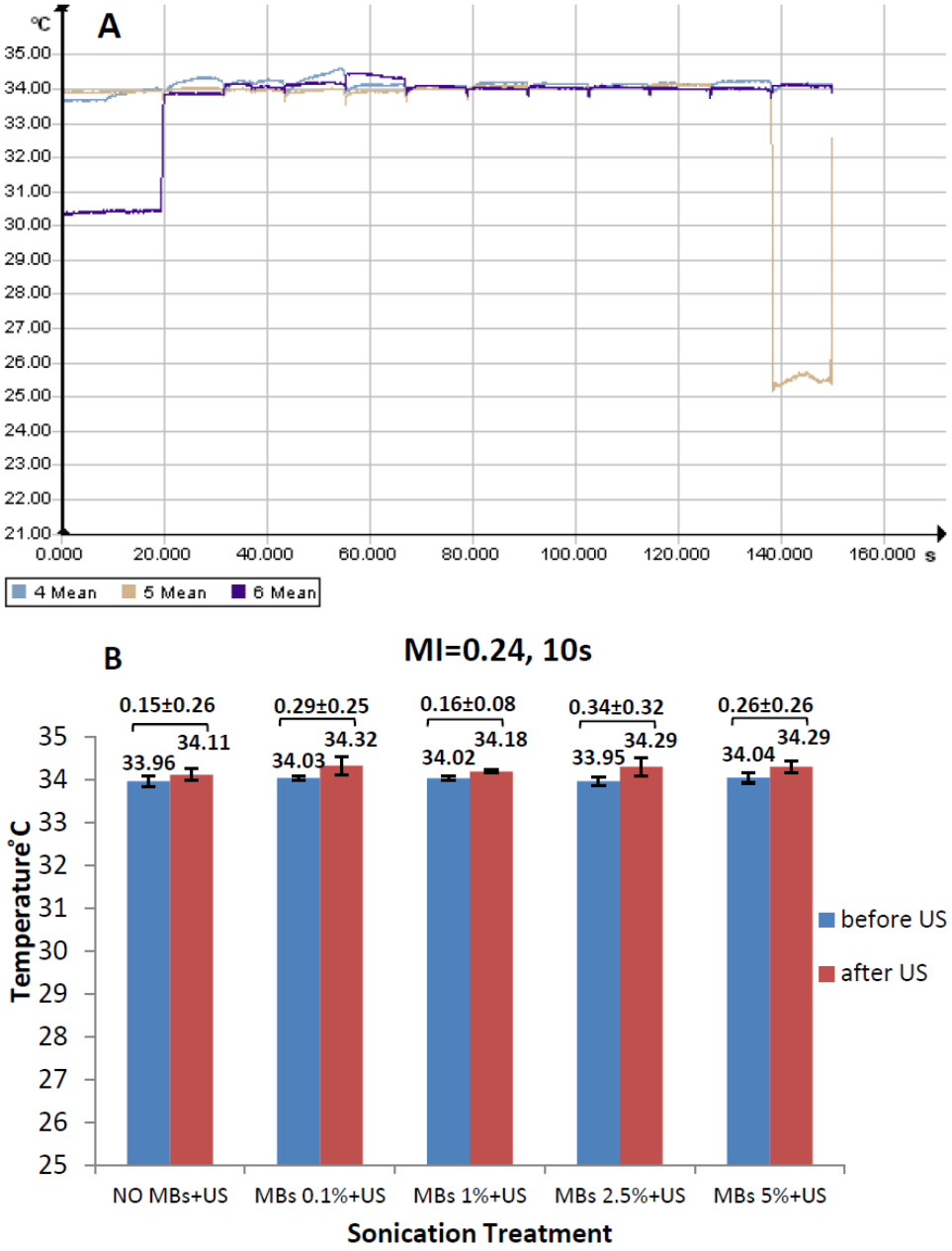

Figure 5.14 Temperature changes by US exposure of MI = 0.24, duration 10 sec, in the absence/presence (0.1%, 1%, 2.5% and 5%) of SonoVue® MBs. Temperature mapping from thermal camera (A); Calculated temperature changes of before and after US treatment (40 msec time record frame) (B)

As can be seen from the thermal camera temperature mapping shows in Figure 5.14 A, temperatures in three wells (position 4, 5 and 6) have been selected to analyse the results. Temperature in position 4 (light blue curve) was the well being sonicated,

position 5 and 6 are the two adjacent wells, 5 would be sonicated next, 6 was the well just been treated (pictures can be found in Figure 5.2 B within this chapter). The temperature mapping indicated not much temperature changes in three interested positions before and after US exposure. In Figure 5.14 B, very little temperature increase (maximum 0.34 ± 0.32 ℃) was observed according to data calculation in all treatment groups.

MI = 0.31

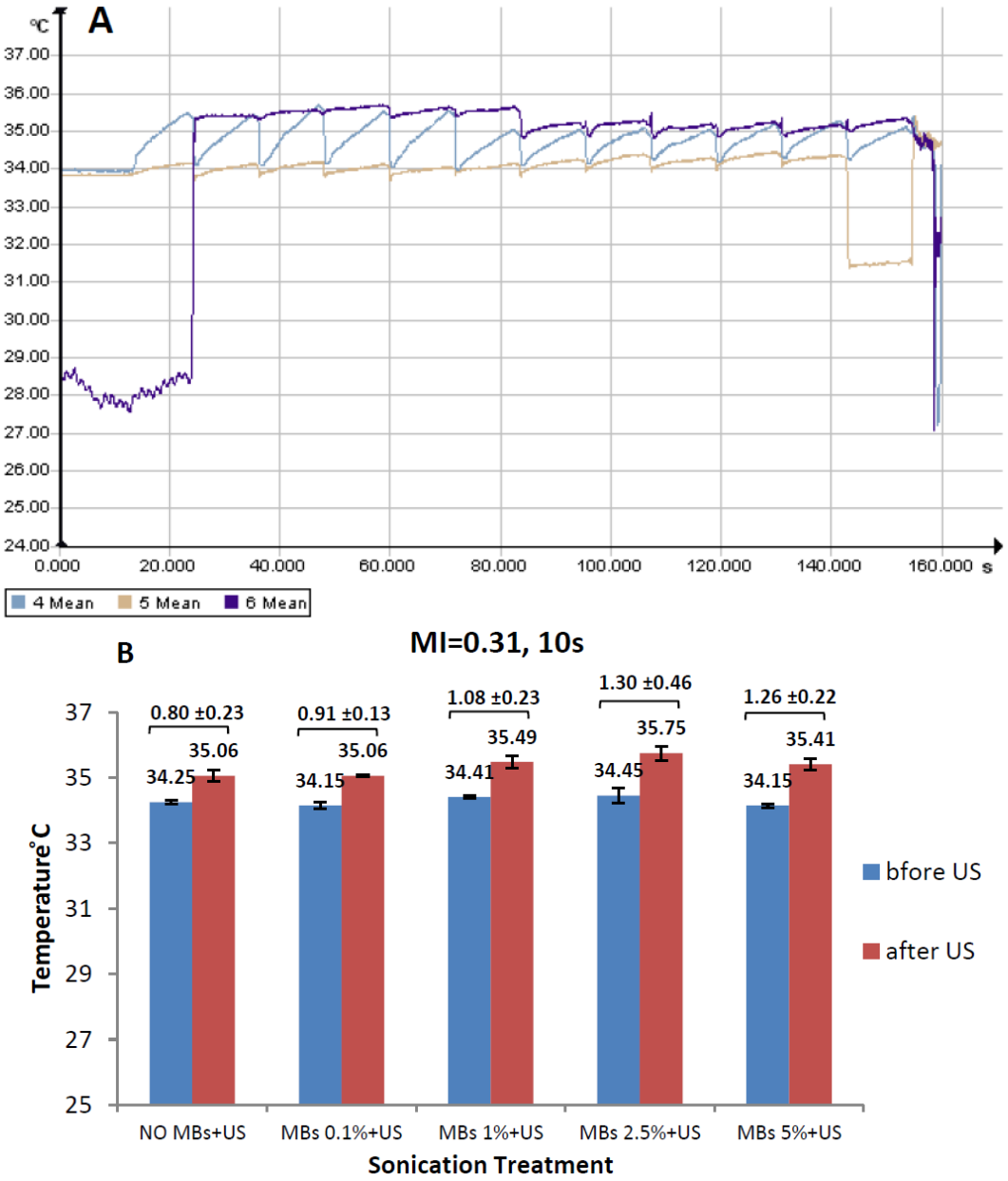

Figure 5.15 Temperature changes by US exposure of MI = 0.31, duration 10 sec, in the absence/presence (0.1%, 1%, 2.5% and 5%) of SonoVue® MBs. Temperature mapping from thermal camera (A); Calculated temperature changes of before and after US treatment (40 msec time record frame) (B).

Different temperature mapping displays in Figure 5.15 A and it illustrates that when MI = 0.31, sonicated well (position 4) had a sharp temperature increase within 10 sec (increasing segment on light blue curve) from around 34 ℃ up to roughly 35.5 ℃. While, temperatures in adjacent position 5 (light brown curve, non-sonicated wells) were not influenced much which stated insignificant heating (< 0.2 ℃) spread to adjacent wells within desired US parameters. Figure 5.15 B further demonstrates calculated temperature changes within this set of US parameters, where, the maximum temperature increase was 1.30 ± 0.46 ℃. Furthermore, the presence of MBs showed no additional thermal effects.

MI = 0.53

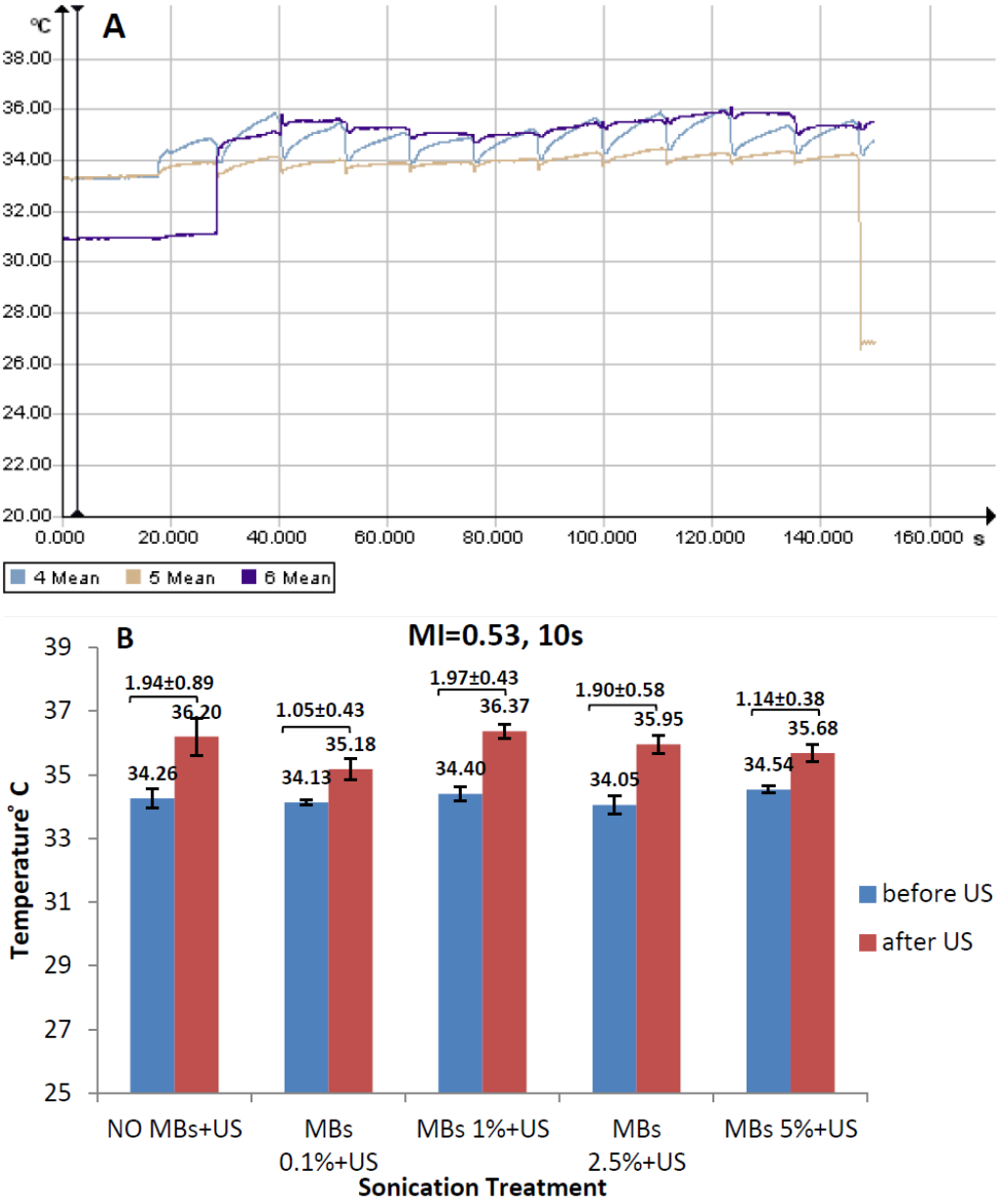

Figure 5.16 Temperature changes by US exposure of MI = 0.53, duration 10 sec, in the absence/presence (0.1%, 1%, 2.5% and 5%) of SonoVue® MBs. Temperature mapping from thermal camera (A); Calculated temperature changes of before and after US treatment (40 msec time record frame) (B).

Results in Figure 5.16 are similar to Figure 5.15, when MI = 0.53 applied, higher temperature increase was observed (maximum 1.97 ± 0.43 ℃), but again, little heating (< 0.5 ℃) spread to adjacent wells and MBs did not affect thermal effects of US treatment.

All temperatures presented here are average temperatures compiled from three

separate experiments performed in triplicates and were expressed as means ± SD.

5.4.2.2 Temperature measurement by thermocouples

Thermocouples are complementary experiments to confirm results obtained by thermal camera. Temperatures by exposure MI = 0.24, 0.31 and 0.53 in the absence of MBs, and MI = 0.53 in the presence of 5% MBs were tested.

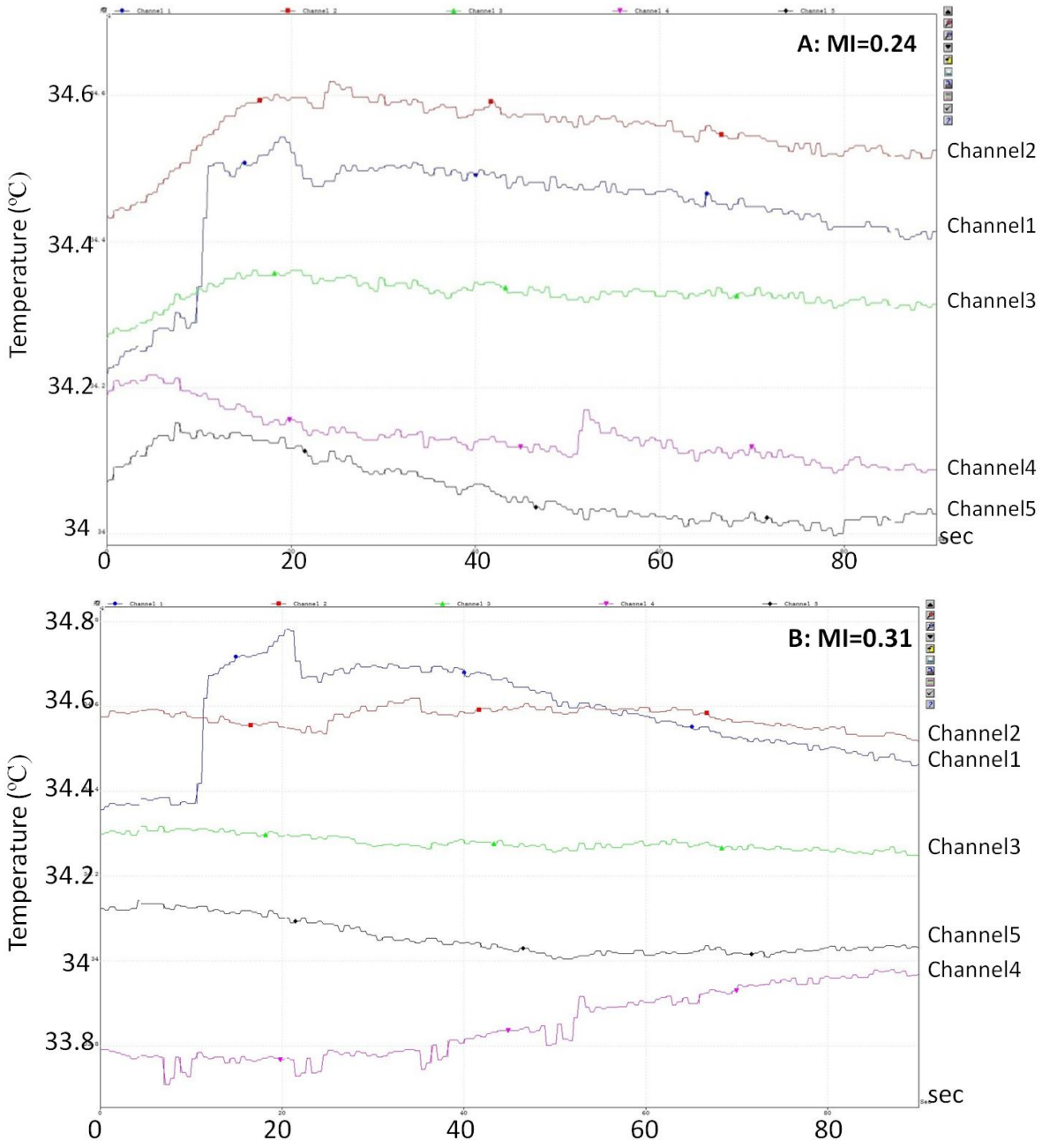

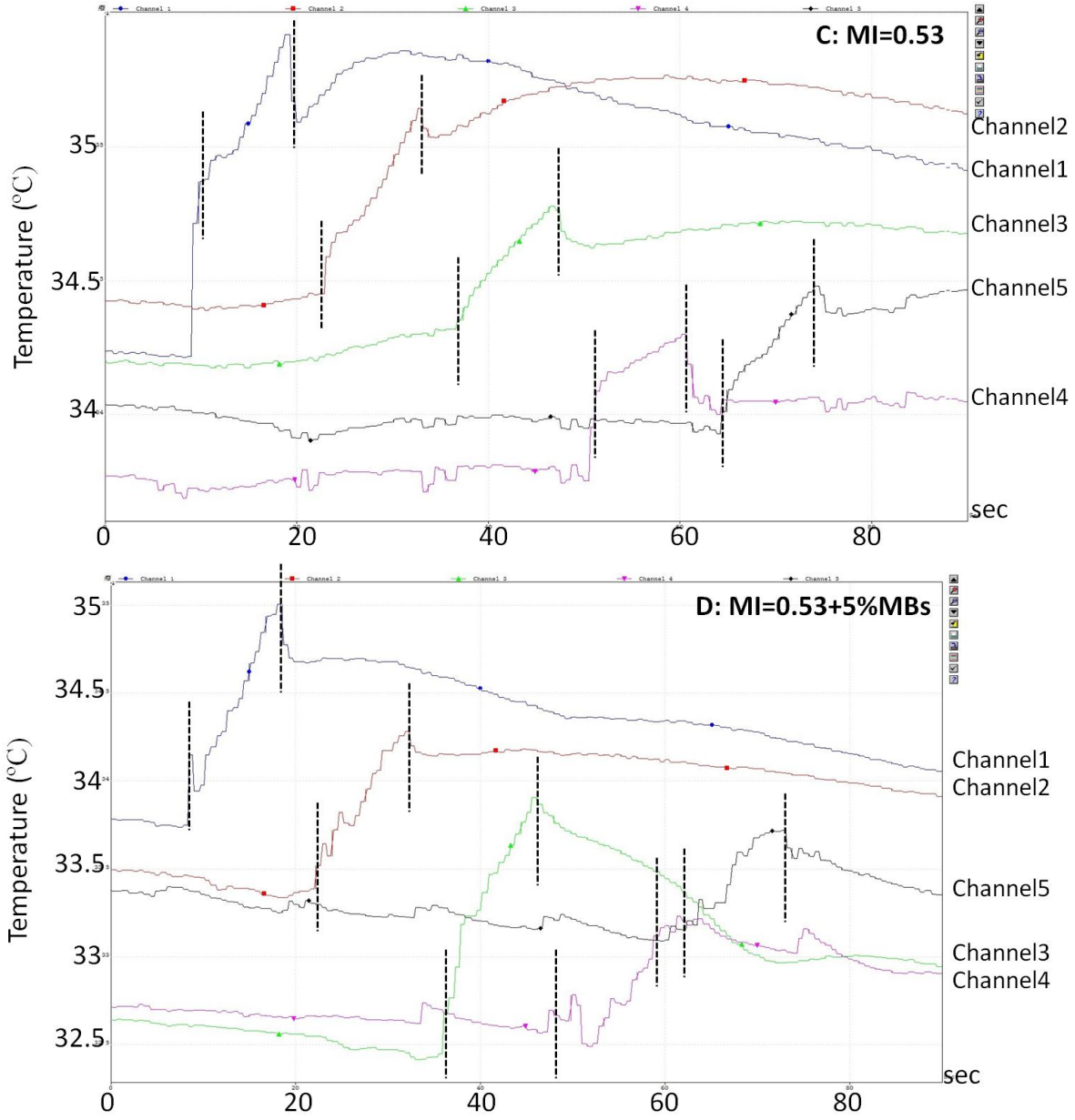

Figure 5.17 Temperature mapping by thermocouples. MI = 0.24, no MBs (A); MI = 0.31, no MBs (B); MI = 0.53, no MBs (C); and MI = 0.53 with 5% MBs (D).

From Figure 5.17 A and B, very little temperature increase (< 0.5 ℃) was received when MI = 0.24 and 0.31. To be noticed in both A and B, channel 1 exhibits a sharp temperature increase segment where channel 1 thermocouples was placed in the first sonicated well, this phenomenon suggested the very first sonication might be subjected to a split-second higher US power then desired, at the moment of switching on the power amplifier.

In Figure 5.17 C and D, obvious temperature rise (marked ascendant part of curve by black dotted line) happened to all thermocouples channels when US MI = 0.53 was employed; the maximum temperature increase was around 2 ℃, which was consistent with data received by thermal camera.

Temperature evaluation within selected US parameters is critical reference for the next carrier-drug binding test and drug cellular uptake assays, which helps to distinguish what is the main effects (thermal or mechanical) to cause drug release or increased cellular drug uptake.

5.4.3 Cavitation

By exposure FUS to TA solutions to test fluorescence intensity changes by selected low acoustic parameters; no obvious increasing of fluorescent signals was received after 10 sec sonication.

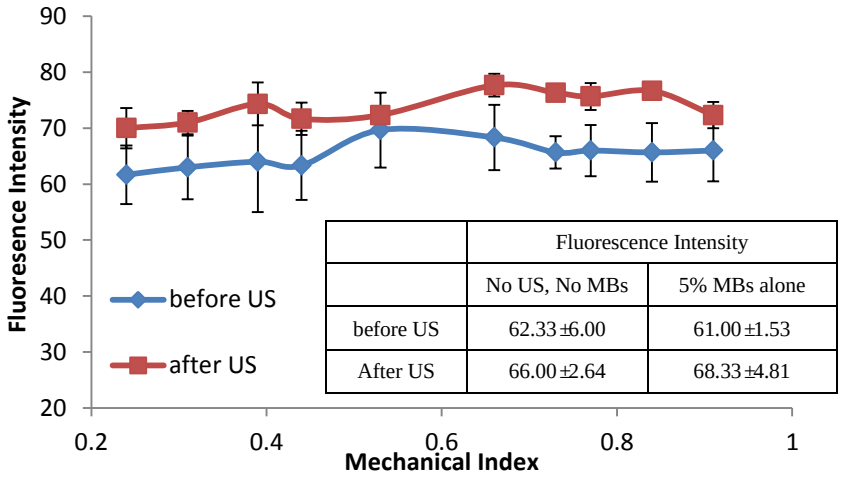

	Fluorescence Intensity	
	No US, No MBs	5% MBs alone
before US	62.33 ±6.00	61.00 ±1.53
After US	66.00 ±2.64	68.33 ±4.81

Figure 5.18 Fluorescence intensity changes of TA solutions post US exposure in the presence of 5% MBs. The embedded table lists fluorescence intensities of two control samples: TA with no MBs no US and TA with 5% MBs no US.

In Figure 5.18, a slight increase of fluorescence intensity was detected, however, in comparison to two control groups of data displays in the table embedded in Figure 5.18, TA solution without MBs with no US treatment also has an increasing of fluorescence intensity from 62.33 ± 6.00 to 66.00 ± 2.64, and TA solution with 5% of MBs but no US treatment was also observed fluorescence intensity increased from 61.00 ± 1.53 to 68.33 ± 4.81. Data of TA with 2.5% MBs will not present here as

similar results gained as above.

Thus, observation of increased fluorescent signal was believed not due to inertial cavitations occurring, it is suggested to be physical influences such as temperature, exposure time in air and etc. Therefore, it is difficult to say inertial cavitations were induced by desired low acoustic parameters. However, it is also hard to conclude that only stable cavitations existed. Better analysis methods are needed to clarify this point.

All data presented here is average fluorescence intensity compiled from three separate experiments performed in triplicates and were expressed as means ± SD.

5.4.4 Carrier-drug Binding Results

Carrier-DOX inclusion solution was exposed to FUS and their encapsulation changes were obtained.

Table 5.2 Encapsulation percentage of DOX by the carrier before and post 10 sec US sonication treatment at MI = 0.24, 0.31 and 0.53 in the presence of MBs (0.1%, 1%, 2.5% and 5%)

	Encapsulation (% of control) Before US	Encapsulation (% of control) After US		
No US, No MBs	81.06±1.19	MI=0.24	MI=0.31	MI=0.53
No MBs+US	81.21±0.29	77.69±0.37	77.60±0.08	77.88±0.12
0.1% MBs+US	81.28±0.39	77.96±0.22	77.20±0.15	78.56±0.14
1% MBs+US	80.19±0.48	77.37±0.14	76.89±0.04	77.12±0.19
2.5% MBs+US	80.84±0.22	77.11±0.20	76.61±0.27	76.48±0.08
5% MBs+US	85.32±0.21	78.20±0.30	78.57±0.30	78.68±0.56

*The results are presented from three separate experiments carried out in triplicates and were expressed as means±SD.

As can be seen from Table 5.2, encapsulation efficacy of DOX by the carrier is over 80% before US treatment. Three groups of US treatment showed slightly DOX release after sonication, minimum encapsulation rate was 76.48 ± 0.08%. However, this ~ 4% 'drug release' was believed not attributed to US mechanical effects and it is suggested to be triggered by US thermal effect mainly.

The explanation, first of all, is the procedure of transferring little volume of 420 μL/well pre-heated carrier-DOX solution into 96-well plate has been implemented at

room temperature, in which, such a small volume of test solution is difficult to be maintained at pre-heated temperature of 37 °C. Nonetheless, DOX's encapsulation efficiency was measured at room temperature before US exposure, whereas the sonicator water bath was maintained at 34 ℃ that warmed up test solution when the plate was in. Furthermore, sonication also generated minor heating. Therefore, lower encapsulation observed of carrier-DOX system after sonication was suggested to be carrier's responsivity to thermal effect, according to 'thermal-sensitive' conclusion stated in Chapter 3. Moreover, no additional changes of encapsulation rate were observed in Table 5.3 when different MI were applied, either in the presence of different concentrations of MBs, which is the second explanation of this non-mechanical-sensitive carrier-drug system. Nonetheless, because very low US powers were employed and only 10 sec duration were applied for each single cell culture well, that are insufficient to induce drug release from the complex inclusion.

5.4.5 Cell Viability in The Presence of MBs

After temperature and carrier-responsivity investigation of selected sets of acoustic parameters, more *in-vitro* cell culture studies were performed to optimise applicable parameters in TDD drug delivery. Cell viability test in the presence of MBs was conducted firstly by inspection of both KB and HCT116 cell lines.

KB cells

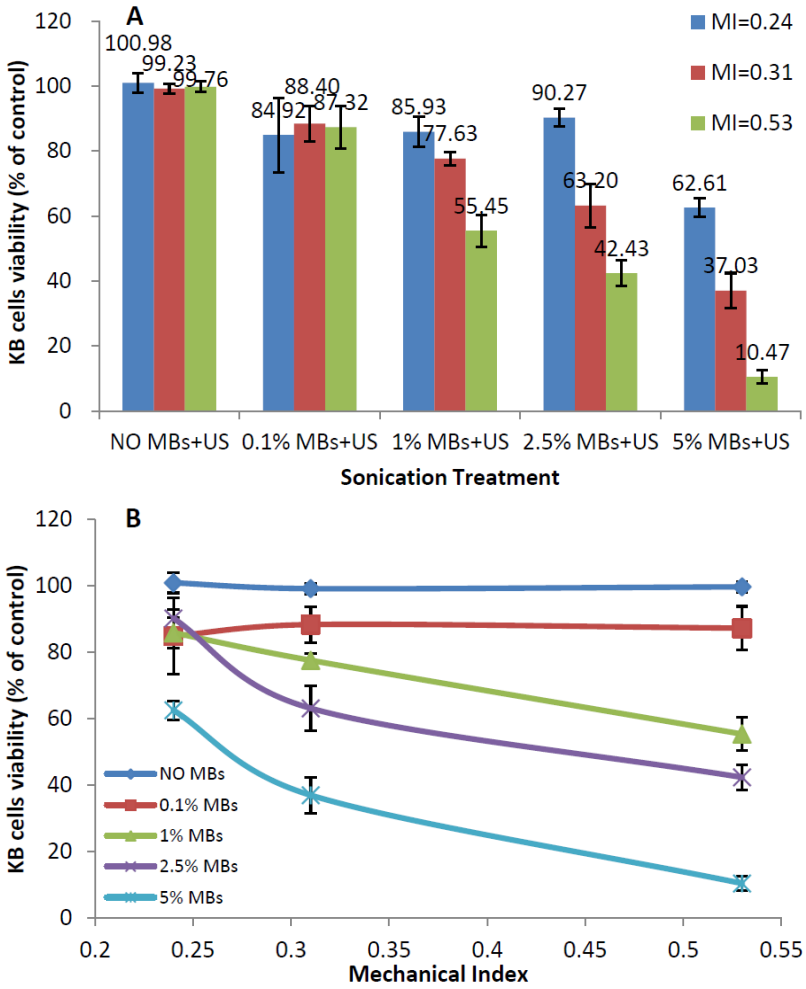

Figure 5.19 KB cells viability (% of control) 48 hr post sonication in the absence/presence of MBs. KB cells viability as a function of MBs' concentration (A); KB cells viability as a function of US mechanical index (B).

From Figure 5.19 A, KB cells expressed high viable rate (over 85%) when lowest MI of 0.24 was applied except in the presence of the highest MBs of 5% (62.61%). In parallel, under the same MI, viabilities of KB cells were high when MBs concentration $\leq$ 0.1%. Along with either increased MI or concentrations of MBs, the viable KB cells decreased correspondingly.

Figure 5.19 B presents cell viability in another way by different MIs, in which, clear observation of decreasing trend of viable cells with increasing MI and concentrations of MBs can been seen.

HCT116 cells

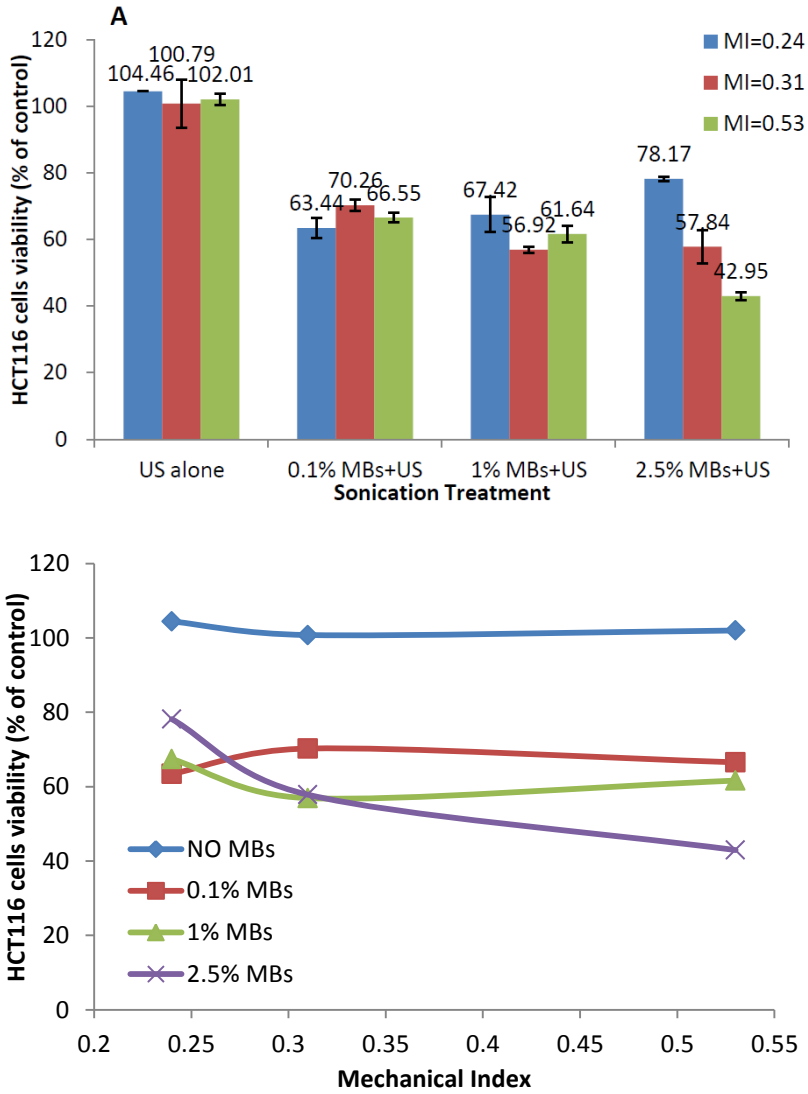

Figure 5.20 HCT116 cells viability (% of control) 48 hr post sonication in the absence/presence of MBs. HCT116 cells viability as a function of MBs' concentration (A); HCT116 cells viability as a function of US mechanical index (B).

As can be seen from Figure 5.20, HCT116 cells behaved more sensitive to US exposure in the presence of MBs, viable HCT116 cells were lower than that of KB cells. The results were consistent with observation of HCT116 cells which exhibited less-stable adhesion property in Chapter 4, therefore, HCT116 cells were more vulnerable to US exposure. This is why the highest 5% of MBs was not applied for HCT116 cells. Again, except MI = 0.24, cell viability decreased when increased either MI or concentrations of MBs.

5.4.6 Cellular Drug Uptake

To evaluate the efficiency of FUS as a drug uptake stimulant for encapsulated carrier-drug inclusion, drug cellular uptake experiments were performed on the basis of above results of temperature investigation, cavitations detection, carrier's responsivity measurements and cell viability evaluation.

KB cells

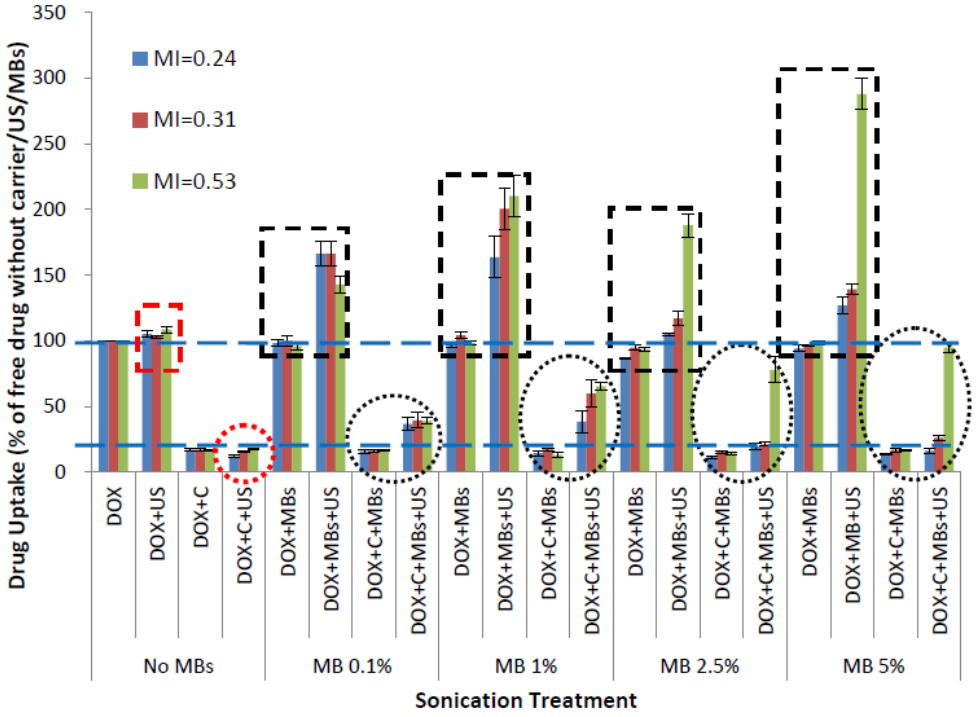

Figure 5.21 DOX cellular update in KB cells after US exposure in the presence of drug carrier and MBs.

Figure 5.21 shows drug cellular uptake (% of control) of KB cells post sonication in the presence of drug carrier without / with MBs. Bars highlighted by squares are data of cells exposed to no carriers containing DOX solutions, where, cellular drug uptake increased sharply (from ~ 100% up to ~ 280%) along with both increased MI and MBs concentrations. This suggested cell sonoporation occurred and the pore size of cell membrane was enlarged to induce more drug molecule intercalation.

By looking at bars highlighted by circles in Figure 5.21, drug uptake of cell samples exposed to protected drug solutions are presented. In which, successful

protection of DOX by the carrier can be seen as very low drug uptake was obtained (~ 15%), which supported those results achieved in Chapter 4. Besides, no significant increase of cellular uptake was recorded in cell samples exposed to carrier-drug solutions without MBs but with US treatment (bars in red circle) only. However, cellular DOX uptake increased when concentrations of MBs rose up. Detailed analysis of increased drug uptake shows in Table 5.3.

Table 5.3 Increased fold of KB cells DOX cellular uptake of (DOX+C*+MBs+US) treatment compared to (DOX+C*+US) treatment at different MI

	Increased fold of DOX uptake		
[MBs]	MI=0.24	MI=0.31	MI=0.53
0.1% MBs	3.03	2.56	2.25
1% MBs	3.17	3.89	3.78
2.5% MBs	1.61	1.38	4.51
5% MBs	1.34	1.69	5.49

*C stands for carrier.

Table 5.3 aims to express significant factors of increased drug uptake between cell samples subjected to protected drug solutions with MBs and without MBs. From this table, minimum 1.34-fold of DOX uptake was achieved by employing MI of 0.24 with 5% MBs. While maximum of 5.49-fold drug uptake was obtained by using MI of 0.53 with 5% MBs. However, when concentration of MBs was 1%, minimum 3.17-fold and maximum 3.78-fold were received. As well as sonication with 0.1% of MBs by MI of 0.24, 3.03-fold drug uptake was get. The results suggested again sonoporation happened in the presence of MBs and MBs' oscillation / collapse stimulated more drug uptake by KB cells, and, another possibility was drug released from the carrier by minor thermal effect, or by mechanical effect.

HCT116 cells

Similar experiments were performed for HCT116 cells. According to experience from its viability test, as significant cell loss was obtained with 5% of MBs, and less effective of 0.1% MBs, only two intermediate concentrations of 1% and 2.5% of MBs were employed to HCT116 cells.

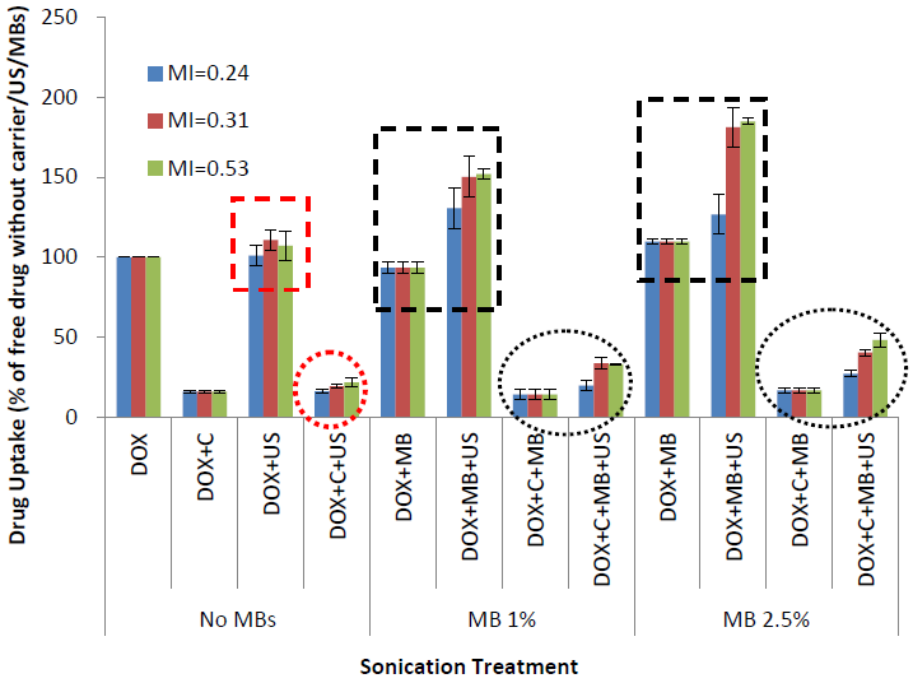

Figure 5.22 DOX cellular update in HCT116 cells after US exposure in the presence of drug carrier and MBs.

Table 5.4 Increased fold of HCT116 cells DOX cellular uptake of (DOX+C*+MB+US) treatment compared to (DOX+C*+US) treatment at different MI

	Increased fold of DOX uptake		
[MBs]	MI=0.24	MI=0.31	MI=0.53
1% MBs	1.40	2.38	2.33
2.5% MBs	1.62	2.42	2.89

*C stands for carrier.

As expected, similar results were delivered and show in Figure 5.22 for drug uptake situation by HCT116 cells. No significant cellular drug uptake increased in US treatment without MBs for protected DOX (red circle area). Apparently, enhanced DOX uptake was observed in cell samples subjected to both DOX alone and protected DOX in the presence of MBs, and treated by sonications. Table 5.4 shows significant increased factors of DOX uptake between sonication with MBs and without MBs for cells were exposed to protected DOX solutions. Minimum of 1.4-fold was achieved of MI = 0.24 with 1% of MBs, while maximum of 2.89-fold was obtained when MI = 0.53 with 2.5% of MBs.

To summarise, mechanical insensitivity of the carrier-drug inclusion was

suggested in section *5.4.4* in this chapter. However, significant increased DOX cellular drug uptake by both KB and HCT116 cells occurred in the presence of MBs with US treatment illustrates important cell response to MBs-induced mechanical effects such as cavitations.

5.4.7 AFM Measurement of Cell Sonoporation

Short time membrane morphology and topography changes of KB cells were inspected by AFM post sonication with and without SonoVue® MBs by various frequencies of FUS transducers.

Transducer *f* = 1.467 MHz

AFM images of KB cells sonicated 60 sec by *f* = 1.467 MHz in continuous FUS wave without MBs show in Figure 5.23.

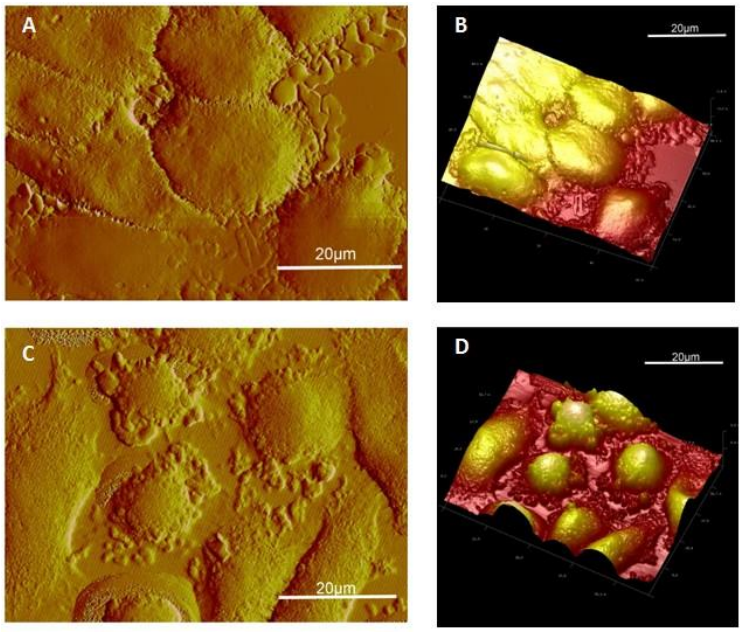

Figure 5.23 AFM cell surface morphology and topography of KB cells before and after *f* = 1.467 MHz sonication. Surface of cells before US treatment (A); 3D image of cells before US treatment (B); surface of cells after sonication (C); and 3D image of cells after sonication (D).

As can be seen from Figure 5.23, smoother cell membrane (Figure 5.23 A) and normal 3D sharp of cells (Figure 5.23 B) were observed before US treatment, while uneven cell membrane (Figure 5.23 C) and more protrusion shape of cells (Figure 5.23

D) can be seen after sonication treatment. The results indicate stress/strain response of cells to pressures came from acoustic wave.

Transducer *f* = 1.142 MHz

KB cells were sonicated 60 sec by *f* = 1.142 MHz in continuous FUS wave, where, 5% MBs was added.

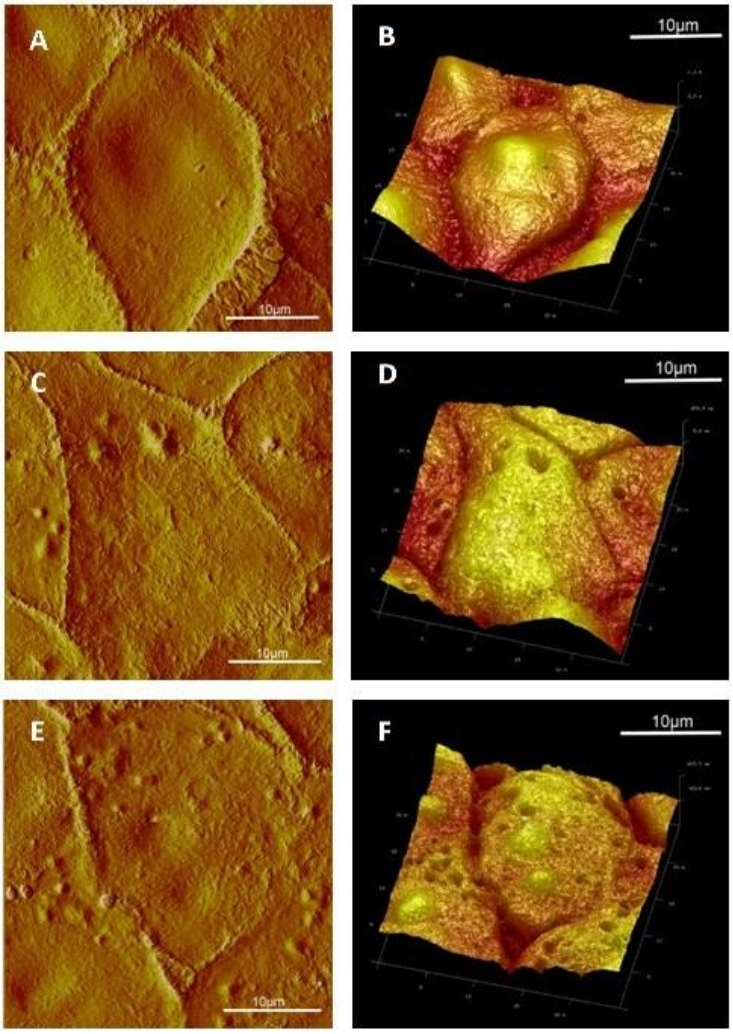

Figure 5.24 AFM cell surface morphology and topography of KB cells before and after *f* = 1.142 MHz sonication. Surface of cells before US treatment (A); 3D image of cells before US treatment (B); surface of cells after sonication without MBs (C); 3D image of cells after sonication without MBs (D); surface of cells after sonication with 5% MBs (E); and 3D image of cells after sonication with MBs (F).

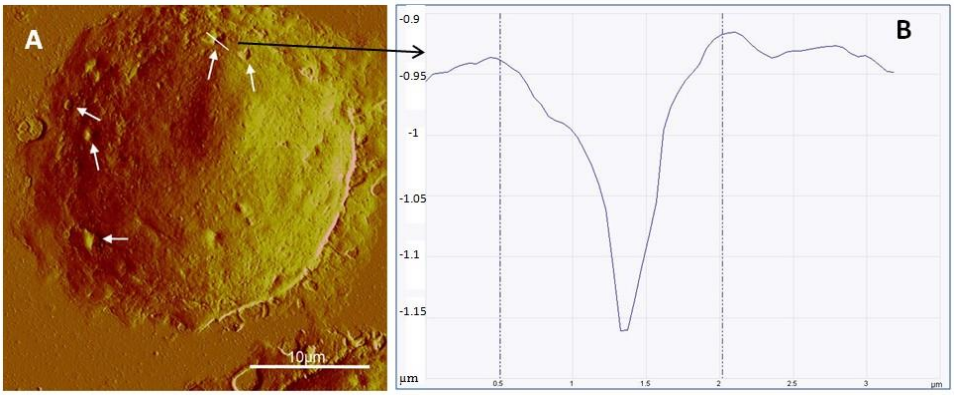

Figure 5.25 AFM cell surface morphology and sonoporation observation of KB cells after *f* = 1.142 MHz sonication with 5% MBs. Surface of KB cells after sonication with 5% MBs (A); and selected sonoporation plot depth and width of a defect (B).

<u>Transducer *f* = 0.4868 MHz</u>

KB cells were sonicated 10sec by *f* = 0.4868 MHz in continuous FUS wave in the absence/presence (2.5%) MBs.

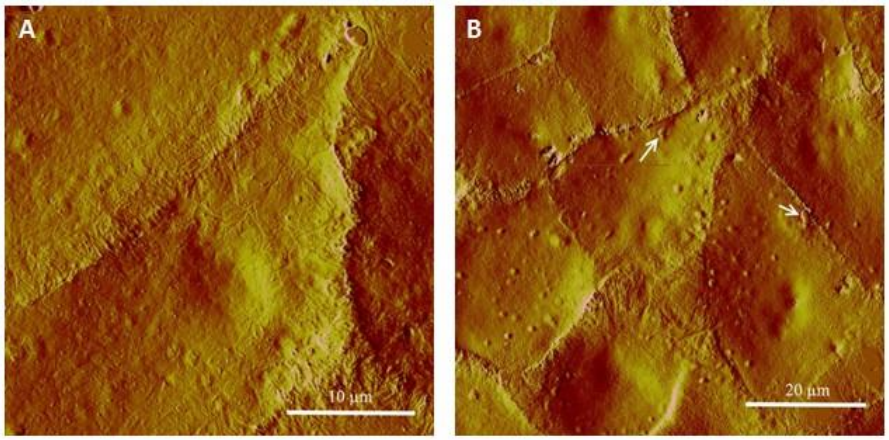

Figure 5.26 AFM cell surface morphology comparison of KB cells before (A) and after (B) *f* = 0.4868 MHz sonication with 2.5% MBs.

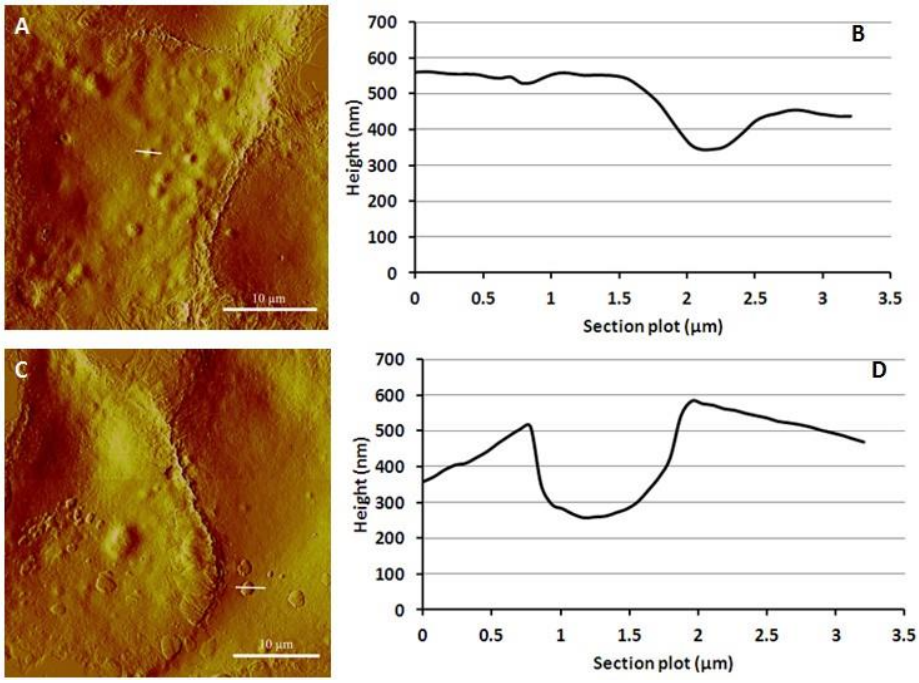

Figure 5.27 AFM cell surface morphology of KB cells after *f*=0.4868MHz sonication with and without 2.5% MBs. Surface image of cells after sonication without MBs (A); selected sonoporation plot depth and width of defects in picture A (B); surface image of cells after sonication with MBs (C); and selected sonoporation plot depth and width of defects in picture C (D).

From Figure 5.24 A and B, Figure 5.26 A, all non-treated cells possessed normal shape and size, with highly rich surface profiles observed, in terms of cell cytoskeleton structures (fibre structures), etc. After the US treatments, flatter cell membranes were documented by the AFM (with much less fibre structures observed). Small pits were found on the cell membranes with depth of 100 – 200 nm (Figure 5.25 and Figure 5.27 A and B). These observations were speculated to be caused by US, which induced non-uniform pressure (or stress & strain) on the cells, resulting in the changes of cell topography (Figure 5.24 C and D).

By adding the MBs to the US treatments, a significant difference in membrane structural topography was seen immediately when compared to the previous experimental groups. Cell membranes were covered with different kind of pore structures with very sharp edges (Figure 5.24 E and F, Figure 5.25 and Figure 5.27 C and D), which it is thought are the disrupted membranes, sonoporated by FUS+MBs treatment (Prentice, Cuschieri et al. 2005). It should be noted that these pore structures

were not observed on all the treated cells (Figure 26 B).

AFM study was a complementary method in this thesis research for cell morphology and topography observation to further investigate cell membrane sonoporation situation in FUS-triggered TDD. The above AFM images illustrate potent sonoporation occurred in the presence of additional MBs, which is an explanation to increased drug uptake observed in section *5.4.6*.

5.5 Conclusions

In this chapter, it was expected that the use of a standardised *in vitro* sonication device and experimental method would reduce instrument-related variability in reported results, reduce the time associated with the US exposure of a large number of wells of a 96-well plate and thus increase the accuracy of exposure durations of cells to both encapsulated and non-encapsulated drugs.

The carrier-DOX drug delivery system was validated to be mechanically (low acoustic power induced) stable, and, by adding additional ultrasound contrast agent of SonoVue® MBs into the system, cell membrane sonoporation with exposure to FUS was confirmed through both cellular drug uptake and AFM studies.

In spite of that, answers to some questions are still unclear, including the form of cavitation (stable / inertial), DOX release / uptake mechanism (such as whether the carrier-DOX complex penetrates the cell membrane intact before the DOX is released) and biochemistry response of cells (cell signalling pathway) to US exposure. Possible methodologies to clarify these will be discussed in Chapter 7.

Chapter 6

Animal House Design and Experimental Planning for Clinical MR-guided FUS System

6.1 Introduction

An extensive cell culture study had been carried out to investigate thermal-responsivity and mechanical-responsivity of the carrier-DOX complex inclusion by thermo oven and FUS, respectively. The logical continuation of this work is the initiation of *in vivo* study to confirm the ability of ultrasound to locally release cytotoxic drug and increase cellular drug uptake by tumour tissues employing the combination of thermal and mechanical effects of FUS under MRI guidance. However, before starting experiments with live animal, setup configuration, MR and ultrasound parameters should be evaluated in a series of experiments that will simulate as close as possible real *in vivo* experiments conditions, but without complexity involved in treating anaesthetised live animals. The perfect model for this purpose is mice cadavers, since they provide same positioning challenges as live mice, same anatomical details and similar acoustic properties.

Thus, this chapter aims to introduce the establishment and verification of 1) animal model: small rodents with and without tumours; 2) imaging and positioning of mice cadavers (with and without tumours); 3) sonication trials for optimisation of FUS sonication mode and acoustic parameters; 4) best MR imaging coils, and 5) procedure time frame. All experiments were carried out using clinical MR-guided FUS system - ExAblate 2000.

6.2 Animal Model and Clinical MR-guided FUS System

6.2.1 Animal Model

Small animal resource unit (RU)

A standard RU for handling immune-compromised live mice with or without tumours during daily experiments was setup. It comprises an internally ventilated cages (IVC) rack with an air handling unit and a high-efficiency particulate absorption (HEPA) filter. For transfer of mice from IVC to other housing boxes and for other procedures a Class II Bio-safety cabinet is available.

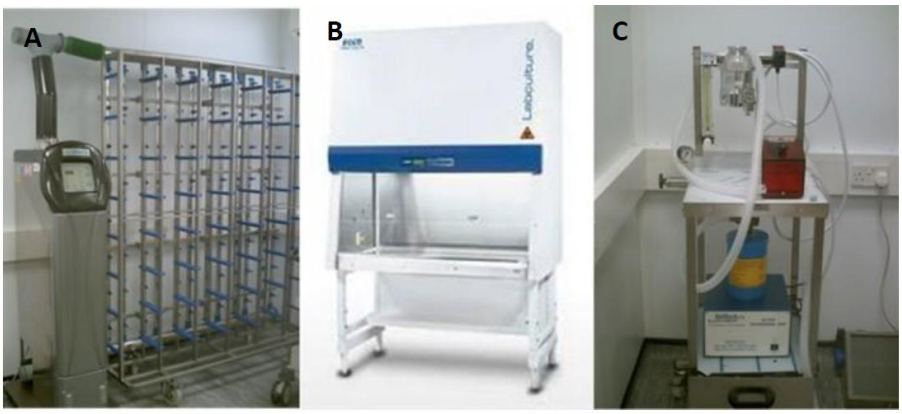

Figure 6.1 Mice housing system for internally ventilated cages (IVC) rack with a high-efficiency particulate absorption (HEPA) filter (A); Class II Bio-safety cabinet (B); MRI compatible anaesthetic device (C).

Nude mice (Fogh and Giovanella 1978; Fogh and Giovanella 1982)

Nude mouse is a laboratory mouse strain with genetic mutant (disruption of the FOXN1 gene) that has a deteriorated or removed thymus, resulting in an inhibited immune system due to a greatly reduced number of T cells. The main characteristic of nude mouse is lack of body hair, which gives this mutant strain the name of 'nude'. Nude mice are valuable to oncology research because these are well-established as tumour xenografts recipients due to no rejection response. Such xenografts are often established in research to test new diagnostic and therapeutic methods. Hence, nude mice model is ideal for the current research reported here. Figure 6.2 shows a laboratory nude mouse model.

Figure 6.2 A nude mouse (From http://en.wikipedia.org/wiki/Nude_mouse, created by Armin Kübelbeck).

6.2.2 Clinical MR-guided FUS System-ExAblate 2000 for Animal

1.5 Tesla MRI system

MRI is a medical imaging technique used in radiology to investigate the anatomy and function of the body in both health and disease. MRI is potent at finding and pinpointing some cancers. Main application in cancer diagnosis contains: 1) an MRI with contrast agent is the best combination to see such as brain tumours; 2) by MRI, doctors can sometimes distinguish whether a tumour is benign or malignant; 3) MRI can also be used to look for signs that cancer may have metastasised from where it started to another part of the body; 4) MRI images can help to be as an efficient guidance in treatment such as surgery, radiation therapy or chemotherapy. MRI is the investigation of choice in the preoperative staging of cancers, and has a role in the diagnosis, staging, and follow-up of other tumours (Husband and Padhani 2006). Wider interest in solid tumour microenvironment has come from more and more exquisite data available by employing MRI (Gillies, Raghunand et al. 2002).

In the thesis reports here, a 1.5 Tesla MR scanner was used for the guidance of treatment with FUS. The MR imaging was performed using either a single-channel surface coil or two versions of the 8-channel DUOFLEX interventional coil: a 10 cm × 10 cm surface coil and 24 cm × 24 cm surface coil.

ExAblate 2000

ExAblate 2000 system deliveries FUS energy into human body in a minimal-invasive manner. In a matter of seconds, the tissue at the focal spot of the ultrasound beam is heated to the point of irreversible thermal coagulation, while nearby tissue remains unaffected.

ExAblate 2000 (Figure 6.3) is a clinical approved FUS surgery system which consists of a bowl shaped transducer (Figure 6.3 D) with 208 transmitting ultrasonic elements. The system controls each element and has the ability for continuous power and phase modulation individually. Additional bowl shaped element (Figure 6.3 D, red circle) is acting as a receiver and it is located in the middle of the transducer. The element is used for the spectrum measurements.

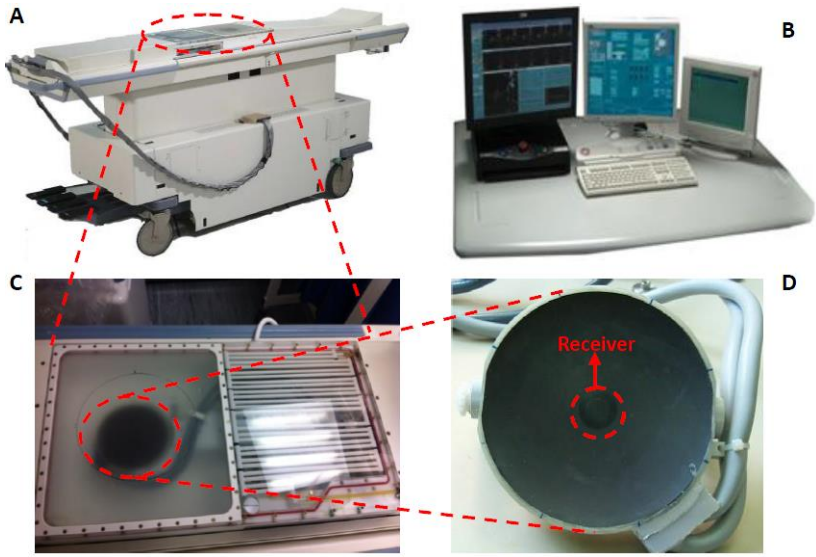

Figure 6.3 ExAblate 2000. Cradle (A); Operator console (B); Table components in degased water (C); Bowl shaped transducer (removed) (D).

ExAblate 2000's FUS system operates inside a MRI scanner that used to provide images of the patient's anatomy, and prepare an appropriate treatment plan. The MRI also measures temperature changes inside the body during FUS treatment. The system acquires MR images and runs dedicated sequences to display temperature maps. The temperature maps are used to calculate the extent of thermal ablation and to help ensure safety and efficacy. In terms of operating site, ExAblate operator has full control of all acoustic parameters, so system performance can be adjusted to do

hyperthermia instead of ablation and ‘irreversible tissue damage’. ExAblate 2000 was used as the sonication platform for the *ex vivo* study within this thesis report.

6.3 Materials and Methods

6.3.1 Materials

Consumables, animals and equipment	Manufacturer and place of origin	Specification
MycoAlertTM PLUS Mycoplasma Detection Kit	Lonza, Rockland, ME USA	
High concentration Matrigel	BD Biosciences, Two Oak Park, Bedford, MA USA	
McCoy's 5A (Modified) Medium	Gibco® Invitrogen, UK	[+] High Glucose [+] L-Glutamine [+] Bacto-peptone [+] Phenol Red [−] Sodium Pyruvate [−] HEPES
Fetal Bovine Serum (FBS)	Gibco Invitrogen, UK	Origin: South America
Gentamycin	Gibco® Invitrogen, UK	10 mg/mL
Nu/nu mice	Clare Hall Laboratories, London, UK	4 females
1.5 Tesla MRI system	General Electric, USA	Signa HDX
ExAblate 2000	InSightec LTD, Israel	UF
Single channel surface coil	InSightec LTD, Israel	5GP breast
8-channel DUOFLEX interventional coil	MR Instruments ltd. Minneapolis, USA	10 cm×10 cm 24 cm×24 cm

6.3.2 Methods

6.3.2.1 *Ex vivo* MR imaging and FUS sonication

Preliminary set up testing was done on nude mice cadavers (obtained from Animal Resource Unit of university) were used in this *ex vivo* study as a simulation for *in vivo* experiment. Lack of fur in these animals presents additional benefit for FUS experiments, since it is possible to create good acoustic coupling without shaving.

MRgFUS procedures were performed on the hind leg muscle of 5 nude mice

cadavers, from same day culling. ExAblate 2000 (uterine fibroid, UF) system was used in the experiments. The system's targeting accuracy was verified with tissue mimicking phantom on the day prior to beginning of experiment.

During the procedure, the mouse was positioned above the ExAblate 2000 system therapy table, on its right side, on top of coupling gel-pad, so that right leg of the animal was entirely immersed in a small cut-out of the gel filled with degassed water (Figure 6.4 C). In the experiments the gel-pad with mouse cadaver was placed inside a rodent chamber (Figure 6.4 A and 6.4 B), especially designed for *in vivo* experiments to provide sterile and controlled environment for the anaesthetised animal during the experiment and to prevent animal's escape in case anaesthesia level drops.. The chamber consists of Plexiglas box with Mylar surface on the bottom to allow access for the focused ultrasound.

Two gloves filled with water were arranged around the mouse cadaver, so that its head was kept above water level and right and left legs were fully separated to avoid passage of ultrasound to non-targeted leg (in *in vivo* experiment it is proposed to use mice with tumours grown on both sides, but only one will be sonicated, leaving the second one for control). Another purpose of gloves was to simulate conditions for *in vivo* experiments in which a glove with warm water is planned be used as heating source to maintain animals' body temperature during MR scanning and FUS sonication.

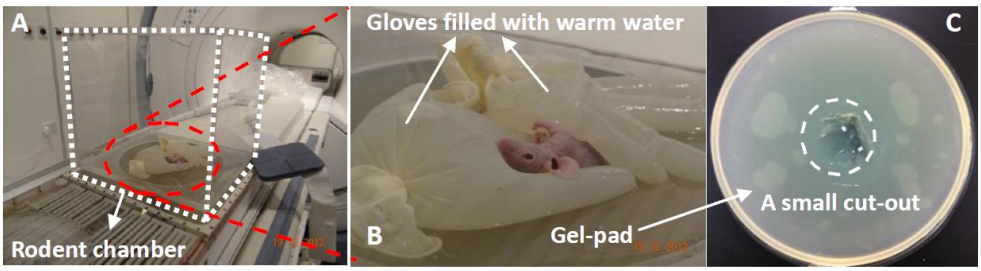

Figure 6.4 Animal positioning on ExAblate 2000 table inside rodent chamber (A); mouse was protected by gloves filled with water (B); on top of coupling gel-pad with a small cut-out (C).

Several imaging coils were evaluated in different experiments for best image quality including DUOFLEX Interventional 8-channel phased array coil 24×24 cm

and 10 × 10 cm, DUOFLEX interventional single channel coil and InSightec 5GP breast coil, respectively (Figure 6.5).

Figure 6.5 DUOFLEX interventional 8-channel phased array coil 24 × 24 cm (A) and 10 × 10 cm (B); DUOFLEX interventional single channel coil (C); and InSightec 5GP breast coil (D).

A short 3-plane localiser scan was performed to verify proper positioning, followed by Coronal and Sagittal T2-weighted FSE MR imaging sequences with the following parameters: TE = 84 msec, TR = 200 msec, flip angle 80 °, field of view 16 × 16 cm, receiver bandwidth 10 kHz and 384 × 384 matrix. The treatment region was outlined using those MR images, see Figure 6.6.

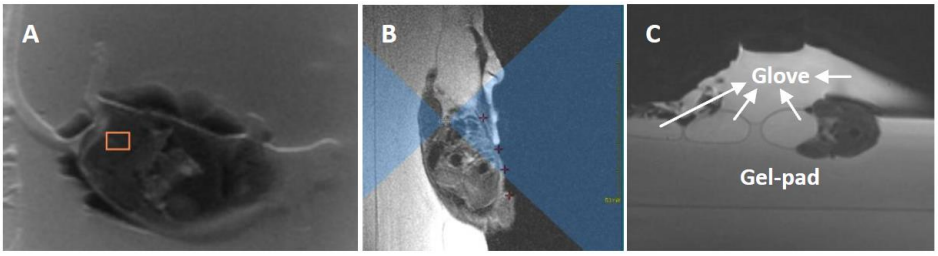

Figure 6.6 Planning of sonication. Coronal T2-weighted image, showing targeted treatment location (A); Sagittal T2-weighted image showing one of the performed sonication spots, blue area designates passage of ultrasound beam (B) and Axial T2-weighted image showing glove position around the animal (C).

Following verification, several (6 – 8) sonications were performed, with a 'hyperthermia' sonication mode, using acoustic power of 4 – 5W. Hyperthermia

sonication mode consisted in the first part of 20 sec long continuous sonication and in the second part of 54 sec long pulsed sonication with 1 sec power ON and 2.5 sec power OFF cycle. These parameters were evaluated in phantom session prior to the experiment. Highest available acoustic frequency (1.35 MHz) was selected to avoid deep penetration of US into tissue. Focal point of sonications was placed at the distal edge of the targeted muscle to increase distance to skin, which even with this measure was still smaller than ExAblate software recommends, but since sonications planned to be of very low power as compared to ablation levels, skin to focal distance was considered within safety limits.

During the sonications, real time MR thermometry was used to monitor and control spot position and tissue temperature. Reference temperature for thermometry calculation was updated in ExAblate software to be 20 ℃, as was room temperature on the day of experiment. ExAblate thermal imaging protocol was adjusted for imaging of small sample, providing good spatial resolution and reasonable Signal-to-Noise Ratio (SNR) on the same time. Resulting scan time, 10sec per thermal image, was longer than in clinical system, but since performed sonications were rather long (74 sec), temporal resolution did not suffer much.

Immediately following the procedure, a set of high quality images was acquired to find any potential changes in tissue due to MRgFUS procedure; however since cadavers lack perfusion and the energies used were very low, no radiological findings were anticipated. After the imaging, the mice cadavers were examined for any evidence of skin damage or any other noticeable treatment effect.

6.3.2.2 *Ex vivo* and *in vivo* MR imaging

Followed the above nude mice cadavers' MR imaging and ExAblate FUS sonication simulations, a human colorectal xenograft (HCT116) was implanted in live nude mice and tumour growth has been monitored regularly until tumours reached to certain sizes which were suitable (large enough) for *in vivo* MR imaging.

Tumour injection, growth and monitoring

HCT116 cell line has been introduced and employed in Chapter 4 for *in vitro* cell

culture study and they are tumourigenic in nude mice. For mice implantation, HCT116 cells were grown in McCoys 5A (modified) growth medium containing 10% FBS and 0.5% Gentamycin at 37 ℃ with 5% CO_2. Cultured HCT116 cells were tested for mycoplasma prior to harvesting. Mycoplasma-free cells were trypsinised, harvested, rinsed, and then suspended at ratio of 1 : 1 (50 µl : 50 µl) McCoys 5A medium (modified) and high concentration matrigel. The suspension was kept below 4 ℃ at all times. Xenograft studies with HCT116 were carried out under project licence PPL 60/4462 and personal licence PIL 60/14010 in accordance with the guidelines of the United Kingdom Coordinating Committee on Cancer Research (UKCCCR).

Four female nude mice were obtained at age of 4 weeks and breed in cage No.27 (C27), and they were weighed around 20 g and identified as C27.4, C27.6, C27.40 and C27. NM (No Mark) by ear mark positioning prior to tumour implantation. Mice were then injected subcutaneously in the right flank (Figure 6.7 D) with 100 µl of McCoys 5A medium (modified) and matrigel (50 µl : 50 µl) suspension, containing 1×10^8 HCT116 cells. The mice were housed under aseptic conditions, in individually ventilated cages with full records in a temperature (24 ℃) and light-controlled (12 hr/day) environment (Kang, Oh et al. 2011).

After injection, mice were checked daily and weighed weekly. Tumour measurements were carried out for monitoring. Tumour dimensions were measured twice a week using calliper. Tumour sizes were calculated according to spherical tumour volume (V) Equation 6.1(Tomayko and Reynolds 1989):

$$V = 4/3\pi[(d_1 + d_2)/4)]^3$$

Equation 6.1 Tumour volume calculation

Where, d_1 and d_2 are tumour's horizontal and vertical diameters (mm), respectively.

MR imaging procedure

MR imaging procedures for mice cadaver with tumours and live mouse with tumour were the same as *ex vivo* MR imaging described in section *6.3.2.1*. Several

MRI experiments were carried out to acquire magnetic resonance images of mice with tumours. Different rodent chambers and MR coils (Figure 6.7 B and D) were used to find the optimal set.

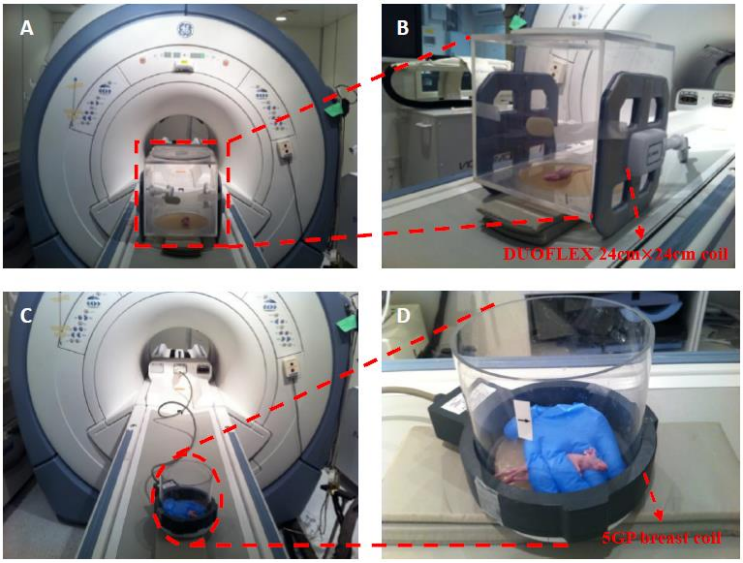

Figure 6.7 Comparison between different rodent chambers and different MR imaging coils. Big Perspex chamber with DUOFLEX interventional phased array 24 cm × 24 cm coil (A and B); small bucket chamber with InSightec 5GP breast coil (C and D).

6.4 Results and Discussion

6.4.1 *Ex vivo* Mice Cadaver MR Imaging and Sonications

6.4.1.1 MR imaging parameters

MR imaging parameters were optimised to provide the best image quality for the spatial resolution required to image such as small samples. The following imaging parameters were selected (Table 6.1):

Table 6.1 Selected MR imaging parameters

	Planning images	Thermometry
Field of View (FOV, cm)	16×16	16×16
Matrix	256×256	256×128
Slice thickness (mm)	3	3
Bandwidth (kHz)	15.6	5.7
TE (msec)	85	15
TR (msec)	3600	28
Number of averages (NEX)	2	3
Echo train length	15	N/A

For the comparison among different MR imaging coils, the coil which provided the best image quality was the single-channel surface coil (InSightec's Breast coil 5GP) (Figure 6.8 C and c), it provided best image quality both in treatment planning and in thermometry. The 8-channel DUOFLEX interventional coil also produced images of reasonable quality (Figure 6.8 B and b), although lower when compared to the single-channel surface coil. However, this coil currently cannot be used with rodent chamber, since its cable is too short and there is currently no opening in the rodent chamber to provide access for the coil. When DUOFLEX interventional phased array (24×24 cm and 10×10 cm) coil was used, no reliable thermometry could be measured, since the distance to the receiver element of the coil for such a small sample is too great to collect reliable data. Figure 6.8 illustrates difference in image quality of the scans performed with the same parameters, but with different imaging coils.

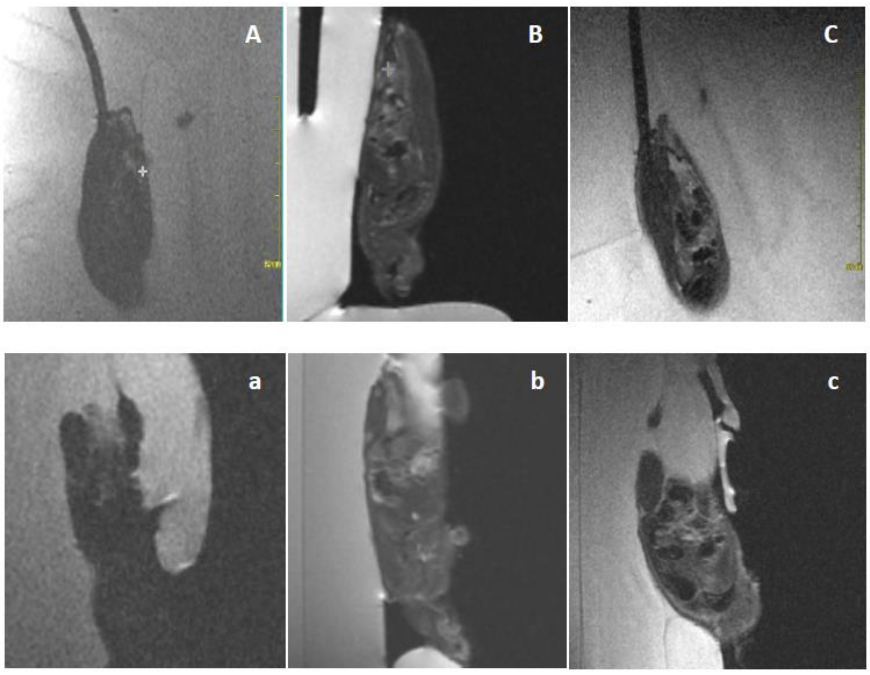

Figure 6.8 Comparison of MR scans with different imaging coils, Coronal T2-weighted planning images on the upper row (A, B and C) and Sagittal T2-weighted planning images on the lower row (a, b and c) acquired with DUOFLEX interventional phased array 10 cm × 10 cm coil (A and a); DUOFLEX interventional single channel coil (B and b); and InSightec's Breast coil (5GP) (C and c).

6.4.1.2 Sonication mode and acoustic parameters

One of the goals of these experiments was to select sonication mode that will create sufficient temperature rise (8 – 10 ℃) to cause hyperthermia (typically 40 – 47 ℃), but will still be below the level of ablation (higher than 57 ℃).

After thorough phantom tests the following sonication regime was selected: 20 sec continuous sonication, followed by pulsed sonication with 1 sec ON, 2.5 sec OFF cycle. This mode consistently created required heating pattern in phantom: rapid temperature rise of 8 – 10 ℃ in the beginning of sonication followed by temperature plateau till energy delivery stops. Continuous part of sonication is responsible for the initial temperature rise, while pulses maintain temperature at the same level. Power of 4 W was used for both parts of sonication.

Hyperthermia sonications were then performed in 5 *ex vivo* mice treatments, targeting right leg of the animal, 6 – 8 sonications per treatment. Temperature pattern

observed in dead mice tissue was similar to one seen in phantom tests: temperature rise of 7 – 10 ℃ in the beginning of sonication followed by constant temperature till sonication is over. Temperature graph of the typical sonication is shown in Figure 6.9. Some sonications resulted in higher temperature rise of 10 – 12 ℃ (which is still below ablation level), probably due to the presence of bony structures in the acoustic pass zone.

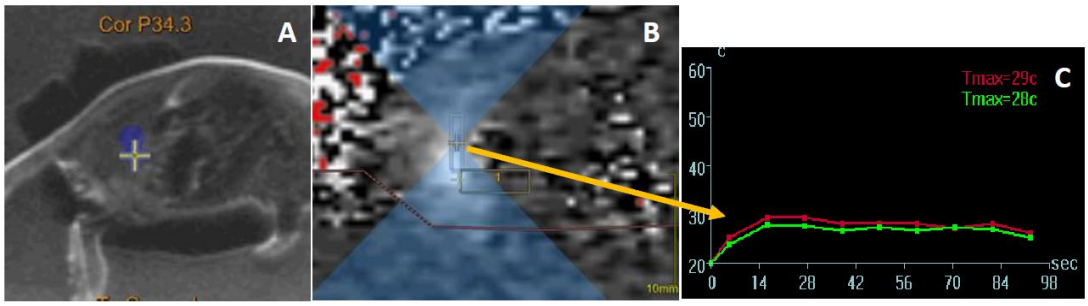

Figure 6.9 Thermal monitoring during the sonication. Coronal T2-weighted image showing planned spot location (A); Sagittal thermal image showing area of temperature rise (bright) around focal point (B); and Temperature graph showing temperature during the sonication (red line designates maximum temperature at the selected point and green line designates the average temperature over the 3 × 3 pixel area around the selected point) (C).

Sonications with power of 5 W produced considerably higher thermal rise (12 – 15 ℃) than required and it was noticed that heating was less uniform (Figure 6.10).

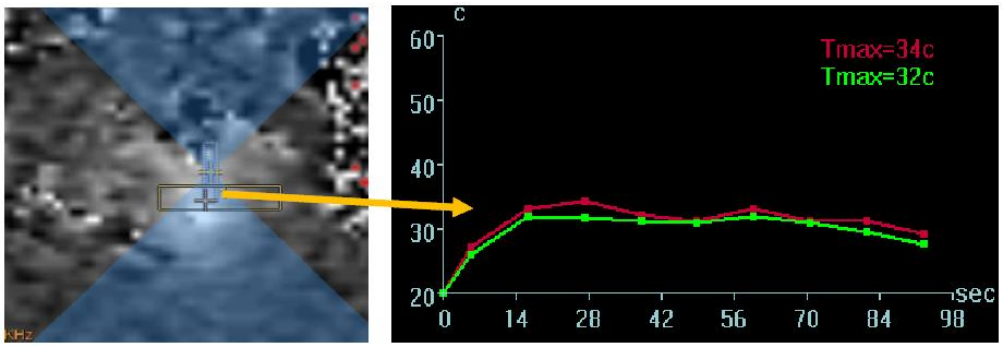

Figure 6.10 An example of sonications with power of 5 W and less uniformity of temperature rising.

In most sonications, the heating occurred just below focal point, with a constant shift of 5 – 6 mm towards the transducer. After noticing this shift, focal point was moved up, increasing skin-to-focal distance, and thus the treatment safety. Each time,

the heated spot covered roughly a circular area with diameter of ~ 10 mm. Assuming maximal tumour diameter of 15 mm, a treatment of 6 to 8 sonications should cover the required volume (tumour + margins) with sufficient overlap.

Post treatment mice cadavers were closely examined to find any skin damage or any other treatment effect. There were no signs on skin in any of the treated animals. No radiological findings were observed on post-treatment MR images.

6.4.1.3 Evaluation of rodent chamber and experimental time frame

Although the rodent chamber served its function well in above *ex vivo* experiments, several weak points were noted as MR images did not have the desired quality. Some modifications were required prior to initiation of live animals study.

The weak points and necessary improvements include: 1) the box is too deep as it was designed to be suitable for rats and guinea pigs as well as mice, so working inside the chamber with both hands during the positioning for example, is very uncomfortable, which will be even more so in *in vivo* experiment when injections will have to be performed inside the chamber (for administration of contrast agent or MBs) and the environment must stay sterile during the entire procedure; 2) two openings for gloved hands from the opposite sides of the box would increase the level of comfort significantly; 3) another opening in the box should be created for the imaging coil, which should be placed around the animal; 4) alternatively, a smaller round box can be constructed especially for mice experiments, preferably with size that will fit inside the Breast coil.

In terms of experiments time frame, the average treatment time (sonications time) was 30 min for 8 sonications, while imaging before and after treatment took additional 20 min in average. Since *in vivo* experiments are planned to be performed using gas anaesthesia, the experiment time of up to 1 hr is considered acceptable.

6.4.2 Tumour Growth and Monitoring for *ex vivo* and *in vivo* Experiments

Mice C27.4, C27.6 and C27.40 were subjected to HCT116 human colorectal cancer cells subcutaneous injection in the same day at the beginning as these three mice were proposed to be scanned by MR under terminal anaesthesia. Mouse C27.NM was injected HCT116 cells a week after, which was for conducting MR scanning under normal anaesthesia with full recovery.

After subcutaneous injection of HCT116 colon cancer cells, tumour volumes were monitored and mice weights measurements were conducted regularly. Tumour monitoring progress is shown in Figures 6.13 – 6.16 for each mouse. The values for the volume of the tumours are shown in Table 6.2 and tumour growth evolution in time in Figure 6.17, respectively. The mice weights measurements are shown in Table 6.3.

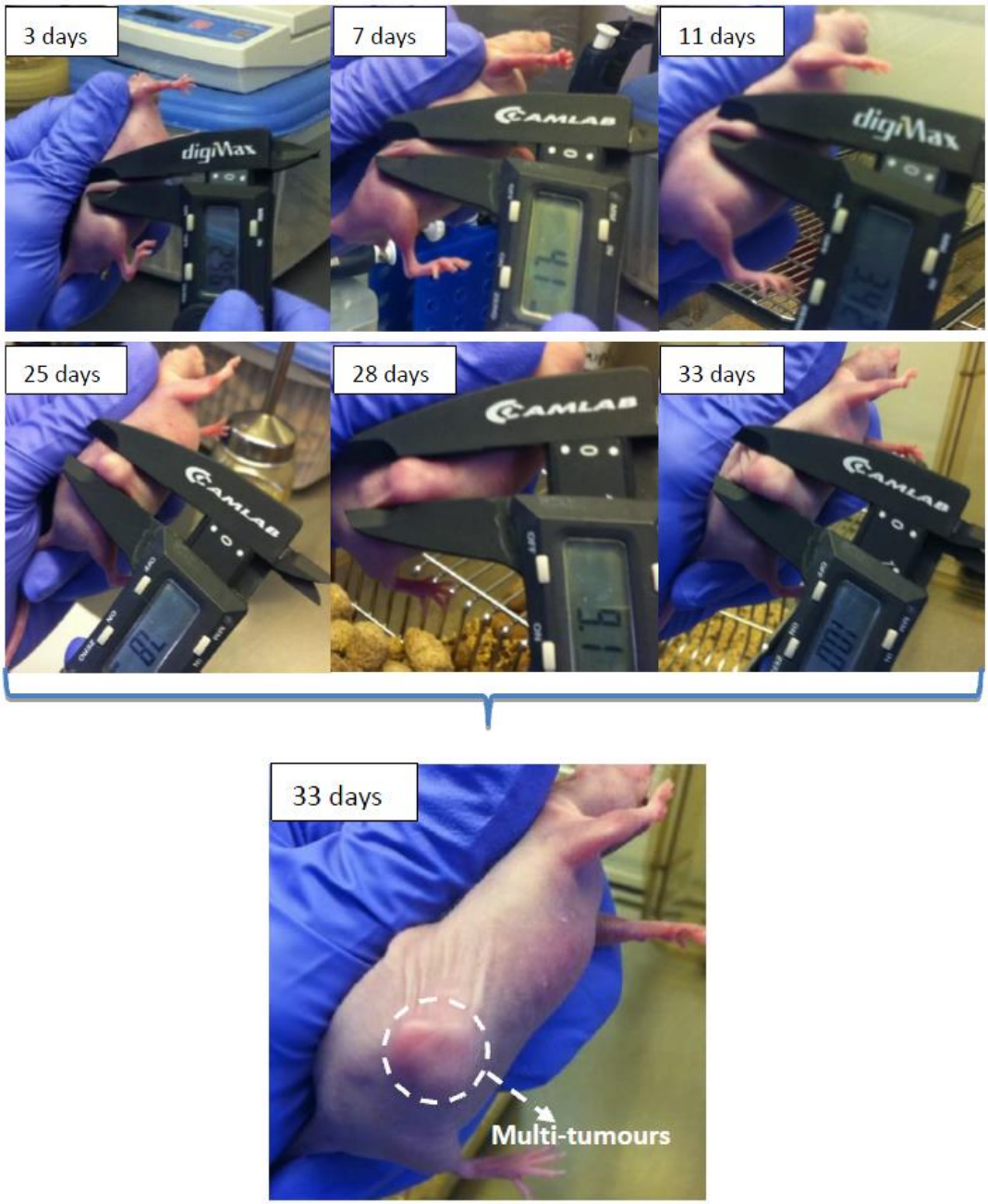

Figure 6.11 Mouse C27.4 tumour growth and monitoring until sacrifice (33 days after injection HCT116 cells).

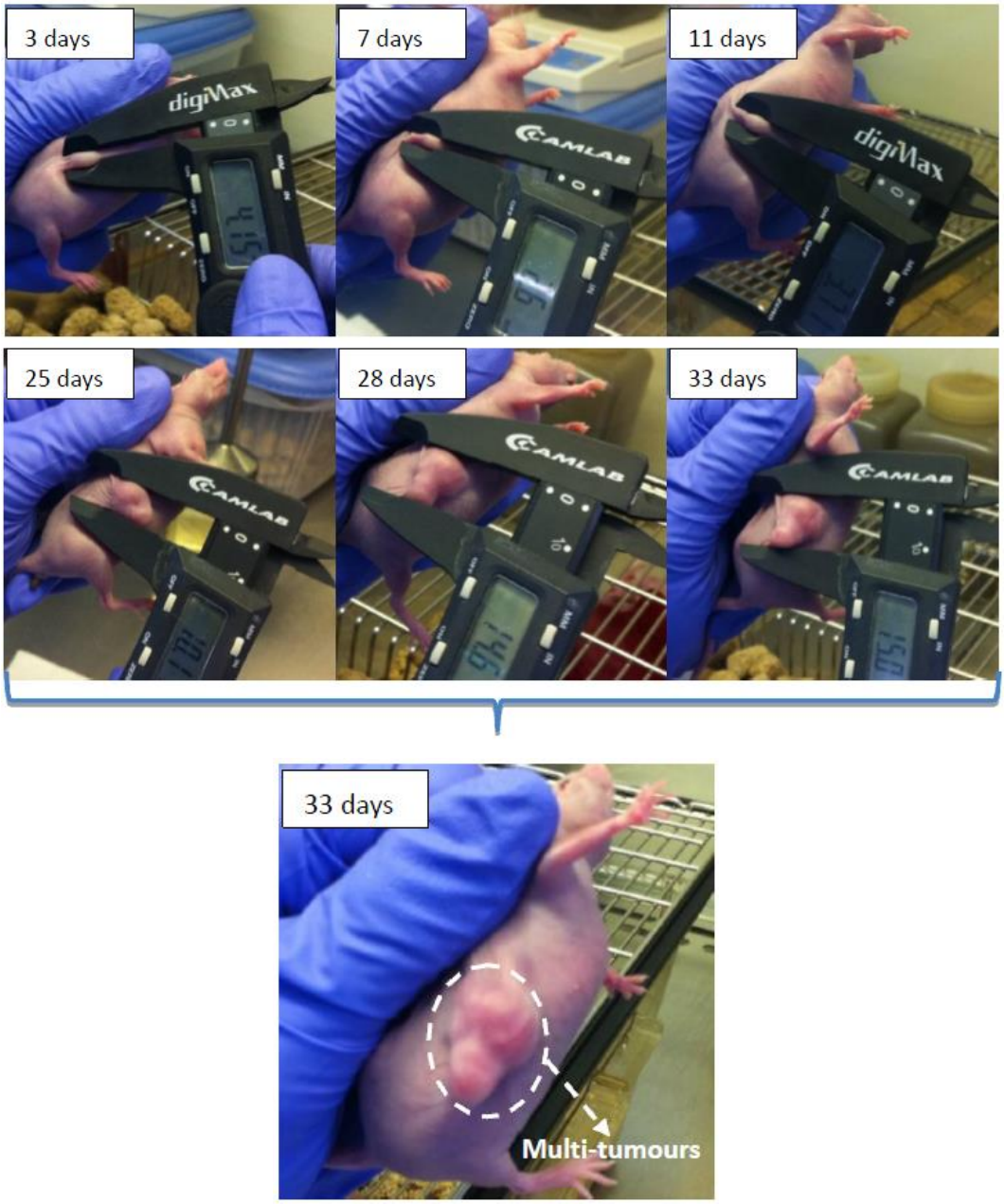

Figure 6.12 Mouse C27.6 tumour growth and monitoring until sacrifice (33 days after injection HCT116 cells).

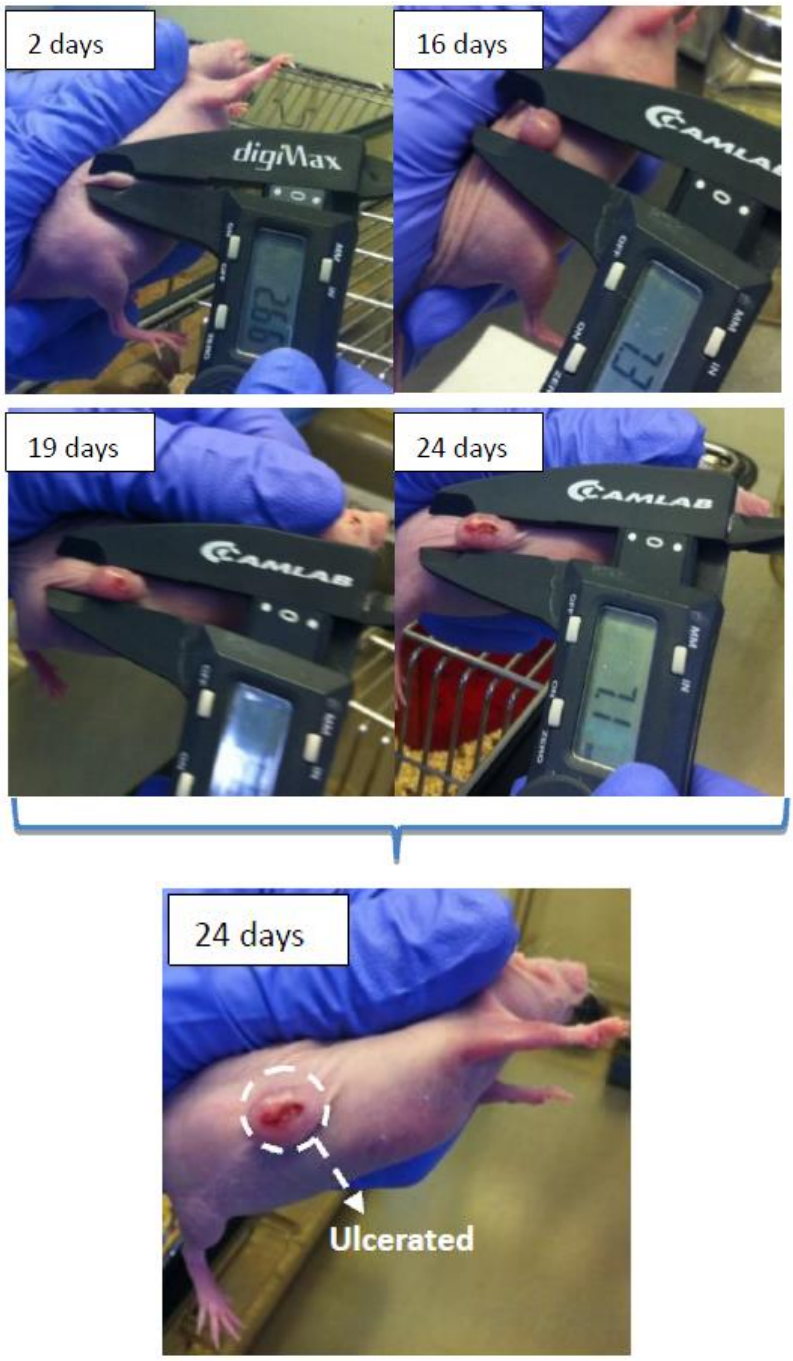

Figure 6.13 Mouse C27.NM tumour growth and monitoring until sacrifice (24 days after injection HCT116 cells, ulcerated).

Tumour monitoring revealed that tumour implanted for mouse C27.NM (Figure 6.13) was ulcerated after 24 days post injection, and it was suggested to euthanise the animal as soon as possible to minimise its suffering. Therefore, mouse C27.NM (exchanged with mouse C27.40) together with mouse C27.4 (Figure 6.11) and C27.6 (Figure 6.12), whose tumours grew faster in comparison to mouse C27.40 (Figure 6.14),

were terminated by CO_2 euthanasia after 24 days (mouse C27.NM) and 33 days (mouse C27.4 and C27.6) post injection of HCT116 cells. Right before termination, tumour volume of three mice was 332.98 mm^3 (mouse C27.NM), 572.04 mm^3 (mouse C27.4) and 1059.71 mm^3 (mouse C27.6), respectively. Moreover, tumours of mouse C27.4 and C27.6 appeared as a multi-tumours shape.

Figure 6.14 Mouse C27.40 tumour growth and monitoring until after injection 33 days.

On the contrary, mouse C27.40, which was supposed to be sacrificed and to undergo MR imaging as a cadaver, replaced mouse C27.NM and was scanned as live due to its relatively slower tumour growth rate and smaller tumour volume (Figure 6.14).

Table 6.2 lists detailed information of tumours' monitoring process and their sizes in different stages. Figure 6.15 shows by curves the overall trend of tumour growth of four mice.

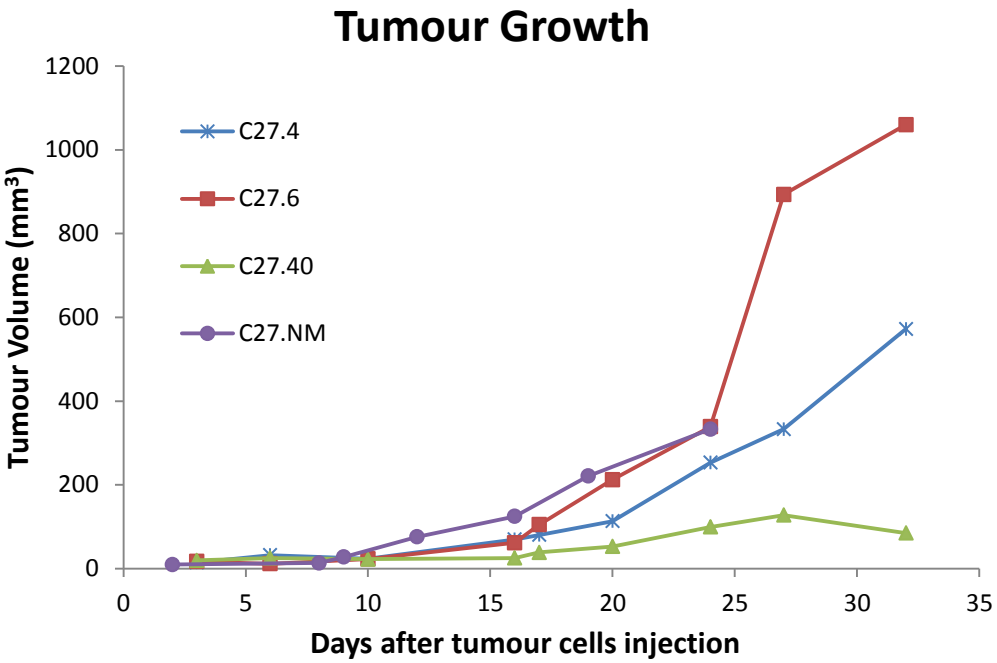

Figure 6.15 Tumour growth curves of four mice.

Table 6.2 Tumour growth and volume (mm^3) monitoring

# Mouse	Dates	29-04-13	02-05-13	06-05-13	12-05-13	13-05-13	16-05-13	20-05-13	23-05-13	28-05-13
C27.4	d_1/d_2 (mm)	2.96/3.1	4.1/3.8	3.38/3.7	4.8/5.4	5.2/5.5	5.6/6.4	7.9/7.8	8.1/9.1	10/10.6
	Tumour Volume(mm^3)	14.56	32.26	23.22	69.44	80.16	113.08	253.24	332.98	572.04
C27.6	d_1/d_2 (mm)	3.22/3.15	2.6/3.0	3.42/3.63	4.7/5.1	5.7/6.0	7.0/7.8	10.1/7.2	14.6/9.3	15.0/10.3
	Tumour Volume(mm^3)	16.91	11.49	22.93	61.59	104.81	212.13	338.82	893.35	1059.71
C27.NM	d_1/d_2 (mm)			2.64/2.61	3.1/2.8	4.2/3.3	4.5/6.0	7.3/5.1	6.6/8.4	7.1/10.1
	Tumour Volume(mm^3)			9.47	13.44	27.61	75.75	124.76	220.85	332.98
C27.40	d_1/d_2 (mm)	3.31/3.39	4.0/3.3	3.3/3.82	3.5/3.8	4.4/4.0	4.6/4.7	5.5/6.0	6.3/6.2	5.5/5.4
	Tumour Volume(mm3)	19.68	25.46	22.54	25.46	38.79	52.64	99.52	127.81	84.74

In parallel, all mice weights were measured once a week. Table 6.3 presents weights of four mice after tumour implantation. For mouse C27.4 and C27.NM, their weights were increasing every week due to tumours growth. In contrast, weights of mouse C27.6 and mouse C27.40 were decreasing after 3 weeks of tumour implantation; it might be because their body had relevant pathological response to the tumour xenografts such as loosing weights.

Table 6.3 Mice weights monitoring

Dates / Weight (g) / #Mouse	29-04-13	02-05-13	09-05-13	13-05-13	20-05-13	28-05-13
C27.4	18.5	20.1	22.1	22.9	22.5	23.2
C27.6	19.7	22.0	24.4	24.1	23.3	22.7
C27.NM	21.5	22.4	25.2	25.3	25.5	26.1
C27.40	20.5	22.3	24.4	23.9	23.0	22.6

6.4.3 *Ex vivo* Mice Cadaver Bearing Tumours MR Imaging

The following tables (Table 6.4 – 6.6) list selected MR parameters for scanning three mice (C27.4, C27.6 and C27.NM) cadavers bearing tumours.

Mouse C27.4

Table 6.4 Mouse C27.4 MR imaging parameters

	Mouse C27.4			
Coil	DUOFLEX 10×10	DUOFLEX 24×24	5GP breast	
Sequence	FRFSE-XL	FRFSE-XL	FSE-XL	FRFSE-XL
TR (ms)	5880	6480	580	3260
TE (ms)	84.5	84.5	8.2	85
Bandwidth (kHz)	10	10	31.2	10
FOV (cm)	14×14	14×14	14×14	13×13
Slice thickness (mm)	2	2	2	2
Number of averages (NEX)	2	3	2	2

Three groups of MR scans were conducted for the first mouse C27.4 by using MR parameters list in Table 6.4 and three different coils (DUOFLEX interventional phased

array 10 × 10 cm, 24 × 24 cm coil, and InSightec 5GP breast coil) were used under different set of MR parameters according to different coils' property.

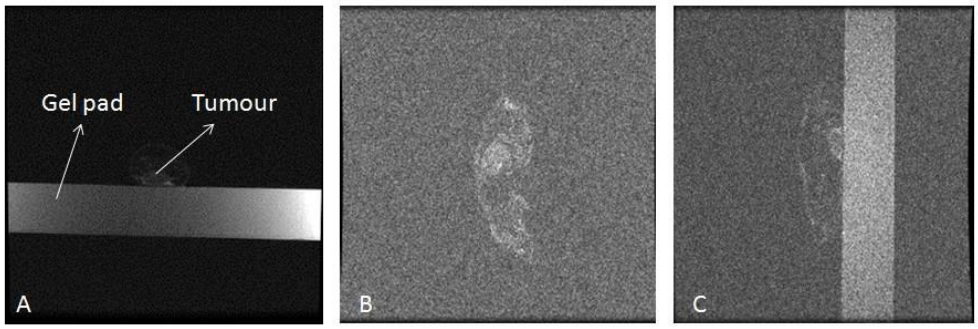

Figure 6.16 MR images of mouse C27.4 placed inside big Perspex rodent chamber and scanned by DUOFLEX interventional phased array 10 × 10 cm coil. Axial (A); coronal (B); and sagittal (C) T2-weighted scans of the animal lying on a gel pad were taken to visualise the tumour.

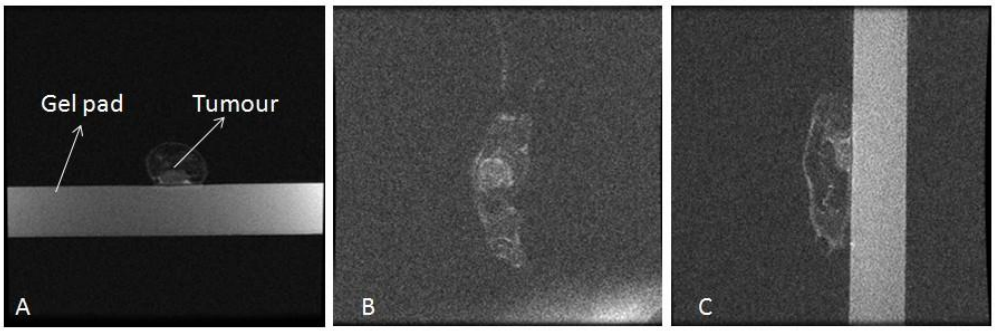

Figure 6.17 MR images of mouse C27.4 placed inside big Perspex rodent chamber and scanned by DUOFLEX interventional phased array 24 × 24 cm coil. Axial (A), coronal (B) and sagittal (C) T2-weighted scans of the mouse lying on a gel pad, were taken to visualise the tumour.

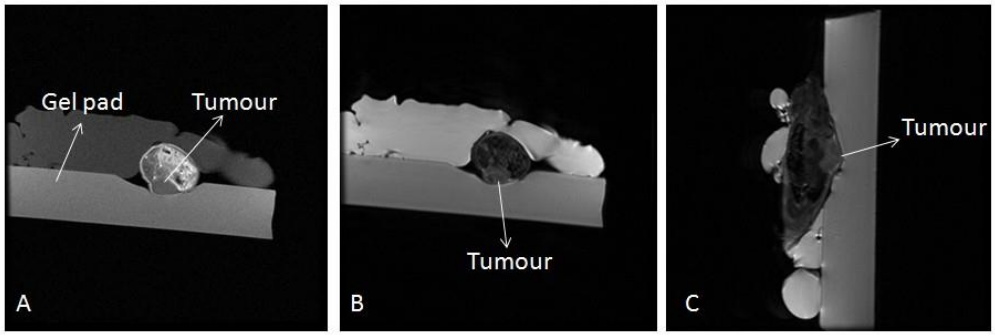

Figure 6.18 MR images of mouse C27.4 placed inside small Bucket rodent chamber and scanned by InSightec 5GP breast coil. An axial T1-weighted MR image was first taken to plan the scan (A); axial T2-weighted; (B) and sagittal T2-weighted (C) images of the animal were taken to visualise the tumour.

Figure 6.16 shows MR images of mouse C27.4 scanned by DUOFLEX interventional phased array 10 × 10 cm coil. The image quality was not good enough to observe the exact location of tumour especially when the image orientations were coronal and sagittal. The reason was that the small mouse cadaver inside the big Perspex rodent chamber was located too far from the receiving elements of the coil. Similarly, images obtained by using DUOFLEX interventional phased array 24 × 24 cm coil were not satisfactory either because big rodent chamber was still keeping the mouse cadaver too far from the coil. However, when using DUOFLEX 24 × 24 cm coil higher image quality was achieved (Figure 6.17 A) than DUOFLEX 10×10cm coil as can be seen from the clear tumour position in the axial image.

In comparison to Figure 6.16 and 6.17, much clear MR anatomy images of the mouse were obtained by using InSightec 5GP breast coil which was set up around a small round Bucket chamber. As can be seen from Figure 6.18, both mouse anatomy and location of the tumour were clearly seen in both axial and sagittal orientations as opposed to Figure 6.16 and 6.17. This was because the scanned object (mouse) was nearer to the imaging coil.

Mouse C27.6

Based on scanning parameters for the above mouse C27.4, for the second mouse C27.6, only two coils (DUOFLEX interventional phased array 24 × 24 cm coil and InSightec 5GP breast coil) were used. Two sets of scans were conducted according to the parameters list in Table 6.5, respectively.

Table 6.5 Mouse C27.6 MR imaging parameters

	Mouse C27.6		
Coil	DUOFLEX 24×24	5GP breast	
Sequence	FRFSE-XL	FSE-XL	FRFSE-XL
TR (ms)	3260	740	3600
TE (ms)	85	8.2	85.2
Bandwidth (kHz)	10	31.2	10
FOV (cm)	13×13	14×14	14×14
Slice thickness (mm)	3	2	2
Number of averages (NEX)	3	3	3

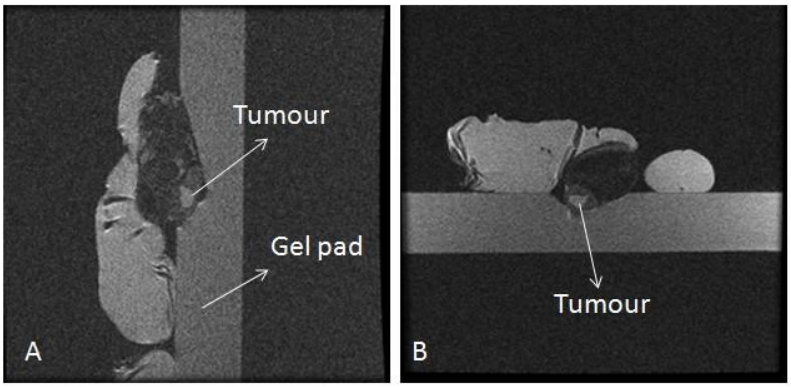

Figure 6.19 MR images of mouse C27.4 placed inside big Perspex rodent chamber and scanned by DUOFLEX interventional phased array 24 × 24 cm coil. Sagittal (A) and axial (B) T2-weighted scans of the mouse lying on a gel pad were taken to visualise the tumour.

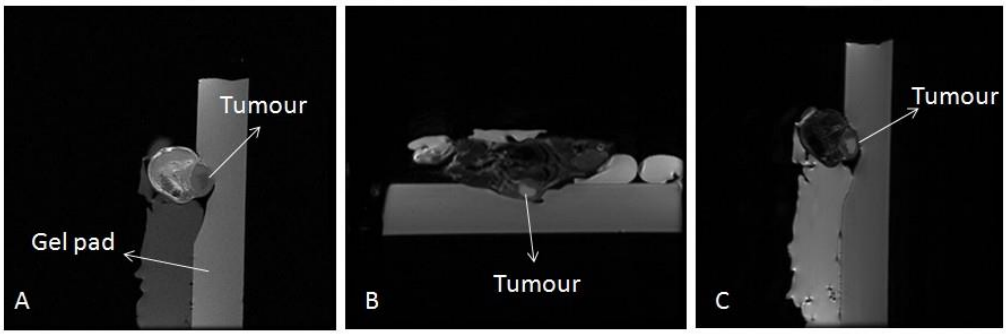

Figure 6.20 MR images of mouse C27.4 placed inside small Bucket rodent chamber and scanned by InSightec 5GP breast coil. A sagittal T1-weighted MR image was first taken to plan the scan (A); axial (B) and sagittal (C) images of the animal were taken to visualise the tumour.

The MRI images obtained for mouse C27.6 were similar to the ones for C27.4. Images obtained by using DUOFLEX interventional phased array 24 × 24 cm coil were less clear (Figure 6.19). This was due to the mouse placing inside the big Perspex animal chamber which kept the mouse far away from the coil. 5GP breast coil gave better image quality (Figure 6.20) by fixed around the small bucket animal chamber where the coil was located nearer to the mouse cadaver.

Mouse C27.NM

For the last mouse cadaver C27.NM, only 5GP breast coil was used for MR scanning. Table 6.6 lists MR scanning parameters used for C27.NM.

Table 6.6 Mouse C27.NM MR imaging parameters

	Mouse C27.NM	
Coil	5GP breast	
Sequence	FSE-XL	FRFSE-XL
TR (ms)	580	2940
TE (ms)	8.2	84.5
Bandwidth (kHz)	31.2	10
FOV (cm)	14×14	14×14
Slice thickness (mm)	2	2
Number of averages (NEX)	3	2

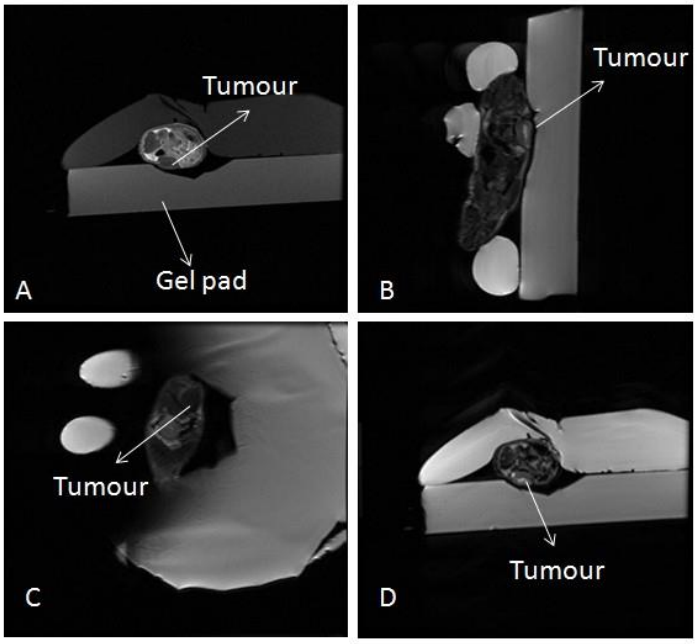

Figure 6.21 MR images of mouse C27.NM placed inside small Bucket rodent chamber and scanned by InSightec 5GP breast coil. An axial T1-weighted MR image was first taken to plan the scan (A); sagittal (B), coronal (C) and axial (D) images of the animal were taken to visualise the tumour.

InSightec 5GP breast coil gave the best image quality among all the other coils, this coil and set up were further adopted for the next step: *in vivo* MR imaging.

6.4.4 *In vivo* Live Mice Bearing Tumours Anaesthesia and MR Imaging

Mouse C27.40

For anaesthesia procedure, it was administered 0.23 ml of the ketamine/xylazine mixture to mouse C27.40 according to its weight was 23 g by intra-peritoneal injection. The full surgical anaesthesia was achieved approximately 3 min later. The mouse was inspected according to MR imaging protocol shows in Table 6.6 in section *6.4.3*, by employing InSightec 5GP breast coil. Coronal, axial and sagittal MR images were obtained for mouse C27.40 can be seen in Figure 6.22.

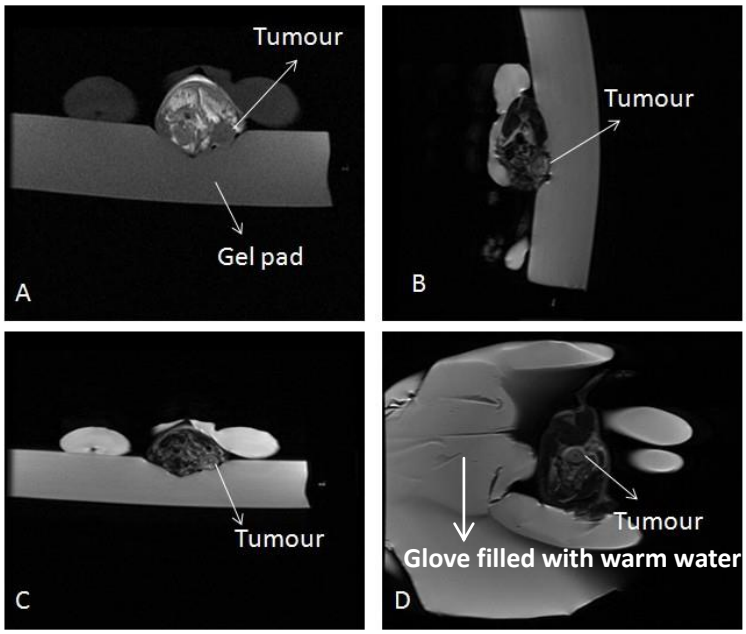

Figure 6.22 MR images of live mouse C27.40 placed inside small Bucket rodent chamber and scanned by InSightec 5GP breast coil. An axial T1-weighted MR image was first taken to plan the scan (A); sagittal (B), axial (C) and coronal (D) images of the mouse were taken to visualise the tumour.

From Figure 6.22, high resolution live mouse anatomy images were obtained by MR with clear localisation of the implanted tumour. During MR scanning, the mouse was surrounded by gloves filled with warm water (~ 50 ℃) (Figure 6.22 D) for maintaining mouse's normal body temperature. After 35 min MR scanning, it was

noticed that the mouse was coming out of deep anaesthesia and was responding to painful stimuli, which confirmed the proper anaesthesia administration of ketamine / xylazine mixture for desired mouse recovery time frame at around 30 min. Warm water filled gloves successfully maintained mouse's normal body temperature during the entire imaging procedure in the cold environment of MRI room.

As the procedure was proposed to be conducted continually under terminal anaesthesia without recovery, a further dose of 0.1 ml of ketamine / xylazine mixture was given, which achieved full surgical anaesthesia again in approximately 1min. The warm water filled glove was then replaced with one filled with freshly heated water and it was resumed the imaging procedure for a last scan. This procedure lasted approximately 12 min and the mouse was found to be dead at the end.

6.5 Conclusions

In this study, the optimal experimental set-up and the MR imaging protocol that gives the best images for the tumour visualisation were found. The optimal set up for the MR imaging included the receive-only InSightec 5GP Breast coil and the small cylindrical mouse house. It was found during procedure that for optimal imaging results the mouse house and coil were best sited on some pads to raise them to (or as near to) the isocentre of the magnet. For ease of localisation and prescribing subsequent scans the animal should be placed either head or feet first into the scanner.

The experimental arrangement was tested firstly in ex-vivo experiments in which mice cadavers were used prior to conducting the first experiments with live animals. These *ex vivo* experiments were successfully conducted and the parameters (sonication parameters as well as MR imaging parameters and imaging coil) for the future in-vivo experiments have been optimised, and such a protocol was considered as a general hands-on rehearsal for the research team before the first live animal experiments was carried out.

HCT116 tumour xenografts were successfully implanted and grew well in the rodent mode of female nude mice. Tumour growth monitoring and tumour volume

measurement were conducted according to standard routines. The high resolution MR images of dead/live mice bearing tumour xenografts ensured the future *in vivo* sonication experiments will be conducted under precise imaging guidance. Together with the FUS parameters, these parameters form a set that will allow application of MRgFUS treatments to live mice bearing tumours under anesthesia with full recovery.

Chapter 7

Discussions and Conclusions

7.1 Discussions and Prospects

This thesis has presented comprehensive research on a TDD vehicle for potential joint chemotherapy for cancer from the chemical design and synthesis of nanocarriers through *in vitro* work to *in vivo* trials. Many achievements were made but these are also accompanied with many future prospects.

CDs' deviation as TDD nanocarriers

First of all, CDs are multi-functional agents that have attracted much attention and use in the pharmaceutical field. Research in both humans and animals has illustrated that CDs can be utilised to improve drug delivery for almost any type of drug formulation. The properties of bio-adaptability and multi-functionality make CDs capable of alleviating those undesirable characteristics of drug molecules in various routes of administration through the formation of CD-drug inclusion complexes.

Knowledge of different impact factors which can influence complex formation to obtain clinically applicable CD-drug complexes with potently desirable properties is essential. However, adding CDs to existing drug molecules without further optimisation will seldom result in an acceptable outcome. Thus, the work for this thesis sought to explore chemical modification based on native CDs in the design of an innovative TDD system with existing anticancer drugs.

Since CDs are capable of extending the function of pharmaceutical additives, the combination of molecular encapsulation with other possible materials will become effective and a valuable tool for the improvement of drug formulation in the manner of stability and circulation time *in vivo*. Moreover, the most desirable attribute for a drug carrier is the ability to deliver enough potency of a drug to a targeted site. For the novel synthesised **carrier 3b** discussed in this study, a hypothesised model of possible

conjugation with polymers or peptides to further improve its drug delivery properties, and rational tagging with a delivery ligand is presented in Figure 7.1.

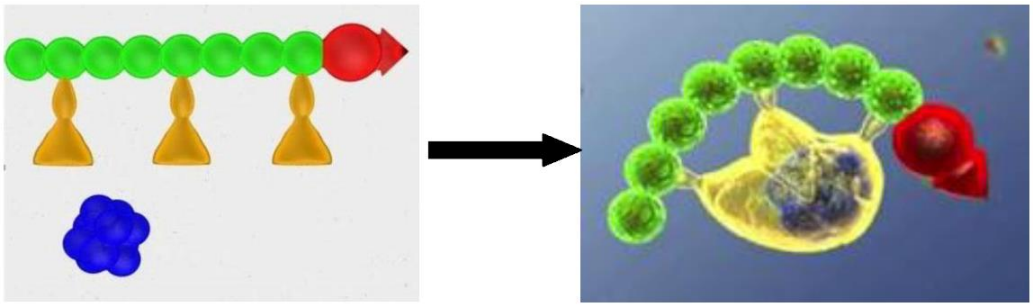

Figure 7.1 γ-CD based drug delivery vehicle.

Here, the yellow part is γ-CD derivative monomers; several of them will capture a drug molecule (blue balls); the green chain could be a polymer or peptide to carry the monomer CD carriers and the red arrow molecule represents a targeting ligand that will recognise certain receptors of tumours. The targeting ligand could be a folate receptor (FR) acceptor which can recognise high FR-expressing tumour cells such as the KB cells discussed in this thesis.

The conjugation of a drug with CD can be a versatile means to construct a new class of novel drug delivery systems like liposomes, microspheres, peptides, nanoparticles and site specific prodrugs. Thus, there is scope for a vibrant future in the research and development of CD based drug delivery systems (Arun, Ashok et al. 2008).

Establishment of *in vitro* human cancer cell models for FUS-mediated TDD

Chemical modification, characterisation and analysis are very early stage investigations relating to the inclusion of CD-drug complexation; whether the same strong encapsulation affinity between modified CD and the drug will be observed *in vivo* or in further clinical studies, *in vitro* experiments are indispensable. A typical and reliable *in vitro* study for a novel exploited TDD system is performed by using cultured human cancer cells which usually express a unique surface marker specifically entrusted with the task of testing the targeted delivery strategy (Bae and Park 2011). Cytotoxicity and cellular drug uptake are commonly examined by exposure of drug delivery systems

directly to those cells grown as monolayers or in suspension under various environmental conditions.

Two human cancer cell lines: KB and HCT116, were successfully tested *in vitro*, leading to the achievement of the objective of fast screening of the carriers' encapsulation potency to different drug molecules, investigation of drug release factors and confirmation of sonoporation. A particularly interesting contribution was the establishment of a precise sonoporation protocol for cell monolayers in a 96-well plate. In terms of *in vitro* cell sonoporation reported in the current literatures, they are mostly carried out with cell suspensions (Ashush, Rozenszajn et al. 2000; Guzman, Nguyen et al. 2001; Sundaram, Mellein et al. 2003; Karshafian, Bevan et al. 2009) rather than adhesion cell monolayers, despite the fact that cell suspensions are believed to be far away from the real cell conditions *in vivo*. Secondly, sonications were commonly performed in physical environments such as an Opti-cell chamber (Yudina, de Smet et al. 2011) or a petri-dish (Liu, Cho et al. 2001), in which, cells are cultured in a unitary environment without the possibility of isolated control samples undergoing the same sonication conditions.

Taking the above aspects into account, the sonicator device for cell monolayer sonication in a 96-well plate was established as a unique but standardised and precisely repeatable US applicator. A sonication protocol with cell monolayers in a single well achieved experimental conditions with the following features:

1) the cell monolayer more closely resembles the conditions of cells in tissue;

2) single wells are isolated from each other and can be treated and examined separately;

3) sonication groups with various US parameters together with control groups can be easily arranged within a single 96-well plate.

MBs-involved FUS-mediated TDD under non-thermal effects

Through the application of the *in vitro* sonicator, another contribution was to prevent FUS induced thermal effects and thus to investigate cells' response only to mechanical effects by employing very low acoustic power. It has been shown in the *in vitro* sonication results that MB-stimulated oscillation (e.g. microstreaming) or

cavitation involved in cell sonoporation occurred with negligible thermal effects detected and that sonoporation in human cancer cells is directly related to MB concentration (Ward, Wu et al. 2000). This indicated FUS-mediated drug delivery in the presence of MBs is effective; however, much more work needs to be carried out to demonstrate the precise mechanisms of this action.

Although the acoustic pressure threshold of oscillation or cavitation from MBs is not fully understood, several parameters, including the abundance of cavitation nuclei in the exposed medium, affect the process (Han, Ikegami et al. 2007). Other factors affecting sonoporation include MI, acoustic pressure amplitude, exposure time, duty cycle and pulse repetition frequency (PRF). Sonoporation efficiency improved (as shown by enhanced cell permeability and cellular drug uptake) with increased values of MI, acoustic pressure amplitude and FUS exposure time in the present study.

The conclusion that follows is that the method of *in vitro* cell cultivation and sonoporation is a very useful tool in FUS-mediated TDD, recognizing that certain methods cannot be examined with *in vivo* models directly before validation of their safety. However, it is generally believed that the most trustworthy preclinical experiments are animal studies. Nevertheless, methods to eliminate any pain or distress in trials involving live animals are continuously advocated. Hence there is a steady and increasing demand to replace animal studies by *in vitro* experiments in research, leading to the need for better understanding of the replacement of *in vivo* by *in vitro* methods. Many questions certainly can be answered by *in vitro* experiments, but these cannot cover the whole area of scientific research. Working with live animals means the examination of questions in their full complexity; whereas *in vitro* experiments may be able to answer only one special aspect of a question (Varga 2011).

MRgFUS-ExAblate 2000: *ex vivo* and *in vivo* pre-clinical studies

Although the *in vitro* cell sonicator has the potential to become a potent instrument for prolonged application and investigation in FUS-involved TDD, in practice, efficient monitoring tools for sonication parameters, cavitation detection and thermal isolation are still under development. The sonicator cannot be used in *in vivo* studies in its current state and it is not MR compatible; hence results could not be translated

directly into clinical use. Therefore, a clinically approved MRgFUS system–ExAblate 2000 was adopted to perform *in vivo* trials by utilising a small rodent model to further evaluate the FUS-induced TDD systems developed in this study.

Before exposure of any animals to either FUS or encapsulated drugs, *post mortem* and *in vivo* MRI scans and ExAblate sonications were performed and optimised MRI and FUS parameters were determined. *In vivo* carrier-drug distribution was also investigated by intravenous administration of encapsulated DOX and DOX alone to healthy mice. In the later studies, mice were sacrificed immediately and 0.5 min, 2 min, 2 hr, 4 hr and 10 hr after drug / encapsulated drug administration, respectively. Necessary organs were extracted and homogenised.

Following the results achieved with optimised MRI and FUS parameters, validated potency of drug protection *in vivo* and the significant drug release in the presence of hyperthermia and FUS with MBs, the *in vivo* release of encapsulated DOX from the carriers by application of MRgFUS on a targeted region was considered. The purpose of the experiment described next was to evaluate encapsulation and drug release by the use of MRgFUS in the quadriceps muscles of living healthy mice. A total of five mice were involved; four of these were treated with MRgFUS and one remained as a non-sonicated control.

The applied acoustic power (4 W) and sonication duration (14 min) failed to produce the desired temperature increase of 6 – 8 ℃, as was initially planned and seen *ex vivo*. Chemical analyses showed that although there was a fluorescent signal of DOX in the collected organs (blood, liver and kidney), there were no detectable signals in the quadriceps muscles samples. This indicated that there might be a problem with the length of exposure time to DOX. Previous *in vivo* experiments showed that the optimal time for encapsulated DOX absorption in the quadriceps muscles is about 10 hr following injection, strongly suggesting that the short exposure time of 14 min would not be enough to produce a clear DOX signal from this tissue.

Future experiments should consider the application of higher powers as well as the examination of different time points of DOX exposure both before and after MRgFUS application. The sonoporation stimulus of MB USCA should also be considered for

injection with encapsulated DOX. Still more specifically, the proof of efficacy of the drug delivery system developed in the work reported here requires *in vivo* experiments with xenografts of human cancer in mice, rabbits or rats in the near future. The experiments should be conducted following percutaneous or image guided orthotopic implantation of human tumour cell lines such as ultrasound monitored prostate orthotopic tumour reported by Saar *et al.* (Saar, Körbel et al. 2012) and orthotopic U87 gliomas assessed by MRI present by Weidensteriner *et al.* (Weidensteiner, Reichardt et al. 2013). When the tumour size reaches 5 – 10 mm, the cytotoxic drug bound to the nano-carrier and/or MBs suspension should be injected intravenously. MRI guided insonation of the tumour should then be carried out using protocols established by previous *in vitro* and *in vivo* studies.

7.2 Conclusions

Overall, this thesis study concludes feasibiltiy of a MRgFUS mediated TDD vehicle from:

1) rational design and synthesis of natural γ-CD as an encapsulation and transport nanocarrier for DOX;

2) full chemical characterisation of desired **carrier 3b**;

3) comprehensive inclusion affinity and drug release analysis of the carrier-DOX complex;

4) successful establishment of *in vitro* human cancer cell models;

5) validation of the encapsulation efficiency both *in vitro* and *in vivo*, as well as thermo-sensitivity of carrier-DOX inclusion in monolayers of cells;

6) successful *in vitro* sonoporation application of a unique sonicator in combination with MBs;

7) successful optimisation of clinical MRI and FUS parameters *ex vivo* and *in vivo*.

The results from this study confirm the possibility of translation of the constructed γ-CD derived carrier into clinical use as a delivery vehicle of DOX for release with combined thermal and mechanical mechanisms by clinically applicable

MRgFUS-triggered TDD for cancer therapy.

The Thesis provides better understanding of the mechanism of and potential for this novel delivery approach: MRI-guided, ultrasound-mediated, site-specific drug delivery assisted by MB contrast agents. It is likely that this novel technology will enter the clinical arena in the near future, based on the ever-increasing scientific contributions from researchers. The chemical modifications and *in vitro*, *ex vivo* and *in vivo* preclinical studies discussed here represent only a glimpse into the future of clinical application.

Finally, to master MRgFUS-mediated therapeutic applications of the kind presented here and to translated them into the clinic still requires interdisciplinary collaborations. Much effort is being dedicated to technological advancement in all aspects of the drug delivery platform: hardware, software, and wetware (protocols and molecular devices used in molecular biology and synthetic biology) (Castle, Butts et al. 2013). Expertise in the fields of physical chemistry, cellular physiology, genetics, ultrasound physics and imaging must come together with shared goals. Following relationships formed in the Nanoporation project, it is conceivable that new strategic partnerships will be developed among the partners, to involve pharmaceutical companies, and clinical reseach to provide the necessary translation of MRgFUS-based TDD into cancer therapy .

Appendices

1 Standardisation, Apparatus and Set-up of *in vitro* FUS Device for TDD

In the current setup, the acoustic fields of four interchangeable custom transducers, built *in-house*, were simulated using a model created in MATLAB and the results were compared with output measurements from each transducer, taken with a needle hydrophone. Frequencies of desired transducers are 0.486 MHz, 1.142 MHz, 1.467 MHz and 2.022 MHz, which can deliver maximum acoustic powers, $5 < P_{ac} < 25$ W, depending on the transducer and its efficiency. The range of frequencies was chosen to cover clinically available FUS system ExAblate in order to produce relevant guidance for pre-clinical studies (Chapter 6).

The device (Figure A.1 A) consists of a Perspex box with several separate compartments including a larger one for the water bath in which the ultrasound sources and the 96-well plate are placed. Degassed water is circulated to prevent air bubble formation beneath the plate interfering with the FUS propagation and its temperature is kept close to physiological levels (37 ℃) using an external heater. A smaller compartment inside the water bath ($14 \times 10.5 \times 6$ cm^3) accommodates detachable nylon housing (Figure A.1 D) for the transducers. These are activated with a signal generator (Figure A.1 F) that can generate various wave-forms amplified with an A075 RF power amplifier (Figure A.1 G). Alongside the water bath, a linear stage translates a Perspex transducer holder (Figure A.1 E) for a 96-well plate through the water above the transducers on two parallel aluminum tracks, using small linear bearing carriages.

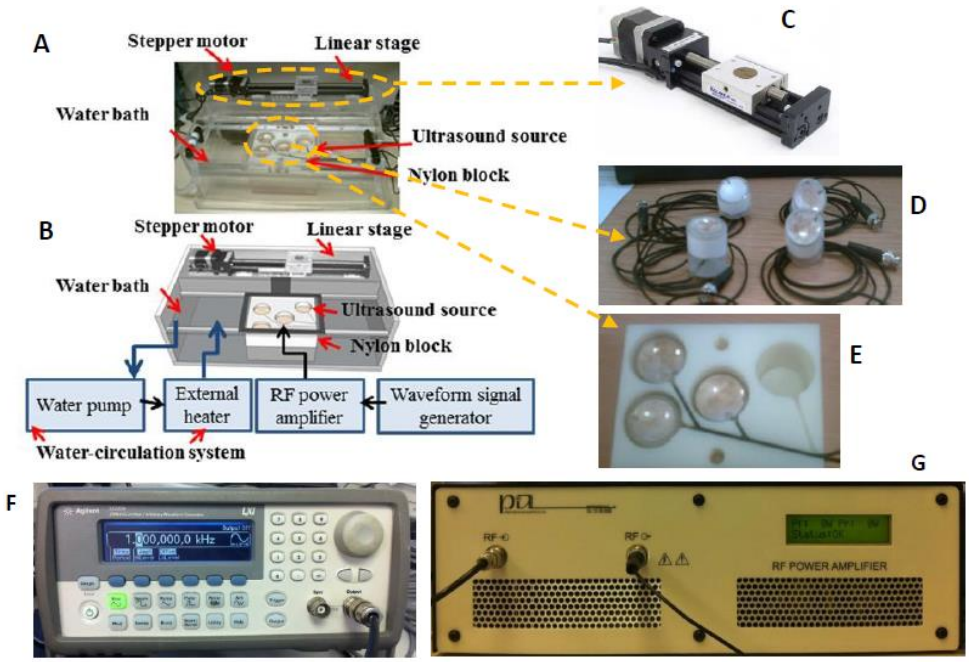

Figure A.1 Photograph (A) and schematic drawing (B) of the sonicator; stepper motor (C) to move the plate holder; piezoceramic bowl transducers within nylon housing (D); Perspex transducer cases (E); signal generator (F); and RF power amplifier (G).

The plate holder (Figure A.2 C) has two cutout adaptors (Figure A.2 A, B) for precise inverted (Figure A.2 D) or normal positioning (Figure A.2 E) of the 96-well plate and accurate horizontal location of the ultrasound focal point at the centre of each well (Figure A.2 F). Inverted plates allow FUS propagation within the wells, to minimise possible acoustic scattering or reflection from the bottom of the plate. The positions of the holes housing the transducers were chosen to allow sonication of all lines of a 96-well plate: lines A, B, D and F and then C, E, G and H after a manual rotation through 180 ° according to transducer positions 1, 2, 3 and 4 respectively, in the horizontal plane of the plate.

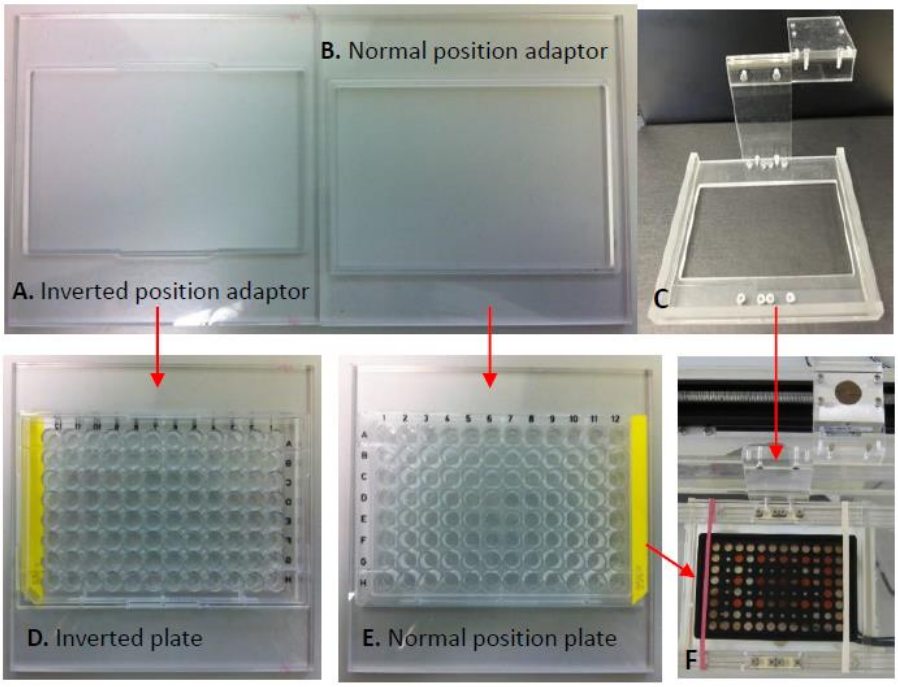

Figure A.2 Two cutout adaptors for plates (A, B); plate holder (C); inverted plate places in the adaptor (D); normal position plate places in the adaptor (E); and inverted plate in the adaptor fixed in the plate holder within the sonicator (F).

The water in the bath is heated by an ETH200 heater (Figure A.3 A) using Positive Thermal Coefficient (PTC) of resistance technology and thus acting as its own thermostat. It is returned to the reservoir using a micro-pump. This system maintains the temperature (measured with a glass thermometer) at 34 ℃ (Figure A.3 B), a few degrees below human body temperature, to avoid critical overheating (> 43 ℃) of the biological material on exposure to FUS. To avoid air bubble formation and to maintain the water temperature at a desired level, the pump drive voltage was reduced to 6 or 9 V to lower the flow.

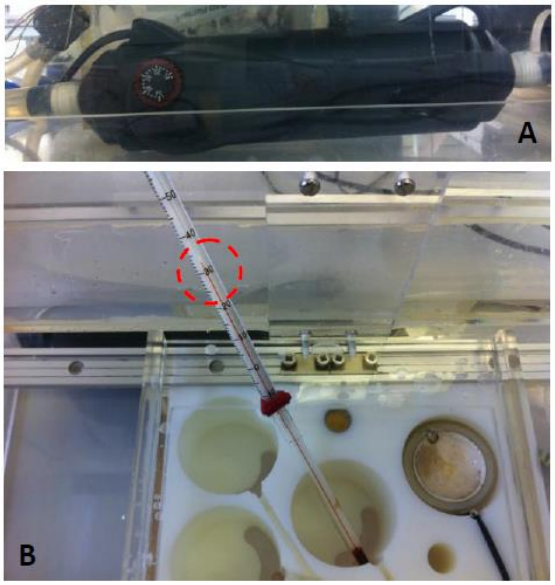

Figure A.3 The ETH200 heater system (A); water bath temperature maintain at ~ 34 ℃ constantly (B).

An X-slide linear stage connected to a programmable VXM motor controller and a NEMA 17 stepper motor are the main components of the motion system. The LabVIEW software allows the user to choose between four starting positions corresponding to the lateral centers of the FUS sources and then sends commands to the VXM controller to activate the stepper motor. The motor advances the stage 0.5×10^{-2} mm/step for precise positioning of the focal regions at the centres of the wells. Once a sequence of sonications in the same line is completed, the plate can be re-positioned manually above different US sources. All 12 wells in a line on the 96-well plate can be sonicated or only certain wells can be selected, as required. This is very useful to minimise the heat transfer from the site of sonication to adjacent wells, as discussed later.

For FUS sources, four transducers were made with geometrically-focused piezoceramic bowls (Figure A.4) with dimensions and type of piezoceramic specified in Table A.1.

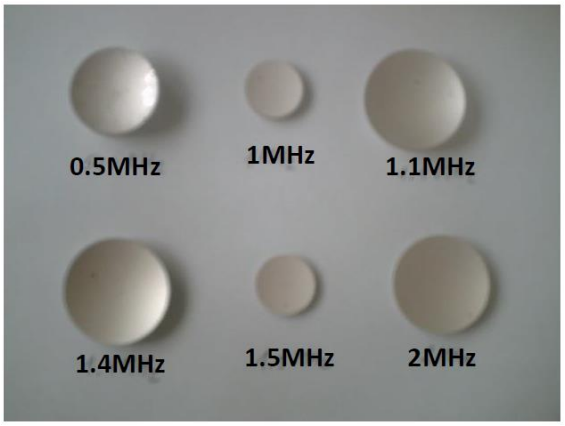

Figure A.4 Various frequencies geometrically-focused piezoceramic bowls.

Table A.1 Dimensions of US focal zone at (-6 dB) for the four transducers, and measured values of efficiency and electrical impedance in water

Frequency (MHz)	Beam Diameter (calculated) (mm)	Beam Diameter (from scan) (mm)	Beam Length (calculated) (mm)	Efficiency %	Impedance in water at 24 ℃ (Ω)	Impedance in water at 34 ℃ (Ω)
0.4868	3.14	5.30	20.34	19	82.1	83.5
1.142	1.34	3.04	9.70	28	46.4	46.7
1.467	1.25	1.60	10.94	76	54.0	67.1
2.022	1.16	1.60	12.81	50	20.2	20.7

The outer diameters (ODs) of the piezoceramics were in the range 30 – 35 mm, the focal distances 30 – 50 mm, and the resonance frequencies are 0.4868 – 2.022 MHz. The transducers cases were made from Perspex tube (OD = 40 mm) with a bowl positioned at the top of each case. Adapted lengths were cut for the transducer cases, in the range 20 – 40 mm, to position the focus of the field exactly at the bottom of the 96-well plate.

The input commands for the linear stage as well as the sonication parameters defined by the waveform generator including exposure duration, duty cycle, voltage amplitude, frequency, and wave form type (sinusoidal, pulsed and other options) are provided through a user friendly interface (Figure A.5) implemented in LabVIEW.

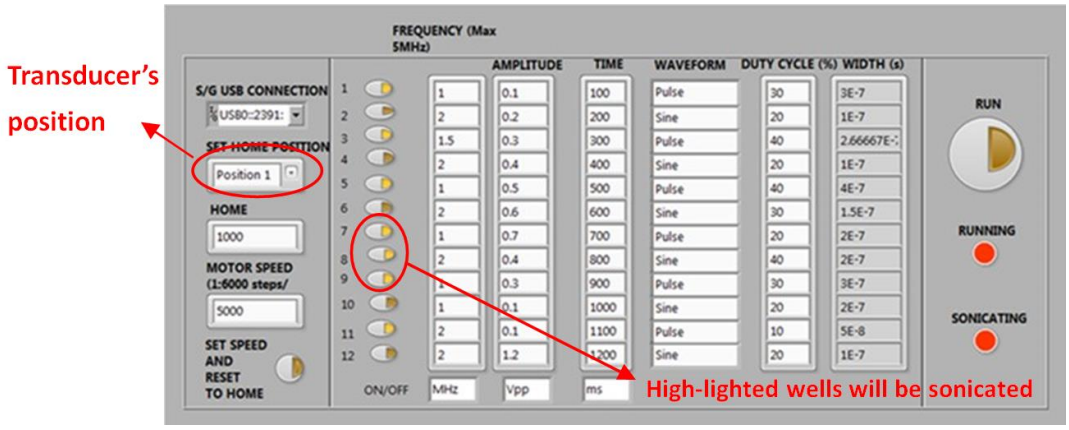

Figure A.5 LabVIEW interface allows control of numerical values for acoustic parameters at the focal point through the amplitude of the applied voltage, wave form (pulsed, sinusoidal), frequency, US duty cycle and to a sequence of individually selected wells in the plate (out of 12 wells in each line) to be sonicated.

Acoustic field characterisations (can be found in Appendices) of all transducers have been fully conducted and confirmed by needle hydrophone and MATLAB simulations to make an accurate assessment before performing sonoporation to cells.

2 The MATLAB Simulations and Real Acoustic Field Scan for 1W of Transducers 1.142MHz, 0.4868MHz, 1.467 MHz and 2.022MHz

2.1 Transducer *f* = 0.4868MHz:

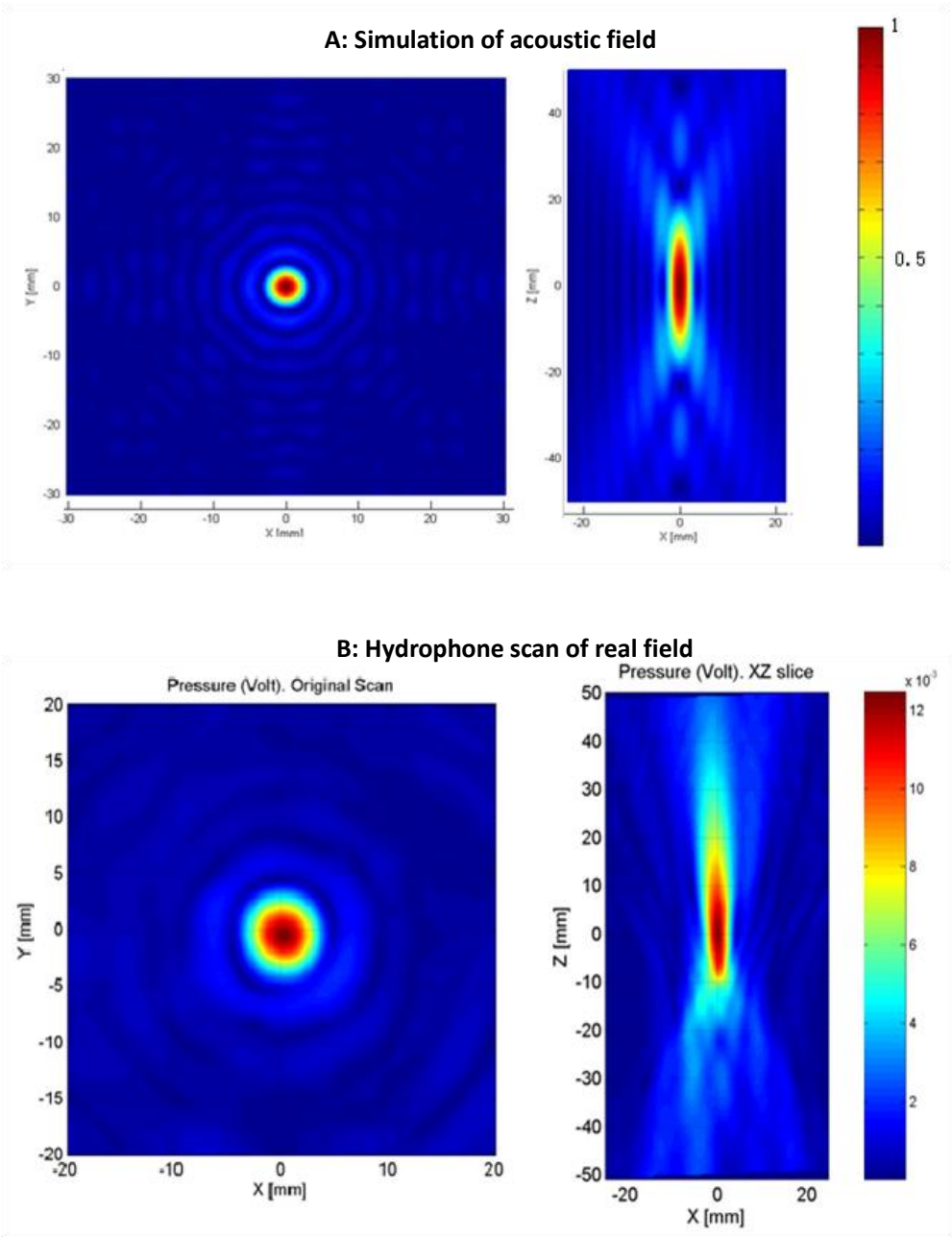

Figure A.6 Simulation (A) and Hydrophone (B) scan of acoustic field for 0.4868 MHz FUS transducer.

2.2 Transducer *f* = 1.142MHz:

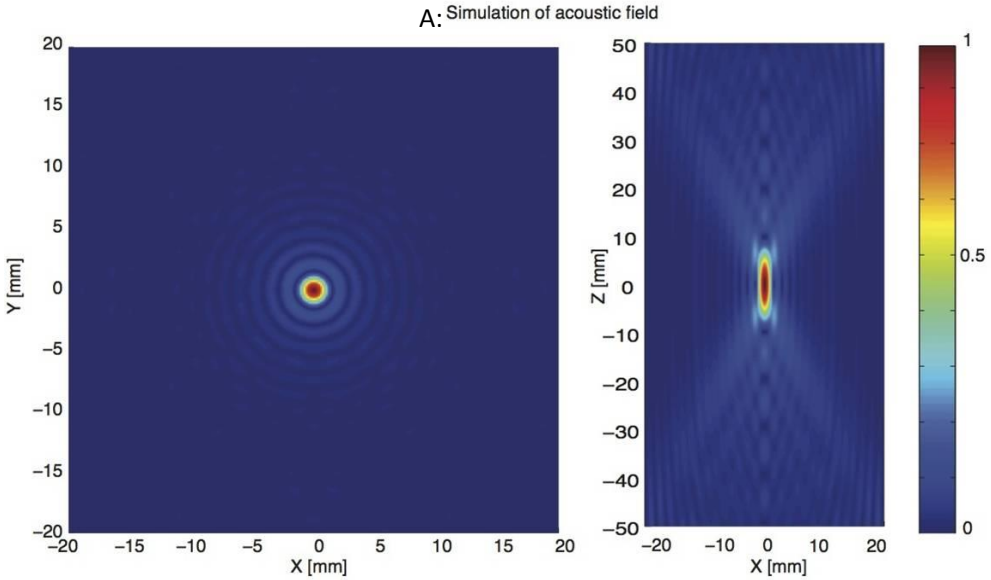

Figure A.7 Simulation (A) and Hydrophone (B) scan of acoustic field for 1.142 MHz FUS transducer.

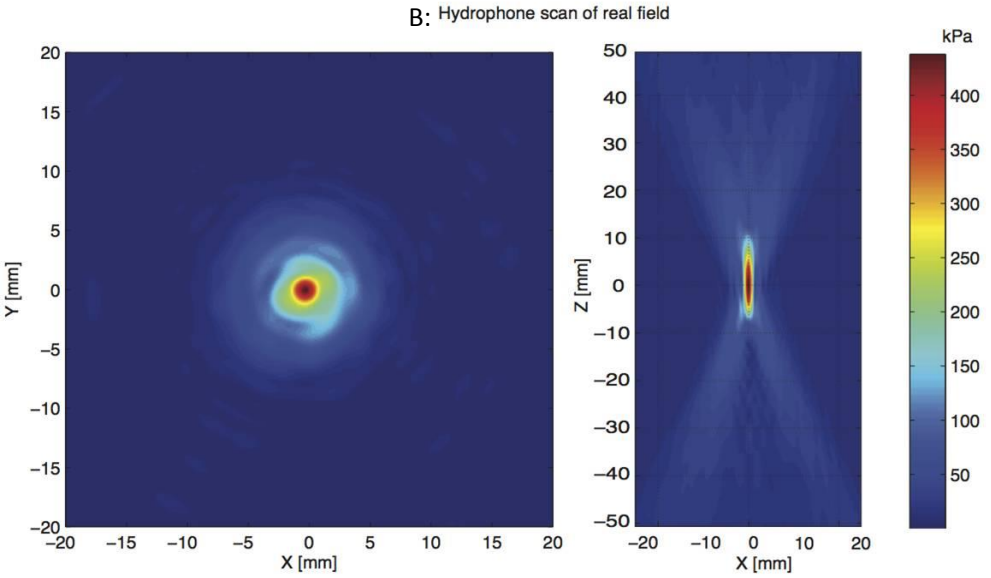

2.3 Transducer *f* = 1.467MHz:

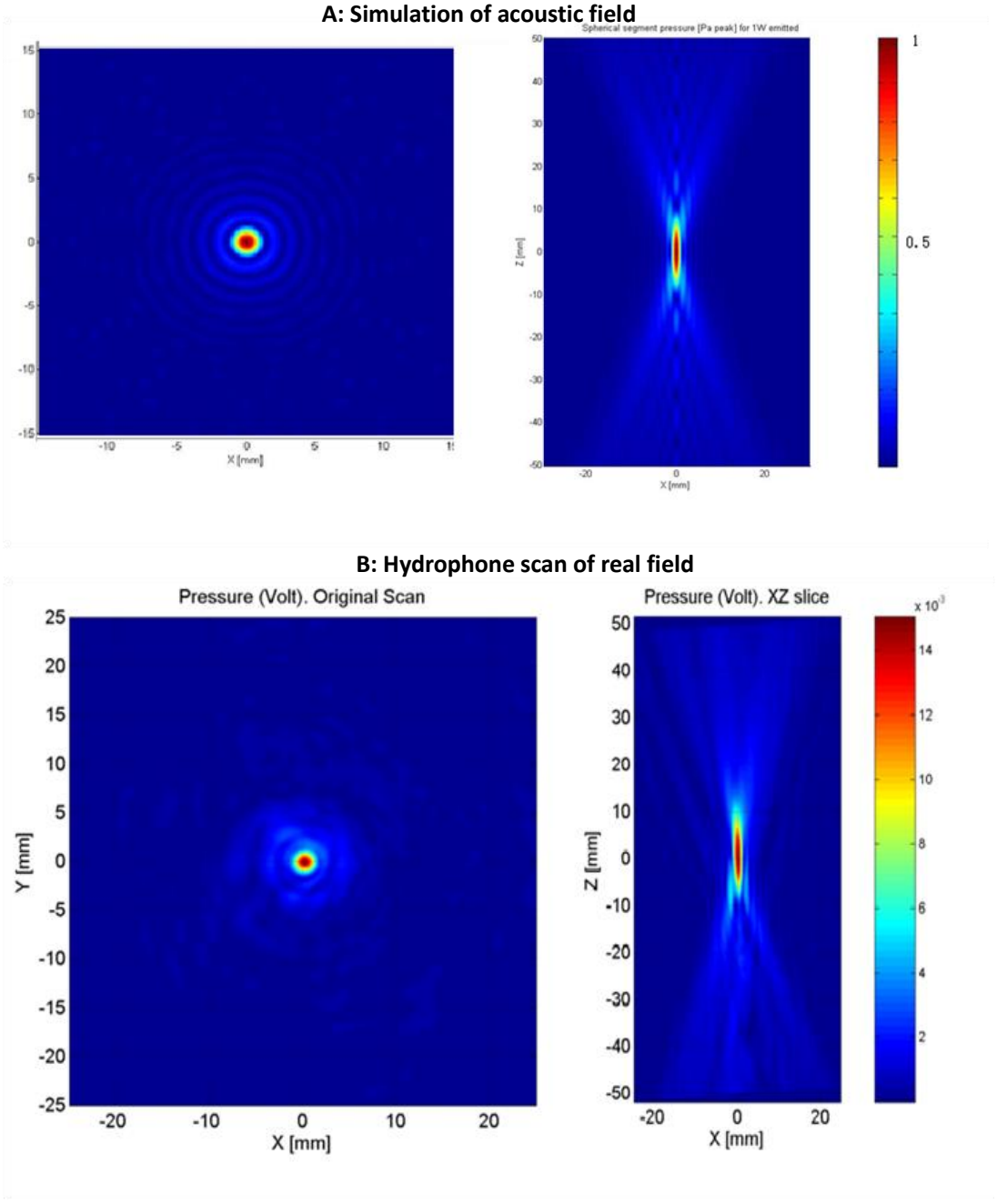

Figure A.8 Simulation (A) and Hydrophone (B) scan of acoustic field for 1.467 MHz FUS transducer.

2.4 Transducer *f* = 2.022MHz:

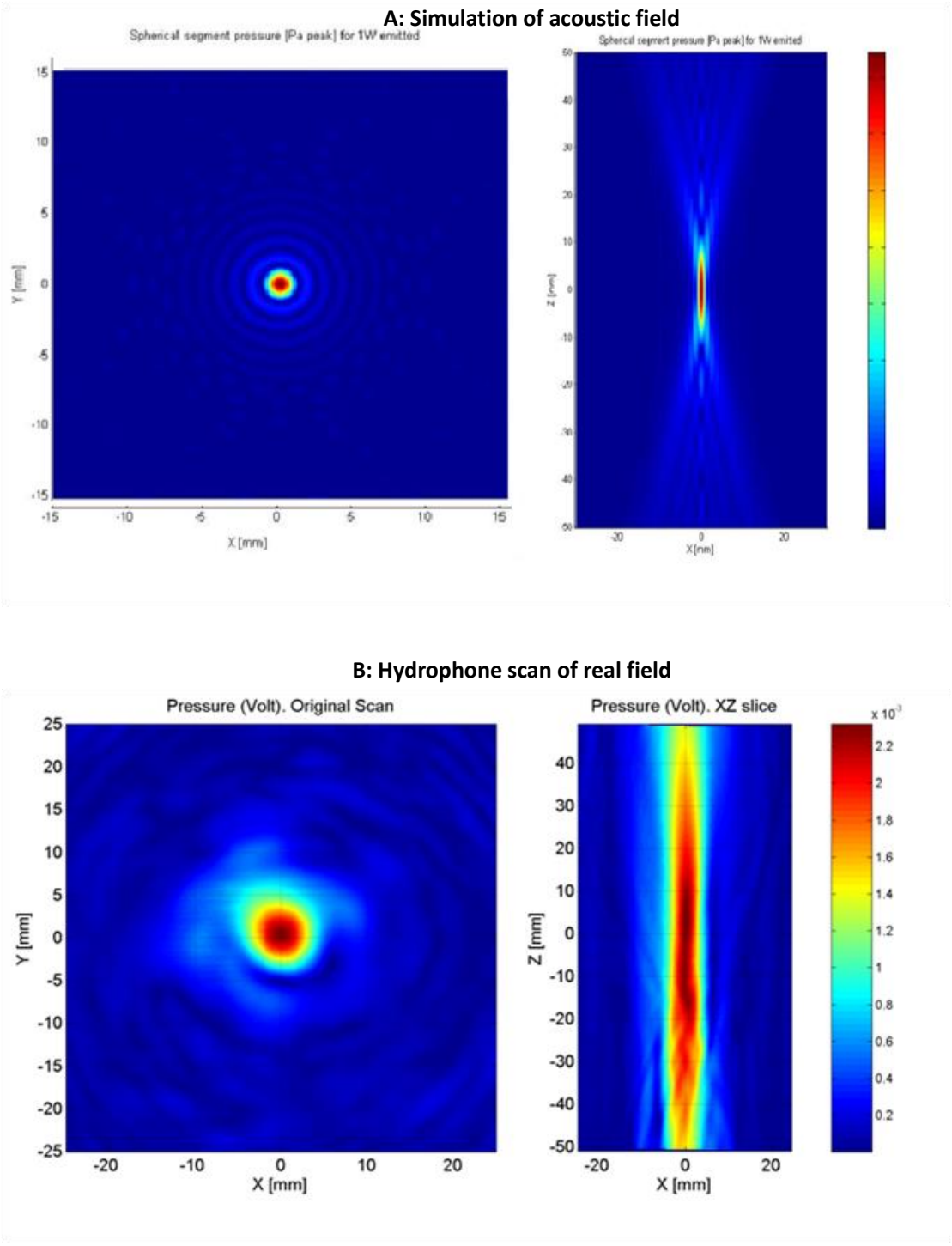

Figure A.9 Simulation (A) and Hydrophone (B) scan of acoustic field for 2.022 MHz FUS transducer.

3 Acoustic Intensity and Mechanical Index were Calculated for Various Acoustic Powers of Transducers 1.142MHz, 0.4868MHz, 1.467 MHz and 2.022MHz

3.1 Transducer *f*=0.4868MHz, Efficiency=19%:

Signal Gen. Voltage Vpp (mV)	Acoustic power [W]	Beam Diameter [mm]	Beam Length [mm]	Intensity [W/mm^2]	Intensity [W/cm^2]	Pressure [MPa]	Mechanical Index
120.00	0.25	3.14	20.34	0.03	3.22	0.22	0.31
160.00	0.50	3.14	20.34	0.06	6.44	0.31	0.44
190.00	0.75	3.14	20.34	0.10	9.66	0.38	0.54
230.00	1.00	3.14	20.34	0.13	12.88	0.44	0.63
250.00	1.25	3.14	20.34	0.16	16.10	0.49	0.70
280.00	1.50	3.14	20.34	0.19	19.32	0.54	0.77
310.00	1.75	3.14	20.34	0.23	22.54	0.58	0.83
330.00	2.00	3.14	20.34	0.26	25.76	0.62	0.89
340.00	2.25	3.14	20.34	0.29	28.98	0.66	0.94
360.00	2.50	3.14	20.34	0.32	32.20	0.69	0.99
380.00	2.75	3.14	20.34	0.35	35.42	0.73	1.04
400.00	3.00	3.14	20.34	0.39	38.64	0.76	1.09
430.00	3.50	3.14	20.34	0.45	45.08	0.82	1.17
450.00	4.00	3.14	20.34	0.52	51.52	0.88	1.26
470.00	4.25	3.14	20.34	0.55	54.74	0.90	1.29
500.00	5.00	3.14	20.34	0.64	64.40	0.98	1.40

3.2 Transducer *f*=1.142MHz, Efficiency=28.75%:

Signal Gen. Voltage Vpp (mV)	Acoustic power [W]	Beam Diameter [mm]	Beam Length [mm]	Intensity [W/mm^2]	Intensity [W/cm^2]	Pressure [MPa]	Mechanical Index
80.00	0.25	1.34	9.70	0.18	17.78	0.51	0.48
110.00	0.50	1.34	9.70	0.36	35.57	0.73	0.68
130.00	0.75	1.34	9.70	0.53	53.35	0.89	0.83
160.00	1.00	1.34	9.70	0.71	71.13	1.03	0.96
190.00	1.50	1.34	9.70	1.07	106.70	1.26	1.18
220.00	2.00	1.34	9.70	1.42	142.27	1.46	1.36
240.00	2.50	1.34	9.70	1.78	177.84	1.63	1.52
260.00	3.00	1.34	9.70	2.13	213.40	1.78	1.67
280.00	3.50	1.34	9.70	2.49	248.97	1.93	1.80
300.00	4.00	1.34	9.70	2.85	284.54	2.06	1.93
350.00	5.50	1.34	9.70	3.56	355.67	2.30	2.15
370.00	6.00	1.34	9.70	4.27	426.81	2.52	2.36
400.00	7.00	1.34	9.70	4.98	497.94	2.72	2.55
430.00	8.50	1.34	9.70	5.69	569.08	2.91	2.72
450.00	9.00	1.34	9.70	6.40	640.21	3.09	2.89
470.00	10.00	1.34	9.70	7.11	711.34	3.26	3.04
500.00	11.50	1.34	9.70	7.82	782.48	3.41	3.19

3.3 Transducer *f*=1.467MHz, Efficiency= 76.4%:

Signal Gen. Voltage Vpp (mV)	Acoustic power [W]	Beam Diameter [mm]	Beam Length [mm]	Intensity [W/mm^2]	Intensity [W/cm^2]	Pressure [MPa]	Mechanical Index
15.00	0.25	1.25	10.94	0.20	20.31	0.55	0.45
20.00	0.50	1.25	10.94	0.41	40.62	0.78	0.64
25.00	1.00	1.25	10.94	0.81	81.23	1.10	0.91
30.00	1.75	1.25	10.94	1.42	142.16	1.46	1.20
35.00	2.50	1.25	10.94	2.03	203.08	1.74	1.44
40.00	3.25	1.25	10.94	2.64	264.00	1.98	1.64
45.00	4.25	1.25	10.94	3.45	345.23	2.27	1.87
50.00	5.25	1.25	10.94	4.26	426.47	2.52	2.08
55.00	6.50	1.25	10.94	5.28	528.01	2.80	2.32
60.00	7.50	1.25	10.94	6.09	609.24	3.01	2.49
65.00	9.00	1.25	10.94	7.31	731.08	3.30	2.72
70.00	10.50	1.25	10.94	8.53	852.93	3.56	2.94
75.00	12.00	1.25	10.94	9.75	974.78	3.81	3.15
80.00	14.00	1.25	10.94	11.37	1137.24	4.12	3.40
85.00	15.75	1.25	10.94	12.79	1279.40	4.37	3.60
90.00	18.00	1.25	10.94	14.62	1462.17	4.67	3.85

3.4 Transducer *f*=2.022MHz, Efficiency= 50.3%:

Signal Gen. Voltage Vpp (mV)	Acoustic power [W]	Beam Diameter [mm]	Beam Length [mm]	Intensity [W/mm^2]	Intensity [W/cm^2]	Pressure [MPa]	Mechanical Index
70.00	0.25	1.16	12.81	0.24	23.68	0.59	0.42
100.00	0.50	1.16	12.81	0.47	47.35	0.84	0.59
140.00	1.00	1.16	12.81	0.95	94.71	1.19	0.84
160.00	1.25	1.16	12.81	1.18	118.38	1.33	0.94
180.00	1.50	1.16	12.81	1.42	142.06	1.45	1.03
200.00	1.75	1.16	12.81	1.66	165.73	1.57	1.11
250.00	2.75	1.16	12.81	2.60	260.44	1.97	1.39
280.00	3.25	1.16	12.81	3.08	307.79	2.14	1.51
340.00	4.75	1.16	12.81	4.50	449.85	2.59	1.83
400.00	6.50	1.16	12.81	6.16	615.59	3.03	2.14
470.00	9.00	1.16	12.81	8.52	852.35	3.56	2.52
530.00	11.25	1.16	12.81	10.65	1065.44	3.98	2.82
590.00	13.00	1.16	12.81	12.31	1231.17	4.28	3.03
660.00	17.00	1.16	12.81	16.10	1609.99	4.90	3.46
710.00	20.00	1.16	12.81	18.94	1894.11	5.31	3.76
780.00	23.00	1.16	12.81	21.78	2178.23	5.70	4.03

4 The Maximum Temperature Achieved for Four Transducers

4.1 Maximum temperature achieved for four transducers (*T refers to thermocouples):

Frequency (MHz)	Power (W)	Time (s)	Maximum Temperature (℃)						
			*T1	T2	T5	T3	T4	T6	T7
0.4868	1	20	34.16	37.02	38.35	37.35	36.4	34.64	40.1
		40	34.19	37.83	39.06	38.64	38.03	35.02	41.01
		60	34.49	39.51	40.34	39.75	38.91	35.44	43.99
	2.5	20	34.28	39.31	43.69	41.56	41	35.22	45.14
		40	34.46	43.64	46.85	43.93	45.38	36.21	49.74
		60	34.68	46.09	50.78	45.21	46.38	36.98	51.66
	5	20	34.53	43.15	47.53	46.91	53.92	35.75	49.19
		40	35.08	49.4	64.02	53.29	65.49	38.86	55.29
		60	35.54	53.12	65.14	56.07	62.19	39.25	56.17
1.142	1	20	33.84	35.46	35.21	36.06	34.62	34.26	36
		40	33.97	36.4	36.24	37.36	35.64	34.55	37.15
		60	33.94	36.51	36.71	37.89	36.15	34.87	37.73
	2.5	20	34.18	37.83	36.88	38.58	36.6	34.64	39.5
		40	34.35	40.02	38.71	41.59	48.8	35.41	42.5
		60	34.42	40.59	39.91	42.97	39.82	35.79	43.5
	5	20	34.34	41.32	38.96	42.32	39.59	35.42	46.11
		40	34.43	44.21	41.99	47.83	42.34	36.7	50.48
		60	34.67	45.2	44.17	49.5	44.27	37.55	52.47
1.467	1	20	34.49	35.97	36.36	36.35	36.15	35.37	37.06
		40	34.07	36.55	36.55	36.96	36.48	35.33	37.74
		60	34.06	37.29	37.1	37.54	37.06	35.68	38.42
	2.5	20	34.06	36.53	36.23	36.56	36.22	35.12	38.37
		40	34.16	38.02	37.98	38.28	37.85	35.96	39.32
		60	34.27	39.37	38.78	39.49	38.54	36.68	39.85
	5	20	34.2	38.58	38.06	38.64	38.06	36.03	40.29
		40	34.27	41.69	40.96	41.55	40.3	37.63	41.95
		60	34.33	41.02	41.02	42.26	41.39	37.79	43.4
2.022	1	20	33.97	35.77	39.08	35.8	36.26	34.17	37.82
		40	34.2	37.16	41.57	37.94	37.87	34.52	37.82
		60	34.29	37.86	42.71	38.81	38.62	34.42	40.07
	2.5	20	34.03	37.42	41.51	38.64	38.44	34.42	40.07
		40	33.93	37.67	37.81	37.89	37.43	35.98	39.4
		60	34.1	40.52	44.47	42.63	41.87	35.05	44.16
	5	20	33.98	40.15	44.54	42.79	40.87	34.73	43.47
		40	34.23	43.1	49.19	49.66	45.22	35.65	45.48
		60	34.29	44.94	49.62	52.39	46.93	36.25	50.02

4.2 Distribution of Thermocouples Inside the Wells of A 96-well Plate:

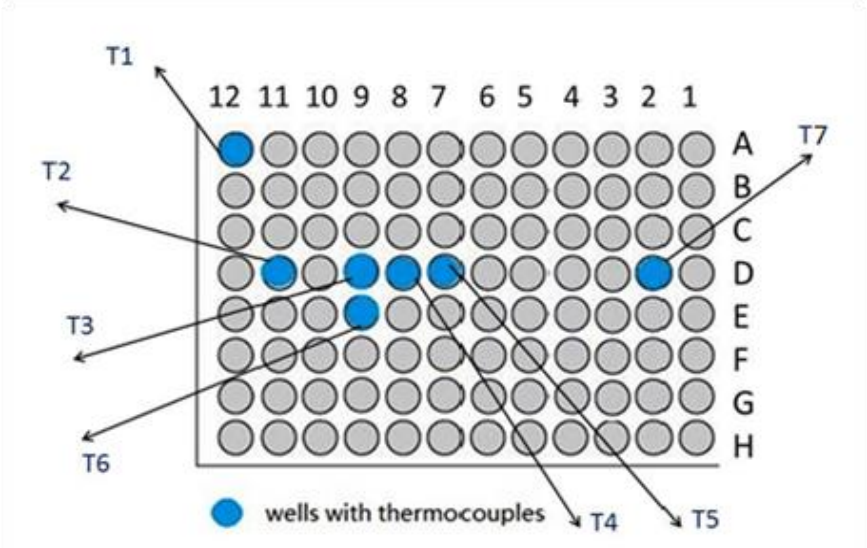

4.3 The Average Temperature of 1W, 2.5 W and 5W

Power	Time	T1	T2	T5	T3	T4	T6	T7
1W	20s	34.1	36.1	37.3	36.4	35.9	34.6	37.7
	40s	34.1	37.0	38.4	37.7	37.0	34.9	38.4
	60s	34.2	37.8	39.2	38.5	37.7	35.1	40.1
2.5W	20s	34.1	37.8	39.6	38.8	38.1	34.9	40.8
	40s	34.2	39.8	40.3	40.4	42.4	35.9	42.7
	60s	34.4	41.6	43.5	42.6	41.7	36.1	44.8
5W	20s	34.3	40.8	42.3	42.7	43.1	35.5	44.8
	40s	34.5	44.6	49.0	48.1	48.3	37.2	48.3
	60s	34.7	46.1	50.0	50.1	48.7	37.7	50.5
Average		34.3	40.2	42.2	41.7	41.4	35.8	43.1

References

Abedin, M. and N. King (2010). "Diverse evolutionary paths to cell adhesion." Trends Cell Biol **20**(12): 734-742.

Adler, A. D., F. R. Longo, et al. (1967). "A simplified synthesis for meso-tetraphenylporphine." The Journal of Organic Chemistry **32**(2): 476-476.

Adler, A. D., F. R. Longo, et al. (1970). "On the preparation of metalloporphyrins." Journal of Inorganic and Nuclear Chemistry **32**(7): 2443-2445.

Afadzi, M., L. Davies Cde, et al. (2012). "Effect of ultrasound parameters on the release of liposomal calcein." Ultrasound Med Biol **38**(3): 476-486.

Agrawal, P., S. K. Barthwal, et al. (2009). "Studies on self-aggregation of anthracycline drugs by restrained molecular dynamics approach using nuclear magnetic resonance spectroscopy supported by absorption, fluorescence, diffusion ordered spectroscopy and mass spectrometry." European Journal of Medicinal Chemistry **44**(4): 1437-1451.

Agrawal, P., S. K. Barthwal, et al. (2009). "Studies on self-aggregation of anthracycline drugs by restrained molecular dynamics approach using nuclear magnetic resonance spectroscopy supported by absorption, fluorescence, diffusion ordered spectroscopy and mass spectrometry." Eur J Med Chem **44**(4): 1437-1451.

Ahmad, I. and T. M. Allen (1992). "Antibody-mediated specific binding and cytotoxicity of liposome-entrapped doxorubicin to lung cancer cells in vitro." Cancer Res **52**(17): 4817-4820.

Ahmad, I., M. Longenecker, et al. (1993). "Antibody-targeted delivery of doxorubicin entrapped in sterically stabilized liposomes can eradicate lung cancer in mice." Cancer Res **53**(7): 1484-1488.

Ahmed, H. U., E. Zacharakis, et al. (2009). "High-intensity-focused ultrasound in the treatment of primary prostate cancer: the first UK series." Br J Cancer **101**(1): 19-26.

Akerman, M. E., W. C. Chan, et al. (2002). "Nanocrystal targeting in vivo." Proc Natl Acad Sci U S A **99**(20): 12617-12621.

Al-Bataineh, O., J. Jenne, et al. (2012). "Clinical and future applications of high intensity focused ultrasound in cancer." Cancer Treat Rev **38**(5): 346-353.

Alexis, F., E. M. Pridgen, et al. (2010). "Nanoparticle technologies for cancer therapy." Handb Exp Pharmacol(197): 55-86.

Alfarouk, K. O., A. K. Muddathir, et al. (2011). "Tumor Acidity as Evolutionary Spite." Cancers **3**(1): 408-414.

Allegre, M. and A. Deratani (1994). "Cyclodextrin uses: From concept to industrial reality." Agro. Food Ind. Technol. **31**: 9-17.

Allen, C., D. Maysinger, et al. (1999). "Nano-engineering block copolymer aggregates for drug delivery." Colloids and Surfaces B: Biointerfaces **16**(1–4): 3-27.

Allen, T. M., A. K. Agrawal, et al. (1994). "Antibody-Mediated Targeting of Long-Circulating (StealthR) Liposomes." Journal of Liposome Research **4**(1): 1-25.

Allen, T. M., E. Brandeis, et al. (1995). "A new strategy for attachment of antibodies to sterically stabilized liposomes resulting in efficient targeting to cancer cells." Biochim Biophys Acta **26**(2): 99-108.

Allen, T. M. and P. R. Cullis (2013). "Liposomal drug delivery systems: from concept to clinical

applications." Adv Drug Deliv Rev **65**(1): 36-48.

Allen, T. M., C. Hansen, et al. (1991). "Liposomes containing synthetic lipid derivatives of poly(ethylene glycol) show prolonged circulation half-lives in vivo." Biochimica et Biophysica Acta (BBA) - Biomembranes **1066**(1): 29-36.

Alley, M. C., D. A. Scudiero, et al. (1988). "Feasibility of drug screening with panels of human tumor cell lines using a microculture tetrazolium assay." Cancer Res **48**(3): 589-601.

Anand, R., S. Ottani, et al. (2012). "A close-up on doxorubicin binding to γ-cyclodextrin: an elucidating spectroscopic, photophysical and conformational study." RSC Advan. **2**: 2346-2357.

Anand, R., S. Ottani, et al. (2012). "A close-up on doxorubicin binding to γ-cyclodextrin: an elucidating spectroscopic, photophysical and conformational study." RSC Advances **2**: 2346-2357.

Antony, A. C., M. A. Kane, et al. (1989). "Folate (pteroylglutamate) uptake in human red blood cells, erythroid precursors and KB cells at high extracellular folate concentrations. Evidence against a role for specific folate-binding and transport proteins." Biochem J **260**(2): 401-411.

Anyarambhatla, G. R. and D. Needham (1999). "Enhancement of the Phase Transition Permeability of DPPC Liposomes by Incorporation of MPPC: A New Temperature-Sensitive Liposome for use with Mild Hyperthermia." J Liposome Res **9**(4): 491-506.

Arima, H., H. Adachi, et al. (1990). "Enhancement of the antiinflammatory effect of ethyl 4-biphenylyl acetate in ointment by beta-cyclodextrin derivatives: increased absorption and localized activation of the prodrug in rats." Pharm Res **7**(11): 1152-1156.

Armarego, W. L. F. and C. L. L. Chai (2003). Chapter 1 - Common Physical Techniques used in Purification. Purification of Laboratory Chemicals (Fifth Edition). W. L. F. Armarego and C. L. L. Chai. Burlington, Butterworth-Heinemann**:** 1-52.

Arun, R., K. C. K. Ashok, et al. (2008). "Cyclodextrins as Drug Carrier Molecule: A Review." Scientia Pharmaceutica **76**(4): 567-598.

Ashush, H., L. A. Rozenszajn, et al. (2000). "Apoptosis induction of human myeloid leukemic cells by ultrasound exposure." Cancer Res **60**(4): 1014-1020.

Bader, H., H. Ringsdorf, et al. (1984). "Watersoluble polymers in medicine." Die Angewandte Makromolekulare Chemie **123**(1): 457-485.

Bae, Y. H. and K. Park (2011). "Targeted drug delivery to tumors: myths, reality and possibility." J Control Release **153**(3): 198-205.

Baguley, B. C., K. O. Hicks, et al. (2002). "Chapter15 tumor cell cultures in drug development." ANTICANCER DRUG DEVELOPMENT: 269-284.

Bakker-Woudenberg, I. A., A. F. Lokerse, et al. (1992). "Enhanced localization of liposomes with prolonged blood circulation time in infected lung tissue." Biochim Biophys Acta **14**(4): 318-326.

Balamuralidhara, V., T. M. Pramodkumar, et al. (2011). "pH Sensitive Drug Delivery Systems: A Review." Am. J. Drug Discovery Dev. **1**: 24-48.

Balci, M. (2005). Basic 1H-and 13C-NMR spectroscopy, Elsevier.

Ballou, B., B. C. Lagerholm, et al. (2004). "Noninvasive imaging of quantum dots in mice." Bioconjug Chem **15**(1): 79-86.

Baptista, P., E. Pereira, et al. (2008). "Gold nanoparticles for the development of clinical diagnosis methods." Anal Bioanal Chem **391**(3): 943-950.

Barenholz, Y., S. Amselem, et al. (1993). "Stability of liposomal-doxorubicin formulation: problems and prospects." Med Res Rev **13**: 449-491.

Barnett, S. B., G. R. ter Haar, et al. (1994). "Current status of research on biophysical effects of ultrasound." Ultrasound Med Biol **20**(3): 205-218.

Bawarski, W. E., E. Chidlowsky, et al. (2008). "Emerging nanopharmaceuticals." Nanomedicine **4**(4): 273-282.

Bekers, O., J. H. Beijnen, et al. (1990). "Inclusion complexation of doxorubicin and daunorubicin with cyclodextrins." J Pharm Biomed Anal **8**(8-12): 671-674.

Bekers, O., J. H. Beijnen, et al. (1990). "Inclusion complexation of doxorubicin and daunorubicin with cyclodextrins." Journal of Pharmaceutical and Biomedical Analysis **8**(8–12): 671-674.

Bekers, O., J. H. Beijnen, et al. (1991). "Effect of cyclodextrin complexation on the chemical stability of doxorubicin and daunorubicin in aqueous solutions." International Journal of Pharmaceutics **72**(2): 123-130.

Belotti, D. (1996). "The microtubule-affecting drug paclitaxel has antiangiogenic activity." Clinical Cancer Research **2**(11): 1843.

Bender, M. L. and M. Komiyama (1978). "Cyclodextrin Chemistry." Springer-Verlag, Berlin.

Bergeron, R. J. (1984). "Cycloamylose-substrate binding. In: Attwood, J.L., Bavies, J.E.D., MacNicol, D.D. (Eds.)." Inclusion Compounds. Academic Press, London: 391-443.

Berridge, M. and C. Rao (1993). "Characterization of the cellular reduction of 3-(4,5-dimethylthiazol-2-yl)-2,5-diphenyltetrazolium bromide (MTT): subcellular localization, substrate dependence, and involvement of mitochondrial electron transport in MTT reduction. ." Archives Biochem Biophys **303**: 474-482.

Bhardwaj, R., R. T. Dorr, et al. (2000). "Approaches to reducing toxicity of parenteral anticancer drug formulations using cyclodextrins." PDA J Pharm Sci Technol **54**(3): 233-239.

Bianco, A. and M. Prato (2003). "Can Carbon Nanotubes be Considered Useful Tools for Biological Applications?" Advanced Materials **15**(20): 1765-1768.

Blanco, E., A. Hsiao, et al. (2011). "Nanomedicine in cancer therapy: innovative trends and prospects." Cancer Sci **102**(7): 1247-1252.

Blanco, E., C. W. Kessinger, et al. (2009). "Multifunctional micellar nanomedicine for cancer therapy." Exp Biol Med (Maywood) **234**(2): 123-131.

Blume, G. and G. Cevc (1990). "Liposomes for the sustained drug release in vivo." Biochim Biophys Acta **2**(1): 91-97.

Blume, G., G. Cevc, et al. (1993). "Specific targeting with poly(ethylene glycol)-modified liposomes: coupling of homing devices to the ends of the polymeric chains combines effective target binding with long circulation times." Biochim Biophys Acta **18**(1): 180-184.

Bohmer, M. R., C. H. Chlon, et al. (2010). "Focused ultrasound and microbubbles for enhanced extravasation." J Control Release **148**(1): 18-24.

Bontha, S., A. V. Kabanov, et al. (2006). "Polymer micelles with cross-linked ionic cores for delivery of anticancer drugs." Journal of Controlled Release **114**(2): 163-174.

Bosman, A. W., H. M. Janssen, et al. (1999). "About Dendrimers: Structure, Physical Properties, and Applications." Chem Rev **99**(7): 1665-1688.

Brewster, M. E. and T. Loftsson (2007). "Cyclodextrins as pharmaceutical solubilizers." Advanced Drug Delivery Reviews **59**(7): 645-666.

Burgess, A. and K. Hynynen (2013). "Noninvasive and targeted drug delivery to the brain using focused ultrasound." ACS Chem Neurosci **4**(4): 519-526.

Busbee, B. D., S. O. Obare, et al. (2003). "An Improved Synthesis of High-Aspect-Ratio Gold

Nanorods." Advanced Materials **15**(5): 414-416.

Busch, K. W., I. M. Swamidoss, et al. (2003). "Determination of the enantiomeric composition of guest molecules by chemometric analysis of the UV-visible spectra of cyclodextrin guest-host complexes." J Am Chem Soc **125**(7): 1690-1691.

Cabuy, E. (2011). "Hyperthermia in cancer treatment " Reliable Cancer Therapies. Energy based therapies **1**(2): 1-48.

Castle, J., M. Butts, et al. (2013). "Ultrasound-mediated targeted drug delivery: recent success and remaining challenges." Am J Physiol Heart Circ Physiol **304**(3): 30.

Chavez-Gutierrez, L., L. Bammens, et al. (2012). "The mechanism of gamma-Secretase dysfunction in familial Alzheimer disease." Embo J **31**(10): 2261-2274.

Chen, R. J., S. Bangsaruntip, et al. (2003). "Noncovalent functionalization of carbon nanotubes for highly specific electronic biosensors." Proceedings of the National Academy of Sciences **100**(9): 4984-4989.

Chen, Y., T. Xu, et al. (2005). "Temperature dependence of the inclusion–dissociation behavior of the inclusion complexes between cationic substituted 3H-indoles and β-cyclodextrin: Design of a novel type of semi-rotaxane." Journal of Photochemistry and Photobiology A: Chemistry **173**(1): 42-50.

Cheng, J. F.-K., Kay T., K. F.-D. Khin, Mark E., et al. (2004). "Antitumor activity of beta-cyclodextrin polymer-camptothecin conjugates." Mol Pharm **1**(3): 183-193.

Cheng, J. F.-K., Kay T., K. F.-J. Khin, Gregory S., et al. (2003). "Synthesis of linear, beta-cyclodextrin-based polymers and their camptothecin conjugates." Bioconjug Chem **14**(5): 1007-1017.

Cheng, Y., C. S. A, et al. (2008). "Highly efficient drug delivery with gold nanoparticle vectors for in vivo photodynamic therapy of cancer." J Am Chem Soc **130**(32): 10643-10647.

Cheng, Y., J. Wang, et al. (2008). "Pharmaceutical applications of dendrimers: promising nanocarriers for drug delivery." Front Biosci **13**: 1447-1471.

Choi, Y., T. Thomas, et al. (2005). "Synthesis and functional evaluation of DNA-assembled polyamidoamine dendrimer clusters for cancer cell-specific targeting." Chem Biol **12**(1): 35-43.

Collins, P. G., K. Bradley, et al. (2000). "Extreme Oxygen Sensitivity of Electronic Properties of Carbon Nanotubes." Science **287**(5459): 1801-1804.

Connors, K. A. (1995). "Population characteristics of cyclodextrin complex stabilities in aqueous solution." J Pharm Sci **84**(7): 843-848.

Connors, K. A. (1997). "The Stability of Cyclodextrin Complexes in Solution." Chem Rev **97**(5): 1325-1358.

Conti, L., P. Grimaldi, et al. (2010). "Effects induced in cells by ultrasound revealed by ATR-FTIR spectroscopy." Vibrational Spectroscopy **52**(1): 79-84.

Corsi, C. (2014). Infrared: A Key Technology for Security Systems. Sensors. F. Baldini, A. D'Amico, C. Di Nataleet al, Springer New York. **162:** 37-42.

Cory, A. H., T. C. Owen, et al. (1991). "Use of an aqueous soluble tetrazolium/formazan assay for cell growth assays in culture." Cancer Commun **3**(7): 207-212.

Coussios, C. C., C. H. Farny, et al. (2007). "Role of acoustic cavitation in the delivery and monitoring of cancer treatment by high-intensity focused ultrasound (HIFU)." Int J Hyperthermia **23**(2): 105-120.

Cramer, F. (1954). "Einschlussverbindungen." Springer-Verlag, Berlin.

Dai, X., Z. Yue, et al. (2008). "Fluorescence intensity and lifetime imaging of free and micellar-encapsulated doxorubicin in living cells." Nanomedicine **4**(1): 49-56.

Davis, M. (2009). "- Design and development of IT-101, a cyclodextrin-containing polymer conjugate of camptothecin." Adv Drug Deliv Rev **61**(13): 1189-1192.

Davis, M. E., Z. G. Chen, et al. (2008). "Nanoparticle therapeutics: an emerging treatment modality for cancer." Nat Rev Drug Discov **7**(9): 771-782.

Davis, M. E., H. Gonzalez, et al. (2004). "Cyclodextrin-based pharmaceutics: past, present and future." Nat Rev Drug Discov **3**(12): 1023-1035.

De Jong, N. (2002). "Mechanical index." European Journal of Echocardiography **3**(1): 73-74.

Deckers, R. and C. T. Moonen (2010). "Ultrasound triggered, image guided, local drug delivery." J Control Release **148**(1): 25-33.

Deckers, R. and C. T. W. Moonen (2010). "Ultrasound triggered, image guided, local drug delivery." Journal of Controlled Release **148**(1): 25-33.

Deckers, R., C. Rome, et al. (2008). "The role of ultrasound and magnetic resonance in local drug delivery." J Magn Reson Imaging **27**(2): 400-409.

Deng, C. X., F. Sieling, et al. (2004). "Ultrasound-induced cell membrane porosity." Ultrasound Med Biol **30**(4): 519-526.

Denkewalter, R. G., J. F. Kolc, et al. (1981). "Macromolecular highly branched homogeneous compound." Allied Corporation.

Derfus, A. M., W. C. W. Chan, et al. (2004). "Probing the Cytotoxicity of Semiconductor Quantum Dots." Nano Letters **4**(1): 11-18.

Dewhirst, M. W., C. D. Landon, et al. (2013). "Novel approaches to treatment of hepatocellular carcinoma and hepatic metastases using thermal ablation and thermosensitive liposomes." Surgical oncology clinics of North America **22**(3): 545-561.

Dick, E. A. and W. M. Gedroyc (2010). "ExAblate magnetic resonance-guided focused ultrasound system in multiple body applications." Expert Rev Med Devices **7**(5): 589-597.

Djukovic, D., G. A. Nagana Gowda, et al. (2013). Chapter 18 - Mass Spectrometry and NMR Spectroscopy–Based Quantitative Metabolomics. Proteomic and Metabolomic Approaches to Biomarker Discovery. H. J. Issaq and T. D. Veenstra. Boston, Academic Press**:** 279-297.

Donald, A. T. (2005). Dendrimeric Supramolecular and Supramacromolecular Assemblies. Supramolecular Polymers, Second Edition, CRC Press.

Draper, D. O., J. C. Castel, et al. (1995). "Rate of temperature increase in human muscle during 1 MHz and 3 MHz continuous ultrasound." J Orthop Sports Phys Ther **22**(4): 142-150.

Dreher, M. R., D. Raucher, et al. (2003). "Evaluation of an elastin-like polypeptide-doxorubicin conjugate for cancer therapy." J Control Release **91**(1-2): 31-43.

Dromi, S., V. Frenkel, et al. (2007). "Pulsed-high intensity focused ultrasound and low temperature-sensitive liposomes for enhanced targeted drug delivery and antitumor effect." Clin Cancer Res **13**(9): 2722-2727.

Drummond, D. C., C. O. Noble, et al. (2008). "Pharmacokinetics and in vivo drug release rates in liposomal nanocarrier development." J Pharm Sci **97**(11): 4696-4740.

Duck, F. A., A. C. Baker, et al. (1998). Ultrasound in Medicine, Taylor & Francis.

Duncan, R. (2003). "The dawning era of polymer therapeutics." Nat Rev Drug Discov **2**(5): 347-360.

Dupont, J., C. S. Consorti, et al. (2003). Preparation of 1-Butyl-3-Methyl Imidazolium-Based Room Temperature Ionic Liquids. Organic Syntheses, John Wiley & Sons, Inc.

E.Buhleier, W. W., F. Vögtle (1978). ""Cascade"- and "Nonskid-Chain-like" Syntheses of Molecular Cavity Topologies." Synthesis **2**: 155-158.

Eisenbrey, J. R., P. Huang, et al. (2009). "Ultrasound triggered cell death in vitro with doxorubicin loaded poly lactic-acid contrast agents." Ultrasonics **49**(8): 628-633.

El-Sayed, M. E., A. S. Hoffman, et al. (2005). "Rational design of composition and activity correlations for pH-sensitive and glutathione-reactive polymer therapeutics." J Control Release **101**(1-3): 47-58.

El Fegoun, A. B., E. Barret, et al. (2011). "Focal therapy with high-intensity focused ultrasound for prostate cancer in the elderly. A feasibility study with 10 years follow-up." Int Braz J Urol **37**(2): 213-219.

Elwood, P. C. (1989). "Molecular cloning and characterization of the human folate-binding protein cDNA from placenta and malignant tissue culture (KB) cells." J Biol Chem **264**(25): 14893-14901.

Emara S, M. I., Tamura K, Razee S, Masujima T, Mohamed HA, El-Gizawy SM, El-Rabbat NA. (2000). "Effect of cyclodextrins on the stability of adriamycin, adriamycinol, adriamycinone and daunomycin." Talanta **51**(2): 359-364.

Esenaliev, R. O., I. V. Larina, et al. (2001). Cavitation-induced drug delivery in tumors for cancer chemotherapy: animal studies.

Fang, X., G. Mark, et al. (1996). "OH radical formation by ultrasound in aqueous solutions Part I: the chemistry underlying the terephthalate dosimeter." Ultrasonics Sonochemistry **3**(1): 57-63.

Farlow, J., D. Seo, et al. (2013). "Formation of targeted monovalent quantum dots by steric exclusion." Nat Meth **advance online publication**.

Farokhzad, O. C. and R. Langer (2009). "Impact of nanotechnology on drug delivery." ACS Nano **3**(1): 16-20.

Feril, L., Jr., K. Tachibana, et al. (2010). "Hypotonia-induced cell swelling enhances ultrasound-induced mechanical damage to cancer cells." Journal of Medical Ultrasonics **37**(1): 3-8.

Feril, L. B., Jr., T. Kondo, et al. (2002). "Enhancement of hyperthermia-induced apoptosis by non-thermal effects of ultrasound." Cancer Lett **178**(1): 63-70.

Fernandez, A.-M., K. V. derpoorten, et al. (2001). "N-Succinyl-(β-alanyl-l-leucyl-l-alanyl-l-leucyl)doxorubicin: An Extracellularly Tumor-Activated Prodrug Devoid of Intravenous Acute Toxicity." J. Med. Chem. **44**: 3750-3753.

Ferrari, M. (2005). "Cancer nanotechnology: opportunities and challenges." Nat Rev Cancer **5**(3): 161-171.

Finlay, G. J., W. R. Wilson, et al. (1986). "Comparison of in vitro activity of cytotoxic drugs towards human carcinoma and leukaemia cell lines." Eur J Cancer Clin Oncol **22**(6): 655-662.

Fogh, J. and B. C. Giovanella (1978). "The Nude Mouse in Experimental and Clinical Research (Vol.1)." (eds) Academic Press.

Fogh, J. and B. C. Giovanella (1982). "The Nude Mouse in Experimental and Clinical Research(Vol.2)." (eds) Academic Press.

Fréchet, J. M. J., Tomalia, D.A. (2001). "Dendrimers and Other Dendritic Polymers." Wiley, Chichester.

French, D., Pulley, A.O., Effenberger, J.A., Rougvie, M.A., Abdullah, M. (1965). "Studies on the Schardinger dextrins. XII. The molecular size and structure of the δ-, ε-, ζ-, and η-dextrins. ." Arch. Biochem. Biophys. **111**: 153-160.

Frenkel, V. (2008). "Ultrasound mediated delivery of drugs and genes to solid tumors." Adv Drug Deliv Rev **60**(10): 1193-1208.

Frenkel, V., A. Etherington, et al. (2006). "Delivery of liposomal doxorubicin (Doxil) in a breast cancer tumor model: investigation of potential enhancement by pulsed-high intensity focused ultrasound exposure." Acad Radiol **13**(4): 469-479.

Freudenberg, K. and F. Cramer (1948). "Die Konstitution der Schardinger-Dextrine α, β und γ. Z." Naturforsch **3b**: 464.

Freudenberg, K., Cramer, F., Plieninger, H. (1953). "Verfahren zur Herstellung von Einschlusverbindungen physiologisch wirksamer organischer Verbindungen." Knoll A.-G. Chemische Fabriken, Germany, Patent No. 895,769.

Freudenberg, K. and R. Jacobi (1935). "U ¨ber Schardinger Dextrine aus Sta ¨rke." Liebigs Ann. Chem. **518**: 102-108.

Fridborg, H., P. Nygren, et al. (1995). "Relationship between pharmacokinetic parameters in patients and cytotoxicity in vitro of standard and investigational anticancer drugs." Anticancer Drugs **6**(1): 64-69.

Fruehauf, J. H., W. Back, et al. (2008). "High-intensity focused ultrasound for the targeted destruction of uterine tissues: experiences from a pilot study using a mobile HIFU unit." Arch Gynecol Obstet **277**(2): 143-150.

Fry, W. J. (1950). "Physical factors involved in ultrasonically Induced Changes in Living Systems: I. Identification of Non-Temperature Effects." J ACOUST SOC AMER **22**(6): 867-876.

Fujiwara, A., T. Hoshino, et al. (1985). "Anthracycline Antibiotics." Critical Reviews in Biotechnology **3**(2): 133-157.

Furgeson, D. Y., M. R. Dreher, et al. (2006). "Structural optimization of a "smart" doxorubicin-polypeptide conjugate for thermally targeted delivery to solid tumors." J Control Release **110**(2): 362-369.

Furnari, B., N. Rhind, et al. (1997). "Cdc25 mitotic inducer targeted by chk1 DNA damage checkpoint kinase." Science **277**(5331): 1495-1497.

Furusawa, H., K. Namba, et al. (2007). "The evolving non-surgical ablation of breast cancer: MR guided focused ultrasound (MRgFUS)." Breast Cancer **14**(1): 55-58.

Gaber, M. H., N. Z. Wu, et al. (1996). "Thermosensitive liposomes: extravasation and release of contents in tumor microvascular networks." Int J Radiat Oncol Biol Phys **36**(5): 1177-1187.

Gabizon, A., R. Catane, et al. (1994). "Prolonged circulation time and enhanced accumulation in malignant exudates of doxorubicin encapsulated in polyethylene-glycol coated liposomes." Cancer Res **54**(4): 987-992.

Gabizon, A., R. Chisin, et al. (1991). "Pharmacokinetic and imaging studies in patients receiving a formulation of liposome-associated adriamycin." Br. J. Cancer **64**(6): 1125-1132.

Gabizon, A., T. Peretz, et al. (1989). "Systemic administration of doxorubicin-containing liposomes in cancer patients: a phase I study." Eur J Cancer Clin Oncol **25**(12): 1795-1803.

Gao, X., Y. Cui, et al. (2004). "In vivo cancer targeting and imaging with semiconductor quantum dots." Nature Biotechnology **22**(8): 969-976.

Gao, X., L. Yang, et al. (2005). "In vivo molecular and cellular imaging with quantum dots." Current Opinion in Biotechnology **16**(1): 63-72.

Gatenby, R. A., E. T. Gawlinski, et al. (2006). "Acid-mediated tumor invasion: a multidisciplinary study." Cancer Res **66**(10): 5216-5223.

Gatenby, R. A. and R. J. Gillies (2004). "Why do cancers have high aerobic glycolysis?" Nat Rev Cancer **4**(11): 891-899.

Gaucher, G., M. H. Dufresne, et al. (2005). "Block copolymer micelles: preparation, characterization and application in drug delivery." J Control Release **109**(1-3): 169-188.

Gaur, S., L. Chen, et al. (2012). "Preclinical study of the cyclodextrin-polymer conjugate of camptothecin CRLX101 for the treatment of gastric cancer." Nanomedicine: Nanotechnology, Biology and Medicine **8**(5): 721-730.

Gerlóczy, A., S. Antal, et al. (1988). Percutaneous Absorption of Heptakis-(2,6-Di-O-14C-Methyl)-β-Cyclodextrin in Rats. Proceedings of the Fourth International Symposium on Cyclodextrins. O. Huber and J. Szejtli, Springer Netherlands. **5:** 415-420.

Gerold, B., D. Gourevich, et al. (2012). Applicator for in-vitro ultrasound-activated targeted drug delivery. 11TH INTERNATIONAL SYMPOSIUM ON THERAPEUTIC ULTRASOUND, AIP Publishing.

Gerweck, L. E. and K. Seetharaman (1996). "Cellular pH Gradient in Tumor versus Normal Tissue - Potential Exploitation for the treatment of cancer." CANCER RESEARCH **56**: 1194-1198.

Gianfelice, D., A. Khiat, et al. (2003). "MR imaging-guided focused US ablation of breast cancer: histopathologic assessment of effectiveness-- initial experience." Radiology **227**(3): 849-855.

Gilchrist, A., M. Bunemann, et al. (1999). "A dominant-negative strategy for studying roles of G proteins in vivo." J Biol Chem **274**(10): 6610-6616.

Gillies, E. R. and J. M. Frechet (2005). "Dendrimers and dendritic polymers in drug delivery." Drug Discov Today **10**(1): 35-43.

Gillies, R. J., N. Raghunand, et al. (2002). "MRI of the tumor microenvironment." J Magn Reson Imaging **16**(4): 430-450.

Giordano, F., C. Novak, et al. (2001). "Thermal analysis of cyclodextrins and their inclusion compounds." Thermochimica Acta **380**: 123-151.

Giraudeau, P., N. Guignard, et al. (2007). "Optimization of homonuclear 2D NMR for fast quantitative analysis: Application to tropine–nortropine mixtures." Journal of Pharmaceutical and Biomedical Analysis **43**(4): 1243-1248.

Gong, J., M. Chen, et al. (2012). "Polymeric micelles drug delivery system in oncology." J Control Release **159**(3): 312-323.

Gorin, B. I., R. J. Riopelle, et al. (1996). "Efficient perfacial derivatization of cyclodextrins at the primary face." Tetrahedron Letters **37**(27): 4647-4650.

Gourevich, D., O. Dogadkin, et al. (2013). "Ultrasound-mediated targeted drug delivery with a novel cyclodextrin-based drug carrier by mechanical and thermal mechanisms." J Control Release **170**(3): 316-324.

Grazú, V., M. Moros, et al. (2012). "Chapter 14 – Nanocarriers as Nanomedicines: Design Concepts and Recent Advances." Frontiers of Nanoscience: 337-440.

Greenleaf, W. J., M. E. Bolander, et al. (1998). "Artificial cavitation nuclei significantly enhance acoustically induced cell transfection." Ultrasound Med Biol **24**(4): 587-595.

Gregoriadis, G. (1995). "Engineering targeted liposomes: progress and problems." Trends in Biotechnol. **13**: 527-537.

Gregoriadis, G. and J. Wiley (1988). "Liposomes as drug carriers: recent trends and progress." Chicester: 52-61.

Gros, L., H. Ringsdorf, et al. (1981). "Polymeric Antitumor Agents on a Molecular and on a Cellular

Level?" Angewandte Chemie International Edition in English **20**(4): 305-325.

Grosse, P. Y., F. Bressolle, et al. (1999). "Methyl-β-cyclodextrin and doxorubicin pharmacokinetics and tissue concentrations following bolus injection of these drugs alone or together in the rabbit." International Journal of Pharmaceutics. **180**(2): 215-223.

Guzman, H. R., D. X. Nguyen, et al. (2001). "Ultrasound-mediated disruption of cell membranes. I. Quantification of molecular uptake and cell viability." J Acoust Soc Am **110**(1): 588-596.

Guzman, H. R., D. X. Nguyen, et al. (2002). "Equilibrium loading of cells with macromolecules by ultrasound: effects of molecular size and acoustic energy." J Pharm Sci **91**(7): 1693-1701.

Hainfeld, J., D. Slatkin, et al. (2004). "The use of gold nanoparticles to enhance radiotherapy in mice." Phys Med Biol **49**(18): N309-315.

Hamaguchi, T., T. Doi, et al. (2010). "Phase I study of NK012, a novel SN-38-incorporating micellar nanoparticle, in adult patients with solid tumors." Clin Cancer Res **16**(20): 5058-5066.

Hamaguchi, T., K. Kato, et al. (2007). "A phase I and pharmacokinetic study of NK105, a paclitaxel-incorporating micellar nanoparticle formulation." Br J Cancer **97**(2): 170-176.

Hamaguchi, T., Y. Matsumura, et al. (2005). "NK105, a paclitaxel-incorporating micellar nanoparticle formulation, can extend in vivo antitumour activity and reduce the neurotoxicity of paclitaxel." Br J Cancer **92**(7): 1240-1246.

Han, G., P. Ghosh, et al. (2007). Multi-Functional Gold Nanoparticles for Drug Delivery. Bio-Applications of Nanoparticles. W. W. Chan, Springer New York. **620:** 48-56.

Han, Y. W., A. Ikegami, et al. (2007). "Sonoporation is an efficient tool for intracellular fluorescent dextran delivery and one-step double-crossover mutant construction in Fusobacterium nucleatum." Appl Environ Microbiol **73**(11): 3677-3683.

Hansen, C. B., G. Y. Kao, et al. (1995). "Attachment of antibodies to sterically stabilized liposomes: evaluation, comparison and optimization of coupling procedures." Biochimica et Biophysica Acta (BBA) - Biomembranes **1239**(2): 133-144.

Harwood, L. M. (1989). Experimental organic chemistry : principles and practice. C. Moody. Oxford [England] ;, Blackwell Scientific Publications**:** 127-132.

Hattori, K., A. Kenmoku, et al. (2006). "Saccharide-branched Cyclodextrins as Targeting Drug Carriers." J. Incl. Phen. Macr. Chem. **56**: 9-16.

Hawker, C. J. and J. M. J. Frechet (1990). "Preparation of polymers with controlled molecular architecture. A new convergent approach to dendritic macromolecules." Journal of the American Chemical Society **112**(21): 7638-7647.

Heath, T. D., R. T. Fraley, et al. (1980). "Antibody targeting of liposomes: cell specificity obtained by conjugation of F(ab')2 to vesicle surface." Science **210**(4469): 539-541.

Heath, T. D., J. A. Montgomery, et al. (1983). "Antibody-targeted liposomes: increase in specific toxicity of methotrexate-gamma-aspartate." Proc Natl Acad Sci U S A **80**(5): 1377-1381.

Hensel, K., M. P. Mienkina, et al. (2011). "Analysis of ultrasound fields in cell culture wells for in vitro ultrasound therapy experiments." Ultrasound Med Biol **37**(12): 2105-2115.

Hernot, S. and A. L. Klibanov (2008). "Microbubbles in ultrasound-triggered drug and gene delivery." Adv Drug Deliv Rev **60**(10): 1153-1166.

Herschel, W. (1800). "Experiments on the refrangibility of the visible rays of the sun." Philosophical Transactions of the Royal Society of London **90**: 284-292.

Hill, C. R. and G. R. ter Haar (1995). "Review article: high intensity focused ultrasound--potential for cancer treatment." Br J Radiol **68**(816): 1296-1303.

Hillebrenner, H., F. Buyukserin, et al. (2006). "Template synthesized nanotubes for biomedical delivery applications." Nanomedicine **1**(1): 39-50.

Hirayama, F., M. Yamamoto, et al. (1992). "Acid - catalyzed hydrolysis of maltosyl - β - cyclodextrin." Journal of Pharmaceutical Science **89**(9): 913-916.

Holister, P., C. R. Vas, et al. (2003). "Dendrimers." Cientifica **Technology White Papers nr.6**.

Hoskins, P., K. Martin, et al. (2010). Diagnostic Ultrasound: Physics and Equipment, New York: Cambridge University Press.

Howarth, M., W. Liu, et al. (2008). "Monovalent, reduced-size quantum dots for imaging receptors on living cells." Nat Methods **5**(5): 397-399.

Hrkach, J., D. Von Hoff, et al. (2012). "Preclinical development and clinical translation of a PSMA-targeted docetaxel nanoparticle with a differentiated pharmacological profile." Sci Transl Med **4**(128): 3003651.

Hu, C. M. and L. Zhang (2012). "Nanoparticle-based combination therapy toward overcoming drug resistance in cancer." Biochem Pharmacol **83**(8): 1104-1111.

Huang, X., P. Jain, et al. (2007). "Gold nanoparticles: interesting optical properties and recent applications in cancer diagnostics and therapy." Nanomedicine **2**(5): 681-693.

Huber, P. E., J. W. Jenne, et al. (2001). "A new noninvasive approach in breast cancer therapy using magnetic resonance imaging-guided focused ultrasound surgery." Cancer Res **61**(23): 8441-8447.

Hundt, W., S. Steinbach, et al. (2009). "The effect of high intensity focused ultrasound on luciferase activity on two tumor cell lines in vitro, under the control of a CMV promoter." Ultrasonics **49**(3): 312-318.

Husain, N., T. T. Ndou, et al. (1992). "Complexation of doxorubicin with β- and γ-cyclodextrins." Applied Spectroscopy **46**(4): 652-658.

Husband, J. and A. Padhani (2006). "Recommendations for Cross-Sectional Imaging in Cancer Management:

Computed Tomography - CT

Magnetic Resonance Imaging - MRI

Positron Emission Tomography - PET-CT." Royal College of Radiologists(2).

Husseini, G. A. and W. G. Pitt (2008). "Micelles and Nanoparticles for Ultrasonic Drug and Gene Deliver." Adv Drug Deliv Rev. **60**(10): 1137-1152.

Husseini, G. A. and W. G. Pitt (2008). "Micelles and nanoparticles for ultrasonic drug and gene delivery." Adv Drug Deliv Rev **60**(10): 1137-1152.

Ibsen, S., M. Benchimol, et al. (2011). "A novel nested liposome drug delivery vehicle capable of ultrasound triggered release of its payload." J Control Release **155**(3): 358-366.

Illing, R. O., J. E. Kennedy, et al. (2005). "The safety and feasibility of extracorporeal high-intensity focused ultrasound (HIFU) for the treatment of liver and kidney tumours in a Western population." Br J Cancer **93**(8): 890-895.

Irie, T. and K. Uekama (1997). "Pharmaceutical applications of cyclodextrins. III. Toxicological issues and safety evaluation." J Pharm Sci **86**(2): 147-162.

Jain, R. K. (1999). Transport of molecules, particles, and cells in solid tumors**:** 241-263.

Jain, R. K. (2001). "Delivery of molecular medicine to solid tumors: Lessons from in vivo imaging of gene expression and function." Journal of Controlled Release **74**(1-3): 7-25.

James, N. D., R. J. Coker, et al. (1994). "Liposomal doxorubicin (Doxil): An effective new treatment for

Kaposi's sarcoma in AIDS." Clinical Oncology **6**(5): 294-296.

James R. Dewald, D. A. T. (1983). "Dense star polymers having core, core branches, terminal groups." The Dow Chemical Corporation.

Jemal, A., R. Siegel, et al. (2010). "Cancer statistics, 2010." CA Cancer J Clin **60**(5): 277-300.

Jenne, J. W., T. Preusser, et al. (2012). "High-intensity focused ultrasound: Principles, therapy guidance, simulations and applications." Zeitschrift für Medizinische Physik **22**(4): 311-322.

Johannsen, M., U. Gneveckow, et al. (2007). "Thermotherapy of prostate cancer using magnetic nanoparticles: feasibility, imaging, and three-dimensional temperature distribution." Eur Urol **52**(6): 1653-1661.

Jolesz, F. A. and N. McDannold (2008). "Current status and future potential of MRI-guided focused ultrasound surgery." J Magn Reson Imaging **27**(2): 391-399.

Jolesz, F. A. and N. J. McDannold (2014). "Magnetic resonance-guided focused ultrasound: a new technology for clinical neurosciences." Neurol Clin **32**(1): 253-269.

Jones, M.-C. and J.-C. Leroux (1999). "Polymeric micelles – a new generation of colloidal drug carriers." European Journal of Pharmaceutics and Biopharmaceutics **48**(2): 101-111.

Kamaly, N., T. Kalber, et al. (2009). "Folate Receptor Targeted Bimodal Liposomes for Tumor Magnetic Resonance Imaging." Bioconjugate Chemistry **20**(4): 648-655.

Kamimura, M., T. Furukawa, et al. (2013). "Enhanced intracellular drug delivery of pH-sensitive doxorubicin/poly(ethylene glycol)-block-poly(4-vinylbenzylphosphonate) nanoparticles in multi-drug resistant human epidermoid KB carcinoma cells." Biomaterials Science **1**(4): 361-367.

Kanazawa, S., T. Furuki, et al. "Measurement of OH Radicals in Aqueous Solution Produced by Atmospheric-pressure LF Plasma Jet."

Kang, K., S. H. Oh, et al. (2011). "A novel topoisomerase inhibitor, daurinol, suppresses growth of HCT116 cells with low hematological toxicity compared to etoposide." Neoplasia **13**(11): 1043-1057.

Karino, T., S. Koga, et al. (1988). "Experimental studies of the effects of local hyperthermia on blood flow, oxygen pressure and pH in tumors." Jpn J Surg **18**(3): 276-283.

Karshafian, R., P. D. Bevan, et al. (2009). "Sonoporation by ultrasound-activated microbubble contrast agents: effect of acoustic exposure parameters on cell membrane permeability and cell viability." Ultrasound Med Biol **35**(5): 847-860.

Kasai, S., H. Nagasawa, et al. (2002). "Design and synthesis of antiangiogenic/heparin-binding arginine dendrimer mimicking the surface of endostatin." Bioorg Med Chem Lett **12**(6): 951-954.

Keenan, J., Y. Liang, et al. (2004). "Two-deoxyglucose as an anti-metabolite in human carcinoma cell line RPMI-2650 and drug-resistant variants." Anticancer Res **24**(2A): 433-440.

Kennedy, J. E., G. R. Ter Haar, et al. (2003). "High intensity focused ultrasound: surgery of the future?" Br J Radiol **76**(909): 590-599.

Kerry K. Karukstis, E. H. Z. T., Jennifer A. Whiles, and R. J. Rosenfeld (1998). "Deciphering the fluorescence signature of daunomycin and doxorubicin." Biophysical Chemistry **73**: 249-263.

Khan, M. K., S. S. Nigavekar, et al. (2005). "In vivo biodistribution of dendrimers and dendrimer nanocomposites -- implications for cancer imaging and therapy." Technol Cancer Res Treat **4**(6): 603-613.

Kim, C. S., G. Y. Tonga, et al. (2013). "Inorganic nanosystems for therapeutic delivery: status and prospects." Adv Drug Deliv Rev **65**(1): 93-99.

Kim, J. W. and C. V. Dang (2006). "Cancer's molecular sweet tooth and the Warburg effect." Cancer Res **66**(18): 8927-8930.

Kim, S. Y., I. G. Shin, et al. (1998). "Preparation and characterization of biodegradable nanospheres composed of methoxy poly(ethylene glycol) and DL-lactide block copolymer as novel drug carriers." J Control Release **56**(1-3): 197-208.

Kim, T. Y., D. W. Kim, et al. (2004). "Phase I and pharmacokinetic study of Genexol-PM, a Cremophor-free, polymeric micelle-formulated paclitaxel, in patients with advanced malignancies." Clinical Cancer Research **10**(11): 3708-3716.

Kleinstreuer, C., E. Childress, et al. (2013). Chapter 10 - Targeted Drug Delivery: Multifunctional Nanoparticles and Direct Micro-Drug Delivery to Tumors. Transport in Biological Media. S. M. Becker and A. V. Kuznetsov. Boston, Elsevier**:** 391-416.

Klibanov, A. L. (2006). "Microbubble contrast agents: targeted ultrasound imaging and ultrasound-assisted drug-delivery applications." Invest Radiol **41**(3): 354-362.

Klibanov, A. L., K. Maruyama, et al. (1990). "Amphipathic polyethyleneglycols effectively prolong the circulation time of liposomes." FEBS Lett **268**(1): 235-237.

Klingler, H. C., M. Susani, et al. (2008). "A novel approach to energy ablative therapy of small renal tumours: laparoscopic high-intensity focused ultrasound." Eur Urol **53**(4): 810-816.

Kobayashi, T., S. Tsukagoshi, et al. (1975). "Enhancement of the cancer chemotherapeutic effect of cytosine arabinoside entrapped in liposomes on mouse leukemia L-1210." Gann **66**(6): 719-720.

Kohori, F., K. Sakai, et al. (1998). "Preparation and characterization of thermally responsive block copolymer micelles comprising poly(N-isopropylacrylamide-b-dl-lactide)." Journal of Controlled Release **55**(1): 87-98.

Kong, G., R. D. Braun, et al. (2000). "Hyperthermia enables tumor-specific nanoparticle delivery: effect of particle size." Cancer Res **60**(16): 4440-4445.

Kong, G., R. D. Braun, et al. (2001). "Characterization of the effect of hyperthermia on nanoparticle extravasation from tumor vasculature." Cancer Res **61**(7): 3027-3032.

Kong, J., N. R. Franklin, et al. (2000). "Nanotube Molecular Wires as Chemical Sensors." Science **287**(5453): 622-625.

Koning, G. A., A. M. Eggermont, et al. (2010). "Hyperthermia and thermosensitive liposomes for improved delivery of chemotherapeutic drugs to solid tumors." Pharm Res **27**(8): 1750-1754.

Kost, J., K. Leong, et al. (1989). "Ultrasound-enhanced polymer degradation and release of incorporated substances." Proc Natl Acad Sci U S A **86**(20): 7663-7666.

Kostarelos, K., L. Lacerda, et al. (2007). "Cellular uptake of functionalized carbon nanotubes is independent of functional group and cell type." Nat Nano **2**(2): 108-113.

Kralova, J., Z. Konak, et al. (2010). "Porphyrin-Cyclodextrin Conjugates as a Nanosystem for Versatile Drug Delivery and Multimodal

Cancer Therapy." J. Med. Chem. **53**: 128-138.

Kudo, N., K. Okada, et al. (2009). "Sonoporation by single-shot pulsed ultrasound with microbubbles adjacent to cells." Biophys J **96**(12): 4866-4876.

Kukowska-Latallo, J. F., K. A. Candido, et al. (2005). "Nanoparticle targeting of anticancer drug improves therapeutic response in animal model of human epithelial cancer." Cancer Res **65**(12): 5317-5324.

Kumar, S. (2006). "Spectroscopy of Organic Compounds." Cosmic rays **10**: 4.

Kurkov, S. V. and T. Loftsson (2012). "Cyclodextrins." International Journal of Pharmaceutics **453**(1): 167-180.

Kwon, G., S. Suwa, et al. (1994). "Enhanced tumor accumulation and prolonged circulation times of micelle-forming poly (ethylene oxide-aspartate) block copolymer-adriamycin conjugates." Journal of Controlled Release **29**(1–2): 17-23.

Lacerda, L., A. Bianco, et al. (2006). "Carbon nanotubes as nanomedicines: from toxicology to pharmacology." Adv Drug Deliv Rev **58**(14): 1460-1470.

Lakshmanan, S., G. K. Gupta, et al. (2013). "Physical energy for drug delivery; poration, concentration and activation." Adv Drug Deliv Rev **7**(13): 00148-00148.

Lam, C. W., J. T. James, et al. (2004). "Pulmonary toxicity of single-wall carbon nanotubes in mice 7 and 90 days after intratracheal instillation." Toxicol Sci **77**(1): 126-134.

Langdon, S. P. (2003). "Cancer Cell Culture: Methods and Protocols."

Langer, M. G. and A. Koitschev (2002). Chapter 7 The biophysics of sensory cells of the inner ear examined by atomic force microscopy and patch clamp. Methods in Cell Biology. H. J. K. H. Bhanu P. Jena, Academic Press. **Volume 68:** 141-169.

Larina, I. V., B. M. Evers, et al. (2005). "Optimal drug and gene delivery in cancer cells by ultrasound-induced cavitation." Anticancer Res **25**(1A): 149-156.

Lasic, D. D. (1998). "Novel applications of liposomes." TIBTECH **16**: 307-321.

Lasic, D. D. and D. Papahadjopoulos (1998). "Medical Applications of Liposomes." Elsevier.

Lavon, I. and J. Kost (2004). "Ultrasound and transdermal drug delivery." Drug Discovery Today **9**(15): 670-676.

Leamon, C. P. and P. S. Low (1991). "Delivery of macromolecules into living cells: a method that exploits folate receptor endocytosis." Proceedings of the National Academy of Sciences **88**(13): 5572-5576.

Lee, C. C., J. A. MacKay, et al. (2005). "Designing dendrimers for biological applications." Nat Biotech **23**(12): 1517-1526.

Lee, E. S., K. Na, et al. (2003). "Polymeric micelle for tumor pH and folate-mediated targeting." J Control Release **91**(1-2): 103-113.

Lee, H. M., J. H. Hong, et al. (2006). "High-intensity focused ultrasound therapy for clinically localized prostate cancer." Prostate Cancer Prostatic Dis **9**(4): 439-443.

Lee, I. O. S.-K. (1998). "Photoluminescent determination of oxygen using metalloporphyrin-polymer sensing systems." Spectrochimica Acta Part A: Molecular and Biomolecular Spectroscopy **54**: 91-100.

Lee, R. J. and P. S. Low (1994). "Delivery of liposomes into cultured KB cells via folate receptor-mediated endocytosis." J Biol Chem **269**(5): 3198-3204.

Lee, S.-K. and I. Okura (1998). "Photoluminescent determination of oxygen using metalloporphyrin-polymer sensing systems." Spectrochimica Acta Part A **54**: 91-100.

Lee, S.-K., Y. B. Shin, et al. (2001). "Highly Sensitive Optical Oxygen Sensing Material:

Thin Silica Xerogel Doped with Tris(4,7-diphenyl-1,10-phenanthroline)ruthenium." Chemistry Letters: 310-311.

Lefor, A. T., S. Makohon, et al. (1985). "The effects of hyperthermia on vascular permeability in experimental liver metastasis." J Surg Oncol **28**(4): 297-300.

Lehrer, S. S. (1971). "Solute Perturbation of Protein Fluorescence The Quenching of the Tryptophyl Fluorescence of Model Compounds and of Lysozyme by Iodide Ion." BIOCHEMISTRY

10(17): 3254-3263.

Leighton, T. G. (1994). The Acoustic Bubble, Academic Press.

Leighton, T. G. (1994). "The Acoustic Bubble." London: Academic ed.

Leighton, T. G., B. T. Cox, et al. (2000). "The Rayleigh-like collapse of a conical bubble." J Acoust Soc Am **107**(1): 130-142.

Lentacker, I., I. De Cock, et al. (2013). "Understanding ultrasound induced sonoporation: Definitions and underlying mechanisms." Adv Drug Deliv Rev **21**(13): 00267-00266.

Leong, T., M. Ashokkumar, et al. (2011). "THE FUNDAMENTALS OF POWER ULTRASOUND-A REVIEW." Acoustics Australia **39**(2).

Leong, T. S., T. J. Wooster, et al. (2009). "Minimising oil droplet size using ultrasonic emulsification." Ultrason Sonochem **16**(6): 721-727.

Leserman, L. D., J. N. Weinstein, et al. (1980). "Receptor-mediated endocytosis of antibody-opsonized liposomes by tumor cells." Proc Natl Acad Sci U S A **77**(7): 4089-4093.

Leskinen, J. J. and K. Hynynen (2012). "Study of factors affecting the magnitude and nature of ultrasound exposure with in vitro set-ups." Ultrasound Med Biol **38**(5): 777-794.

Li, C., M. Curreli, et al. (2005). "Complementary detection of prostate-specific antigen using In2O3 nanowires and carbon nanotubes." J Am Chem Soc **127**(36): 12484-12485.

Li, L., M. Zhao, et al. (2012). "Self-complexation and complexation-controlled target cancer therapy." MedChemComm **3**(9): 1059.

Li, X., Y. P. Zhang, et al. (2005). "Gene therapy for prostate cancer by controlling adenovirus E1a and E4 gene expression with PSES enhancer." Cancer Res **65**(5): 1941-1951.

Li, Y. Y., W. H. Sha, et al. (2007). "Short and long term efficacy of high intensity focused ultrasound therapy for advanced hepatocellular carcinoma." J Gastroenterol Hepatol **22**(12): 2148-2154.

Li, Y. Y., X. Z. Zhang, et al. (2006). "Thermosensitive Y-Shaped Micelles of Poly(oleic acid-Y-N-isopropylacrylamide) for Drug Delivery." Small **2**(7): 917-923.

Lim, E.-K., Y.-M. Huh, et al. (2011). "pH-Triggered Drug-Releasing Magnetic Nanoparticles for Cancer Therapy Guided by Molecular Imaging by MRI." Advanced Materials **23**(21): 2436-2442.

Lim, J. and E. E. Simanek (2012). "Triazine dendrimers as drug delivery systems: from synthesis to therapy." Adv Drug Deliv Rev **64**(9): 826-835.

Lin, C.-Y., J.-R. Li, et al. (2012). "Enhancement of focused ultrasound with microbubbles on the treatments of anticancer nanodrug in mouse tumors." Nanomedicine: Nanotechnology, Biology and Medicine **8**(6): 900-907.

Lin, C. Y., Y. L. Huang, et al. (2010). "Effects of focused ultrasound and microbubbles on the vascular permeability of nanoparticles delivered into mouse tumors." Ultrasound Med Biol **36**(9): 1460-1469.

Lindner, J. R. (2002). "Contrast echocardiography." Current Problems in Cardiology **27**(11): 454-519.

Liu, S.-Q., N. Wiradharmaa, et al. (2007). "Bio-functional micelles self-assembled from a folate-conjugated block copolymer for targeted intracellular delivery of anticancer drugs." Biomaterials **28**(7): 1423-1433.

Liu, Y., C.-W. Cho, et al. (2001). "Ultrasound-Induced hyperthermia increases cellular Uptake and Cytotoxicity of P-Glycoprotein

Substrates in Multi-Drug

Resistant Cells." Pharmaceutical Research **18**(9).

Liu, Y., D. A. Peterson, et al. (1997). "Mechanism of cellular

3-(4,5-dimethylthiazol-2-yl)-2,5-diphenyltetrazolium bromide (MTT) reduction." J Neurochem **69**(2): 581-593.

Lo, Y.-L., C.-S. Chu, et al. (2008). "Temperature compensation of fluorescence intensity-based fiber-optic oxygen sensors using modified Stern–Volmer model." Sensors and Actuators B: Chemical **131**(2): 479-488.

Loftsson, T. and N. Bodor (1995). "Effect of cyclodextrins on percutaneous transport of drugs. In: Smith, E.W.,

Maibach, H.I. (Eds.),." Percutaneous Penetration Enhancers. CRC Press, Boca Raton, FL,: 335-342.

Loftsson, T. and M. E. Brewster (1996). "Pharmaceutical applications of cyclodextrins. 1. Drug solubilization and stabilization." J Pharm Sci **85**(10): 1017-1025.

Loftsson, T. and D. Duchene (2007). "Cyclodextrins and their pharmaceutical applications." International Journal of Pharmaceutics **329**(1-2): 1-11.

Loftsson, T. and M. Masson (2001). "Cyclodextrins in topical drug formulations: theory and practice." International Journal of Pharmaceutics **225**: 15-30.

Low, P. S. and A. C. Antony (2004). "Folate receptor-targeted drugs for cancer and inflammatory diseases." Adv. Drug Deliv. Rev. **56**(8): 1055-1058.

Lu, Y. and K. Park (2013). "Polymeric micelles and alternative nanonized delivery vehicles for poorly soluble drugs." International Journal of Pharmaceutics **453**(1): 198-214.

Lukyanov, A. N., T. A. Elbayoumi, et al. (2004). "Tumor-targeted liposomes: doxorubicin-loaded long-circulating liposomes modified with anti-cancer antibody." J. Control. Rel. **100**(1): 135-144.

Madersbacher, S. and M. Marberger (2003). "High-energy shockwaves and extracorporeal high-intensity focused ultrasound." J Endourol **17**(8): 667-672.

Martin, F. J., W. L. Hubbell, et al. (1981). "Immunospecific targeting of liposomes to cells: a novel and efficient method for covalent attachment of Fab' fragments via disulfide bonds." BIOCHEMISTRY **20**(14): 4229-4238.

Martone, R. L., H. Zhou, et al. (2009). "Begacestat (GSI-953): a novel, selective thiophene sulfonamide inhibitor of amyloid precursor protein gamma-secretase for the treatment of Alzheimer's disease." J Pharmacol Exp Ther **331**(2): 598-608.

Maruyama, K., T. Takizawa, et al. (1995). "Targetability of novel immunoliposomes modified with amphipathic poly(ethylene glycol)s conjugated at their distal terminals to monoclonal antibodies." Biochim Biophys Acta **8**(1): 74-80.

Maruyama, K., T. Yuda, et al. (1991). "Effect of molecular weight in amphipathic polyethyleneglycol on prolonging the circulation time of large unilamellar liposomes." Chem Pharm Bull **39**(6): 1620-1622.

Masayuki, Y., M. Mizue, et al. (1990). "Polymer micelles as novel drug carrier: Adriamycin-conjugated poly(ethylene glycol)-poly(aspartic acid) block copolymer." Journal of Controlled Release **11**(1–3): 269-278.

Mason, T. J., J. P. Lorimer, et al. (1994). "Dosimetry in sonochemistry: the use of aqueous terephthalate ion as a fluorescence monitor." Ultrasonics Sonochemistry **1**(2): S91-S95.

Matsumura, Y., T. Hamaguchi, et al. (2004). "Phase I clinical trial and pharmacokinetic evaluation of NK911, a micelle-encapsulated doxorubicin." British Journal of Cancer **91**(10): 1775-1781.

Matsumura, Y. and K. Kataoka (2009). "Preclinical and clinical studies of anticancer agent-incorporating polymer micelles." Cancer Science **100**(4): 572-579.

Mattheolabakis, G., B. Rigas, et al. (2012). "Nanodelivery strategies in cancer chemotherapy: biological rationale and pharmaceutical perspectives." Nanomedicine **7**(10): 1577-1590.

May, D. J., J. S. Allen, et al. (2002). "Dynamics and fragmentation of thick-shelled microbubbles." Ultrasonics, Ferroelectrics and Frequency Control, IEEE Transactions on **49**(10): 1400-1410.

May, J. P. and S.-D. Li (2013). "Hyperthermia-induced drug targeting." Expert Opinion on Drug Delivery **10**(4): 511-527.

Mayhew, E., D. Papahadjopoulos, et al. (1976). "Inhibition of tumor cell growth in vitro and in vivo by 1-beta-D-arabinofuranosylcytosine entrapped within phospholipid vesicles." Cancer Res **36**(12): 4406-4411.

Mayhew, E. G., D. Lasic, et al. (1992). "Pharmacokinetics and antitumor activity of epirubicin encapsulated in long-circulating liposomes incorporating a polyethylene glycol-derivatized phospholipid." Int J Cancer **51**(2): 302-309.

McDannold, N., C. D. Arvanitis, et al. (2012). "Temporary disruption of the blood-brain barrier by use of ultrasound and microbubbles: safety and efficacy evaluation in rhesus macaques." Cancer Res **72**(14): 3652-3663.

McLean, J. R. and A. J. Mortimer (1988). "A cavitation and free radical dosimeter for ultrasound." Ultrasound Med Biol **14**(1): 59-64.

McNaught, A. D. and A. Wilkinson (2012). IUPAC. Compendium of Chemical Terminology, 2nd ed. (the "Gold Book"), WileyBlackwell; 2nd Revised edition edition.

Merkus, F. W., J. C. Verhoef, et al. (1999). "Cyclodextrins in nasal drug delivery." Adv Drug Deliv Rev **36**(1): 41-57.

Miller, M. W., D. L. Miller, et al. (1996). "A review of in vitro bioeffects of inertial ultrasonic cavitation from a mechanistic perspective." Ultrasound Med Biol **22**(9): 1131-1154.

Mills, J. K. and D. Needham (1999). "Targeted drug delivery." Expert Opinion on Therapeutic Patents **9**(11): 1499-1513.

Mody, V., R. Siwale, et al. (2010). "Introduction to metallic nanoparticles." J Pharm Bioallied Sci **2**(4): 282-289.

Mohammadi, A. and F. Bahrami (2014). "A nonlinear eigenvalue problem arising in a nanostructured quantum dot." Communications in Nonlinear Science and Numerical Simulation **19**(9): 3053-3062.

Mohan, C. (2003). "Buffers." Calbiochem: 18-23.

Mosmann, T. (1983). "Rapid colorimetric assay for cellular growth and survival: application to proliferation and cytotoxicity assays." J Immunol Methods **65**(1-2): 55-63.

Mousa, S. A. and D. J. Bharali (2011). "Nanotechnology-Based Detection and Targeted Therapy in Cancer: Nano-Bio Paradigms and Applications." Cancers **3**(4): 2888-2903.

Muggia, F. M. and M. D. Green (1991). "New anthracycline antitumor antibiotics." Crit. Rev. Oncol. Hematol. **11**(1): 43-64.

Myhr, G. and J. Moan (2006). "Synergistic and tumour selective effects of chemotherapy and ultrasound treatment." Cancer Lett **232**(2): 206-213.

Naji Meidani, A. R. and M. Hasan (2004). "Mathematical and physical modelling of bubble growth due to ultrasound." Applied Mathematical Modelling **28**(4): 333-351.

Nanjwade, B. K., H. M. Bechra, et al. (2009). "Dendrimers: Emerging polymers for drug-delivery systems." European Journal of Pharmaceutical Sciences **38**(3): 185-196.

Needham, D., G. Anyarambhatla, et al. (2000). "A new temperature-sensitive liposome for use with mild

hyperthermia: characterization and testing in a human tumor xenograft model." Cancer Res **60**(5): 1197-1201.

Negussie, A. H., P. S. Yarmolenko, et al. (2011). "Formulation and characterisation of magnetic resonance imageable thermally sensitive liposomes for use with magnetic resonance-guided high intensity focused ultrasound." Int J Hyperthermia **27**(2): 140-155.

Newkome, G. R., Z. Yao, et al. (1985). "Micelles. Part 1. Cascade molecules: a new approach to micelles. A [27]-arborol." The Journal of Organic Chemistry **50**(11): 2003-2004.

O'Neill, C. F., M. G. Ormerod, et al. (1996). "Apoptotic and non-apoptotic cell death induced by cis and trans analogues of a novel ammine(cyclohexylamine)dihydroxodichloroplatinum(IV) complex." Br J Cancer **74**(7): 1037-1045.

Oda, Y., N. Kobayashi, et al. (2008). "β-Cyclodextrin Conjugates with Glucose Moieties Designed as Drug Carriers: Their Syntheses, Evaluations Using Concanavalin A and Doxorubicin, and Structural Analyses by NMR Spectroscopy." Med. Chem. **4**(3): 244-255.

Oda, Y., M. Miura, et al. (2009). "Syntheses and Doxorubicin-Inclusion Abilities of β-Cyclodextrin Derivatives with a Hydroquinone α-Glycoside Residue Attached at the Primary Side." Chem. Pharm. Bull. **57**(1): 74-78.

Oda, Y., H. Yanagisawa, et al. (2008). "Design, synthesis and evaluation of d-galactose-β-cyclodextrin conjugates as drug-carrying molecules." Bioorg. Med. Chem. **16**(19): 8830-8840.

Okada, A., Y. Morita, et al. (2009). "Non-invasive magnetic resonance-guided focused ultrasound treatment of uterine fibroids in a large Japanese population: impact of the learning curve on patient outcome." Ultrasound Obstet Gynecol **34**(5): 579-583.

Paciotti, G. F., L. Myer, et al. (2004). "Colloidal gold: a novel nanoparticle vector for tumor directed drug delivery." Drug Deliv **11**(3): 169-183.

Pantarotto, D., R. Singh, et al. (2004). "Functionalized carbon nanotubes for plasmid DNA gene delivery." Angew Chem Int Ed Engl **43**(39): 5242-5246.

Papahadjopoulos, D., T. M. Allen, et al. (1991). "Sterically stabilized liposomes: improvements in pharmacokinetics and antitumor therapeutic efficacy." Proc Natl Acad Sci U S A **88**(24): 11460-11464.

Papahadjopoulos, D. and A. Gabizon (1987). "Targeting of liposomes to tumor cells in vivo." Ann. N. Y. Acad. Sci **507**: 64-74.

Park, J. W. (2002). "Liposome-based drug delivery in breast cancer treatment." Breast Cancer Res **4**(3): 95-99.

Park, J. W. (2006). Chapter 1 - Fluorescence Methods for Studies of Cyclodextrin Inclusion Complexation and Excitation Transfer in Cyclodextrin Complexes. Cyclodextrin Materials Photochemistry, Photophysics and Photobiology. A. Douhal. Amsterdam, Elsevier. **1:** 1-26.

Park, J. W. (2006). Cyclodextrin Materials Photochemistry, Photophysics and Photobiology.

Patri, A. K., J. F. Kukowska-Latallo, et al. (2005). "Targeted drug delivery with dendrimers: comparison of the release kinetics of covalently conjugated drug and non-covalent drug inclusion complex." Adv Drug Deliv Rev **57**(15): 2203-2214.

Peer, D., J. M. Karp, et al. (2007). "Nanocarriers as an emerging platform for cancer therapy." Nat Nano **2**(12): 751-760.

Pisanic, T. R., J. D. Blackwell, et al. (2007). "Nanotoxicity of iron oxide nanoparticle internalization in growing neurons." Biomaterials **28**(16): 2572-2581.

Pitt, W. G., G. A. Husseini, et al. (2004). "Ultrasonic drug delivery--a general review." Expert Opin

Drug Deliv **1**(1): 37-56.

Pitt, W. G. and S. A. Ross (2003). "Ultrasound Increases the Rate of Bacterial Cell Growth." Biotechnology Progress **19**(3): 1038-1044.

Ponce, A. M., Z. Vujaskovic, et al. (2006). "Hyperthermia mediated liposomal drug delivery." Int J Hyperthermia **22**(3): 205-213.

Prentice, P., A. Cuschieri, et al. (2005). "Membrane disruption by optically controlled microbubble cavitation." Nat Phys **1**(2): 107-110.

Presant, C. A., D. Blayney, et al. (1990). "Preliminary report: imaging of Kaposi sarcoma and lymphoma in AIDS with indium-111-labelled liposomes." The Lancet **335**(8701): 1307-1309.

Presant, C. A., R. T. Proffitt, et al. (1988). "Successful Imaging of human cancer with Indium-111-labeled phospholipid vesiccles." Cancer **62**: 905.

Price, R., J. Chappell, et al. (2006). "Nanoparticle delivery into biological tissues by ultrasonic microbubble destruction." Nanomedicine **2**(4): 273.

Primeau, A. J., A. Rendon, et al. (2005). "The distribution of the anticancer drug Doxorubicin in relation to blood vessels in solid tumors." Clin Cancer Res **11**(24 Pt 1): 8782-8788.

Purushotham, S., P. E. Chang, et al. (2009). "Thermoresponsive core-shell magnetic nanoparticles for combined modalities of cancer therapy." Nanotechnology **20**(30): 0957-4484.

Qian, W. Y., D. M. Sun, et al. (2012). "pH-sensitive strontium carbonate nanoparticles as new anticancer vehicles for controlled etoposide release." Int J Nanomedicine **7**: 5781-5792.

Qian, X., X. Peng, et al. (2008). "In vivo tumor targeting and spectroscopic detection with surface-enhanced Raman nanoparticle tags." Nat Biotechnol **26**(1): 83-90.

Quate, C. and C. Gerber (1986). "Atomic Force Microscopy."

Quintana, A., E. Raczka, et al. (2002). "Design and function of a dendrimer-based therapeutic nanodevice targeted to tumor cells through the folate receptor." Pharm Res **19**(9): 1310-1316.

Radmacher, M. (1997). "Measuring the elastic properties of biological samples with the AFM." IEEE Eng Med Biol Mag **16**(2): 47-57.

Rahimi, M., S. Kilaru, et al. (2008). "Synthesis and Characterization of Thermo-Sensitive Nanoparticles for Drug Delivery Applications." J Biomed Nanotechnol **4**(4): 482-490.

Rajewski, R. A. and V. J. Stella (1996). "Pharmaceutical applications of cyclodextrins. 2. In vivo drug delivery." J Pharm Sci **85**(11): 1142-1169.

Ranjan, A., G. C. Jacobs, et al. (2012). "Image-guided drug delivery with magnetic resonance guided high intensity focused ultrasound and temperature sensitive liposomes in a rabbit Vx2 tumor model." J Control Release **158**(3): 487-494.

Rapoport, N. Y., A. M. Kennedy, et al. (2009). "Controlled and targeted tumor chemotherapy by ultrasound-activated nanoemulsions/microbubbles." J Control Release **138**(3): 268-276.

Reeuwijk, H. J. E. M., H. Irth, et al. (1993). "Liquid chromatographic determination of β-cyclodextrin derivatives based on fluorescene enhancement after inclusion complexation." J. Chromatogr **614**: 95-101.

Reilly, R. M. (2007). "Carbon nanotubes: potential benefits and risks of nanotechnology in nuclear medicine." J Nucl Med **48**(7): 1039-1042.

Rekharsky, M. V. and Y. Inoue (1998). "Complexation Thermodynamics of Cyclodextrins." Chem Rev **98**(5): 1875-1918.

Rodriguez, M. A., R. Pytlik, et al. (2009). "Vincristine sulfate liposomes injection (Marqibo) in heavily pretreated patients with refractory aggressive non-Hodgkin lymphoma: report of the pivotal

phase 2 study." Cancer **115**(15): 3475-3482.

Saar, M., C. Körbel, et al. (2012). "Experimental orthotopic prostate tumor in nude mice: Techniques for local cell inoculation and three-dimensional ultrasound monitoring." Urologic Oncology: Seminars and Original Investigations **30**(3): 330-338.

Sætern, A. M., N. B. Nguyen, et al. (2004). "Effect of hydroxypropyl-β-cyclodextrin-complexation and pH on solubility of camptothecin." International Journal of Pharmaceutics **284**(1–2): 61-68.

Safinya, C. R. and K. K. Ewert (2012). "Materials chemistry: Liposomes derived from molecular vases." Nature **489**(7416): 372-374.

Saikawa, Y., C. B. Knight, et al. (1993). "Decreased expression of the human folate receptor mediates transport-defective methotrexate resistance in KB cells." J Biol Chem **268**(7): 5293-5301.

Sampathkumar, S.-G. and K. J. Yarema (2007). "Dendrimers in Cancer Treatment and Diagnosis, Edited by Challa S. S. R. Kumar " Nanomaterials for Cancer Diagnosis, Nanotechnologies for the Life Sciences **7**: 1-43.

Sarker, D. and P. Workman (2007). "Pharmacodynamic biomarkers for molecular cancer therapeutics." Adv Cancer Res **96**: 213-268.

Sarris, A. H., F. Hagemeister, et al. (2000). "Liposomal vincristine in relapsed non-Hodgkin's lymphomas: early results of an ongoing phase II trial." Ann Oncol **11**(1): 69-72.

Schaaf, A., S. Langbein, et al. (2003). "In vitro transfection of human bladder cancer cells by acoustic energy." Anticancer Res **23**(6C): 4871-4875.

Schardinger, F. (1903). "U¨ ber Thermophile Bakterien aus verschiedenen Speisen und Milch, sowie ¨uber einige Umsetzungsprodukte derselben in kohlenhydrathaltigen N¨ahrl¨osungen, darunter krystallisierte Polysaccharide (Dextrine) aus St¨arke." Z. Untersuch. Nahr. u. Genussm. **6**: 865-880.

Schardinger, F. (1911). "Bildung kristallisierter Polysaccharide (Dextrine) aus St¨arkekleister durch Microben. Zentralbl." Bakteriol. Parasitenk. Abt. II **29**: 188-197.

Schlicher, R. K., H. Radhakrishna, et al. (2006). "Mechanism of intracellular delivery by acoustic cavitation." Ultrasound Med Biol **32**(6): 915-924.

Schmaljohann, D. (2006). "Thermo- and pH-responsive polymers in drug delivery." Advanced Drug Delivery Reviews **58**(15): 1655-1670.

Schmaljohann, D. (2006). "Thermo- and pH-responsive polymers in drug delivery." Advanced Drug Delivery Reviews **58**(15): 1655-1670.

Schneider, H., F. Hacket, et al. (1998). "NMR Studies of Cyclodextrins and Cyclodextrin Complexes." Chem Rev **98**(5): 1755-1786.

Schülke, N., O. A. Varlamova, et al. (2003). "The homodimer of prostate-specific membrane antigen is a functional target for cancer therapy." Proceedings of the National Academy of Sciences of the United States of America **100**(22): 12590-12595.

Scudiero, D. A., R. H. Shoemaker, et al. (1988). "Evaluation of a soluble tetrazolium/formazan assay for cell growth and drug sensitivity in culture using human and other tumor cell lines." Cancer Res **48**(17): 4827-4833.

Selvan, S. T., T. T. Y. Tan, et al. (2009). "Functional and Multifunctional Nanoparticles for Bioimaging and Biosensing." Langmuir **26**(14): 11631-11641.

Senior, J., C. Delgado, et al. (1991). "Influence of surface hydrophilicity of liposomes on their interaction with plasma protein and clearance from the circulation: studies with poly(ethylene glycol)-coated vesicles." Biochim Biophys Acta **11**(1): 77-82.

Shen, D. W., Y. G. Lu, et al. (1991). "Human hepatocellular carcinoma cell lines exhibit multidrug resistance unrelated to MRD1 gene expression." J Cell Sci **98**(Pt 3): 317-322.

Shim, M., A. Javey, et al. (2001). "Polymer functionalization for air-stable n-type carbon nanotube field-effect transistors." J Am Chem Soc **123**(46): 11512-11513.

Shimamura, M., S. Kasai, et al. (2006). "Angiogenesis inhibition of arginine-rich dendrimers, TX-1943 and TX-1944, which mimic the surface structure of endostatin." Vascul Pharmacol **45**(3): 0-0.

Singh, M., R. Sharma, et al. (2002). "Biotechnological applications of cyclodextrins." Biotechnology Advances **20**: 341-359.

Singh, R., Bharti, N., Madan, J. & Hiremath, S.N. (2010). "Characterization of cyclodextrin inclusion complexes – A review." Journal of Pharmaceutical Science and Technology **2**(3): 171-183.

Skoog, D. A. C. S. R. H. F. J. (2007). Principles of instrumental analysis. Belmont, CA, Thomson Brooks/Cole.

Smith, A., H. Duan, et al. (2008). "Bioconjugated quantum dots for in vivo molecular and cellular imaging." Adv Drug Deliv Rev **60**(11): 1226-1240.

Son, S. J., X. Bai, et al. (2007). "Inorganic hollow nanoparticles and nanotubes in nanomedicine: Part 1. Drug/gene delivery applications." Drug Discovery Today **12**(15–16): 650-656.

Soppimath, K. S., C. W. Tan, et al. (2005). "pH-Triggered thermally responsive polymer core-shell nanoparticles for targeted drug delivery." Adv. Mater. **17**: 318-323.

Sorokin, A. V., I. I. Fylymonova, et al. (2012). "Exciton transport in amphi-PIC J-aggregates formed in polymer films." Optical Materials **34**(12): 2091-2094.

Sorokin, A. V., I. I. Fylymonova, et al. (2012). "Exciton transport in amphi-PIC J-aggregates formed in polymer films." Opt. Mater. **34**: 2091-2094.

Sparkman, O. D. (2000). Mass spectrometry desk reference. Pittsburgh, Pa., Global View Pub.

Stella, V. J. and Q. He (2008). "Cyclodextrins." Toxicol Pathol **36**(1): 30-42.

Stella, V. J. and R. A. Rajewski (1997). "Cyclodextrins: their future in drug formulation and delivery." Pharm Res **14**(5): 556-567.

Stewart, M. J. and I. D. Watson (1983). "Standard units for expressing drug concentrations in biological fluids." British Journal of Clinical Pharmacology **16**(1): 3-7.

Straubinger, R. M., K. Hong, et al. (1983). "Endocytosis of liposomes and intracellular fate of encapsulated molecules: encounter with a low pH compartment after internalization in coated vesicles." Cell **32**(4): 1069-1079.

Sun, C., O. Veiseh, et al. (2008). "In vivo MRI detection of gliomas by chlorotoxin-conjugated superparamagnetic nanoprobes." Small **4**(3): 372-379.

Sundaram, J., B. R. Mellein, et al. (2003). "An experimental and theoretical analysis of ultrasound-induced permeabilization of cell membranes." Biophys J **84**(5): 3087-3101.

Suslick, K. S. and L. A. Crum (1998). Sonochemistry and sonoluminescence, Wiley-Interscience: New York.

Suzuki, S., S. Watanabe, et al. (1995). "Preparation of long-circulating immunoliposomes containing adriamycin by a novel method to coat immunoliposomes with poly(ethylene glycol)." Biochim Biophys Acta **17**(1): 9-16.

Svenson, S. and D. A. Tomalia (2005). "Dendrimers in biomedical applications--reflections on the field." Adv Drug Deliv Rev **57**(15): 2106-2129.

Swiech, O., A. Mieczkowska, et al. (2012). "Intermolecular interactions between doxorubicin and beta-cyclodextrin 4-methoxyphenol conjugates." J Phys Chem B **116**(6): 1765-1771.

Szatmári, I. and Z. Vargay (1988). Pharmacokinetics of Dimethyl-Beta-Cyclodextrin in Rats. Proceedings of the Fourth International Symposium on Cyclodextrins. O. Huber and J. Szejtli, Springer Netherlands. **5:** 407-413.

Szejtli, J. (1988). Cyclodextrin Technology: 79-306.

T.M. Allen, T. M., C.B. Hansen, Y.C. Chin (1992). "Stealth liposomes: an improved sustained release system for 1-b-D-arabinofuranosylcytosine." Cancer Res. **52**: 2431-2439.

Tabushi, I., Y. Kiyosuke, et al. (1978). "Approach to the aspects of driving force of inclusion by. alpha.-cyclodextrin." J. Am. Chem. Soc. **100**(3): 916-919.

Tacker, J. R. and R. U. Anderson (1982). "Delivery of antitumor drug to bladder cancer by use of phase transition liposomes and hyperthermia." J Urol **127**(6): 1211-1214.

Tafazzoli, M. and M. Ghiasi (2009). "Structure and conformation of α-, β- and γ-cyclodextrin in solution: Theoretical approaches and experimental validation." Carbohydrate Polymers **78**(1): 10-15.

Tanaka, M., Y. Iwata, et al. (1995). "Effect of 2-Hydroxypropyl-β-cyclodextrin on Percutaneous Absorption of Methyl Paraben." Journal of Pharmacy and Pharmacology **47**(11): 897-900.

ter Haar, G. (2007). "Therapeutic applications of ultrasound." Prog Biophys Mol Biol **93**(1-3): 111-129.

ter Haar, G., A. Shaw, et al. (2011). "Guidance on reporting ultrasound exposure conditions for bio-effects studies." Ultrasound Med Biol **37**(2): 177-183.

ter Haar, G. R. (2001). "High intensity focused ultrasound for the treatment of tumors." Echocardiography **18**(4): 317-322.

Thanou, M. and W. Gedroyc (2013). "MRI-Guided Focused Ultrasound as a New Method of Drug Delivery." Journal of Drug Delivery **2013**: 12.

Thomas, M. and A. M. Klibanov (2003). "Conjugation to gold nanoparticles enhances polyethylenimine's transfer of plasmid DNA into mammalian cells." Proceedings of the National Academy of Sciences **100**(16): 9138-9143.

Tinkov, S., R. Bekeredjian, et al. (2009). "Characterization of ultrasound-mediated destruction of drug-loaded microbubbles using an improved in vitro model." Applied Acoustics **70**(10): 1323-1329.

Tiwari, G., R. Tiwari, et al. (2010). "Cyclodextrins in delivery systems: Applications." J Pharm Bioallied Sci **2**(2): 72-79.

Tomalia, D. A., H. Baker, et al. (1985). "A New Class of Polymers: Starburst-Dendritic Macromolecules." Polym J **17**(1): 117-132.

Tomalia, D. A., L. A. Reyna, et al. (2007). "Dendrimers as multi-purpose nanodevices for oncology drug delivery and diagnostic imaging." Biochem Soc Trans **35**(Pt 1): 61-67.

Tomayko, M. and C. P. Reynolds (1989). "Determination of subcutaneous tumor size in athymic (nude) mice." Cancer Chemotherapy and Pharmacology **24**(3): 148-154.

Torchilin, V. P. (2000). "Drug targeting." European Journal of Pharmaceutical Sciences **11, Supplement 2**(0): S81-S91.

Totterman, A. M., N. G. Schipper, et al. (1997). "Intestinal safety of water-soluble β-cyclodextrins in paediatric oral solutions of spironolactone: effects on human intestinal epithelial Caco-2 cells." J. Pharm. Pharmacol. **49**: 43-48.

Treat, L. H., N. McDannold, et al. (2012). "Improved Anti-Tumor Effect of Liposomal Doxorubicin After Targeted Blood-Brain Barrier Disruption by MRI-Guided Focused Ultrasound in Rat Glioma." Ultrasound Med Biol **38**(10): 1716-1725.

Tuszynski, G. P. and A. Murphy (1990). "Spectrophotometric quantitation of anchorage-dependent cell

numbers using the bicinchoninic acid protein assay reagent." Anal Biochem **184**(1): 189-191.

Uekama, K. (2004). "Design and Evaluation of Cyclodextrin-Based Drug Formulation." Chem.Pharm.Bull. **52**(8): 900-915.

Uekama, K., H. Adachi, et al. (1992). "Improved transdermal delivery of prostaglandin E1 through hairless mouse skin: combined use of carboxymethyl-ethyl-beta-cyclodextrin and penetration enhancers." J Pharm Pharmacol **44**(2): 119-121.

Uekama, K., F. Hirayama, et al. (1998). "Cyclodextrin Drug Carrier Systems." Chem. Rev **98**: 2045-2076.

Uekama, K., F. Hirayama, et al. (1998). "Cyclodextrin Drug Carrier Systems." Chem Rev **98**(5): 2045-2076.

Vaage, J., E. Mayhew, et al. (1992). "Therapy of primary and metastatic mouse mammary carcinomas with doxorubicin encapsulated in long circulating liposomes." Int J Cancer **51**(6): 942-948.

van der Zee, J. (2002). "Heating the patient: a promising approach?" Ann Oncol **13**(8): 1173-1184.

van Wamel, A., K. Kooiman, et al. (2006). "Vibrating microbubbles poking individual cells: drug transfer into cells via sonoporation." J Control Release **112**(2): 149-155.

Vandyke, K., M. Y. White, et al. (2007). "Plant-derived MINA-05 inhibits human prostate cancer proliferation in vitro and lymph node spread in vivo." Neoplasia **9**(4): 322-331.

Vardharajula, S., S. Z. Ali, et al. (2012). "Functionalized carbon nanotubes: biomedical applications." Int J Nanomedicine **7**: 5361-5374.

Varga, G. (2011). "Alternative methods In vitro techniques: Cell and tissue cultures." Animal Experiments in Medicine.

Vasir, J. K. and V. Labhasetwar (2005). "Targeted drug delivery in cancer therapy." Technology in cancer research & treatment **4**(4): 363-374.

Vaupel, P., F. Kallinowski, et al. (1989). "Blood flow, oxygen and nutrient supply, and metabolic microenvironment of human tumors: a review." Cancer Res **49**(23): 6449-6465.

Venditto, V. J. and F. C. Szoka Jr (2013). "Cancer nanomedicines: So many papers and so few drugs!" Advanced Drug Delivery Reviews **65**(1): 80-88.

Villeneuve, L., L. Alberti, et al. (2009). "Assay of hydroxyl radicals generated by focused ultrasound." Ultrason Sonochem **16**(3): 339-344.

Villiers, A. (1891). "Sur la fermentation de la f écule par l'action du ferment butyrique." Compt. Rend. Acad. Sci. **112**: 536-538.

Visaria, R. K., R. J. Griffin, et al. (2006). "Enhancement of tumor thermal therapy using gold nanoparticle-assisted tumor necrosis factor-alpha delivery." Mol Cancer Ther **5**(4): 1014-1020.

Vogelson, C. T. (2001). "Advances in drug delivery systems." Modern Drug Discovery **4**(4): 49-50, 52.

Vykhodtseva, N. (2010). Disruption of Blood–Brain Barrier by Focused Ultrasound for Targeted Drug Delivery to the Brain. **45:** 35-62.

Wagner, B. (2003). "Chapter 1 in Handbook of Photochemistry and Photobiology,." in: H. Nalwa (Ed.), Supramolecular Photochemistry, American Scientific Publishers, Stevenson

Ranch, CA, **3**.

Wagner, B., S. Fitzpatrick, et al. (2003). "Fluorescence Suppression of 7-Methoxycoumarin upon Inclusion into Cyclodextrins." Journal of inclusion phenomena and macrocyclic chemistry **47**(3-4): 187-192.

Wagner, B. D. (2006). Chapter 2 - The Effects of Cyclodextrins on Guest Fluorescence. Cyclodextrin Materials Photochemistry, Photophysics and Photobiology. A. Douhal. Amsterdam, Elsevier. **1:**

27-59.

Wang, P., C. Xu, et al. (2010). "Mitochondrial damage in nasopharyngeal carcinoma cells induced by ultrasound radiation in the presence of hypocrellin B." J Ultrasound Med **29**(1): 43-50.

Wang, Y., R. Wang, et al. (2010). "Pegylated phospholipids-based self-assembly with water-soluble drugs." Pharm Res **27**(2): 361-370.

Ward, M., J. Wu, et al. (2000). "Experimental study of the effects of Optison concentration on sonoporation in vitro." Ultrasound Med Biol **26**(7): 1169-1175.

Weidensteiner, C., W. Reichardt, et al. (2013). "Effects of the nitric oxide donor JS-K on the blood-tumor barrier and on orthotopic U87 rat gliomas assessed by MRI." Nitric Oxide **30**(0): 17-25.

Wiener, E. C., M. W. Brechbiel, et al. (1994). "Dendrimer-based metal chelates: a new class of magnetic resonance imaging contrast agents." Magn Reson Med **31**(1): 1-8.

Willis, M. and E. Forssen (1998). "Ligand-targeted liposomes." Adv. Drug Deliv. Rev. **29**(3): 249-271.

Wilson, I. D., R. Plumb, et al. (2005). "HPLC-MS-based methods for the study of metabonomics." Journal of Chromatography B **817**(1): 67-76.

Wolinsky, J. B. and M. W. Grinstaff (2008). "Therapeutic and diagnostic applications of dendrimers for cancer treatment." Adv Drug Deliv Rev **60**(9): 1037-1055.

Woodle, M. C., T. M. Allen, et al. (1992). "In vivo efficacy of vincristine entrapped in long-circulating liposomes." Proc. Am. Assoc. Cancer Res. **33**: 447.

Woodle, M. C., G. Storm, et al. (1992). "Prolonged systemic delivery of peptide drugs by long-circulating liposomes: illustration with vasopressin in the Brattleboro rat." Pharm Res **9**(2): 260-265.

Wu, C., M. W. Brechbiel, et al. (1994). "Metal-chelate-dendrimer-antibody constructs for use in radioimmunotherapy and imaging." Bioorganic & Medicinal Chemistry Letters **4**(3): 449-454.

Wu, F., Z. B. Wang, et al. (2007). ""Wide local ablation" of localized breast cancer using high intensity focused ultrasound." J Surg Oncol **96**(2): 130-136.

Wu, F., Z. B. Wang, et al. (2003). "Preliminary experience using high intensity focused ultrasound for the treatment of patients with advanced stage renal malignancy." J Urol **170**(6 Pt 1): 2237-2240.

Wu, F., Z. B. Wang, et al. (2005). "Feasibility of US-guided high-intensity focused ultrasound treatment in patients with advanced pancreatic cancer: initial experience." Radiology **236**(3): 1034-1040.

Wust, P., B. Hildebrandt, et al. (2002). "Hyperthermia in combined treatment of cancer." Lancet Oncol **3**(8): 487-497.

Xiang, T.-x. and B. Anderson (2002). "Stable Supersaturated Aqueous Solutions of Silatecan 7-t-Butyldimethylsilyl-10-Hydroxycamptothecin via Chemical Conversion in the Presence of a Chemically Modified β-Cyclodextrin." Pharmaceutical Research **19**(8): 1215-1222.

Xiong, L. L., J. H. Hwang, et al. (2009). "Early clinical experience using high intensity focused ultrasound for palliation of inoperable pancreatic cancer." Jop **10**(2): 123-129.

Xu, P., H. Tang, et al. (2004). "Enhanced stability of core-surface cross-linked micelles fabricated from amphiphilic brush copolymers." Biomacromolecules **5**(5): 1736-1744.

Yamanoi, T., N. Kobayashi, et al. (2006). "Preparation of a Cyclodextrin Conjugated With Two Arbutin Moieties as a Drug-Carrier Model, and its High Ability for the Inclusion of Doxorubicin." Letters in Drug Design & Discovery **3**(3): 188-191.

Yamanoi, T., N. Kobayashia, et al. (2006). "Preparation of a Cyclodextrin Conjugated With Two

Arbutin Moieties as a Drug-Carrier Model, and its High Ability for the Inclusion of Doxorubicin." Letters in Drug Design & Discovery(3): 188-191.

Yamanoi, T., N. Yoshida, et al. (2005). "Synthesis of mono-glucose-branched cyclodextrins with a high inclusion ability for doxorubicin and their efficient glycosylation using Mucor hiemalis endo-β-N-acetylglucosaminidase." Bioorg. Medicin. Chem. Let. **15**(4): 1009-1013.

Yang, H. and W. J. Kao (2006). "Dendrimers for pharmaceutical and biomedical applications." J Biomater Sci Polym Ed **17**(1-2): 3-19.

Yokoyama, M., S. Inoue, et al. (1989). "Molecular design for missile drug: Synthesis of adriamycin conjugated with immunoglobulin G using poly(ethylene glycol)-block-poly(aspartic acid) as intermediate carrier." Die Makromolekulare Chemie **190**(9): 2041-2054.

Yokoyama, M., S. Inoue, et al. (1987). "Preparation of adriamycin-conjugated poly(ethylene glycol)-poly(aspartic acid) block copolymer. A new type of polymeric anticancer agent." Die Makromolekulare Chemie, Rapid Communications **8**(9): 431-435.

Yokoyama, M., T. Okano, et al. (1991). "Toxicity and antitumor activity against solid tumors of micelle-forming polymeric anticancer drug and its extremely long circulation in blood." Cancer Res **51**(12): 3229-3236.

Yokoyama, M., T. Okano, et al. (1999). "Selective Delivery of Adiramycin to a Solid Tumor Using a Polymeric Micelle Carrier System." Journal of Drug Targeting **7**(3): 171-186.

Yorozu, T., M. Hoshino, et al. (1982). "Fluorescence studies of pyrene inclusion complexes with .alpha.-, .beta.-, and .gamma.-cyclodextrins in aqueous solutions. Evidence for formation of pyrene dimer in .gamma.-cyclodextrin cavity." The Journal of Physical Chemistry **86**(22): 4426-4429.

Yorozu, T., M. Hoshino, et al. (1982). "Photoexcited inclusion complexes of .beta.-naphthol with .alpha.-, .beta.-, and .gamma.-cyclodextrins in aqueous solutions." The Journal of Physical Chemistry **86**(22): 4422-4426.

Young, F. R. (1999). Cavitation, Imperial College Press.

Yu, T., Z. Wang, et al. (2004). "A review of research into the uses of low level ultrasound in cancer therapy." Ultrasonics Sonochemistry **11**(2): 95-103.

Yudina, A., M. de Smet, et al. (2011). "Ultrasound-mediated intracellular drug delivery using microbubbles and temperature-sensitive liposomes." J Control Release **155**(3): 442-448.

Yudina, A., M. Lepetit-Coiffe, et al. (2011). "Evaluation of the temporal window for drug delivery following ultrasound-mediated membrane permeability enhancement." Mol Imaging Biol **13**(2): 239-249.

Yurkovetskiy, A. F.-F., Robert J. and R. Fram (2009). "- XMT-1001, a novel polymeric camptothecin pro-drug in clinical development for patients with advanced cancer." Adv Drug Deliv Rev **61**(13): 1193-1202.

Zhang, L., W. Z. Chen, et al. (2010). "Feasibility of magnetic resonance imaging-guided high intensity focused ultrasound therapy for ablating uterine fibroids in patients with bowel lies anterior to uterus." Eur J Radiol **73**(2): 396-403.

Zhang, L., H. Zhu, et al. (2009). "High-intensity focused ultrasound (HIFU): effective and safe therapy for hepatocellular carcinoma adjacent to major hepatic veins." Eur Radiol **19**(2): 437-445.

Zhu, H., K. Zhou, et al. (2009). "High intensity focused ultrasound (HIFU) therapy for local treatment of hepatocellular carcinoma: role of partial rib resection." Eur J Radiol **72**(1): 160-166.